ELECTROCHEMICAL, BOND, AND SERVICE LIFE PARAMETERS OF

COATED STEEL - CEMENTITIOUS SYSTEMS EXPOSED TO CHLORIDES

A THESIS

Submitted by

DEEPAK KUMAR KAMDE

for the award of the degree

of

DOCTOR OF PHILOSOPHY

DEPARTMENT OF CIVIL ENGINEERING

INDIAN INSTITUTE OF TECHNOLOGY MADRAS

CHENNAI 600 036, INDIA

June 2020

This page is intentionally left blank

THESIS CERTIFICATE

This is to certify that the thesis titled, **ELECTROCHEMICAL, BOND, AND SERVICE LIFE PARAMETERS OF COATED STEEL - CEMENTITIOUS SYSTEMS EXPOSED TO CHLORIDES**, submitted by **Mr. Deepak Kumar Kamde** (Roll No.: **CE15D074**) to the Indian Institute of Technology Madras, Chennai, for the award of the degree of Doctor of Philosophy, is a bona fide record of the research work done by him under my supervision. The contents of this thesis, in full or in parts, have not been submitted to any other Institute or University for the award of any degree or diploma.

Dr. Radhakrishna G. Pillai
Research Guide & Associate Professor
Department of Civil Engineering
Indian Institute of Technology Madras
Chennai - 600 036, India

This page is intentionally left blank

Dedicated to

my Parents, Mrs. Jyoti Kamde and Mr. Rameshwar Kamde

This page is intentionally left blank

ACKNOWLEDGMENTS

This page is intentionally left blank

ABSTRACT

ELECTROCHEMICAL, BOND, AND SERVICE LIFE PARAMETERS OF COATED STEEL - CEMENTITIOUS SYSTEMS EXPOSED TO CHLORIDES

Currently, many reinforced concrete (RC) structures are designed for a service life of 100+ years. Coated steel reinforcement are widely used in anticipation of enhanced corrosion resistance and service lives of RC systems. The following two types of non-metallic coatings are generally used in the concrete construction industry: (i) fusion-bonded-epoxy (FBE) and (ii) cement-polymer-composite (CPC) coatings. However, in most cases, the FBE coated steel rebars are bent and cut at sites, exposed to sunlight, and poorly handled during the transport, storage, and construction at sites. Also, at many construction sites, it has been observed that the CPC coating is applied without adequate cleaning and preparation (say, sandblasting) of the surface of steel rebars. These inadequate practice can adversely affect the service lives of such steel-coating-concrete systems. To evaluate the performance of coated steel rebars in concrete systems, the first step is the corrosion assessment of coated steel rebars embedded in cementitious systems. Conventional test methodologies may not be able to detect the initiation of corrosion in coated steel rebars embedded in concrete systems. Therefore, there is a dire need to develop a suitable test methodology to detect the initiation of corrosion. Also, the reported chloride threshold values of uncoated rebars and the service life models used for RC systems with uncoated steel rebars may not be valid to estimate the service lives of RC systems with coated steel rebars. Because of these, the practitioners are facing challenges in assessing the corrosion condition and estimating the service lives of RC systems with coated steel rebars, which are the focus of this thesis.

In Objective 1, the feasibility of test methods that are conventionally used for uncoated steels in cementitious systems were evaluated for coated steel rebar systems. Hence, 3-bar

prism specimens and 1-bar lollipop specimens with various uncoated and coated steel rebars were cast and tested using the following techniques: (i) half-cell potential (HCP), (ii) macrocell corrosion current (MCC), (iii) linear polarization resistance (LPR), and (iv) electrochemical impedance spectroscopy (EIS). A total of 50 specimens were tested, and the test durations were about 400 days for prism and 200 days for lollipop specimens. Results indicated that the MCC measurements on prism specimens could not detect the ongoing corrosion activities. The possible reason for the unfeasibility of MCC is the differences in the corrosion circuits in the case of uncoated and coated steel rebars. If the resistances offered by FBE coating (> 30 kΩ) and concrete are significantly high then, the corrosion cell forms across various exposed points on the top rebar itself – without the participation of other rebars. Such corrosion will not be reflected in the current measurements made across multiple rebars. Also, because of the high ohmic drop across the FBE coating, the HCP and LPR measurements could not detect the initiation of corrosion at the steel surfaces. Only EIS measurements could effectively detect the initiation of corrosion in systems with FBE coated steels. Therefore, a test methodology based on the EIS technique using lollipop specimens and a generalized equivalent circuit were proposed to detect the initiation of corrosion. On the other hand, CPC coating offers low resistance (< 0.02 kΩ); therefore, all the studied techniques, except HCP, could detect the initiation of corrosion. Therefore, a test methodology based on LPR and using lollipop specimens was proposed to detect the initiation of corrosion of CPC coated rebars.

In Objective 2, the effect of inadequate construction practices such as exposure of the coated rebars to sunlight (say, UV rays) and mechanical scratch damage on the coating on the coating characteristics, chloride thresholds, and service lives of systems with FBE coated steel rebars were evaluated. To investigate the effect of exposure to sunlight/UV rays on coating characteristics, a total of 45 FBE coating samples were exposed to an accelerated UV weathering chamber for 60 days. The results from micro-analytical studies (using FTIR, SEM,

EDX, etc.) show that the exposure of FBE coated steel rebars to sunlight/UV rays can result in UV-induced chemical changes, shrinkage, and cracking of FBE coating. Then, to investigate the corrosion characteristics of FBE coated steel rebars, a total of 20 lollipop specimens with uncoated, FBE coated steel rebars with no damage (FBEC-ND), with scratch damage (FBEC-SD), and after UV exposure (FBEC-UV) were cast and tested using the proposed methodology from Objective 1. It was found that the FBEC-ND and FBEC-UV coating undergoes a 4-stage (slow) and 2-stage (fast) coating degradation, respectively. Experimental results show that FBE coating with scratch damage and UV exposure can undergo premature initiation of corrosion, the mechanisms involved are proposed. Also, the frameworks to determine the Cl_{th}, $D_{Cl, coating}$, and service lives of RC systems with FBE coated steel rebars are proposed. It was found that exposure to UV rays can significantly increase the $D_{Cl, coating}$ and decrease the Cl_{th} than uncoated steel. The proposed model estimated that the scratch damage and UV exposure of the coating can result in $\approx 70\%$ and 40% reduction, respectively, in the service lives of RC systems.

In Objective 3, the effect of surface preparation on Cl_{th} and the effect of corrosion on bond performance were investigated. For former, a total of 40 3-bar prism and 1-bar lollipop specimens with the following variables were cast and tested: (i) coated and uncoated steel, (ii) with and without sandblasting. Electrochemical data shows that the applications of CPC coating on as-received steel surfaces with rust can significantly reduce the resistance to the initiation of corrosion. Micrographs revealed that when CPC coating is applied on as-received steel rebars with rust, a thin, long, and continuous crack was observed at the steel-coating interface. This crack can provide a low resistive path for the corrosion process – resulting in $\approx 50\%$ less Cl_{th} and $\approx 40\%$ less service lives than that of the adequately coated steel rebars. To investigate the effect of CPC coating and corrosion on bond characteristics, a total of 35 pullout specimens were cast, exposed to chloride solution for about six months, and tested for their

bond strength. It was found that the RC systems with CPC coated steel rebars with no corrosion exhibited about 20% reduction of bond strength (τ_b) than uncoated steel rebars. With negligible corrosion, the bond strengths and stiffnesses of steel-coating-concrete interfaces were reduced by about 50-70%, which is not the case with uncoated steel rebars. Based on the results, bond stress-slip mechanisms are proposed for CPC coated steel rebar without and with corrosion. Also, a service life model for RC systems with CPC coated steel rebars is proposed by considering the initiation of corrosion and resulting in a significant reduction in bond strengths. Using this framework, the service lives of RC systems with inadequate CPC coating (i.e., on as-received rebars with rust) were about 50% less than that of the systems with adequate CPC coating (i.e., on sandblasted rebars).

Based on the experimental results and their detailed analysis, this thesis provides prescriptive and performance specifications for the use of FBE and CPC coated steel rebars in new construction. In addition, the possible remedial measures, which need further study, are suggested for extending the residual service life of the existing structures with FBE or CPC coated steel rebars.
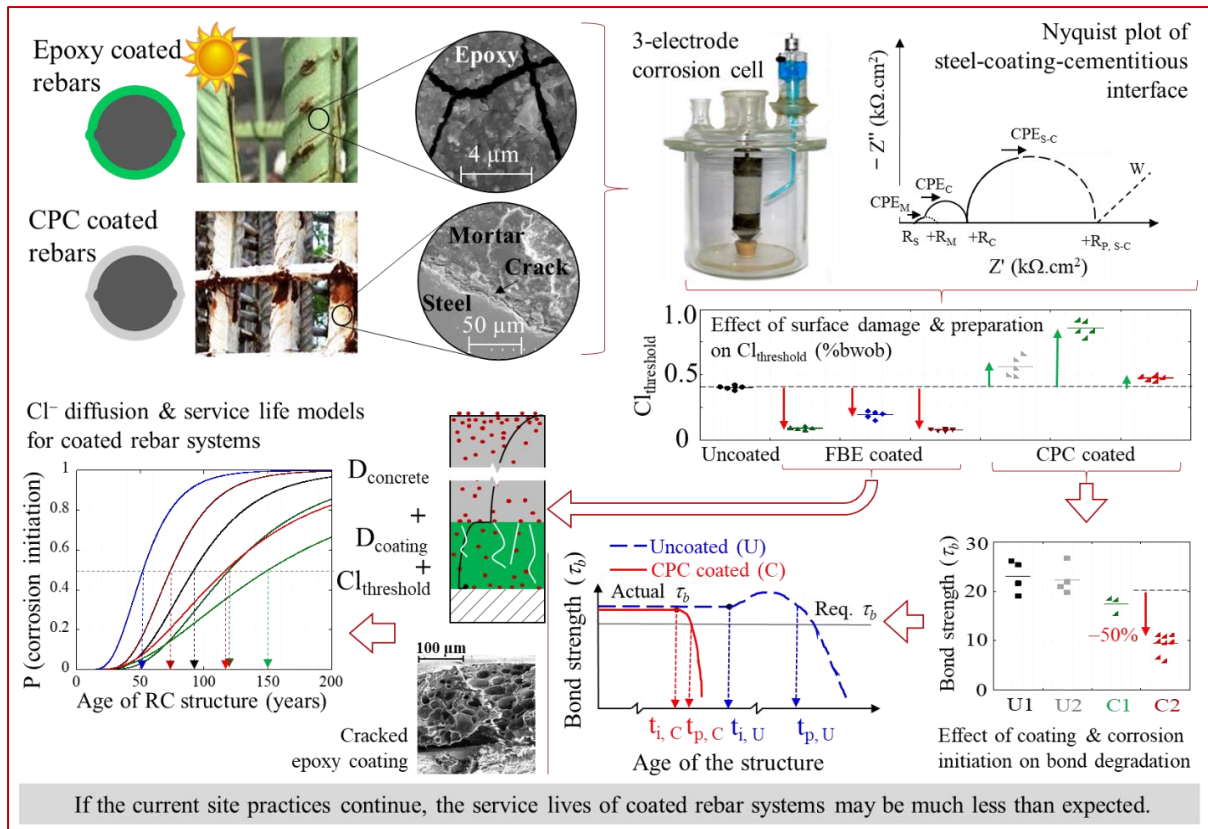
Keywords: Steel, concrete, fusion-bonded-epoxy coating, cement-polymer-composite coating, electrochemical, impedance spectroscopy, initiation of corrosion, depassivation, chloride threshold, bond degradation, durability, service life.

This page is intentionally left blank

TABLE OF CONTENTS

LIST OF FIGURES

LIST OF TABLES

This page is intentionally left blank

NOTATIONS AND ABBREVIATIONS

%bwob	:	% by weight of binder
μ	:	Mean
τ	:	Bond stress
τ_b	:	Bond strength
$\tau_{0.025}$	:	Bond stress at 0.025 mm slip
$\tau_{b, C1}$	:	Bond strength of CPC coated steel rebar and concrete without corrosion of steel and without coating disbondment
$\tau_{b, C2}$	:	Bond strength of CPC coated steel rebar and concrete with negligible corrosion of steel and significant coating disbondment
A	:	Adhesive force
A_{DB}	:	Area of disbondment along the embedded length of MSR
AR	:	As received
AR-CPCC	:	Cement-polymer composite coating applied on steel rebars with the as-received steel surface
C1	:	CPC coated steel rebars embedded in concrete without corrosion and coating disbondment
C2	:	CPC coated steel rebars embedded in concrete with negligible corrosion and significant coating disbondment
CDF	:	Cumulative distribution function
Cl_{th}	:	Critical chloride threshold of steel-coating interface
C_{max}	:	Maximum chloride concentration at the exposed concrete surface
CoV	:	Coefficient of variation
CPC	:	Cement-polymer-composite
CPE_C	:	Capacitance of the coating
CPE_{C-S}	:	Capacitance of the coating-steel interface
CPE_M	:	Capacitance of the mortar
C_s	:	Surface chloride concentration
C (x, t)	:	Chloride concentration at depth 'x' after exposure for 't' seconds
D_{cl}	:	Diffusion coefficient of concrete
DC	:	Direct current
D_{cl}	:	Chloride diffusion coefficient of concrete

$E_{Protection}$	:	Electrochemical potential of steel at passive state
$E_{Pitting}$	:	Electrochemical potential of steel when pitting corrosion starts
EIS	:	Electrochemical impedance spectroscopy
EEC	:	Equivalent Electrical Circuit
erf	:	Error function
F	:	Frictional force
f_c	:	Cube compressive strength of concrete
FBE	:	Fusion-Bonded-Epoxy
FBEC-ND	:	FBE coated steel rebars in as-received condition with no damage/degradation
FBEC-UV	:	FBE coated steel rebars after 10 days of exposure to UV rays
FT-IR	:	Fourier Transform - Infra-Red spectra
K	:	Stiffness of steel-concrete or steel-coating-concrete interface
K_{U1}	:	Stiffness of uncoated steel-concrete interface without corrosion
K_{U2}	:	Stiffness of uncoated steel-concrete interface with negligible corrosion
K_{C1}	:	Stiffness of steel-coating-concrete interface without corrosion and without coating disbondment
K_{C2}	:	Stiffness of steel-coating-concrete interface with negligible corrosion and significant coating disbondment
L_e	:	Embedment length
L_d	:	Development length
L_{d0}	:	Initial development length
$L_{d, U2}$	:	Development length required after the bond loss due to corrosion and coating disbondment
LVDT	:	Linear Variable Differential Transformer
M	:	Compression force due to mechanical interlocking
m	:	Decay constant
MSR	:	Main steel reinforcement
i_a	:	Anodic current
i_c	:	Cathodic current
i_{corr}	:	Rate of corrosion
RC	:	Reinforced concrete
R_C	:	The resistance of the coating

$R_{P,\,C\text{-}S}$	:	Polarization resistance of the coating-steel interface
rpm	:	Rotation per minute
R_M	:	The resistance of the mortar
R_S	:	The resistance offered by the electrolyte solution
s	:	Slip at the free end
s1	:	Slip at the free end during the elastic behavior of steel-concrete or steel-coating-concrete interface
s2	:	Slip at the free end during the plastic behavior of steel-concrete or steel-coating-concrete interface
s3	:	Slip at the free end when the concrete pipe is fully formed, and only frictional force remains at the interface
SB	:	Sandblasted
SB-CPCC	:	Cement-polymer composite coating applied on sandblasted steel rebars
S-C	:	Steel-Coating interface / Steel-cementitious interface
S-C-C	:	Steel-Coating-Concrete interface
SCE	:	Saturated calomel electrode
SEM	:	Scanning electron microscope
s_{U1}	:	Slip corresponding to the steel-concrete interface without corrosion
s_{U2}	:	Slip at the steel-concrete interface with negligible corrosion
s_{C1}	:	Slip at the steel-coating-concrete interface without corrosion and without coating disbondment
s_{C2}	:	Slip at the steel-coating-concrete interface with negligible corrosion and significant coating disbondment
SSR	:	Spiral steel reinforcement
t_i	:	Time to corrosion initiation
$t_{i,\,C}$	:	Time to corrosion initiation of the reinforced concrete system with Cement-polymer-composite coated steel rebars
$t_{i,\,U}$	:	Time to corrosion initiation of the reinforced concrete system with uncoated steel rebars
$t_{p,\,C}$	:	Time to corrosion propagation of reinforced concrete system with Cement-polymer-composite coated steel rebars
$t_{p,\,U}$	:	Time to corrosion propagation of reinforced concrete system with uncoated steel rebars

t	:	Exposure time
t_i	:	Time to corrosion initiation
UV	:	Ultraviolet
U1	:	Uncoated steel rebar without corrosion
U2	:	Uncoated steel rebar with negligible corrosion
wC	:	With coating
woC	:	Without coating
x	:	Depth from the exposed surface of the concrete

1   INTRODUCTION

1.1   PROBLEM STATEMENT

In the past two decades, numerous reinforced concrete (RC) structures, such as highway/railway bridges, high-rise buildings, and power plants, have been constructed along the coastal region with significant chloride exposure and with a target service life of more than 100 years. To achieve this target service life, the steel-cementitious systems in these structures must have good corrosion resistance, especially when exposed to chlorides. In anticipation of enhanced corrosion resistance, the steel reinforcing bars ('rebars,' herein) in many of these structures are coated with organic materials. Usually, these coatings are made of either a polymer or a polymer-modified material and work by (i) providing a shield/physical barrier between the underlying steel and the deleterious elements, such as moisture, oxygen, chlorides, and (ii) restricting the ionic flow between anodic and cathodic areas (Bíaz et al. 2018; Cortés 1998; Kessler et al. 2015). Two coatings are widely used to coat the steel rebars are (i) fusion-bonded-epoxy (FBE) and (ii) cement-polymer-composite (CPC) coating.

FBE coating is obtained by placing the clean and hot (at about 200 $^{\circ}$C) steel rebars in a mist of powdered epoxy, which can fuse and bond to the steel surface. This fusion-bonding and subsequent quenching help to form a uniform, continuous, and well-adhered epoxy coating on the steel surface (McDonald 2016). A good quality FBE coating is expected to insulate and protect the steel surface from the corrosive/chloride environment, and delay the initiation of corrosion. However, Figure 1.1 (a) shows that the FBE coated rebars are inadequately handled during transportation, storage, bending/cutting of rebars, and during the placement/vibration of concrete at construction sites. In addition, Figure 1.1 (b) shows that the FBE coated steel rebars are exposed to sunlight during prolonged storage at manufacturing units, construction sites,

1

and during delayed or staged construction. The poor practices can lead to scratching, cracking, and/or degradation of the epoxy coating, which in turn reduces its corrosion resistance, and results in premature initiation of corrosion (Cividanes et al. 2014; Kamde and Pillai 2017; Singh and Ghosh 2005).

(a) Scratch damage and disbondment of the coating due to poor handling of rebars at sites **(b) Exposure of coated steel to sunlight during storage or delayed construction**

Figure 1.1 Scratch damage and degradation of FBE coating due to inadequate construction practices

The cement-polymer-composite (CPC) coated steel rebars with acrylic based coating modified with cement as additives are widely used in the construction industry. As per the specifications, the CPC coating is supposed to be applied onto sand-blasted (SB) rebars and is applied at the construction sites to avoid the scratch damage to the coating during transportation, bending, and other construction practices. CPC coated steel rebars are expected to protect the steel from corrosion by providing a physical barrier and a passive film by reacting with the metal surface. Figure 1.2 shows that many site personnel do not insist on sandblasting the rebars prior to applying the CPC coating; and use the as-received (AR) rebars with rust on

the surface, which can lead to premature initiation of corrosion. Also, the effect of corrosion on the bond strength of such steel-coating-concrete systems is not reported.
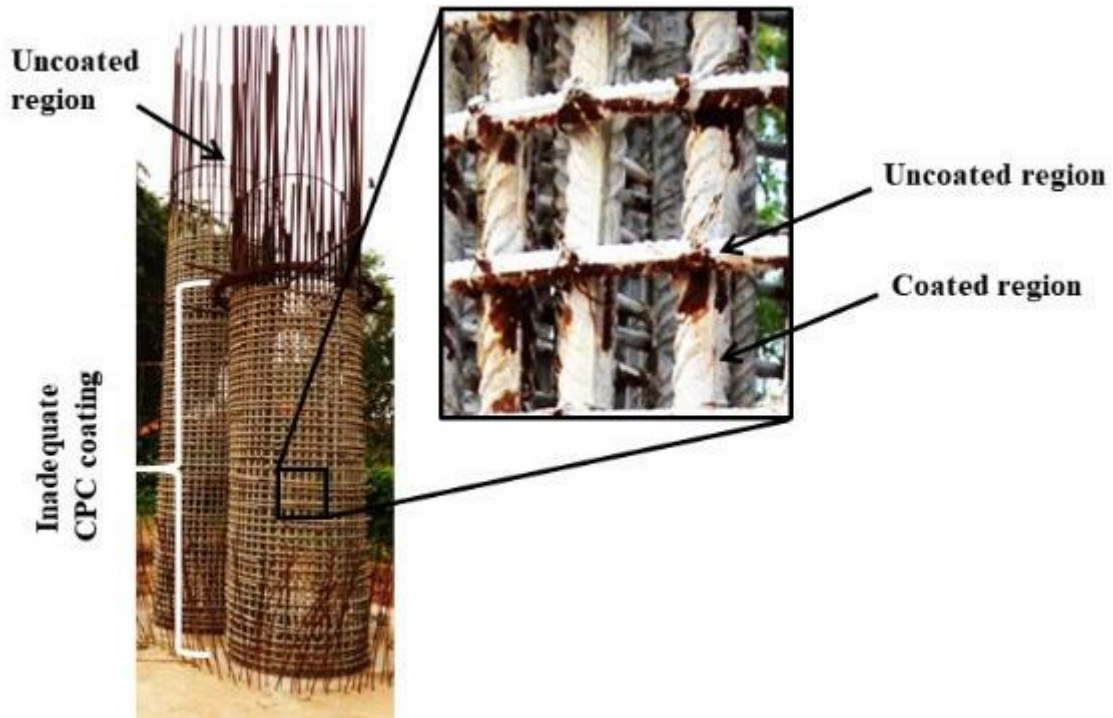
Figure 1.2 Photograph of a column under construction with CPC coated rebars and close-up showing inadequate CPC coating on rebar

Considering the current quality control measures, it is challenging to avoid scratch damage and degradation of coating at construction sites. As a result, many field studies on coated steel rebars report the premature initiation of corrosion, disbondment of coating, or permanent corrosion-induced failure of structures (Kim et al. 2007; Manning 1996; McDonald 2009; Pyć et al. 2000; Zemajtis et al. 1998). On the other hand, many laboratory studies report good performance of coated steel rebars (Ababneh et al. 2012; Kahhaleh et al. 1998; Mohammed et al. 2014; Scannell and Clear 1990; Swamy and Koyama 1989; Vedalakshmi et al. 2000). This difference in opinion from lab and field studies can be due to differences in

3

(i) quality of coated steel rebars used at sites and at laboratories, (ii) the techniques used for assessing corrosion. Due to the unavailability of standard test methods, the practitioners tend to use existing/conventional test methods that are meant for uncoated steel rebars. A few literature report the assessment or comparison of coated steel rebars embedded in cementitious systems using EIS (Cambier et al. 2014; Jolivet et al. 2007; Kranc and Alberto A. Sagues 2001; Lau and Sagüés 2007; Ryou et al. 2005). However, the candidate could not find literature with a suitable standard test method to detect the 'initiation' of corrosion of FBE and CPC coated rebars embedded in concrete. Therefore, there is a dire need to develop a standard test method for assessing the corrosion activities, especially the test methodology to detect the initiation of corrosion.

Traditionally and conservatively, the service life of RC systems is defined as the time to the initiation of corrosion of rebars (t_i) (Bhattacharjee 2012; Karuppanasamy and Pillai 2017a; Tuutti 1982). The estimation of t_i necessitates the estimation of the chloride threshold of embedded steel systems. However, literature do not provide enough quantitative and probabilistic data on the chloride thresholds of coated steel rebar systems. This makes it difficult to estimate the service lives of such systems. Also, the existing service life models made for uncoated steel rebars are not valid for systems with coated steel rebars because they do not consider the chloride ingress through the coating and the associated corrosion initiation and bond degradations with the initiation of corrosion. Therefore, there is a need to develop a frameworks to estimate the service lives of RC systems with coated steel rebars, especially for cases with inadequate coating application and site practices.

1.2 MOTIVATION FOR THE STUDY

Worldwide, many countries/states have either banned or recommended not to use the FBE coated steel rebars. In India and in many other developed/developing nations, still, a large number of infrastructure are being constructed using FBE and CPC coated steel rebars. Many of the structures are built with poor quality control measures. To take any action to regulate the use of coated steel rebars, approving authorities need data showing the performance of coated steel rebars. However, there is a lack of data available on how the poor site conditions and practices affect the coating characteristics, electrochemical characteristics, chloride threshold, and time to corrosion initiation. Also, many personals wrongly believe that the propagation time is longer than the initiation time of coated steel or propagation time of uncoated steel rebars. Therefore, many reported literature focus on the rate of corrosion, mass loss of coated steel rebars, etc. Also, due to the use of inadequate test methods, the reported literatures show different opinion than the performance of FBE coated steel rebars at construction sites. Also, there is a lack of data on the initiation of corrosion and bond performance of CPC coated steel rebars. This thesis will present enough designers and engineers data on service life estimates in terms of both corrosion initiation and bond degradation. Using these data, the Bureau of Indian Standards (IS 13620), American Society of Testing and Materials (ASTM A775), tender documents of public and private organizations, and other specifications can be modified. Also, this thesis will also provide a scientific understanding of corrosion characteristics and mechanisms of initiation of corrosion for both FBE and CPC coated steel rebars.

1.3 DEFINITIONS

Anode: The electrode, where oxidation of metal takes place. The location where electron loss and metal loss takes place.

Bond stress (τ): Bond stress is the resistance to the relative slip between steel rebar and concrete. Generally, chemical adhesion, frictional force, and mechanical interlock between steel rebar and concrete contribution to the bond stress.

Bond strength (τ_b): The bond stress required to break chemical adhesion, frictional force, and mechanical interlock of steel-concrete or steel-coating-concrete interface

Calomel electrode: A reference cell with mercury electrode in potassium chloride solution of specified concentration and saturated with mercurous chloride.

Coating Disbondment: Coating disbondement is the phenomenon of disbondment of coating from the steel surface due to corrosion or due to cathodic reactions.

Corrosion cell: Electrochemical cell on the metal surface because of chemical or physical differences on the metal surface.

Cathode: The electrode where reduction reaction occurs. The location where the electrode accepts electrons.

Chloride threshold (Cl_{th}): The chloride concentration at the steel surface required to initiate the corrosion at the steel surface. This concentration depends on physical and chemical properties at the S-C interface.

Decay constant/maturity constant (m): The decay constant (also known as an aging coefficient or maturity coefficient) reflects the maturity level of concrete and helps in

determining the reduction in the diffusion coefficient over time due to the evolution of the microstructure of the cementitious phase.

Electrode: Electrode is a metallic conductor transporting electricity into non-metallic solid, liqued, gases, vacuums, etc. (Piron, 1994).

Electrolyte: The medium, preferentially conducting in nature, where ions can travel from anode to cathode. In reinforced concrete systems, concrete pore solution is the electrolyte.

Localized corrosion: Corrosion at discrete sites. Pitting corrosion is one of the most common examples of localized corrosion.

Macrocell corrosion (MC): The corrosion cell where anode and cathodes are well-separated (at macro scale).

Maximum surface chloride concentration (C_{max}): The maximum concentration of chloride, which can be accumulated at the concrete surface in the life of the reinforced concrete structure.

Ohmic drop: Potential drop due to electrolytes such as solution, mortar, or anything between the working electrode and the reference electrode.

Passive film: It is an invisible oxide layer on the steel surface. This layer prevents the metal surface from further corrosion when in contact with the environment (moisture, oxygen, and chlorides).

Pitting corrosion: It is one of the forms of localized corrosion by which cavities or pits/holes are formed during the process of corrosion. Pitting corrosion is initiated by localized damage of passive film by acidity, chlorides, low dissolved oxygen concentrations, etc.

Surface chloride concentration on the concrete surface (C_S): Surface chloride concentration (C_s) is the concentration of chlorides accumulated at the exposed concrete surface over time. C_s increases with time and reaches a saturated concentration for a particular concrete in specific exposure condition. This saturated concentration is called maximum surface chloride concentration (C_{max}).

Service life: The duration from the start of exposure of the RC system to the environment until the RC system meets the structural requirements specified by the user. Figure 1.3 shows the widely used service life model for RC structures with uncoated steel rebars. Generally, service life is the summation of time to corrosion initiation and time to corrosion propagation. In this study, time to corrosion initiation is considered to be the end of the service lives of RC systems.
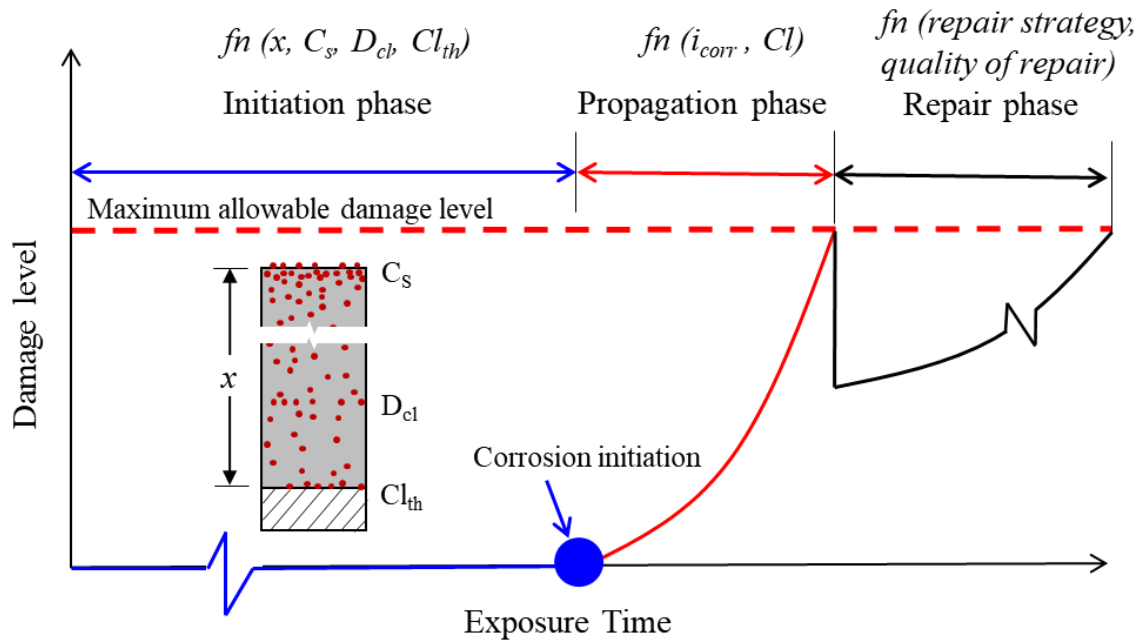
Figure 1.3 Service life model for RC systems with uncoated steel rebars

Three-electrode system: The Three-electrode system consists of the following electrodes: working electrode, reference electrode, and the counter electrode.

- **Working electrode (WE):** The test specimen or the electrode which is anode.

- **Reference electrode (RE)**: The electrode which has accurately maintained potentials, which is used to a reference to measure the potential difference of other electrode.

- **Counter electrode (CE)**: The electrode is usually used for polarization studies to pass current to and from the test electrode. It is made of any non-corroding material. It is also known as the auxiliary electrode.
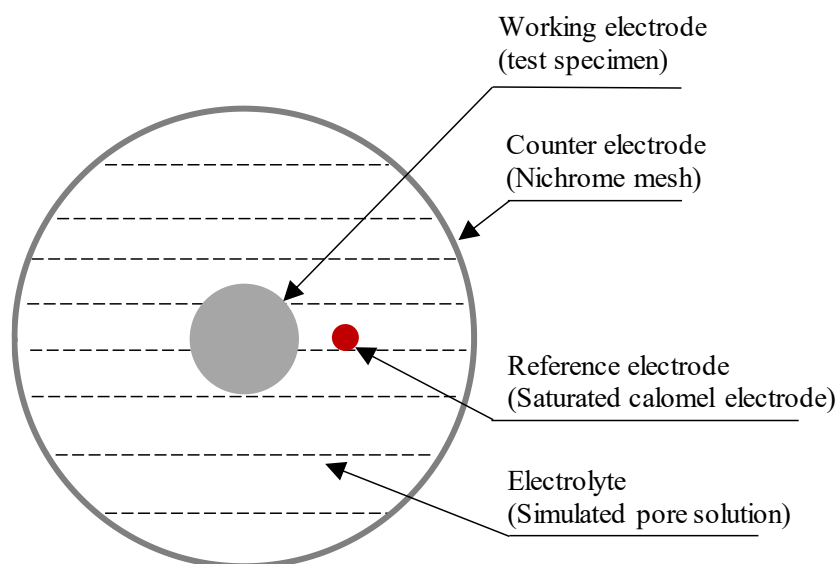
Figure 1.4 Schematic of a typical three-electrode corrosion cell (similar to what is used in this study)

Time to initiation of corrosion: The duration between the start of the exposure of RC systems to the environment until the time of onset of active corrosion. It is the time required for sufficient chlorides to reach the steel surface and initiate the corrosion process (see Figure 1.3). The chloride diffusion coefficient and chloride threshold are two governing parameters to

estimate the time to corrosion initiation. Generally, time to corrosion initiation is considered as the longest duration in the service life of RC systems.

Time to propagation of corrosion: The duration between the time of onset of active corrosion and when the RC system becomes unable to meet the desired structural requirement of RC systems. Corrosion rate and chloride concentration at the steel surface are two governing parameters of corrosion propagation time.

Underfilm corrosion: Corrosion that takes place under the film/coating. This is also known as fillifom corrosion.

Uniform corrosion: Corrosion that takes place uniformly over the metal surface. For example, cast iron and steel corrodes uniformly when exposed to soil, water, etc.

Polarisation resistance (R_P): Resistance of material/metal surface (here, steel in concrete system) to change from its equilibrium potentials.

Resistance of polarisation of the steel-coating-cementitious system ($R_{P, S-C}$): Resistance of steel-coating interface to change from its equilibrium potentials.

Resistance of coating material (R_C): Measured resistance offered by the coating materials on application of potential. This is also an indirect measurement of porosity, moisture uptake, etc.

1.4 RESEARCH QUESTIONS

1. The existing test methods are for the assessment of RC systems with uncoated steel rebars. Can these test methods/techniques be directly used to detect the initiation of corrosion in systems with coated steel rebars (CPC and FBE coated steel rebars)? If not, what are the changes to be incorporated?

2. Are the existing equivalent electrical circuits for coated steels in aqueous solution can fit the EIS response from coated steel rebars embedded in cementitious systems? If not, what are changes should be made?

3. What are the existing corrosion initiation criteria? Can we modify and use them to detect the initiation of corrosion in coated steel rebars embedded in cementitious systems?

4. What is the effect of inadequate application and handling processes such as application of the coating on inadequately cleaned steel surface, bending/dragging of coated steel rebars at the construction sites – resulting in damage, and prolonge outdoor storage of coated steel rebars on chloride thresholds of coated steel rebars?

5. Can the existing approach of defining the chloride thresholds for uncoated steel be used to determine the chloride thresholds of coated steel rebars? If not, what approach should be adopted?

6. Current practices of using the coated steel rebars at construction sites are inadequate, which can lead to premature initiation of corrosion. With this, will the RC systems with inadequate quality of coated steel rebars be able to perform for the designed service lives?

7. What will be the effect of coating thickness and corrosion on the bond strength of steel-coating-concrete systems?

8. Can the existing service life estimation models be used for the estimation of service lives of RC systems with coated steel rebars? If not, what changes should be made to estimate the service lives of RC systems with coated steel rebars?

1.5   OBJECTIVES AND SCOPE

To assess the feasibility of various techniques and develop a suitable test method to detect the initiation of corrosion of steel rebars with FBE and CPC coatings and embedded in cementitious systems

➢ Evaluation of half-cell potential (HCP)

➢ Evaluation of macrocell corrosion current (MCC)

➢ Evaluation of polarization resistance test (LPR)

➢ Evaluation of electrochemical impedance spectroscopy (EIS)

➢ Propose methodology for detecting the initiation of corrosion in FBE and CPC coated steel rebars embedded in cementitious systems

To characterize the various damage/degradation mechanisms and their effects on chloride thresholds; and then, propose a framework to estimate the service life of RC systems with FBE coated steel rebars

➢ Effect of UV-induced cracking/degradation and scratch damage on chloride thresholds

➢ Service life as a function of the diffusion of chlorides through the thin and undamaged FBE coating

➢ Effect of coating thickness on time to corrosion initiation.

To identify the chloride threshold and bond degradation; and then, propose a framework to estimate the service lives of RC systems with CPC coated steel rebars

➢ Effect of surface preparation/sandblasting on the chloride threshold

➢ Effect of corrosion on the bond behavior

➢ Service life as a function of corrosion initiation and immediate bond degradation

1.6 RESEARCH SIGNIFICANCE

Recently, many developing countries are witnessing a construction boom. Unfortunately, many constructions are happening with poor quality materials and inadequate construction practices due to the race for fast-track construction and the low quest for quality/durability among some of the stakeholders. Some of the rising concerns with the performance of RC systems with coated steel rebars are unclear. Based on field studies on concrete core and rebars specimens extracted from structures and laboratory studies such as delamination of coating, degree of corrosion, and visual examination, many agencies in USA, Canada, and Europe have stopped using coated steel rebars in concrete construction (Griffith and Laylor 1999; Hansson et al. 2000; Manning 1996; Pianca et al. 2005; Pyć et al. 2000). However, India, China, Japan, countries in Europe, and some parts of USA are still using them – a few of these are able to strictly enforce stringent quality control measures on materials and construction practices, while many are not able to; the latter case is a huge concern. In such countries, to take any action to regulate the use of coated steel rebars, approving authorities are asking the data showing the performance of coated steel rebars. However, there is a lack of data available on how the poor site conditions and practices affect the electrochemical characteristics, chloride thresholds, and time to corrosion initiation. Also, many personals wrongly believe that the propagation time is longer than the initiation time of coated steel or propagation time of

uncoated steel rebars. Therefore, many reported literature focus on the rate of corrosion, mass loss of coated steel rebars, etc.

Due to the unavailability of standard test methods for assessment of RC systems with coated steel rebars, many practitioners tend to use conventional test methods, which may not represent the true corrosion activities at underlying steels. This thesis reports that the test methods based on techniques such as HCP, LPR, and EIS could not detect the initiation of corrosion in systems with FBE coated steel rebars, and test methods based on HCP could not detect the initiation of corrosion in RC systems with CPC coated steel rebars. Also, a systematic methodology to assess the FBE and CPC coated steel rebars embedded in the cementitious system is proposed to detect the initiation of corrosion, chloride thresholds, and service lives of RC systems with coated steels, which can be used to assess and generate the reliable data for RC systems with coated steel rebars.

This thesis provides an experimental database on adverse effects of damage (by scratches), and degradation (by UV exposure) to coating can significantly reduce the resistance to chloride attack, chloride-induced corrosion, and service life. It was found that the service lives of RC systems with scratch damaged and UV-degraded coating can experience 70% and 40% reduction in the service lives of RC systems with FBE coated steel rebars with no damage/degradation, respectively. Based on the generated database, prescriptive and performance specifications for FBE coated steel rebars are proposed.

In addition, inadequate application of cement-polymer-composite (CPC) coating on rusted or uncleaned steel rebars is widespread. This thesis also provides the experimental data indicating that the use of inadequate application of CPC coating can lead to at least 40% lower service lives than the adequately coated systems (coating on sandblasted rebars). Also, an experimental investigation shows that the negligible corrosion can cause significant

disbondment of coating from the steel surface and reduces the bond strength by 40-80%, which can result in a substantial reduction in the structural capacity.

If the inadequate construction practices associated with coated steel continues, then many large-scale infrastructure systems will incur the high cost of corrosion. This thesis provides a quantitative estimate on the effect of such inadequate construction practices on the service lives of reinforced concrete systems and develops strategies to ensure the use of quality materials and construction/maintenance practices. The generated database will sensitize the engineers and governing bodies to enforce the quality measures and specify stringent specifications (specified in this thesis) for the use of coated steel rebars in constructions.

1.7   RESEARCH METHODOLOGY

Figure 1.5 shows the methodology adopted to achieve the objectives of this thesis. First, the feasibility of existing test methods based on half-cell potential (HCP), macrocell corrosion current (MCC), linear polarization resistance (LPR), and electrochemical impedance spectroscopy (EIS) were evaluated to detect the initiation of corrosion in RC systems with coated steel rebars embedded in cementitious systems were assessed. Then, test methodologies based on EIS and LPR was proposed to assess the RC systems with FBE and CPC coated steel rebars, respectively. Later, these test methodologies were used to quantify the effect of poor construction site practices on chloride thresholds of coated steel rebars, especially for the identified inadequate coating conditions. Then, A existing MATLAB$^{\circledR}$ program was modified to estimate the service life of RC systems with FBE coated steel rebars considering the diffusion of chloride through the coating. In addition, the effect of corrosion on bond characteristics of CPC coated steel rebars was quantified, a framework for estimation of service life based on corrosion and bond characteristics were developed for RC systems with CPC coated steel rebars.
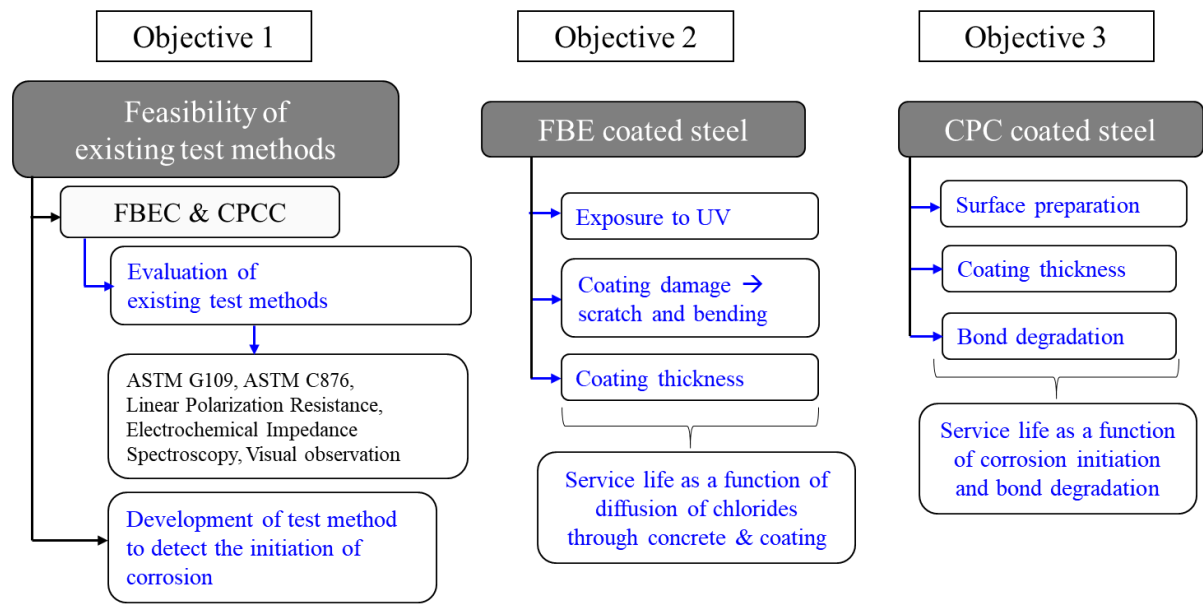
Figure 1.5 Experimental program and methodology

1.8   ORGANIZATION OF THESIS

This thesis is organized by using a chapter-subsection format. There are seven chapters (first level heading) and several subsections to discuss the identified issues highlighted in Section 1.1 (Problem statement). The outline of the chapters is as follows.

- ➢ Chapter 1 (Introduction, the current chapter) introduces the problem statement of this thesis, motivation for the study, followed by research questions and formulated objectives. The impact of the outcomes of this thesis on engineering and scientific sectors is summarised in the research significance section, followed by the methodology adopted is briefly explained.

- ➢ Chapter 2 (Review of literature) provides a review of literature, describing the available knowledge on chloride-induced corrosion, mechanisms, and service lives, especially for coated steel rebars. Chapter 2 provides a detailed history of the use of FBE coated steel rebars. The changes in codes, specifications, and bans of FBE coated steel rebars are discussed in detail. Thereafter, possible strategies

16

to enhance the performance of coated steel rebars are provided. Followed by the performance of various coated steel rebars in the construction industry are discussed. The contradictions in various available literature with respect to the performance of coated steel rebars are discussed, and possible reasons are provided. Then, the effect on coating and corrosion on the bond performance of RC systems are described. Finally, the knowledge gap is summarized.

➢ Chapter 3 (Experimental programs) describes the material properties and experimental programs, used to achieve the objectives of this thesis.

➢ Chapter 4 (Feasibility of the existing test methods to assess corrosion of coated steel rebars) covers the experimental results from 3-bar prism specimens (HCP and MCC), and lollipop specimens (LPR and EIS) for FBE and CPC coated steel rebars. Then, a test methodology is proposed for the assessment of RC systems with uncoated, FBE, and CPC coated steel rebars.

➢ Chapter 5 (Performance of FBE coated steel) provides the micro-analytical and electrochemical data (FTIR/SEM/EDX/EIS) from the tests conducted on FBE coating samples and lollipop specimens with FBE coated steel rebars. Later in Chapter 5, a framework is proposed to determine the chloride threshold, diffusion coefficients of coating, and service lives of RC systems with FBE coated steel rebars. Also, using this methodology, quantitative estimates are made for RC systems with FBE coated steel rebars considering the various inadequate construction practices. Based on the results, performance and prescriptive specifications are recommended for new construction and existing systems with FBE coated steel rebars.

➢ Chapter 6 (Performance of CPC coated steel) provides the micro-analytical and electrochemical data (SEM, MCC, and LPR) from the tests conducted on 3-bar

prism and lollipop specimens with CPC coated steel rebars. Then, the effect of corrosion on the bond performance of RC systems with CPC coated steel rebars are estimated. Later in Chapter 6, a framework is proposed to estimate the service lives of RC systems with CPC coated steel rebars. Also, using this methodology, quantitative estimates are made for RC systems with CPC coated steel rebars considering the inadequate application of CPC coating. Based on the results, performance and prescriptive specifications are recommended for new construction and existing systems with CPC coated steel rebars.

➢ Chapter 7 (Conclusions and recommendations) provides the conclusions from this thesis and recommendations for the use of coated steel rebars in new constructions. Thereafter, remedial measures are provided for the existing structures with FBE and CPC coated steel rebars. Then, major contributions from this thesis and recommendations for future research are provided.

➢ Appendix A provides the procedure to fit EIS response to the equivalent electrical circuit for coated steel rebars

➢ Appendix B provides the procedure to determine the chloride threshold of uncoated and coated steel in cementitious systems

➢ Appendix C describes the modified SL-CHLOR, an in-house developed MATLAB® program for estimation of the service lives of RC systems with coated steel rebars

1.9   SUMMARY

In Chapter 1, the problem statement of this thesis is presented. It was highlighted that the current site practices at construction sites, especially for coated steel rebars. Scratch damage to coating, exposure of coated steel rebars to sunlight, and application of the coating on rusted

steel rebars are widespread. However, such rebars are continued to be used without concern about the service lives of FBE coated steel rebars. Authorities that can regulate the usage of coated steel are not able to make decisions because of the unavailability of scientific and engineering data, being the motivation for the study. Then, research questions, formulated objectives, and the impact of the outcomes of this thesis on engineering and scientific sectors are summarised in the research significance section, followed by the methodology adopted is briefly explained.

This page is intentionally left blank

2   REVIEW OF LITERATURE

2.1   INTRODUCTION

This chapter presents a review of literature relevant to chloride-induced corrosion of RC systems with coated steel rebars and estimation of the service lives of RC systems with coated steel rebars. This chapter includes the review of corrosion initiation mechanisms involved in and critical parameters for the estimation of the service lives of RC systems. Then, the existing test methodologies for assessment of RC systems are discussed in detail, highlighting the drawbacks associated with the existing assessment techniques of coated steel rebars. Then, details on why there is a difference in the field and laboratory experiences with corrosion of RC systems with coated steel rebars are provided. After that, the bond characteristics of RC systems without and with corrosion is discussed. Then, a review is provided to establish the base on why the existing service life models may not work for estimating the life of RC systems with coated steel rebars.

2.2   BASICS OF CORROSION OF UNCOATED STEEL REBARS IN CONCRETE

Figure 2.1 shows that about 90% of publications in corrosion of concrete structures are published in the last two decades. Some questions remain unanswered and still being investigated, corrosion mechanisms, chloride thresholds, and service lives of RC systems are a few of them, especially for coated steel rebars. These aspects are investigated and will be discussed in detail later in this thesis. Note that a total of about 2000 articles on coated steel in concrete (Scopus search with 'Coated' + 'Steel' + 'Concrete') are published until today. These articles include publication with articles focusing on mechanical properties and articles on the coating on the concrete surface also. In short, only about 5% of total articles focus on the corrosion assessment of coated steel in concrete. Recently only about 50 - 70 research articles

per year are published on coated steel rebars embedded in concrete, which substantiate that very little research is carried out or being carried out on evaluating and understanding the performance of coated steel rebars. Therefore, more research is needed in the area of coated steel rebars embedded in the cementitious system. This thesis will highlight various areas, which were not addressed earlier. This section will briefly describe the electrochemistry and mechanisms of corrosion of rebars embedded in concrete.
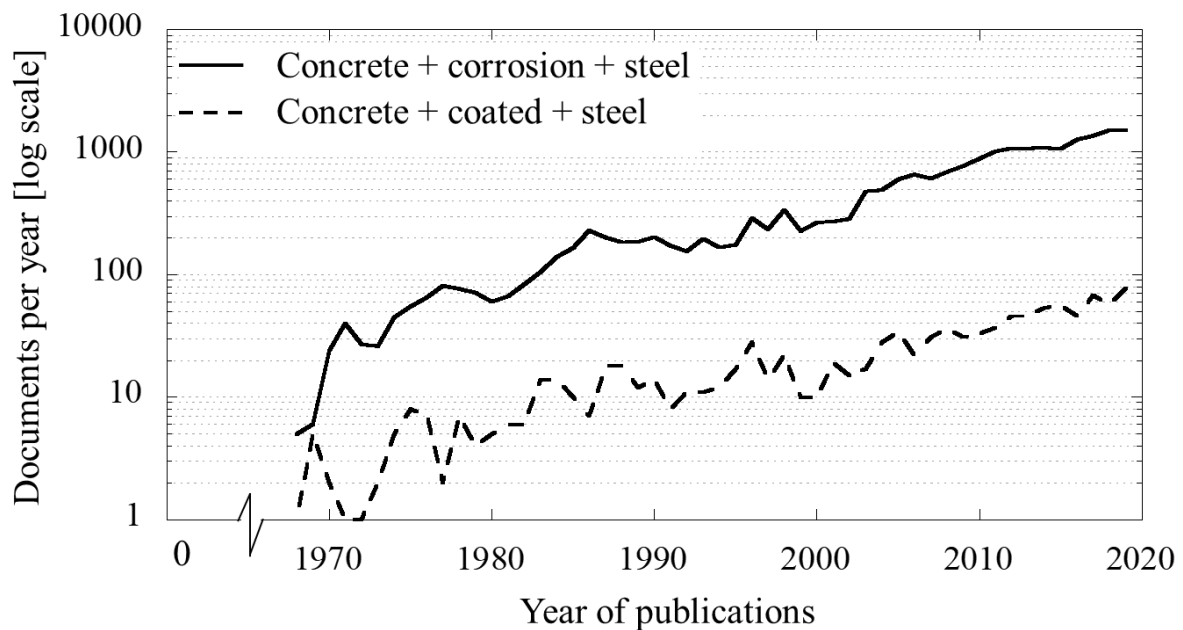
Figure 2.1 Number of publications per year on corrosion in concrete structures (data collected from Scopus with keywords as 'concrete + corrosion + steel' and 'coated + steel + concrete')

Corrosion of reinforcement is one of the major deterioration mechanisms. Worldwide, in the last two decades, many researchers have addressed many aspects of corrosion of steel rebar in concrete. Figure 2.2 shows the Pourbaix diagram for steel. Generally, the pH of concrete is in between the 11.5 to 13.5 (see vertical grey shaded box), and the potential of steel in concrete is about ($-$ 100 mV to $-$ 500 mV) – indicating that the steel is passive in this region – highlighted by the red box in Figure 2.2 (Malik et al. 1992). However, when chlorides

penetrate concrete from the atmosphere (airborne, seawater, deicing salts, etc.), the steel may get depassivated and starts to corrode.
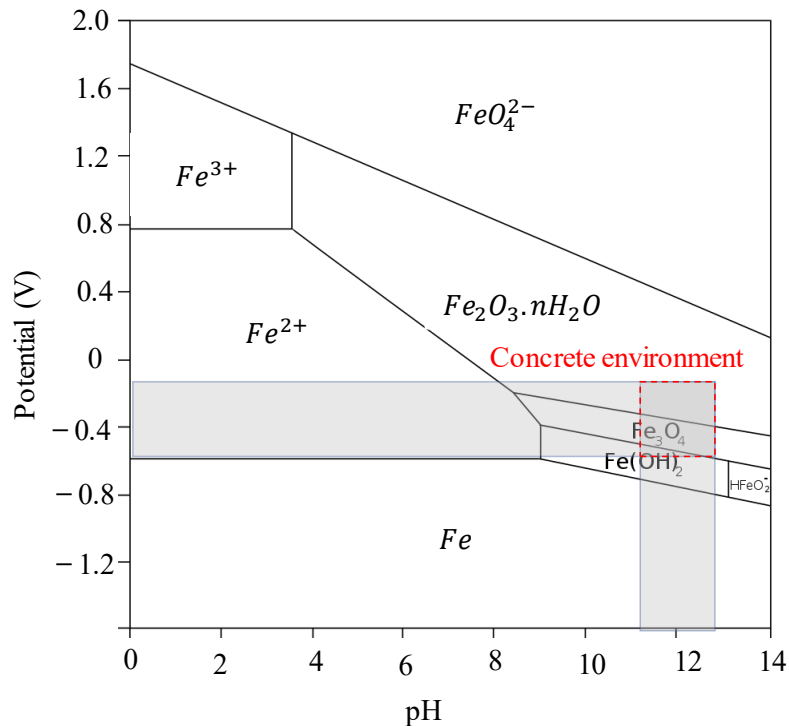
Figure 2.2 Pourbaix diagram of steel

The corrosion of steel occurs when there is electro-physical interaction between iron, water, and oxygen (Hussain et al. 1995; Tuutti 1982). Figure 2.3 shows the corrosion process and four essential elements for the corrosion process, (i) anode, (ii) cathode, (iii) electronic conductor, and (iv) ionic conductor. At Anode, Anodic process liberates electrons and forms ferrous or ferric (Fe^{2+} or Fe^{3+}) (see Eq. 1.1), which later due to hydrolysis results in the formation of iron hydroxide $Fe(OH)_2$ (passive film) and hydrogen ions resulting in a decrease of pH. At the cathode, the reduction of oxygen takes place, where oxygen consumes these electrons and produces hydroxyl ion, resulting in high pH (see Eq. 2.2). The cathodic reaction depends on the availability of oxygen and electronic conduction between anode to cathode. The electric conduction is provided by steel (flow of electrons from anode to cathode). The

corrosion cell is complete when ionic conduction between anode and cathode is established. In the metal industry, electrolyte solutions or salt bridge is an ionic conductor; and in reinforced concrete systems, steel is an electronic conductor, and concrete is an ionic conductor.
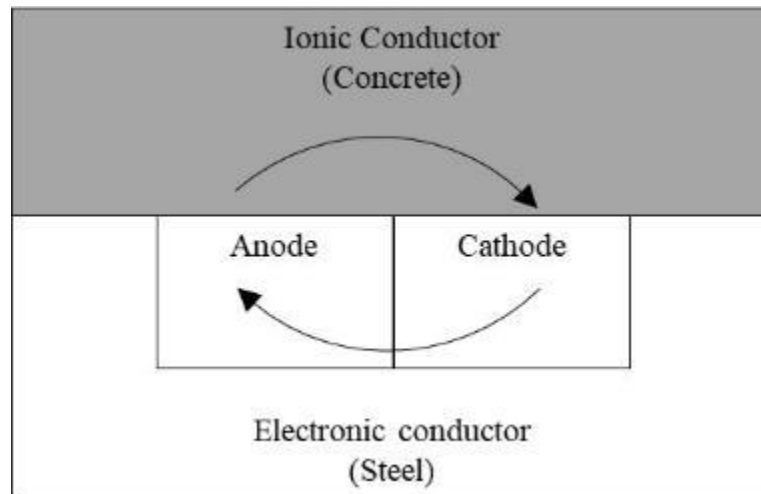
Figure 2.3 Essential elements of a typical corrosion cell

At anode,

$$Fe \rightarrow Fe^{2+} + 2e^- \qquad \qquad 2.1$$

At cathode,

$$O_2 + 2H_2O + 4e^- \rightarrow 4OH^- \qquad \qquad 2.2$$

As discussed, the following four elements are essential to establish a corrosion cell: anode, cathode, electron conductor, and ionic conductor. At equilibrium, the electrons liberated per unit of time at anodic site (i_a), and the electrons consumed per unit time at cathodic sites (i_c) are equal. Therefore, the rate of corrosion (i_{corr}) is equal to i_a and i_c. Note that in RC systems, electrical resistance within reinforcement is very low. Therefore, i_a can always be high. The rate of corrosion is controlled with the cathodic current (i_c). The cathodic current depends on the rate at which oxygen reaches the steel surface to cathodic sites (Walsh and Sagues 2016; Wang et al. 2014b) and the electrical resistivity of concrete (Rengaraju 2019).

Also, the passivation of steel can reduce the rate of cathodic reactions. Therefore, the rate of corrosion can be controlled by oxygen diffusion, ohmic resistance, and passivation of steel.

Curve 1 in Figure 2.4 shows the anodic curve shows the typical anodic polarization curve of steel without any chlorides. Depending on the cathodic reactions, the steel in concrete can have a low to high rate of corrosion based on the electrochemical potential of the steel. The region between $E_{protection}$ and $E_{Pitting}$ (i.e., between two horizontal dash lines) is the long-range of potentials where steel is passive in concrete. When chlorides reach the steel surface, steel depassivates, and start to corrode. The rate of corrosion depends on the concentration of chlorides. Figure 2.4 shows that with chlorides, the passivation range reduces, and anodic polarization curves shift to the right – indicating a higher rate of corrosion with more chloride concentration (Cox and Roetheli 1931; Malik et al. 1992).

Note: not to the scale
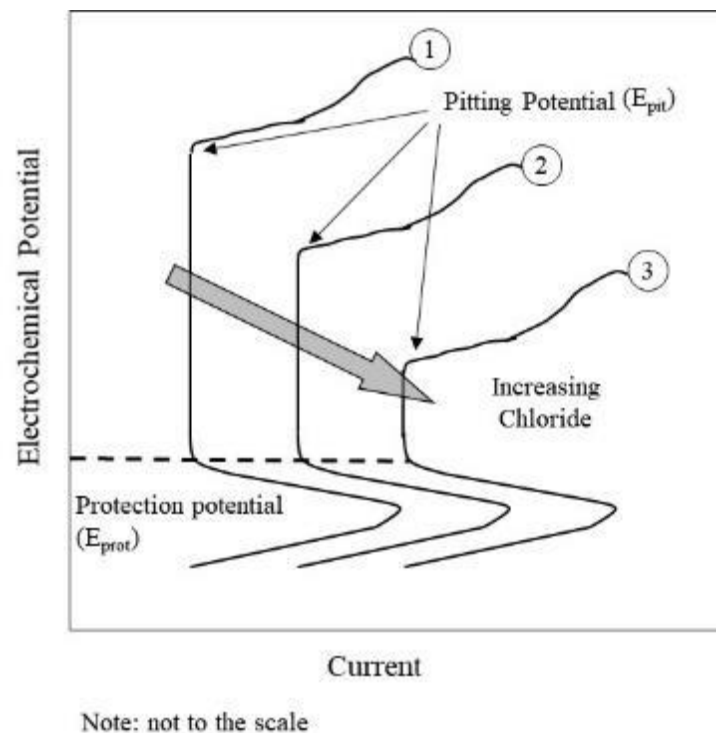
Figure 2.4 Schematic representation of corrosion condition in concrete with different chloride concentration (Malik et al. 1992; Sergi 2018)

2.3 CHLORIDE-INDUCED CORROSION

Nowadays, many infrastructure systems are built in the marine environment, and many of the countries adopt deicing salt for melting the ice. These exposure conditions can lead to penetration/diffusion of chlorides in concrete. When chlorides reach the passive steel surface, it can break the passive layer/oxide layer ($Fe(OH)_2$) and initiate the corrosion. Note that chlorides have higher mobility than hydroxide ions. Therefore, the chlorides can make their way to the steel surfaces by replacing the hydroxide ions of the passive film. Note that the chloride ions with a specific concentration can depassivate the steel surface. Therefore, the chloride concentration required to depassivate the steel surface is known as the critical chloride threshold. Note that the chloride threshold is not the property of steel alone, but of the steel-binder interface, and depends on the micro-environment at the steel-binder interface (Angst 2011). Figure 2.5(a) shows a typical mechanism that takes place in chloride-induced corrosion of steel rebars in concrete. Note that once the chloride-induced corrosion is initiated, the same chlorides can form $FeCl_2$ and disintegrate further to chloride ions. Therefore, corrosion can progress even without the requirement of new chlorides at the rebar level. Figure 2.5(b) shows why corrosion initiates at a specific location. Concrete is a non-homogeneous material. Therefore, when chlorides diffuse through the concrete, different concentration of chlorides can diffuse through different sections of concrete due to the unavailability of aggregates. Therefore, the place where the chloride concentration is exceeding the chloride threshold value, corrosion initiates. Another reason for the preferential site for initiation of corrosion can be the formation of unstable passive film at a few locations due to the presence of pores, aggregates, etc. at the steel-concrete interface.

$$FeCl_2 + 2H_2O \rightarrow 2HCl + Fe\,(OH)_2$$

$$2H^+ + 2\,Cl^-$$

Concrete

$$\tfrac{1}{2}\,O_2 + H_2O + 2e^- \rightarrow 2OH^-$$

$$Fe^{2+} + 2Cl^- \rightarrow FeCl_2$$

$$Fe \rightarrow Fe^{2+} + 2e^-$$

$$2e^-$$

(a) Mechanism

$$Cl^-\qquad Cl^-$$

Multiple corrosion pits
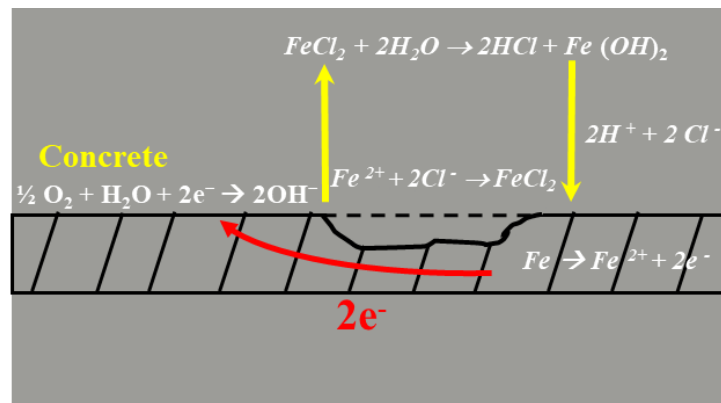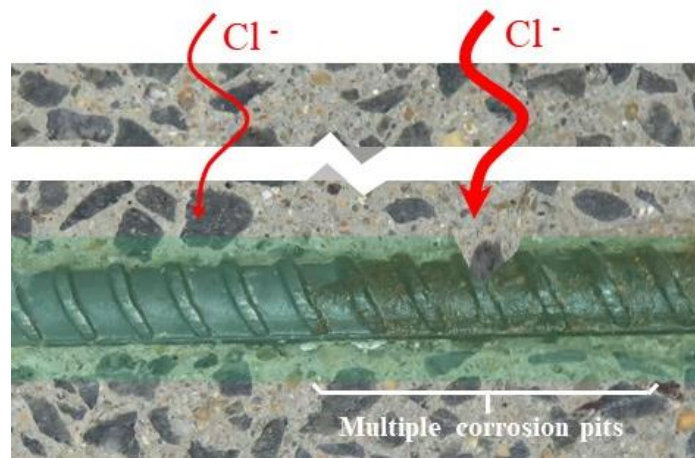
(b) Preferential sites for corrosion initiation

Figure 2.5 Mechanism of chloride-induced corrosion

2.4   APPROACHES FOR ENHANCING CORROSION RESISTANCE

Figure 2.6 shows a pie chart summarising that about 40% of the failure of reinforced concrete structures is due to inadequate use of materials. In many cases, failure can be linked to chloride-induced corrosion of reinforcement in concrete systems. There are various approaches to delay the initiation of corrosion and achieve long service lives. In general, the prescriptive approach (deemed to satisfy) and the performance-based approaches are adopted. In the prescriptive approach, material specifications are prescribed in guidelines of durability-

based specifications or standards based on factors such as exposure class and target service lives of RC systems. Generally, prescriptive approaches instruct on how to do work, limit values for binder content, water to binder ratios, mechanical properties, etc. Therefore, the prescriptive approaches do not allow modern materials, new design strategies, rational approaches, and similar (Alexander and Beushausen 2019). However, the performance of materials in any exposure environment cannot be generalized based on the mix proportion parameters.
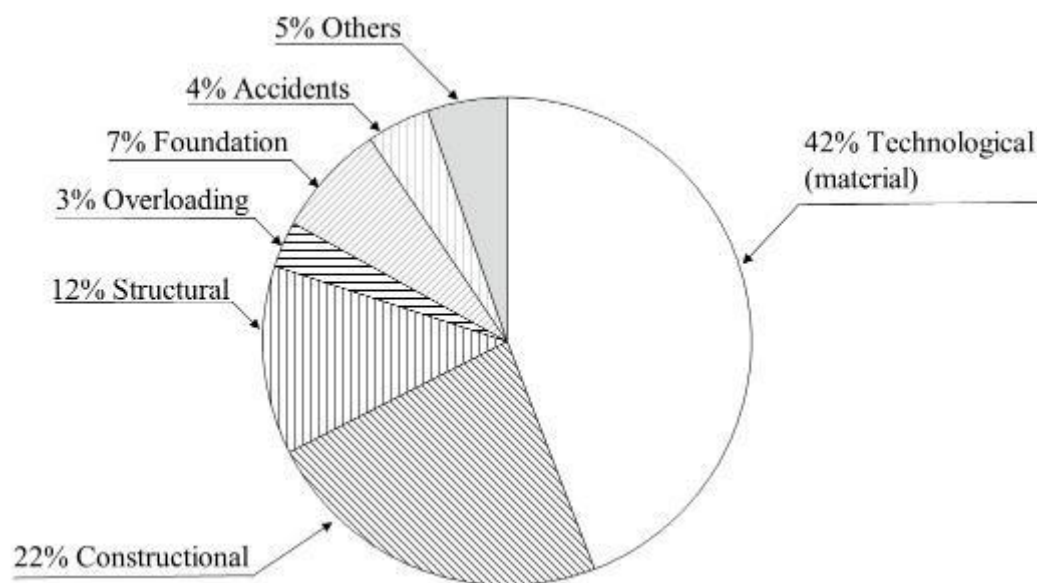
Figure 2.6 Causes of structural failure [data from Vedalakshmi et al. (2005)]

On the other hand, in the performance-based approach, concrete is designed for the durability requirements without limiting any on material characterization. In this approach, materials are assessed at various stages. Depending on the importance of the structures, the type and method of assessment are chosen (Alexander and Beushausen 2019; Dhanya 2015).

The properties of both steel and concrete can influence the service lives of reinforced concrete systems. However, use of best quality of concrete with low diffusion coefficient (by use of supplementary cementitious materials, chemical admixtures, corrosion inhibitors, etc.)

and excellent quality of steel with high chloride thresholds (such as stainless steel, duplex steel rebars) may not be possible due to limitation of the budget of the projects. Also, that may not be economical for the desired service lives of RC infrastructure. Therefore, a balanced approach with the synergistic effect of the properties of concrete and steel needs to be considered (Pillai et al. 2020). Figure 2.7 shows a schematic representing that the balance between properties of steel and concrete can result in a durable and economic structure. This thesis focusses on enhancing the service lives of RC systems by using better quality steel rebars. Various types of steel rebars are commercially available to delay the initiation of corrosion. Note that the mechanical and chemical properties of steel rebars can be altered by modifying the chemical ingredients during or after the molten metal sets and manufacturing processes. For example, the appropriate addition of carbon can alter hardness, strength, weldability, and brittleness of steel rebars (Egorov et al. 1989). Also, the addition of copper, nickel, and/or chromium can alter the corrosion resistance of steel rebars (Cunat 2004; De Lima et al. 2019).
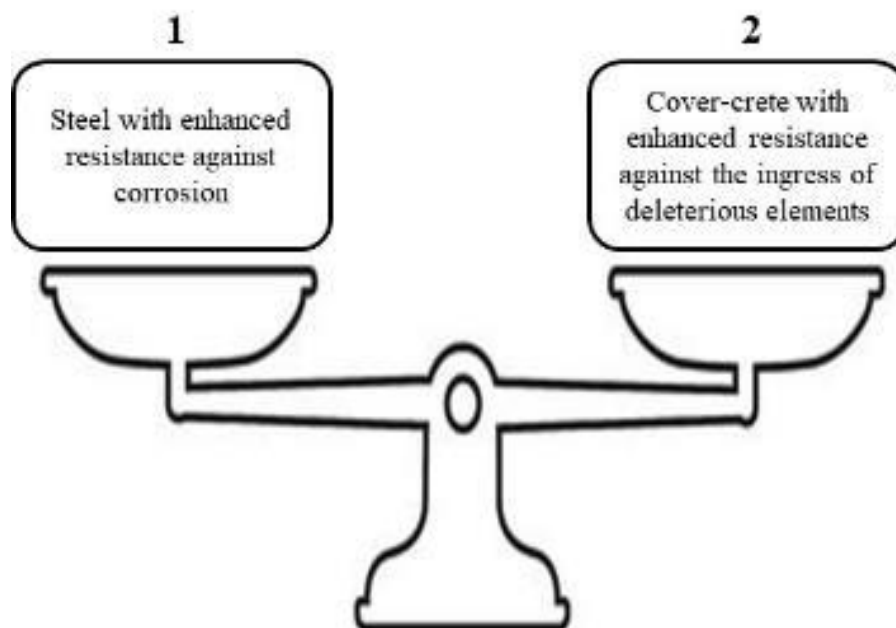
Figure 2.7 Schematic representing that balance between properties of steel and concrete is required to achieve durable reinforced concrete structures

Table 2.1summarizes the introduction/commencement of various steel rebars in the construction industry to achieve better mechanical and corrosion resistance properties than before. Here, the discussion is divided into two categories, uncoated and coated steel rebars, irrespective of the commencement of their use in construction. In the early constructions, plain rebars were used. Plain mild steels were first hot rolled steel rebars used in construction after the use of cold-rolled steel flat/strip reinforcements. However, soon they were out of marker due to the requirement of higher strengths. Then, ribbed bars were used with modified chemical composition to achieve higher strength, and ribs were provided to enhanced bond strength between steel rebars and concrete. However, when higher strength was required, they were cold twisted and deformed (CTD) to increase the yield strength (Ray et al. 1997). As a result of cold twisting, the corrosion resistance of rebars was reduced as compared to ribbed bars, and they are no longer used. Later thermo-mechanically treated (TMT) or quenched and self-tempered (QST) rebars were introduced to the construction industry to achieve both higher yield strength and corrosion resistance and are used in now construction industry. The outer surface of QST (martensite) provides hardness and strength to the steel, and the inner part of the steel (ferrite-pearlite) provides the ductility to the steel reinforcement (Nair and Pillai 2020). As it is a hot rolled steel, they have better resistance to corrosion than cold rolled steel rebars (Nair and Pillai 2017).

Later, when higher resistance to corrosion was required to achieve the desired service lives of RC systems, chemical composition was modified by the use of copper, cadmium, and with higher than usual percentage of phosphorus to get corrosion-resistant-steel (Cunat 2004). However, there are not much reported literature on the performance of corrosion-resistant steel rebars. Another corrosion resistant steel is stainless steel. Stainless steels are reported to have

a significantly high chloride threshold (Trejo and Pillai 2004). Note that stainless steel cannot be used for regular construction projects due to the cost of these steels is about six to seven times the cost of conventional steel rebars. Therefore, they are generally used in the construction of structures with higher importance and where the cost of the structures is not a concern. For example, a few temples and Shivaji statue in India are constructed or planned to be constructed stainless steel rebars.
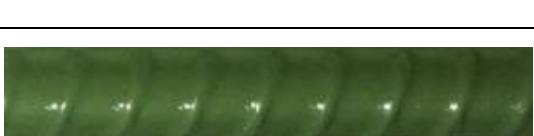
For special requirements such as longer spans with a higher load carrying capacities, prestressing steel was introduced to the construction industry. Prestressing steels are manufactured with higher concentrations of carbon, chromium, nickel, and copper, and a lower concentration of phosphorous content. The prestressing steels are cold drawn through stepwise dices of smaller sizes – resulting in residual stresses on the steel surface and elongated microstructures. Therefore, prestressing steels are more susceptible to stress-induced corrosion. ACI 222R committee reports that chloride thresholds of these steels can be six times lower than that of QST steel rebars (ACI Committee 222 2001). Another concern with prestressing steel is the possibility of localized corrosion that can locally reduce the cross-section of steel – leading to stress-corrosion cracking and failure of prestressing steel and RC systems with prestressing steel (Joseline et al. 2018).

Reinforced concrete systems in the marine environment need higher resistance to corrosion than elsewhere. Therefore, metallic or nonmetallic coated reinforcements are used for construction in coastal regions (Kamde and Pillai 2020a; Pei et al. 2017; Zayed and Sagues 1990). Galvanized steel rebars and organic coated steel reinforcements are a few widely used coated steel rebars. Galvanized rebars are manufactured by a hot-dip zinc bath of molten zinc at the temperature of about 450°C, which results in the metallurgical adhesion between zinc and steel substrate. Coated zinc protect substrate steel by sacrificing itself (Vera et al. 2012).

Therefore, scratch damage to the zinc coatings will not influence the immediate performance of galvanized steel rebars. Note that the metallic coated steel rebars are not used as much as nonmetallic (mostly, organic) coated steel rebars (Manning 1996).

The most widely used organic coated steel rebars are fusion-bonded-epoxy (FBE) coated steel rebar and polymer coating modified by cementitious systems. In India, one of the most commonly used polymer coating modified by the cementitious system is cement-polymer-composite (CPC) coated steel rebars. The FBE coating is epoxy-based polymer applied in the manufacturing unit and expected to insulate the substrate steel from the atmosphere (moisture, oxygen, chlorides) and delay the initiation of corrosion. On the other hand, CPC coating is an acrylic-based polymer applied at the construction sites on sand-blasted steel rebars. The corrosion prevention mechanisms for both are to (i) insulate the substrate steel and environment, (ii) limiting cathodic sites, and (c) limit oxygen supply to the steel surface. Figure 2.8 shows the relative costs of each of these steels for the year 2010. Note that the cost of these steels can vary with time, and it also depends on the demand of each of these steels. This thesis focusses on the performance of organic coated steel, which is discussed in detail next.

Table 2.1 Types of steel rebars used in the construction industry

Type of steel rebars and approximate period of introduction		Photographs
1950s	Plain and ribbed (hot rolled) mild steel rebars	
1970s	Thermo-mechanically treated (TMT) or Quenched and self-tempered steel rebars	
1980s	Cold and twisted deformed (CTD) steel rebars	
1980s	Corrosion resistance steel rebars	
1990s	Stainless steel rebars	
1940s	Prestressing strands	
1950s	Galvanized steel rebars	
1970s	Fusion-bonded-epoxy coated steel rebars	
1990s	Cement-polymer-composite coated steel rebars	
1990s	Fiber-reinforced polymer (FRP) rebars	
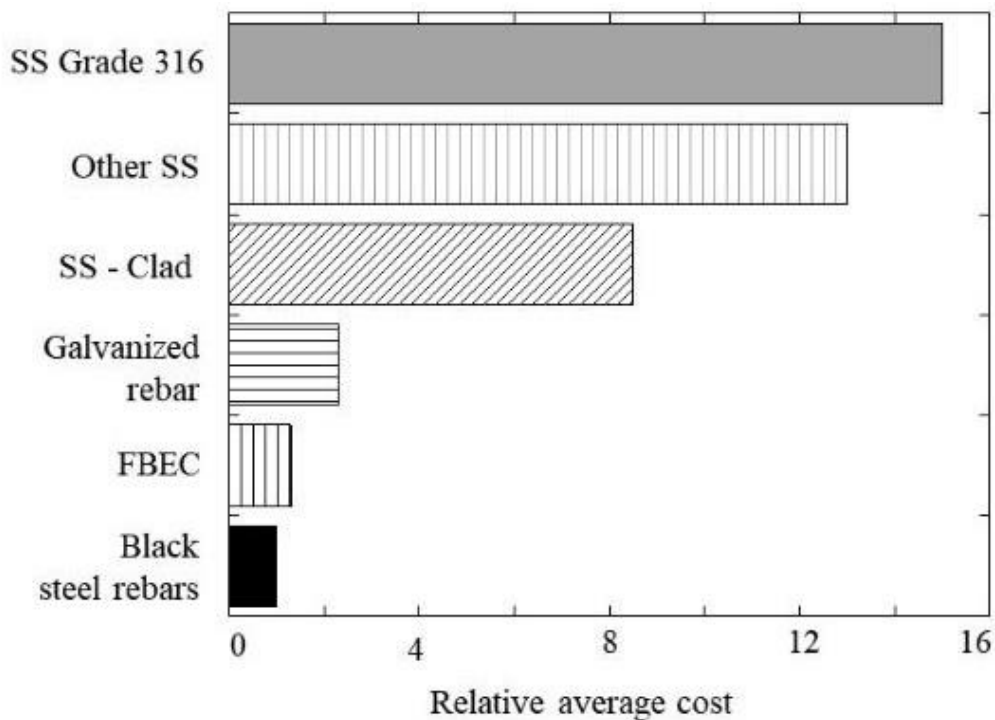
Note: the cost can vary with time and demand of the individual steel rebars

Figure 2.8 Relative costs of reinforcing bars in construction [adapted from (McDonald 2010)]

2.5 FUSION-BONDED-EPOXY (FBE) COATED STEEL REBARS

Figure 2.9 shows the schematic of the cross-section of a typical FBE coated steel rebar embedded in concrete. Typically, FBE coating with a thickness of about 175 to 300 µm is suggested by widely used Indian and international standards (IS 13620 2015; ASTM A775 2017). In general, organic coated steel rebars works by following protection mechanisms (i) barrier between substrate steel and moisture, oxygen, chlorides, etc., (ii) restriction to the ionic conduction between anodic and cathodic sites, and (iii) limit the anodic and cathodic sites (Bíaz et al. 2018; Cortés 1998; Kessler et al. 2015).
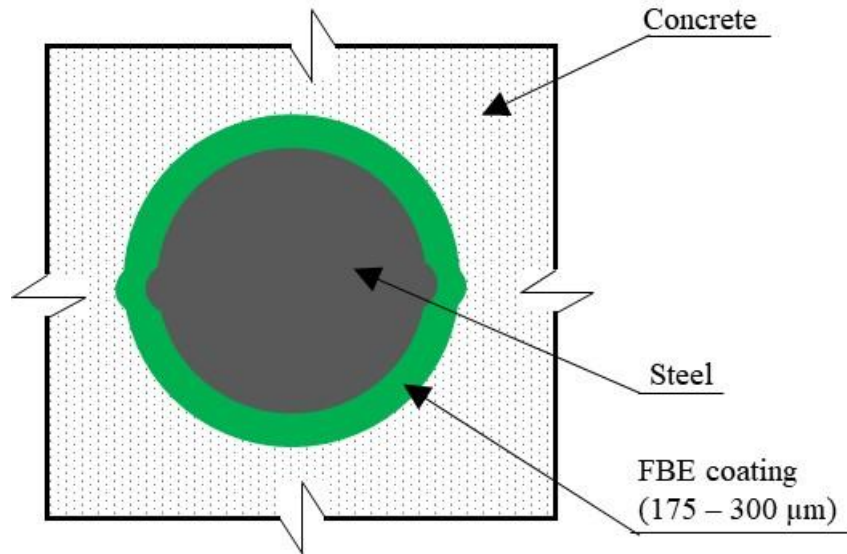
Figure 2.9 Schematic of the cross-section of coated steel rebar embedded in concrete

Figure 2.10 shows the FBE coating process. First, the uncoated steel rebars are sandblasted to remove the rust, dust, mill scale, or any foreign elements. Then, these cleaned steel rebars are heated using electric induction or gas-fired heater in a hot chamber to maintained at the temperature of the surface to about 230ºC. The surface temperatures are monitored using temperature indicators. After that, these heated steel rebars are passed through the chamber with the mist of powdered epoxy, which is allowed to fuse and bond to the steel surface (McDonald 2009). This fusion-bonding and subsequent quenching help to form a uniform, continuous, and well-adhered epoxy coating on the surfaces of steel rebars (Manning 1996).

The epoxy coating is expected to insulate the steel surface from the corrosive environment and delay the initiation of corrosion. However, FBE coating are found to have holidays or pinholes (manufacturing defects). In addition to manufacturing defects, poor handling of FBE coated steel rebars during transportation and at construction sites lead to scratching and cracking of the epoxy coating, which in turn reduces its corrosion resistance, which is reported in many literature (Cividanes et al. 2014; Hansson et al. 2000; Lau and Sagüés

2007; Zemajtis et al. 1998). As many structures in the developed world have experienced premature corrosion of RC systems with FBE coated steel rebars. The governing bodies of many states/countries have made changes whenever required based on the available knowledge during that time. Table 2.2 shows the summary of experiences from fields, major research outputs, and alterations/modifications made in documents/specifications/standards used for manufacturing and construction practices with FBE coated steel rebars. Also, Table 2.3 provides the details of modifications done in ASTM A775 from 1981 to 2017. However, a few of the specified clauses in present ASTM A775 (2017) may need to be revised, and a few of them are addressed in this thesis.
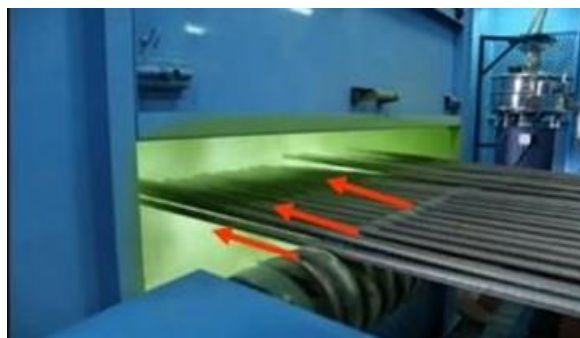
(a) Blasting, cleaning, & heating (220ºC; electrical induction or gas-fired heater)	**(b) Epoxy resin powder is ionized and attracted to the steel surface by electrostatic forces**
(c) Water quenching results in a thermosetting polymer	**(d) Inspection for holidays/damage**
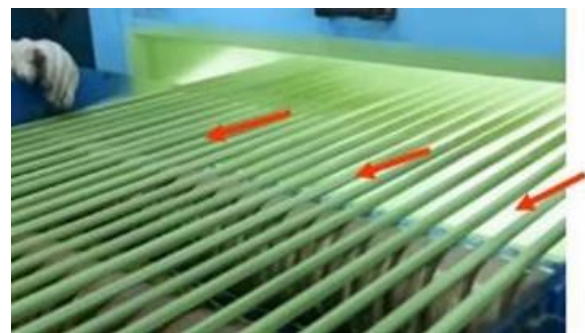
Figure 2.10 Steps to coat FBE on steel rebars at the manufacturing unit (Mitsuba 2016)

Table 2.2 History of the use of coated steels in construction

Year	What happened and what was found/implemented?s	References
1950	Introduction of organic coating to the buried pipelines	(Cortés 1998)
Early 1970	Introduction of FBE coated steel rebars in the construction industry from pipeline industries. Lack of consideration of the effect of concrete, fabrication, damage, etc.	
1973	The first research was carried out by FHWA (Federal Highway Administration). The effect of manufacturing defects and damages at sites were not considered. Coating thickness recommended to be 180 ± 5 µm.	(FHRA 1976; Manning 1996)
1976	Use of Epoxy coated rebars (ECR) gained popularity. Specifications permitted damage up to 2% in straight rebars, 5% in bent rebars, 3% after placement of rebars, and 6 holidays/meter were allowed.	(Manning 1996)
1977	17 states in USA started using FBE coated steel rebars. Therefore, the price difference between uncoated and coated steel came down from 120% to 20 %.	
1970	Construction of structures with mixed FBE coated steel and uncoated steel rebars in Kentucky and Virginia were promoted to reduce the corrosion rate rebars in RC systems. However, the test methodology adopted may not be valid.	(Manning 1996)
1977	ASTM and AASTHO considered to include a specification for FBE coated steel. The specifications were framed based on experiences till date	
1979-1986	Long key bridges in Florida began to show signs of corrosion within five to seven years. The reason for failure was concluded as disbondment, and corrosion aggravated by bending. pH <5. However, the root cause of the problem was not addressed	(Manning 1996)
1980	FHWA conducted research on long-term outdoor exposure of FBE coated steel rebars. The holiday exceeded 80 no./meter, failed to pass the bend test.	FHWA 1980
1981	Introduction of ASTM A775	

Table 2.2 History of the use of coated steels in construction (continued)

Year	What happened and what was found/implemented?	References
1979	Florida Department of Transportation banned the use of FBE coated steel from the use in the bridges.	(Manning 1996)
1980	Concerns with the time gap between sandblasting and coating were raised. The time gap was reduced from 8 hours to 3 hours	(McDonald 2010)
1988	Complete ban from all construction in July 1992. DOT, Florida concluded that FBE coated steel rebar would not provide long-term protection to RC systems	(Manning 1996)
1985	Macrocell corrosion measurements were found to be misguiding the corrosion activities at the rebar surface. Coated steel may provide protection from corrosion only for about four to five years more than the uncoated steel. Increased number of holidays (20 holidays/meter). Underfilm contamination. No change in coating thickness. However, the effect of outdoor exposure on the chloride threshold of FBE coated steel was not explored.	(Manning 1996)
1984-1993	Lessons were not learned from the past failure of structures with FBE coated steel rebars. The rapid increase in the use of ECR by USA and Canada. 70-80% of total steel rebar production	(Manning 1996)
1992	FBE coated steel rebars exhibited coating disbondment, blisters, and cracks under long-term corrosion performance tests	(Hansson et al. 2000)
1993	Introduction to BIS: IS 13620. Most of the specifications were adopted from ASTM 775 version available in 1993. Later no changes are made to date.	(IS 13620 2015)
1981-2007	Later modifications are provided in Table 2. Modification of ASTM A775	See Table 2.3
2000	Virginia transportation research council published a report on the long-term performance of FBE coated steel rebars. Disbondment of the coating was observed within four years of exposure. The coating can become permeable to moisture when embedded in concrete. Recommended to stop using FBECR	(Pyć et al. 2000)
	Many states/countries have banned the use of FBE coated steel rebars.	See Table 2.4

As summarized in Table 2.3, the ASTM A775 was modified based on the timely knowledge up-gradation and construction requirement. However, IS 13620 was introduced in 1993, and no changes/modifications are made to date (May 2020). This raises concerns with the existing specifications prescribed in IS 13620 (2015).

Table 2.3 Modifications made in ASTM A775 from 1981 to present (McDonald 2010)

Year	Changes made
1981	The first version approved
1989	Permissible damage level was reduced to 1 % of the steel surface area
1989	Introduction of anchor profile of 1.5 – 4 mil (38 – 100 µm)
1990	All the damages should be repaired
1993	Limit on coating thickness was introduced (177 - 300 µm)
1994	Flexibility test - The bend angle was increased to 180° from 120°.
1995	Limit on number of holidays - one holiday per foot length is allowed
1995	The coating should be done within 3 hours after cleaning of the steel surface
1997	Coating disbondment test was introduced to check the adhesion between concrete and steel
2004	Coating thickness limit was increased (177 - 400 µm) for larger diameter rebars
2004	Limits on individual measurements were introduced (should not be less than 80 % and should not be more than 120 % of the allowable limits)
2007	Requirements for patching materials were added to the standard

2.5.1 Effect of inadequate site practices of FBE coated steel rebars

Figure 2.11 shows a few of the inadequate practice with FBE coated steel rebars at construction sites. Figure 2.11(a) shows that the FBE coated steel rebars are bent using metallic levers. Note that the bending of rebars is done at construction sites after the coating is applied to the steel rebars. During bending, the coating can crack at the bent locations [see Figure 2.11(b)] and get damaged at the place where rebars were held using the metallic lever. Figure

1.1(a) shows that the coating can get scratched due to dragging the coated steel at construction sites during transporting them from one place to another. Also, the use of metallic tie wires and the use of needle vibrators with metallic vibrating heads for compacting the concrete can lead to severe scratch damage to the FBE coated steel rebars. In the damaged FBE coated steel rebars, some of the damaged portions (pinholes or cracks) can be anodes, and the remaining be the cathodes – resulting in localized crevice/under film corrosion even without chlorides at the steel rebar level (Kessler et al. 2015). Therefore, practitioners should avoid the use of metallic wires, use of needle vibrators while using FBE coated steel rebars. In the 1980s, it was recommended to avoid the bending of FBE coated steel rebars at the construction sites (Cortés 1998), which is still in practice in many parts of the world today. Therefore, the protection mechanisms discussed above may not be valid – leading to premature initiation of corrosion.

(a) FBE coated rebars are bent at a construction site using hard tools   **(b) Cracked FBE coating at the cracked locations**

Figure 2.11 Inadequate construction practices associated with FBE coated steel rebars

Although the FBE steel rebars are expected to have a defect-free and continuous coating, manufacturing defects such as pinholes and varying coating thicknesses have been observed on numerous FBE coated steel rebars (Pyc 1998). In addition, the poor handling during

transportation from factory to the sites and the poor handling (bending, cutting, dragging, stepping/walking over) at construction sites can cause severe damage such as scratches, cracks on the epoxy coating – resulting in premature, localized corrosion (Singh and Ghosh 2005).

In addition, FBE coated steel rebars get exposed to sunlight/ultraviolet (UV) radiation during prolonged storage and delayed construction, which are difficult to avoid at many construction sites. It was reported that five among 300 bridges in Florida, USA faced premature initiation of corrosion due to open storage of FBE coated steel at construction sites (McDonald 2009). Sagues et al. (2008) reported the possible reason of early corrosion in Florida bridges was the result of combination of highly aggressive environment (such as heat cooling cycle, ultraviolet exposure), highly permeable concrete, and flaws & damage to FBE coating. However, the deterioration mechanism was not discussed in the report. The scenario could be worse in many parts of the world with poor handling practices and high UV indices. Therefore, the first-generation epoxy coating material was modified with UV resistant agents and non-bendable epoxy formulations, which exhibited better UV resistance and bonding between the steel and coating and minimized the progression of underfilm corrosion (Cortés 1998) and implemented in Florida, USA. However, the candidate could not find literature reporting the modification of manufacturing processes or coating materials in many parts of the world. Therefore, the coating material characteristics need to be investigated for FBE coatings used in various parts of the world. Figure 2.12 shows that the UV indices in many countries can be more than 8 in the month of October. Also, the UV indices can be significantly high during summer, which can be considered as severe exposure conditions for epoxy-coated steel rebars (Bhattacharya et al. 2012; Heberlein et al. 2008; Singh et al. 2018). It should be noted that most of the construction happens during summer. Also, many construction projects experience delays due to several reasons leading to prolonged exposure of the steel rebars to sunlight/UV rays. Figure 2.13(a), (b), (c), and (d) show the photographs of a FBE coated steel

rebar cage to be used in the pier of the bridge, the FBE steel rebars at pier cap, rebars at the expansion joint, and rebars in the side railing, respectively, are getting exposed to sunlight/UV rays. This indicates that the FBE coated steel rebars gets exposed to construction sites at every stage of construction due to delay in construction or staged construction.
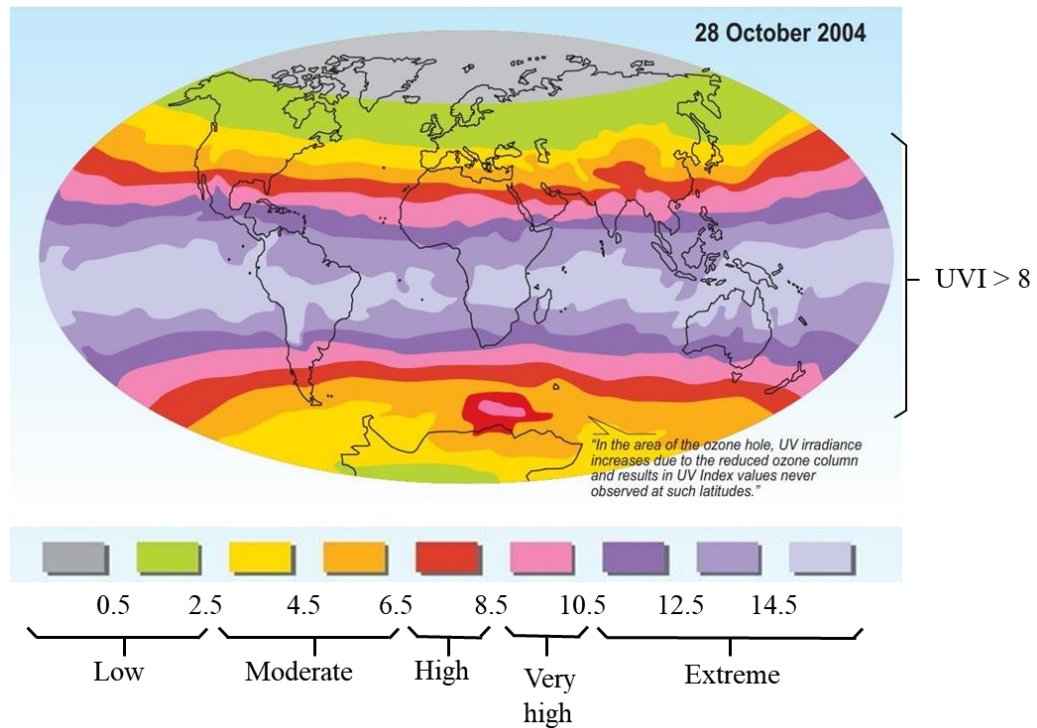
Figure 2.12 Highest UV index in the year 2004 (Heberlein et al. 2008)

Similarly, Figure 2.14(a) shows similar construction practices with FBE coated steel rebars in an under-construction commercial building. Where Figure 2.14(b) and (c) shows how that the FBE coated steel rebars gets damaged (due to bending and dragging at construction sites) and exposed to UV rays (due to delay in construction) before concrete is placed. Note that delay in construction with the case of uncoated steel rebars may not affect the corrosion resistance properties of uncoated steel. However, for FBE coated steel rebars, the coating integrity, chemical resistance, and atomic bonding of coating can get affected, and so the corrosion resistance of FBE coated steel rebars.

(a) Rebars exposed to sunlight during prolonged storage at construction site

(b) Rebars exposed to sunlight at pier cap
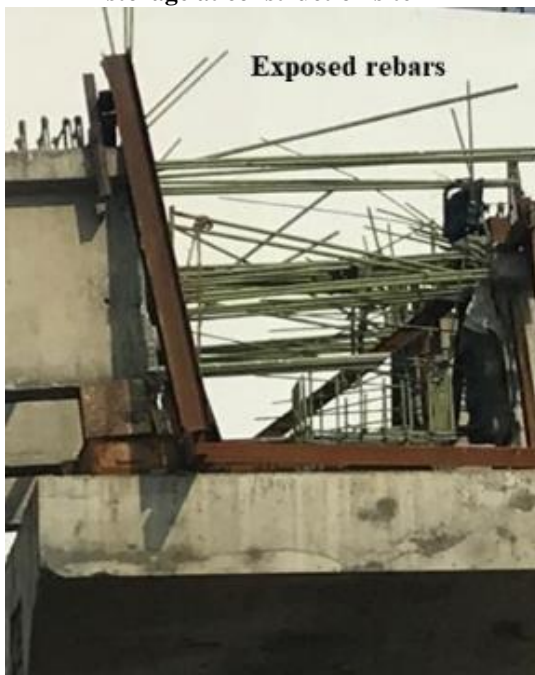
(a) Rebars exposed to sunlight at a construction site

(b) Rebars exposed to sunlight at side railing

Figure 2.13 Exposure of FBE coated steel rebars to sunlight during prolonged storage and delayed/staged constructions

ASTM A775 suggests that 'if circumstances require storing coated steel reinforcing bars outdoors for more than two months, protective storage measures such as steel rebars covered

in opaque polyethylene sheeting shall be implemented to protect the material from sunlight, salt spray and weather exposure' (ASTM A775 2017), which may need modification. Although many agencies in the USA and Europe have banned the use of FBE coated steel rebars (see Table 2.4). Many agencies in the rest of the world are still suggesting using the FBE coated steel rebars in many projects and without modifying the standards/guidelines and adequate practices – a serious concern.

(a) Rebars used in columns

(b) Close-up showing damaged FBE coating steel rebars being used

(c) Damaged coating on straight rebars during to dragging at construction sites

Figure 2.14 Exposure of FBE coated steel rebars in a column of a commercial building to sunlight due to delay in construction

Table 2.4 Details on the ban of FBE coated steel

Country; Reference	Recommendation on the use of FBE coated steel rebars
Florida, USA; (Manning 1996)	In 1979, banned to be used in bridges and large infrastructure
Florida, USA	In 1988, banned from all the construction projects
Oregon, USA; (Griffith and Laylor 1999)	In 1989, (recommended to stop using FBE coated steel rebars
Quebec, Canada; (Pianca et al. 2005)	In 2000, the further use of FBE coated steel rebar was not recommended
Onterio, Canada; (Hansson et al. 2000)	In 2000, The use of FBE coated steel rebar was not recommended based on technical reasons and life-cycle cost analysis
Virginia, USA; (Pyć et al. 2000)	In 2000, recommended stopping to use FBE coated steel rebar

Table 2.5 summarizes the literature on examples of concrete structures with FBE coated steel rebars built with target corrosion-free service lives of about 50 to 75 years; but, showing visible corrosion even within about five years. On the other hand, Table 2.6 shows the summary of laboratory studies indicate mixed opinions (i.e., good and poor performances) on the corrosion resistance of FBE coated systems. The following are the two possible reasons for these differences in opinions between the lab and field studies and between the lab studies. The first reason is the use test methods that do not reflect the long-term field conditions to assess the corrosion of FBE coated systems (see Table 2.6). A few literature suggest to use the electrochemical impedance spectroscopy (EIS) technique to assess the corrosion performance of coated steel systems (Cao-Paz et al. 2010; Lau and Sagüés 2007; Miszczyk and Darowicki 2018; Sagues and Powers 1990; Tang et al. 2014a)– and is adopted in this study. It should be noted that although there are many papers on the corrosion performance of FBE coated steel rebars, reporting the comparative mass loss or cumulative corrosion after periods of exposure to aggressive environments (Al-Amoudi et al. 2004; Cortés 1998; Kahhaleh et al. 1998; Mohammed et al. 2014; Scannell and Clear 1990; Swamy and Koyama 1989). A few literature

report the chloride thresholds of FBE coated steel rebars with damaged FBE coated steel rebars (Kessler et al. 2015). which may be valid for FBE coated steel rebars without damage. In addition, Texas Department of Transportation project reports that the chloride threshold of FBE coated steel rebar 0.34 % by weight of concrete (Vaca-cortes et al. 1998), which is significantly higher than the chloride threshold of uncoated steel rebars (i.e., $\approx$ 0.06 % by weight of concrete). However, these conclusions are also based on half-cell potential measurements, which may not be valid for RC systems with FBE coated steel rebars. In particular, the candidate could not find literature on chloride threshold of FBE coated steel rebars determined using systematic test methods to detect the 'initiation of corrosion', which is needed to quantify service life. The second reason for differences in opinion between lab/field studies is the possible difference between the quality of FBE coated steel rebars tested in the laboratories and that used in construction sites. At sites, by the time the FBE coated steel rebars are placed in concrete, they could experience significant scratch damage and get exposed to sunlight/UV rays during storage and delays in construction stages (see Figure 2.13 and Figure 2.14). Moreover, the candidate could not find literature on the degradation of FBE coated steel rebars due to the exposure to sunlight/UV rays and its effects on the initiation of corrosion and reduction in the service lives of concrete systems, which is the focus of this paper.

Table 2.5 Field studies showing poor performance of FBE coated steel rebars

Location	Age (years)	Conditions/Observations	References
Norway	< 25	50% of bridges experienced corrosion	(McDonald 2009)
Florida, USA	20	Outdoor storage; severe corrosion	
Minnesota, USA	< 35	Cracks and disbondment of coating	
Various states in Canada	5 to 16	Disbondment of coating; under film corrosion	(Griffith and Laylor 1999; Pianca et al. 2005)
Virginia, USA	5	Disbondment of coating	(Pyć et al. 2000)
Various states (MI, WI, NY, PA, OH, VA, and IA) in USA	< 20	Underfilm corrosion, cracking, blistering, and disbondment of coating	(Kim et al. 2007; Zemajtis et al. 1998) (Fanous and Wu 2005)
Various bridges in USA	<30	Early corrosion in Florida bridges was the result of a combination of the highly aggressive environment (such as heat cooling cycle, ultraviolet exposure), highly permeable concrete, and flaws & damage to FBE coating	(Sagüés et al. 2010)

Table 2.6 Laboratory studies and their opinion on the performance of FBE coated steels

Test method/technique	Observations	Opinion	References/ Country
Salt spray, bendability, long-term exposure of prism specimens to artificial and natural exposure conditions	Good adhesion, toughness, good resistance to saltwater spray and alkaline solution	Good	(Swamy and Koyama 1989)/India
Half-Cell-Potential (HCP), Macrocell corrosion current (MCC)	FBE coated steel performs well with a damage to coating < 1% of the defect size.	Good	(Kahhaleh et al. 1998; Mohammed et al. 2014; Swamy and Koyama 1989; Vedalakshmi et al. 2000)/USA, India
HCP, MCC	Performs good when all the condition as per ASTM A775 are satisfied	Conditional	(Kessler et al. 2015, 2016)/Germany
Linear polarization resistance (LPR)/weight loss	The corrosion rate of undamaged FBE was found significantly low. However, the corrosion rate increased with an increase in the damaged area.	Good	(Al-Amoudi et al. 2004)/Saudi Arabia
Visual observation (VOB), HCP, MCC	FBE coated rebars were intact even after exposure to chloride solution for about 8.5 years	Good	(Scannell and Clear 1990)/USA
Electrochemical Impedance Spectroscopy (EIS), VOB	No evidence of corrosion even with cracked concrete; the resistance of the high-frequency loop was low with the damaged coating	Good	(Lau and Sagüés 2007)/USA
HCP, EIS	Measurement of HCP can be misleading, delamination of the coating after 1-year long exposure to 3.5% NaCl solution. However, the corrosion rate was low.	Good	(Darwin and Scantlebury 2002)/UK
VOB, HCP, MCC, EIS	Review paper	Mixed	(Zemajtis et al. 1996)/USA
Coating adhesion, HCP, MCC	No correlation between the rate of corrosion and measured corrosion potential.	Mixed	(Cortés 1998)/USA
LPR, EIS	Underfilm corrosion	Poor	(Singh and Ghosh 2005)/Saudi Arabia

2.5.2 Performance enhancement of epoxy-based coating

Epoxy resin is a combination of chemical bonds (C-H, C-C, C-O-C, N-H, etc.) formed by the polymerization and crosslinking (Nikafshar et al. 2017). The exposure to heat, moisture, sunlight, can alter the mechanical properties of epoxy resins, and it must be considered before using them for a particular engineering application (Cividanes et al. 2014; Peddamallu et al. 2019; Roger et al. 1980). In the case of coatings for steel reinforcement in concrete structures, the desired levels of mechanical properties (i.e., modulus of elasticity, yield strength, and tensile strength) can be achieved by controlled curing and suitable dosage of nanomaterials (Cividanes et al. 2014). For example, barium titanate or barium sulfate is added to control density, achieve high dielectric constant, and tensile strength of epoxy coating (Cheng et al. 2007). Note that the UV-induced changes in the physical and mechanical properties of the epoxy may facilitate oxygen, moisture, and chlorides transport to the steel-coating interface (Séverine Marie Noëlle Cambier 2014). Therefore, the steel-coating interface can degrade via blistering and cathodic delamination. This alteration can lead to physical changes and differences in micro-environment at various locations in the steel-coating interface – leading to the possibility of the formation of preferential sites for initiation of corrosion (Angst et al. 2017). Therefore, reactive diluents and other reactive additives are added to epoxy resin to achieve the desired chemical adhesion with steel and resistance to moisture/alkali in coating (Startsev et al. 2018). Typically, such epoxy materials are used for applications on steel rebars.

The epoxy resin used to coat FBE coated steel rebars is evolved with time. The first generation of FBE coated steel rebars were made with semi-flexible epoxy resin. These rebars could bend after the coating is applied, which resulted in hairline cracking. Later, they were modified to non-bendable epoxy by using additives such as barium sulfate or Barium titanate (Cividanes et al. 2014; Cortés 1998). After the controversies associated with Florida came in

highlights, the epoxy resins were modified by using photo stabilizers. The associated mechanisms and methodology to overcome UV degradation are discussed next.

Total UV irradiance depends on the latitude, altitude above the mean sea level, cloudiness, the time of day, the day of the year, dust in the atmosphere, and on the type and amount of aerosols (Fountoulakis et al. 2018; Sharma et al. 2012). At ground level, the sunlight consists of UVA (315 – 400 nm) and UVB (280 – 315 nm) radiations (Nikafshar et al. 2017). The UV radiation can have higher energy than - C-H, - N-H, and - O-H bonds in epoxy systems – leading to the breakage of such chemical bonds. The regions with broken chemical bonds can get oxidized and degrade the epoxy coating (Nikafshar et al. 2017). The surface of the epoxy can be stabilized by using antioxidants and photo-stabilizers, such as TiO_2, ZnO to resist the degradation of coating (Mahltig et al. 2005b). The dosage of stabilizers/additives could alter the performance of the epoxy coating. For example, an increase in the dosage of carbon black nanoparticles (from 0.7 to 2.5 % by weight of epoxy resin) could improve the UV resistance by two times (increase from 1000 hours to 2000 hours of resistance to degradation with exposure to UV radiations) (Ghasemi-Kahrizsangi et al. 2015a). The particle size of stabilizers can also influence the UV resistance of polymers – the smaller the particle size, the better the UV resistance (Liu and Horrocks 2002). However, the smaller the particle size, the more could be the degree of agglomeration, which can be prevented by dispersing small particles in epoxy by electrostatic forces or ultrasonic waves (Ghasemi-Kahrizsangi et al. 2015b; Löf et al. 2020). The type of additive also influences UV resistance. For example, UV resistance of inorganic and organic additives depends on the kind and degree of crystallinity and the energy bands of molecular systems. Combinations of inorganic and organic additives have been reported to provide enhanced UV resistance (Mahltig et al. 2005a).

The performance of coated steel rebars can be evaluated by the barrier efficiency, coating resistance to electrical or ionic conductivity, resistance to disbondment of coating (Liu et al. 2013; Wang and Gao 2016). It is known that the coatings are permeable to moisture and oxygen (Tator 2015). Tator (2015) reports that the alkaline solution (such as concrete) can break the crosslinking and softens the coating. The disintegration of coating material can lead to a decrease in the ionic or electric resistance of coating (Tator 2015). In addition, exposure to an alkaline environment (here, cementitious systems), coating defects, etc. can result in increase disbondment of coating (Sagues and Powers 1990). Higher the resistance to disbondment of coating lower will be the underfilm/crevice corrosion and its propagation. However, the authors could not find literature on the effects of exposure to sunlight/UV rays on the various characteristics of the coating and its disbondment in the case of FBE coated steel rebars used in concrete construction. The other type of widely used coated steel rebar is cement-polymer-composite coated steel rebars, which is discussed in detail next.

2.6 CEMENT-POLYMER-COMPOSITE (CPC) COATED STEEL REBARS

2.6.1 Performance of cement-modified organic coatings

In the automobile and oil/gas sectors, coatings are applied by skilled workers and only on clean metallic surfaces in a dust-free environment with controlled temperature. In such conditions, coating materials get adhered well to the metal surface and prevent the premature, under film corrosion (Venkatesan et al. 2006a). On the other hand, in the civil construction sector, cementitious coatings to steel reinforcement are often applied by unskilled workers at the construction site. This can lead to various issues associated with poor steel surface preparation and application of coating materials. Figure 2.15 shows one such example of an unskilled worker tying the metallic wires to CPC coated steel rebars. These practices can damage the coating and result in premature initiation of corrosion.

51

Figure 2.15 CPC Coated steel being tied by metallic uncoated tie wires (Central Electrochemical Research Institute Karaikudi 1993)

At present, many organic coatings are commercially available with the following resin as base material: epoxy, acrylic, polyester, etc. If pure organic coatings (i.e., without any additives) are used, then moisture and oxygen can easily penetrate through the coating and result in crevice corrosion and/or under-film corrosion (Fanous and Wu 2005; Griffith and Laylor 1999; Weyers et al. 2000; Zemajtis et al. 1998). However, when additives, such as cement, fly ash, nano-clay, and composites of these materials, are mixed with epoxy/acrylic resins, they can disperse uniformly into small platelets. These small platelets can result in the denser microstructure of the coatings (Biegafiska et al. 1988). Therefore, with the inclusion of additives, the absorption/penetration of water and oxygen can be significantly reduced (Guadagno et al. 2014; Xue et al. 2015). Further, the shape, size, and pH of additives can also influence the migration, inhibition (under-film corrosion or re-passivation), and workability of the coating material. For example, flaky or small-sized additives can provide a tortuous path for corrosion species to travel and offer higher resistance to the penetration of corrosive species (Lyon et al. 2017). Therefore, if cement/fly ash (particle size of about $1 - 100$ μm) is used as

an additive, they can act as a filler and delay the diffusion of corrosive species through the coating (Biegafiska et al. 1988; Xue et al. 2015). They also help in the formation of a strong passive film by providing an alkaline environment to the steel surface (Mayne 1973; Selvaraj et al. 2009). Therefore, this can increase the resistance against the under-film corrosion (Vedalakshmi et al. 2000). In addition, the spherical shape of fly ash can enhance the workability of coating and make it easy to apply on rebars (Biegafiska et al. 1988). All these properties can be achieved only if the steel surface is sandblasted/cleaned adequately. Achieving this is a challenge in the civil construction industry – mainly due to the large-scale usage of rebars and poor workmanship. Literature report on the improved corrosion performance of steel when coated with organic coatings; however, these studies are carried out on cleaned steel surface (Ababneh et al. 2012; Criado et al. 2016; Selvaraj et al. 2009; Tang et al. 2013; Vedalakshmi et al. 2000; Venkatesan et al. 2006b), which is not the usual practice at construction sites. Significant concern exists on the corrosion performance of coated steel reinforcement with the presence of rust beneath the coating (Lyon et al. 2017). Such issues and their impact on the service lives of concrete structures are the focus of this paper.

2.6.2 Performance of the cementitious + organic coatings applied on rebars

Cement-based polymer coatings provide an alkaline environment to the steel surface (Cortés 1998). This may form a stable passive layer on the steel surface. Therefore, high chloride concentration (chloride threshold) may be required to initiate the corrosion activity. But, the literature on the chloride threshold of steels coated with cement-based organic coatings is not available. Note that a few literature focuses on evaluating the performance of organic coating by using various test methods, such as flexibility test, impact resistance test, salt spray test, and quantification of charge transfer resistance (Selvaraj et al. 2009), where four out of 16 coatings could not meet the requirements for the selection of organic coatings (see Table 2.7). Please

note that these test methods will not help in the true estimation of their performance and the service lives of RC systems. Therefore, a study on the determination of chloride threshold of coated steel with cementitious coatings is essential to quantify the service lives of RC structures with coated steel, especially when it is applied inadequately on steel surfaces.

Table 2.7 Performance of various organic coatings

#	Resin							Pigment				Ranking for each test			
	AP	AI	PP	AcR	Ep	Si	PA	TiO_2	$Zn_3(PO_4)_2$	OPC	FA	FT	IRT	SS	CTR
1	Y	Y						Y	Y	Y		1	1	2	Pass
2	Y	Y						Y	Y		Y	1	1	5	Fail
3	Y	Y							Y	Y		1	1	7	Fail
4	Y	Y							Y		Y	1	1	8	Fail
5		Y	Y						Y	Y	Y	1	1	6	Pass
6		Y	Y					Y	Y		Y	1	1	3	Pass
7		Y	Y						Y	Y		1	1	4	Fail
8		Y	Y						Y		Y	1	1	1	Fail
9				Y					Y	Y	Y	2	1	7	Fail
10				Y				Y	Y		Y	1	1	7	Fail
11				Y					Y	Y		2	1	3	Fail
12				Y					Y		Y	1	1	3	Fail
13					Y	Y	Y		Y	Y	Y	1	1	6	Fail
14					Y	Y	Y	Y	Y		Y	1	1	2	Pass
15					Y	Y	Y		Y	Y		1	1	2	Fail
16					Y	Y	Y		Y		Y	1	1	2	Fail
AI : Aromatic isocynate; Acr : Acralic rasin; AP : Acrylic polymer; CTR : Charge transfer resistance; Ep : Epoxy; FA : Fly ash; FT : Flexibility test; IRT : Impact resistance test; OPC: Ordinary Portland Cement; PA: Polyamide; PP: Polyster polyl; Si: Silicon; SS: Salt spray test; Y: Presence of the corresponding element															

The CPC coating consists of two coats (a rapid setting primer coat followed by a cement polymer sealant coat). Both the primer and sealant contain thermoplastic acrylic resins. In

addition, the sealant is mixed with cement powder as an additive. The cement-polymer-composite (CPC) with acrylic base is a type of organic coating that is widely used in the construction industry. Figure 2.16 shows a typical step to be adopted to coat cement-polymer-composites on steel rebars. First, uncoated steel rebars are cleaned using sandblasting to remove the rust, dust, or any other foreign elements. Then, apply the two thin layers of CPC primer coat, followed by two thin layers of CPC sealer coat. The total coating thickness should be between 175 µm to 300 µm. Both the primer and sealant contain thermoplastic acrylic resins (Venkatesan et al. 2006b). In addition, the sealant is mixed with cement powder as an additive. The CPC coating is supposed to be applied on the steel surface after sandblasting/cleaning. Sandblasting can remove the rust, dirt, oil, etc., which could be contaminated by chlorides. Sandblasting results in the large surface area of steel for chemo-mechanical bonding between the bare steel and coating material (Marsh et al. 2001). It may be noted that the cementitious components in the CPC coating can react with the steel surface and form a stable passive layer of oxides.

Figure 2.16 Typical steps for CPC coating

The CPC coating is supposed to be applied onto sand-blasted (SB) rebars at sites. Literature provides sufficient information on the corrosion resistance of SB/clean rebars with CPC and other organic coatings modified with cement/fly ash (Ababneh et al. 2012; Criado et al. 2016; Tang et al. 2013; Vedalakshmi et al. 2000; Venkatesan et al. 2006a). However, it should be noted that many site personnel may not insist on sandblasting or cleaning the rebars prior to applying the CPC coating; and use rebars with as-received (AR) conditions. The as-received steel may have the possible presence of rust on the rebar surface, leading to premature corrosion.

Figure 2.17(a) shows an example of inadequately applied CPC coating on the rebar of a bridge pier of a coastal highway. The photograph was taken during the construction time, and it is evident that the coating is not applied to the top regions of the vertical rebars. Also, incomplete application of CPC coating was observed, especially at the rebar intersections. These indicate that the coating is applied at the site after the rebars are tied in position, and on

'as-received' steel surfaces with rust. However, these inadequately coated steel rebars are not visible after the concrete is placed. Figure 2.17(b) shows the image of the same bridge after the placement of concrete. As these practices are not visible after the placement of concrete, the site personals do not insist on sandblasting/cleaning before the application of CPC coating. The application of the coating on the as-received steel surface can result in inadequate chemo-mechanical bonding and passive film – resulting in premature and/or under film corrosion. The use of CPC coating on as received rebars could lead to a much lower chloride threshold and service lives than the case with CPC coating on SB rebars; however, many site personnel wrongly believe that the CPC coating could perform even without steel surface cleaning. Therefore, one of the focuses of this thesis is to quantify these differences in chloride threshold due to the difference in the surface conditions of the CPC coated steel rebars and their effect on service lives.

(a) Inadequate CPC coating on steel rebars used on bridge piers   **(b) Completed coastal bridge with inadequately coated CPC coated steel rebars (not visible after the concrete is placed)**

Figure 2.17 Highway bridges with CPC coated steel rebars

Though CPC coating (or cement-based polymer modified coating) is widely used in India. Many cement/fly ash-based polymer-modified coatings are being used in different parts of the world. For example, Pei et al. (2015) and Pei et al. (2017) compared the bond and corrosion performance of six combinations of cementitious capillary crystalline waterproofing coating (CCCW), which is widely used in Canada (Pei et al. 2015, 2017). Likewise, Jorge et al. (2012) compared the bond between steel rebars coated with cement-based anticorrosive coatings and repair mortar (Jorge et al. 2012). These coating materials are used for concrete repair in some parts of Europe. In addition, Tang et al. (2012) reported the corrosion performance of cement-modified enamel coatings, showing the use of cement-based coatings in USA (Tang et al. 2013). Likewise, Wang et al. (2014) compared the corrosion performance of polymer-modified cement-based coatings perform superior to FBE coated steel, showing the use of such coated rebar is ongoing in China as well (Wang et al. 2014a). The use of organic coatings modified with cementitious additive is a worldwide practice. Therefore, understanding the corrosion mechanisms of coated steels with cement-based organic coatings will help to overcome the quality issues related to application practices.

2.7 CORROSION OF COATED STEEL REBARS AND ITS TESTING

2.7.1 Assessment of coated metallic structures

The properties of coated metallic structures such as resistance of coatings to degradation in different exposure conditions (Cambier et al. 2014; Nazarov et al. 2008; Zhang et al. 2016), moisture ingress (Liu et al. 2013; Nóvoa et al. 2010; Pathania et al. 2017), and resistance to delamination (Bi and Sykes 2016; Mansfeld and Tsail 1991) are assessed using EIS. In addition, Fourier transform-infrared (FT-IR) spectroscopy is used to quantify the changes in atomic bonding in the organic coatings (Criado et al. 2014; Suliga et al. 2018). Also, scanning electron micrographs are obtained to assess the degree of crosslinking, coating

blistering, coating integrity, and coating delamination (Rajitha et al. 2020). Table 2.8 shows that much of the literature focus on developing new coating, modify the existing coating materials, characterization of coating materials, performance/comparison of various coatings, and effect of damage/degradation to the coating on performance of FBE coated steel rebars. A few literature are available to detect the initiation of corrosion in metallic structures using EIS and/or visual inspection (to list a few (Dhole et al. 2020; Latif et al. 2020)). A few literature reports the comparison of various coated steel rebars embedded in cementitious systems using EIS (Cambier et al. 2014; Jolivet et al. 2007; Kranc and Alberto A. Sagues 2001; Lau and Sagüés 2007; Ryou et al. 2005). However, the candidate could not find literature with test methodology to detect the initiation of corrosion. Also, candidate could not find the data on chloride threshold, and service lives of RC systems with FBE coated steel rebars, which will be addressed in this thesis.

Table 2.8 Major focus of available literature

The focus of available literature	References
Development of new coating/ modification of existing coating material	(Ghasemi-Kahrizsangi et al. 2015a; Parhizkar et al. 2017)
Electrochemical characteristics of coatings	(McHattie et al. 1996; Montes et al. 2004; Tang et al. 2014b)
Performance of coating in aqueous media	(Malik et al. 2002; Tang et al. 2016b; a)
Effect of damage to the coating on corrosion performance	(Kamde and Pillai 2017; Kessler et al. 2015; Sagüés et al. 2010; Vedalakshmi et al. 2000; Zayed and Sagues 1990)
Comparison of various coatings	(Dong et al. 2012; Jalili et al. 2009; Selvaraj et al. 2009; Tang et al. 2012, 2016b; Wang and Gao 2016)
Detection of initiation of corrosion in metal structures	(Dhole et al. 2020; Latif et al. 2020)
Detection of initiation of corrosion in RC structures with FBE coated steel	Candidate could not find literature on methodology to detect the initiation of corrosion

2.7.2 Assessment of coated steel rebars in concrete and challenges

To assess the corrosion activity at the steel surface, the adopted electrochemical technique(s) should be able to account for the high resistance offered by FBE coating. At present, there are no guidelines/standards available for assessing the RC systems with embedded FBE coated steel rebars. Hence, many researchers tend to use the available test methods based on HCP, MCC, LPR, and/or EIS to assess the systems with coated steel rebars (see Table 2.9). Many of these test methods may not be valid in assessing the RC systems with coated steel rebars. The possible challenges associated with the use of these test method in the assessment of the RC systems with FBE coated steel rebars is discussed next.

2.7.2.1 Half-Cell Potential (HCP)

HCP measurement is one of the most widely used techniques for the assessment of RC systems. ASTM C876 (1999) guides evaluating the probability of corrosion activities at the steel rebar surface using HCP measurements on the surface of the concrete (ASTM C876 2015). For RC systems with uncoated steel rebars, the HCP measurements of steel in concrete is challenging due to many factors such as anode area, anode to cathode ratio, concrete cover, relative humidity (induirectly resistitance offered by concrete), but the resistivity of concrete, the varying relative humidity of concrete, etc. (Elsener et al. 2003). Also, the large ohmic drop across coating is a challenge for HCP measurements of RC systems with coated steels. The collective effect of these can lead to erroneous measurements of the corrosion potential of underlying steel in coated rebars (Singh and Ghosh 2005). In addition, if HCP measurement only represent the probability of corrosion activity at the time of measurements, It does not give the information of diffusion of chlorides, the rate of corrosion, and any indication of future corrosion processes(Kessler and Gehlen 2016).

2.7.2.2 Macrocell Corrosion (MC)

Macrocell corrosion current is another test method used for the assessment of corrosion activities in RC systems with uncoated steel rebars. ASTM G109 describes a standard test method for determining the effect of chemical admixtures on corrosion of embedded steel rebars using macrocell corrosion specimens. A typical macrocell corrosion specimen has three steel rebars – one rebar at the top and two rebars at the bottom (ASTM G109-07 2013). The top rebar is close to the reservoir, which is filled with chloride solution during the wet regime, and the reservoir is dried at the starting of the dry regime. During the cyclic wet-dry exposure, the top rebar preferentially gets exposed to chlorides and moisture. Therefore, it is more susceptible to corrosion and acts as an anode. Bottom rebars are relatively away from the

corrosive environment and act as cathode. Once the corrosion is initiated at the top rebar, electrons are expected to travel from top rebar to bottom rebar through the resister connecting them, and ionic conduction is expected to take place through the cementitious system between the bottom and the top steel rebars. However, the resistance offered by FBE coating for ionic conduction is significantly high (Wang and Gao 2016). Therefore, corrosion cell(s) may not form between the top and bottom steel rebars and form within the top rebar itself (Kessler et al. 2015). Therefore, MCC measurements will not represent the corrosion activity of the top rebar (Kamde and Pillai 2017), which may not be suitable for corrosion assessment of concrete systems with FBE coated steel rebars.

2.7.2.3   Linear Polarization Resistance (LPR)

LPR techniques is another widely used technique for measurement of the rate of corrosion. Literature report that the LPR measurements can capture the corrosion activity of the metal surface, where resistance offered by solution/electrolyte is less than 37 kΩ.cm (Kessler and Gehlen 2016; Rengaraju et al. 2019; Tait 2012). The resistance offered by commercially available FBE coating is significantly high (in this study, $\approx 10^3$-10^4 kΩ.cm), which was determined by EIS testing on FBE coated steel. Therefore, such large resistance can result in a significantly high ohmic drop, which can influence the measurements of resistance to polarization using LPR (Rengaraju et al. 2019). In addition to high ohmic drop, non-homogeneous distribution of the absorbed moisture is another challenge associated with the assessment of FBE coated steels – leading to erroneous quantifications of current interruption (Cao-Paz et al. 2010). Therefore, LPR measurements may not be adequate to assess the corrosion activities of coated steels.

2.7.2.4 Electrochemical Impedance Spectroscopy (EIS)

EIS technique is based on application of an alternating signal of small amplitude to the working electrode (in this study, rebar embedded in mortar). When a system has resister in it and an alternating current is applied, it follows the Ohms law. Therefore the resistance of the system can be defined as, R = E/I. However, this relationship is applicable to ideal systems with only resister. However, rebars embedded in concrete or mortar contains other circuit elements. Due to the nonideal behavior, impedance in replacement of resistance. Electrochemical impedance is measured by applying sinusoidal potential excitation and measuring the response as AC current signal. The initial applied potential difference and the response of the electrode are compared by measuring the phase shift between the applied volatage and current. In addition, the amplitude is measured, which is also defined as the resistance of the system to change from its stable state. In short, the electrochemical inpedance, Z is the relation between δE and δI, which described next

When a sinusoidal potential excitation is applied

$$E_t = E_0 \sin(\omega t)$$

where, $\omega = 2\pi f$

The response signal (I_t) is shifted with a phase angle Ø and has a different amplitude than I_0. Therefore, I_t can be defined as

$$I_t = I_0 \sin(\omega t + \emptyset)$$

As per Ohms law, Z is expressed as Z_0 and Ø.

$$Z = E_t/I_t = \frac{E_0 \sin(\omega t)}{I_0 \sin(\omega t + \emptyset)} = Z_0 \frac{\sin(\omega t)}{\sin(\omega t + \emptyset)}$$

63

However, the input AC signal is applied with varied frequencies. Therefore the output current obtained is also at different frequencies. Analysis such response is difficult using the simple formulae presented above. Therefore, to solve them Euler's relationships are used. Therefore, Z is defined as the combination of complex functions. The applied voltage function is

$$E_t = E_0 \exp(j\omega t)$$

And the output current response are

$$I_t = I_0 \exp(j\omega t - \emptyset)$$

Therefore, the impedance is represented as the summation of real and imaginary functions

$$Z(\omega) = \frac{E}{I} = Z_0 \exp(j\emptyset) = Z_0(cos\emptyset + jsin\emptyset)$$

The output from EIS technique is the plot between (i) real and imaginary component of impedance, which is also known as Nyquist plot, (ii) frequency and logarithmic of impedance, and (iii) frequency and phase angle between I and E. The Nyquist is the simplest representation of EIS response. It gives the information on number of interfaces in the system, resistance/impedance of the each layer in the system, the behavior (resistor, capacitor, or constant phase angle) of each layer/element. The drawback of Nyquist plot is that it is not possible to extract information such as the frequency at each point. Whereas, Bode plots give information of impedance and phase angle with respect to frequency. Literature also report that the with the use of EIS following information can be obtained, the presence of surface films, resistance/characteristics of concrete/coating/electrolyte, interfacial corrosion, diffusion/mass transfer phenomena. However, interpreting the results are difficult and need expertise in the subject. Otherwise, wrong interpretations can lead to wrong information on corrosion activity at steel surface inside the concrete. Clear understanding of physical system

can help in arriving at equivalent electrical circuit, which can change according to the conditions of the steel.

Test methods based on EIS have been used to assess the coated metal structures (see Table 2.9). A few literature report that it is possible to overcome challenges such as high resistivity of electrolyte, nonuniform distribution of moisture in the coating, large variation in R_P, by using Electrochemical Impedance Spectroscopy (EIS) technique (Cao-Paz et al. 2010; Miszczyk and Darowicki 2018; Perini et al. 2012). Sagues and Zayed proposed a tentative method for measuring the corrosion current of FBE coated steel rebars in concrete (Sagüés and Zayed 1991). However, this was limited for FBE coated steel rebars with coating damages.

Table 2.9 Reported techniques used to assess RC systems with FBE coated steel rebars in concrete specimens

Test method/technique	Observations	Opinion	Reference
Half-cell potential (HCP), Macrocell corrosion current (MCC), and Visual observation (VOB)	Based on corrosion measurements recorded, FBE coated steel showed better performance than uncoated steels.	Good	(Cortés 1998; Kahhaleh et al. 1998; Mohammed et al. 2014; Vedalakshmi et al. 2000)
HCP, MCC	Performs good when all the condition as per ASTM A775 are satisfied	Conditional	(Kessler et al. 2015, 2016)/Germany
Linear polarization resistance (LPR)	The corrosion rate of undamaged FBE was found significantly low.	Good	(Al-Amoudi et al. 2004)
Electrochemical impedance spectroscopy (EIS) and VOB	The damaged coating can undergo localized/pitting corrosion	Bad	(Lau and Sagüés 2007)
	FBE coated steel rebars can provide an additional five years of service lives as compared to uncoated steel rebars		(Brown et al. 2006)

Also, Scopus search results [with keywords (concrete) AND (corrosion) AND (coated) AND (steel) AND (EIS) or (electrochemical impedance spectroscopy)] show that 15 research articles were published till the year 2006 and about 100 articles were published till April 2020. Many of these articles focus on the assessment of coated steel exposed to the aqueous solution and do not report the studies with FBE coated steel embedded in concrete, which may not simulate the RC systems - indicating that the research on corrosion assessment of coated steel embedded in concrete still needs to be explored. A few literature report the EIS can be one of the techniques capable of assessing coated steel rebars embedded in cementitious systems (Barbucci et al. 1998; Lau and Sagüés 2007; Sagüés and Zayed 1991; Singh and Ghosh 2005; Tang et al. 2012, 2013, 2014a, 2016a), which is adopted in this study. Another advantages of the EIS technique is to obtain reliable data from the EEC by limiting the error of each

component (Chen et al. 2017). By Analysing EIS response with appropriate EEC can provide information on corrosion kinetics, electrochemical control mechanism, if corrosion occurs by activation, concentration or diffusion (Ribeiro and Abrantes 2016). However, it was reported that the representative EEC are not finalized (Tang et al. 2014a), and the candidate could not find a systematic methodology to detect the initiation of corrosion in RC systems with coated steel rebars. Therefore, there is a dire need to investigates the electrochemical response of FBE coated steel rebars with and without damage/degradation to the coating and proposes a systematic methodology using suitable technique and generalized EEC to detect the initiation of corrosion in FBE coated steel rebars embedded in the cementitious system

2.8 BOND CHARACTERISTICS OF UNCOATED AND COATED STEEL EMBEDDED IN CONCRETE

The bond stress (τ) is defined as the shear force per unit surface area of the embedded steel rebars in contact with concrete (Wilkins 1951). The bond stress acts at the interface between rebars and surrounding concrete, and along the direction parallel to steel rebars (Larnach 1952). The τ-slip behavior gets affected by the degree of corrosion of embedded steel rebar (see Figure 2.19). The alteration in the τ-slip response can influence the serviceability of RC elements (Castel et al. 2007; *FIB Model Code* 2010; Mangat and Elgarf 1999; Sajedi and Huang 2017; Tan et al. 2020). However, it was reported that when the mass loss of steel is less than 1%, steel experiences the reactionary confinement from surrounding concrete, and increase in the bond strength (τ_b) (see Figure 2.18). Therefore, with steel mass loss of less than 1%, the structure may not experience any adverse effect on structural performance (*FIB Model Code* 2010). However, RC structures with coated steel can experience adverse effects on structural capacity even without significant corrosion/ steel mass loss (Kamde and Pillai 2018).

2.8.1 Bond mechanism in uncoated Steel-Concrete (S-C) systems

Steel-Concrete (S-C) interfacial forces, i) chemical adhesion (C), ii) friction (F), and iii) mechanical interlock (M) are responsible for the bond between steel rebar and concrete (*FIB Model Code* 2010; Jiang et al. 2018). Figure 2.18 shows the typical bond stress–slip model for uncoated steel embedded in concrete (S-C). τ-slip behavior is characterized by four regions with different τ-slip responses, a, b, c, and d separated by slips vertical lines s1, s2, and s3. Region 'a' (0 - s1) represents an elastic response from the steel-concrete interface. In this region, bond efficiency is due to chemical adhesion between steel and concrete, where concrete remains uncracked. Chemical adhesion is accomplished by micro-interlocking of concrete at the S-C interface (*FIB Model Code* 2010). When stress more than residual shear stress (τ_f) is applied, chemical adhesion breaks and results in the first crack in concrete at S-C interface. Later, if higher bond stresses are applied, frictional force and mechanical interlocking at the S-C interface contribute to resisting the slip due to applied bond stress. During this, cracks spread radially, and result in wedging action, which is enhanced by the crushed concrete stuck at the ribs. Hoop stresses resist outer components of pressure. As a result, surrounding concrete exerts the confining pressure on the S-C interface. This stage can end as soon as the crack radiates to the outer surface, resulting in the splitting of concrete. Therefore, to get the pull-out response, lateral reinforcements/stirrups are provided (Yeih et al. 1997). The stirrups/lateral confinement increases the bond strength – resulting in the maximum bond stress (region 'b'; between s1 and s2). For plain steel rebars, bond stress can suddenly drop by slipping across the S-C interface. When deformed bars are confined using stirrups, under continued loading, plastification of the S-C interface takes place. Therefore, a larger slip is observed with the application of constant load. After that, the S-C interface is smoothened due to wear action – leading to a decrease in τ, i.e., region 'c' (s2–s3). Region 'c' represents the debonding failure after the plastification. The Region 'd' represents the τ-slip response of S-

C interface after the effect of mechanical interlock vanishes, and only frictional force is responsible for the residual bond strength (τ_f) (Tastani and Pantazopoulou 2013).
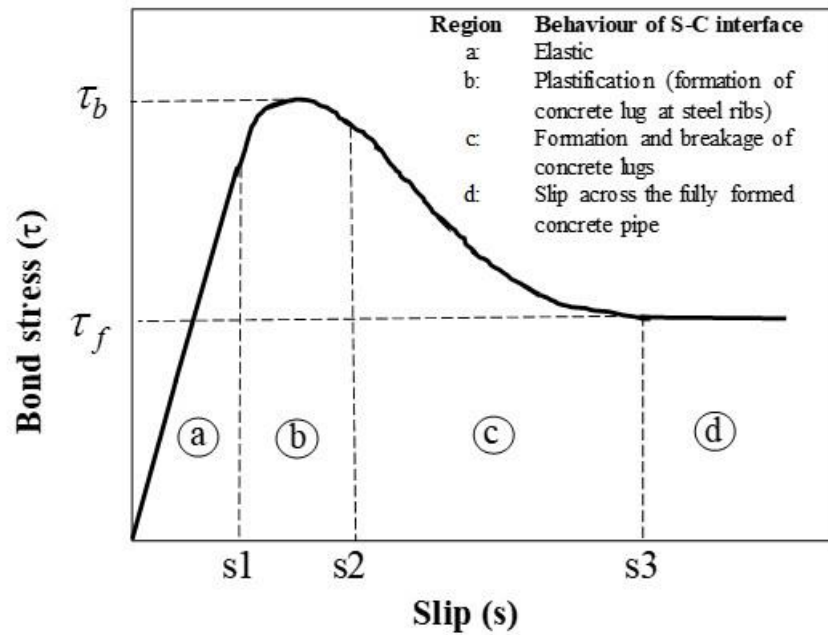
Figure 2.18 Typical bond stress-slip model for uncoated deformed steel rebar embedded in concrete (adapted from FIB Model Code 2010)

IS 2770 (1967) demonstrates the test method for determining the bond between steel and concrete. IS 2770 recommends noting the bond stress value at 0.025 mm, 0.25 mm, and the maximum bond stress. However, it does not define the bond strength. ASTM A1096 (2016) specifies the standard test method for evaluating the bond of individual steel wire or plain rebars for concrete reinforcements (ASTM A1096-M 2016). ASTM A1096-M prescribes the bond strength as equal to the maximum bond stress before or at 2.5 mm. Similarly, ACI 408R-03 defines that the bond strength as the maximum bond stress that may be sustained by the main steel rebar (ACI Committee 408 2003). Therefore, in this study, the maximum bond stress achieved during the test was the bond strength (τ_b).

2.8.2 Factors affecting bond between Steel-Concrete (S-C) and Steel-Coating-Concrete (S-C-C) systems

The τ-slip behavior is affected by following factors: structural characteristics such as rebar properties, concrete properties, concrete cover, rebar spacing; rebar surface condition (ribbed/plain/rusted/uncoated / coated), rib geometry; bar casting position, confinement due to stirrup reinforcement/cover concrete; aggregate type, etc. (ACI Committee 408 2003; Subramanian 2005). Out of these, one of the major parameters influencing the τ_b is the rib face angle, especially when it is determined for coated steel rebars. Literature report that the smaller rib face angles have lesser bond strength between steel and concrete (Gergely and Lutz 1967). For example, plain steel rebar (rib height = 0) and concrete have significantly low τ_b between steel and concrete. Also, it was also reported that a rib face angle greater than 60 degrees could result in the crushing of concrete near the ribs (Hamad 1995). Then, this crushed concrete acts as a rib, instead of ribs on steel rebars, with an effective angle of about 40 degrees. Therefore, the recommended rib face angle is about 45 degrees (Idun and Darwin 1999).

The rib face angle is designed to achieve an adequate bond between uncoated steel rebars and concrete. Note that the coating is applied to the uncoated steel rebar without modifying the rib geometry. In general, the application of the coating on reinforcement reduces the coefficient of friction, rib face angle, and adhesion between coated steel and concrete (Gergely and Lutz 1967; Idun and Darwin 1999; Kobayashi and Takewaka 1984). The combined effect of reduced rib face angle reduced adhesion, and the frictional force between steel and concrete can result in a significant decrease in the τ_b between steel and concrete. The decrease in τ_b due to coating can result in the increase in the development length by 2-3 times the development length (L_d) required for uncoated steel rebar and concrete systems (Pei et al. 2015). Generally, the increase in L_d is considered, and an additional 1.5 times the development length of uncoated steel rebars is provided at the design stage. However, much literature reports that the L_d

depends on various factors, including the coating material properties and variability in coating thickness (Jalili et al. 2009; Kobayashi and Takewaka 1984; Wu et al. 2013). Therefore, it is important to investigate the effect of new coatings on the bond performance of S-C-C systems. Also, the long-term performance of S-C-C systems with coating materials on bond performance should be investigated.

Various coated steel rebars are used in the construction industry, such as fusion-bonded-epoxy coating, enamel coating, polymer-modified cementitious coatings. Much literature reports the bond performance of FBE coated steel rebars embedded in concrete (Assaad and Issa 2012; Idun and Darwin 1999; Kobayashi and Takewaka 1984; Ldun and Darwin 1999; Miller et al. 2003). Without knowing the effect of new coating materials and corrosion on bond performance, many such coated steels have been used in the construction industry. One such coating is a polymer modified cementitious coating, also known as cement-polymer-composite (CPC) coating. CPC coating or similar coatings are widely used cementitious coatings in developed/developing nations (Jorge et al. 2012; Kamde and Pillai 2020a; Pei et al. 2015, 2017; Wang et al. 2014a). The CPC coating contains thermoplastic acrylic resins with cement powder as additives (Kamde and Pillai 2020a; Rajagopalan et al. 2001). Nowadays, many infrastructure systems, especially bridges, are being constructed using CPC coated steel rebars. Generally, CPC coating is applied at the construction sites. Evidence on poor construction practices (inadequate applications of CPC coating on rusted steel surface) is available. This could lead to premature corrosion and a significant reduction in time to initiation of corrosion (Kamde and Pillai 2020a). Many RC structures are built with CPC coated steel rebars without knowing their long-term effect on the bond behavior of steel-coating-concrete (S-C-C) systems. Therefore, one of the focuses of this thesis is to estimate the effect of CPC coating and corrosion on bond behavior of S-C-C systems.

2.8.3 Influence of corrosion on the bond performance of S-C and S-C-C systems

Figure 2.19 shows that many literatures report that up to about 1% of steel mass loss can increase the bond strength due to the increase in frictional force and mechanical bonding due to reactionary confinement (Almusallam et al. 1996; Amleh and Mirza 1999; Auyeung et al. 2000; Bhaskar et al. 2010; Cabrera 1996; Chung et al. 2008; Elbusaefi 2014; Fang et al. 2004; Kearsley and Joyce 2014; Kivell et al. 2011; Lee et al. 2002; Lin and Zhao 2016; Mangat and Elgarf 1999; Rodriguez et al. 1997; Yalciner et al. 2012). When the mass loss is more than 1%, the chemical adhesion between steel and concrete diminishes, and reduced frictional forces and mechanical interlocking are responsible for the bond between steel and concrete (Li et al. 2014). When the corrosion level is about 10%, the bond strength can reduce by about 10 to 25% (Huang 2014). On the other hand, it was reported that when corrosion was induced using voltage application, the bond between uncoated, CPC coated steel rebars, and concrete was not affected (Natarajan et al. 2005). Note that the voltage application can alter the steel-concrete interface and failed to represent the real conditions (Choi et al. 2014). Accumulation of alkali ions (mainly Na^+ and K^+) at the S-C interface during voltage application appears detrimental to the interface integrity – resulting in the alteration of S-C interface properties (Ihekwaba et al. 1996). Another most widely used method of inducing corrosion to the steel rebar is to expose pull-out specimens to cyclic wet and dry regimes with chloride solution (Marcos-Meson et al. 2020; Shang et al. 2019). Generally, pull-out specimens have very large concrete cover to reinforcement. Therefore, this method is time-consuming. Another way to induce corrosion is by premixing of chlorides in concrete, followed by cyclic wetting and drying with chloride/moiture solution. Premixing of chloride represent RC structure after exposure to the marine environment, where chlorides have reached the rebar level. Therefore, the premixing of chloride in concrete can be a short-term methodology to induce corrosion to the reinforcement, which is adopted in this study.
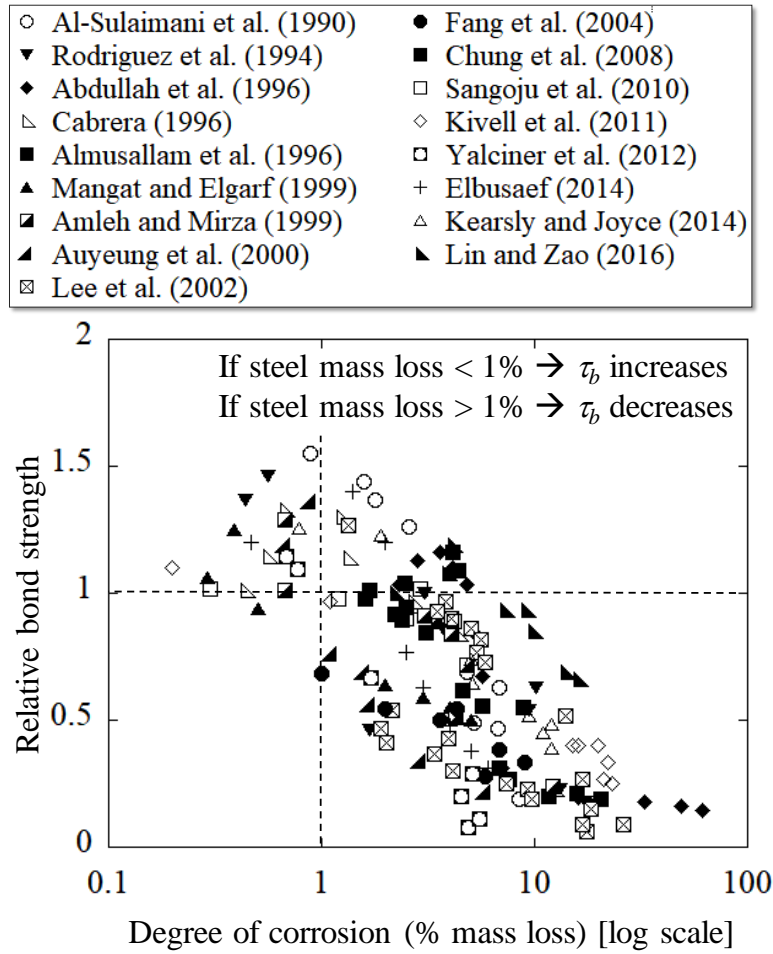
Figure 2.19 Effect of corrosion on bond strength of uncoated steel deformed rebars embedded in concrete (from literature)

2.8.4 Bond degradation and serviceability of systems with coated steel rebars

The service life of reinforced concrete (RC) structures is defined as the duration for which structure safely meets the performance requirements (Zhang et al. 2009). One of the most common serviceability criteria is defined by limiting the crack width and deflection of the flexural member (Cabrera 1996; Li et al. 2014; Rao 2014; Zhang et al. 2009). Much literature provide evidences on the bond strength relates to the deflection of flexural members (Castel et al. 2000; Sajedi and Huang 2017; Zhang et al. 2009). It was reported that the reduction in bond strength could lead to a reduction in the stiffness of the steel-concrete interface (Castel et al.

2000). As a result, when the RC system has low bond strength, the require increased embedded length (lap length) than provided to achieve the bond capacity (Rao 2014). Experimental evidence indicates that the bond strength increases up to about 1% of steel mass loss due to corrosion (see Figure 2.19). Beyond 1% of steel mass loss, the deflection of RC elements increases due to a reduction in the bond strength by about 20% (Zhang et al. 2009). For RC structure with uncoated steel rebars, this duration is usually considered to be less than ten years (Bentz 2003) – with approximately 10% mass loss of steel due to corrosion. During this time, structural properties/appearance such as bond strength, cracks on the concrete surface, and flexural strength can get affected (Jiang et al. 2018; Tan et al. 2020). However, the candidate could not find literature on what will be the effect of corrosion on the bond performance of RC systems with cementitious coatings, which is one of the focuses of this thesis.

2.9 SUMMARY OF KNOWLEDGE GAPS

Worldwide, many countries/states have either banned or recommended not to use the coated steel rebars. In India and many other developing and developed countries, a large number of infrastructure are constructed or being constructed using FBE and CPC coated steel rebars. Many of the structures are built with poor quality control measures. However, there is a lack of data available on how the poor site conditions and practices affect the electrochemical characteristics, chloride thresholds, and time to corrosion initiation of RC systems with coated steel rebars. Also, the current practice of determining the chloride thresholds and service lives of RC systems with uncoated steel rebars do not account for the transport of chloride through the coating. Therefore, they may not be valid for systems with coated steel rebars. Therefore, for reliable estimation of service lives of RC systems with coated steel rebars, a framework considering the important parameters such as chloride diffusion coefficient of coating, chloride thresholds (chloride concentration below coating) is essential, which is not reported in the

literature. To determine the chloride thresholds, it is essential to detect the initiation of corrosion in coated steel rebars using suitable test methodology, which is not reported. Also, the effect of corrosion on bond characteristics of the cementitious coating materials such as CPC coated steel rebars, are not available.

3   EXPERIMENTAL PROGRAM

3.1   INTRODUCTION

This chapter explains the material properties and methodology used in this study. First, the materials are discussed in detail, followed by the various test methodologies adopted to achieve the Objectives 1, 2, and 3.

3.2   MATERIALS USED AND THEIR PROPERTIES

3.2.1   Distilled water

Distilled water was used for the preparation of all the specimens to avoid the mixing of unknown additional chlorides during the preparation of specimens. No ionic impurities were found in distilled water. Also, distilled water was used for the preparation of simulated pore solution for cyclic exposure and electrochemical tests.

3.2.2   Cement and aggregates

Ordinary Portland Cement (OPC) of Grade 53, conforming to IS 12269 (2013), was used to prepare a mortar mix for the casting of modified ASTM G109, lollipop specimens, and pull-out specimens. The specific gravity of OPC was found to be 3.15, meeting the requirements prescribed in (Indian Standards 1988). The fineness of OPC was found to be 310 m^2/kg as per the requirements specified in (ASTM C204-18 2019). Further, Table 3.1 shows the chemical composition and physical properties of OPC used in this study.

Table 3.1 Chemical composition and physical properties of OPC used in this study

Composition (%)						Physical property		
Al_2O_3	Fe_2O_3	CaO	MgO	(Na_2O)	LOI	Mean diameter (μm)	Specific surface area (m^2/kg)	Specific gravity
5.54	4.71	61.7	1.06	0.2	2.27	15	330	3.15

The graded crushed-granite aggregate of maximum minimal sizes 10 and 20 mm were used as the coarse aggregate. The river sand with a maximum nominal size of 4.75 mm conforming to Zone 1 as per IS 383 (1970) was used as the fine aggregate. Table 3.2 shows the physical properties of the aggregates meeting the requirements as per IS 2386-3 (1963). The particle size distribution of these aggregates was determined using sieve analysis as per IS 2386-Part 1 (IS 2386- Part I 1963).

Table 3.2 Physical properties of aggregates

Types of aggregate	Specific gravity	Water absorption (%)
Fine aggregate (river sand)	2.6	0.75
Coarse aggregate (10 mm)	2.8	0.43
Coarse aggregate (20 mm)	2.82	0.40

3.2.3 Cement mortar

Mortar with cement:sand:w/b of 1:2.75:0.5 was used to prepare the 3-bar prism specimens and lollipop specimens. The mixing method prescribed in ASTM C305 (2015) was used for the mixing of mortar using mechanized mortar mixer (ASTM C305 2015). First, mixing water was placed in the bowl. Then, cement was added in the bowl and mixed for 30 seconds at the

speed of 140 ± 5 rotations per minute (rpm). After that, IS 383 (2002) Grade 2 and Grade 3 sand were added to the cement paste within the next 30 seconds, while the mixer is being operated at 140 ± 5 rpm. After that, all the ingredients were mixed for the next 30 seconds at 285 ± 5 rpm. Then, the mixer was stopped, and all the ingredients were scrapped from the base of the mixer to get the proper mix. This process was done within 60 seconds. Then, again the mixer was operated for the next 60 seconds at 285 ± 5 rpm. Then the mortar is ready to place. The placement of mortar for all the specimens was done within 10 minutes to avoid any loss in workability.

3.2.4 Cement concrete

Table 3.3 shows the concrete mix design used in this study to cast pull-out specimens. The measured slump of the concrete was in the range of 60 - 120 mm. Concrete mixtures were prepared in a 300-kg pan mixer. To prepare the concrete mix, concrete mix design shown in Table 3.3 was used. Water correction for superplasticizer (SP) and water absorption from fine and coarse aggregate was adjusted in the mix design. First, all aggregates were dry mixed in the mixer for about five minutes. Then, one-third of the total water was added to the dry mixed aggregates and further mixed for about two minutes. Later, mixing was stopped for about 3 to 4 minutes. This rest time was given for aggregates to absorb the water. Later, cement was added, and mixed until the cement is coated on all the aggregates, usually for about 5 minutes. Then, the required SP was mixed with the remaining two-thirds of water and added to the mixture and mixed for about five minutes. The slump was determined for each batch of concrete. The concrete mix was discarded if the slump was found less than 60 mm.

Table 3.3 Concrete mix design used in this study

Ingredients	Quantity (kg/m^3)
Cement	380
Water	171
Aggregate 10 mm	450
Aggregate 20 mm	620
Sand (<3.75 mm)	800
Superplasticizer	2.3
NaCl	7.6

3.2.5 Uncoated steel rebars

The thermo-mechanically treated (TMT) or quenched and self tempered (QST) steel rebars were used for this study. For the corrosion study, 8 mm diameter rebars were used for the preparation of 3-bar prism and lollipop specimens. For the bond study, 12 mm diameter rebars were used to prepare the pull-out specimens. The steel with tensile strength of 550 MPa were used for both the studies.

3.2.6 Fusion-bonded-epoxy (FBE) coated steel rebars

Fusion-Bonded-Epoxy (FBE) coated steel rebars were used in as-received condition from the manufacturing unit. Following properties were assessed for FBE coated steel in as-received condition: coating thickness, coating continuity, coating flexibility.

3.2.6.1 Coating thickness

Fusion Bonded Epoxy coated steel rebars from 10 different lots were considered in this part of the study. The 8 mm diameter rebars were cut to a length of 150 mm using an oil-water emulsion-based coolant cutter. Coolant cutter was used to avoid the effect of heat generated

during cutting on the coating properties. Then, electromagnetic coating thickness gauge was used to measure the coating thickness of FBE coated steel rebars. A total of 20 measurements were taken in the central 100 mm length of the 150 mm long cut FBE coated steel rebars. The coating thicknesses were measured in between the ribs and at the tip of the ribs. The coating thicknesses were not measured at the inclined face of the rib.

Figure 3.1 shows the FBE coated steel rebar with the diameter 8 mm and desired coating thickness of 300 µm to 350 µm. Figure 3.2 shows the variation of FBE coating thicknesses (CT) in the rebars from each lot. Three horizontal lines represent the minimum and maximum limits for CT in FBE coated steel rebars. The red dash line corresponding to LLI and black dash line corresponding to LLA represents the lower limit prescribed by IS 13620 (2015) and ASTM A775 (2017), respectively. The solid black line corresponding to UL represents the maximum CT specified by IS 13620 (2015) and ASTM A775 (2017). The line with the unfilled circular markers represents the CT measured on the FBE coated steel rebars at locations between two ribs and on the top of ribs. It was found that the commercially available FBE coated steel rebars has CT ranging from about 100 µm to about 1000 µm. IS 13620 (2015) recommends the minimum CT as 100 µm. Note the the CT < 200 µm can result in premature initiation of corrosion (Kobayashi and Takewaka 1984), which will be presented in this thesis. In most of the locations, the CT was found to be more than the CT specified by the standards, which can result in a reduction in bond strength between steel and concrete (Kobayashi and Takewaka 1984; Miller et al. 2003).
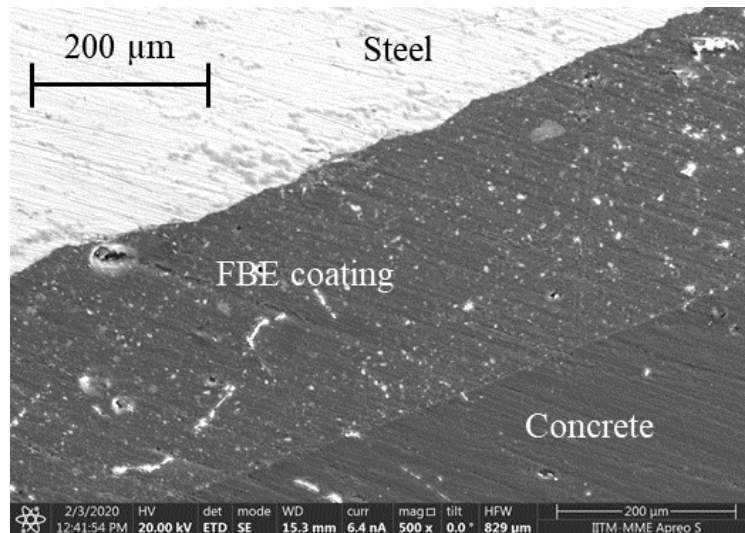
Figure 3.1 Cross-section of FBE coated steel rebar embedded in cementitious system
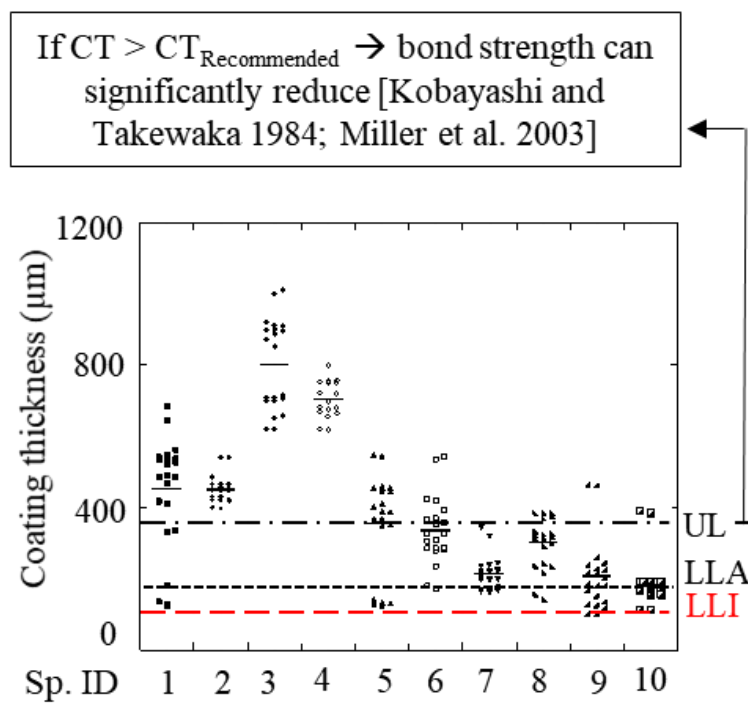
Figure 3.2Variation of coating thickness in commercially available FBE coated steel rebars

3.2.6.2 Coating Continuity

ASTM A775 recommends to use holiday detector for assessing the coating continuity. But, the commercially available holiday detectors are designed for the assessment of coating continuity of coated pipelines. When the holiday detector brush is moved on coated metal surface, each beep sound represents one holiday. The assessment of coated steel rebars using the holiday detector is challenging because of their small surface area of coated steel rebars. Also, holiday detectors can not detect the pinhole or defect unless there is an electrical short circuit between the brush and the underlying steel. When FBE coated steel rebars are exposed to sunlight/UV rays, FBE coating cracks (Nikafshar et al. 2017). At early exposure times, the cracks may not be deep enough to get the electrical short circuit between the brush and underlying steel. Therefore, coating continuity was checked used visual inspectiation (for macro cracks/defects), holiday detector (for through damage), and scanning electron micrographs (cracks/damaged with or without possible electrical short circulit). For this, 8 mm diameter rebars were cut to a length of 150 mm length and visually inspected, and discontineouty, if any were recorded. Then, the holidays were recorded by using a holiday detector as per the guidelines priscribed in ASTM A775 (2017). Then Micrographs of FBE coating peeled off from as-received coated steel specimens were obtained using the scanning electron microscope (SEM) and an effect on coating continuity was evaluated. Effect of UV exposure on coating continuity is discussed in Section 3.4.2.

FBE coated steel rebar specimens were visually inspected and no damage or cracks were observed; see the first photograph and first micrograph (at 300X) in Figure 3.3(a). However, an inspection using a holiday detector indicated many holidays in the coating of the same specimens; see second micrograph (at 5000X) in Figure 3.3(a). These holidays are of about 10 µm diameter, which are not visible to the naked eyes. Then, additional specimens were

exposed to sunlight for 12 days in UV chamber (see ASTM G154), which is equivalent to one month of sunlight exposure. The specimens were visually inspected and no cracks were observed with naked eyes. However, the first micrograph (from the same specimen; at 300X) in Figure 3.3(b) shows that the FBE coating can undergo UV-degradation resulting in new pinholes (see black regions/dots on the surface of epoxy coating) with diameter ranging up to 100 µm. The appearance of new pinholes in large number can be attributed to the evaporation of volatile materials in the coating; indicating inadequate chemical composition of coating material. In addition, UV/sunlight exposure also led to microcracks, which are due to restrained shrinkage of coating, see second micrograph (at 5000X) in Figure 3.3(b). This is mainly an effect of inadequate polymer structure and composition. Therefore, visual inspecton alone is inadequate and the authors recommend to measure the number of pinholes/cracks/scratches at the manufacturing plant and at construction site; in particular, just before the placement of concrete around the rebars. Such approach will force the builders to handle the rebars with care to avoid abrasion-induced scratching and to prevent the prolonged exposure to sunlight/UV (even after the rebar cages are in place).

(a) Before exposure to sunlight

(b) After one month of exposure to sunlight
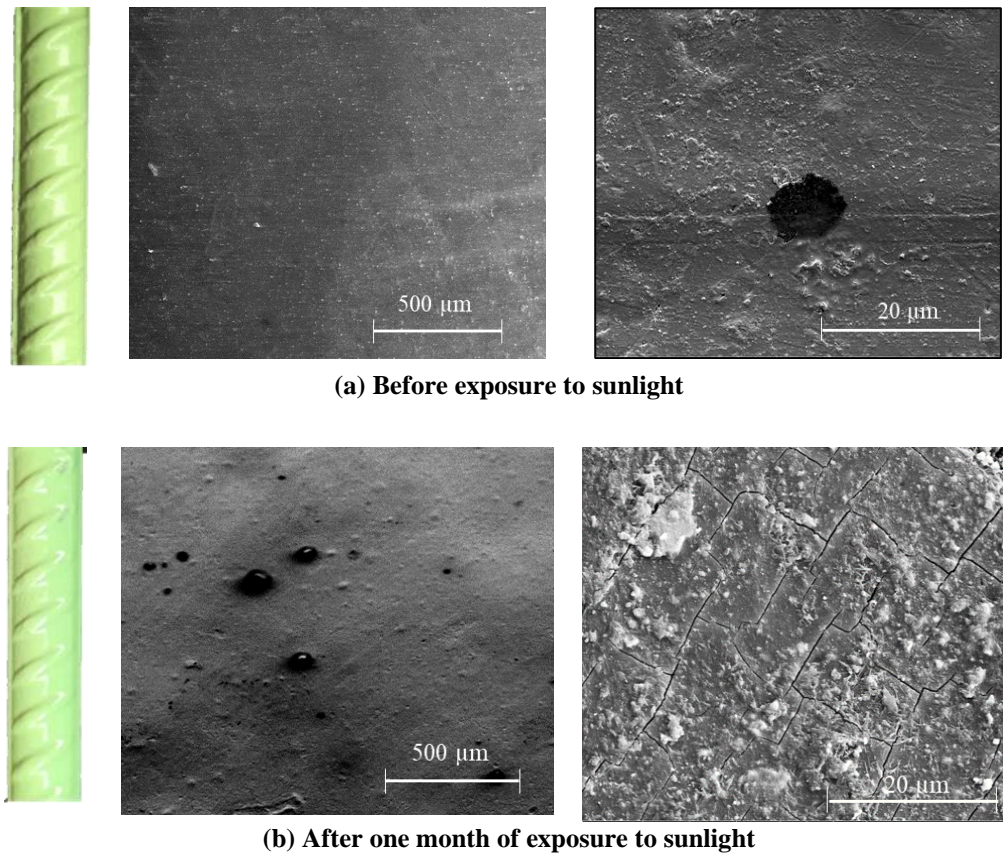
Figure 3.3 Effect of exposure to sunlight/UV on FBE coating
(obtained from same rebar lot)

3.2.6.3   Coating flexibility

Coating flexibility tests were performed as per ASTM A775. For this 8 mm diameter rebars were bent to the angle of $90°$ (instead of $180°$). After bending, the rebars were visually assessed for cracks, debonded coating, and damage to the coating.   Figure 3.4 shows that the commecially available FBE coating can crack when bent to only $90°$ (instead of $180°$, which is recommended by ASTM A775).   Bending to $180°$ can lead to wider cracks and more disbondment of coating. The cracking of coating and disbondment of coating was observed in all the ten specimens tested. Therefore, the quality of coating in commercially available FBE coated steel rebars is inferior than required for desired performance. Therefore, to achieve the good quality coating, the manufacturing process needs to be standarized. Also, the bending of

84

epoxy coated steel on site should be avoided. As suggested by ASTM A775 (2017), the FBE coated stee rebars should be coated after bending. However, providing the guidelines for bending to check the flexibility in the Table 1 of ASTM A775 (2017) can misguide the practitioners to bend the coated steel steel rebars.
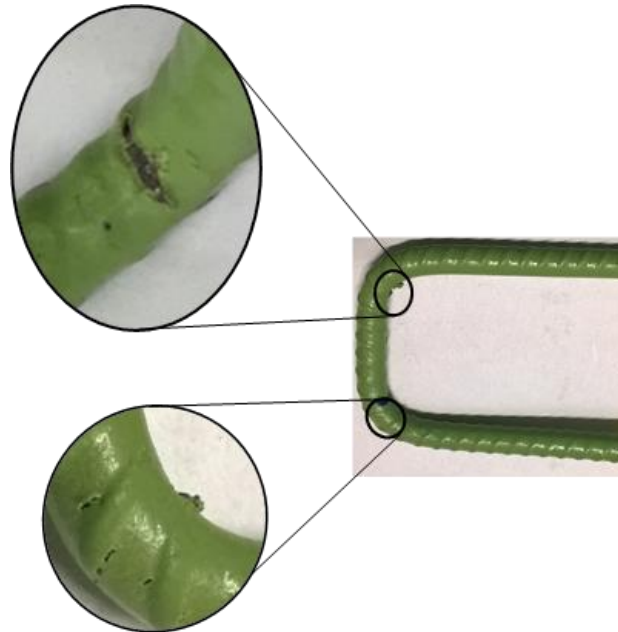
Figure 3.4 Damage to FBE coating due to bending to 90 ° (instead of 180 ° as specified by ASTM A775)

3.2.7   Cement-polymer-composite (CPC) coated steel rebars

The CPC coating consists of two coats (a rapid setting primer coat followed by a cement polymer sealant coat). Both the primer and sealant contain thermoplastic acrylic resins. In addition, the sealant is mixed with cement powder as an additive. CPC coated steel rebars are prepared as follows.

   ➢   Sandblast the steel surface

   ➢   Apply a thin layer of CPC primer; allow it to dry for a minimum of 30 minutes

   ➢   Apply the second layer of CPC primer coat; allowed to dry for 30 minutes

- Apply sealant on the primer coated steel surface; allow it to cure for a minimum of 6 hours (as per manufacturer's guideline)

- Check average final coating thickness was measured using an electromagnetic coating thickness gauge. Ensure that the coating thickness is more than the minimum recommended coating thickness of 175 μm (ASTM A775 2017). Coating thickness was maintained between 175 μm and 275 μm unless required for another testing, such as the effect of coating thickness on corrosion and bond performance.

- Moisture absorption test was conducted on ten CPC coated steels. The following test procedure was followed: Uncoated steels were weighed to the precision of 0.0001 gm (W1). Then, CPC coating was applied on the surfaces of the steel. Then, the CPC coated steels were weighed to the precision of 0.0001 gm (W2). After that, Each coated steel was immersed in a concrete simulated pore solution for 24 hours. Later, these coated steels were removed from the solution and were wiped using a cotton cloth to surface dry condition; and weighed to the precision of 0.0001 gm (W3). The difference in the mass (W3-W2) is the moisture absorbed by the coating material. The average absorbed moisture $[((W3-W2)/(W2-W1))\times100]$ after 24 hours immersion of CPC coated steel was found to be [mean:25, standard deviation: 1.33] % by weight of coating material.

- Note that the coating flexibility test was not conducted on CPC coated steel rebars because CPC coating is applied at construction sites after the rebars are bent. Also, coating contonuity test were not consucted because the mechanism of corrosion prevention of CPC coating is to provide a highly alkaline environment to delay the initiation of corrosion.

3.3 TEST PROGRAM 1: FEASIBILITY OF EXISTING TECHNIQUES FOR COATED STEEL REBARS

This objective focuses on evaluating the feasibility of conventional test methods that are used for uncoated steel rebars such as half-cell potential (HCP), macrocell corrosion current (MCC), linear polarization resistance (LPR), electrochemical impedance spectroscopy (EIS) for assessing the FBE and CPC coated steel rebars. Table 3.4 shows the test variables and the number of specimens used for Test Program 1. First, the feasibility of HCP and MCC was evaluated. Then feasibility of LPR and EIS was assessed either because the time taken to capture the initiation of corrosion was too long or because the HCP and MCC could not detect the initiation of corrosion. For this, five each of 3-bar prism and lollipop specimens were cast with following rebars: (i) uncoated, (ii) FBE coated steel with no damage (FBEC-ND), (iii) FBE coated steel rebars with scratch damage (FBEC-SD, and (iv) CPC coated steel rebar with coating on sandblasted steel surface (CPCC-AR). Here, 'no damage' indicates that no intentional damage were made on the specimens.

Table 3.4 Test variables and number of specimens for Test Program 1

Type of specimen	Testing technique	Steel surface condition	Number of specimens
3-bar prism specimens	HCP and MCC	Uncoated	5
		FBEC-ND	5
		FBEC-SD	5
		CPCC-SD	5
Total number of 3-bar prism specimens			**20**
Lollipop specimens	LPR and EIS	Uncoated	5
		FBEC-ND	5
		CPCC-SD	5
Total number of 1-bar lollipop specimens			**15**

3.3.1   3-bar prism specimens to assess the feasibility of HCP and MCC

3.3.1.1   Specimen preparation

Figure 3.6(a) shows the photograph and schematic of 3-bar prism specimens (200 × 75 × 75) mm prepared with following steel rebars (i) uncoated, (ii) FBEC-ND, (iii) FBEC-SD, and CPCC-SB (see Figure 3.5).

The rebars are placed such that the top rebar is the anode, and two bottom rebars act as a cathode, similar to the 3-bar prism specimen prescribed in (ASTM G109-07 2013). For the preparation of 3-bar prism specimens, five uncoated steel, five sandblasted uncoated steel rebars, and 15 FBE coated steel rebars of 8 mm diameter were cut to the length of 200 mm. Then, five sandblasted steel rebars were coated with CPC coating, as described in 3.2.7. To simulate the scratch damage similar to damaged coated steel rebars the construction sites, the coating for 15 rebars at the center for about 50 mm was damaged by scratching the coating on each side of the ribs of coated steel using emery paper. In total, the coating on about 7 to 9 ribs was scratched off on each coated steel rebar. Figure 3.5(b) shows the damaged FBE coated steel rebar surface. The anode-to-cathode ratio of all the specimens was maintained to 0.5, as in ASTM G109-17a (ASTM G109-07 2013). After that, 25 mm long region on both ends of all the steel was covered with electroplaters tape. This region was further covered with a heat-shrink tube to avoid entry of moisture, oxygen, or chlorides (see Figure 3.6)

(a) Uncoated steel rebar

(b) FBE coated steel with no damage

(c) FBE coated steel with scratch damage to the coating

(d) CPC coating on sandblasted steel
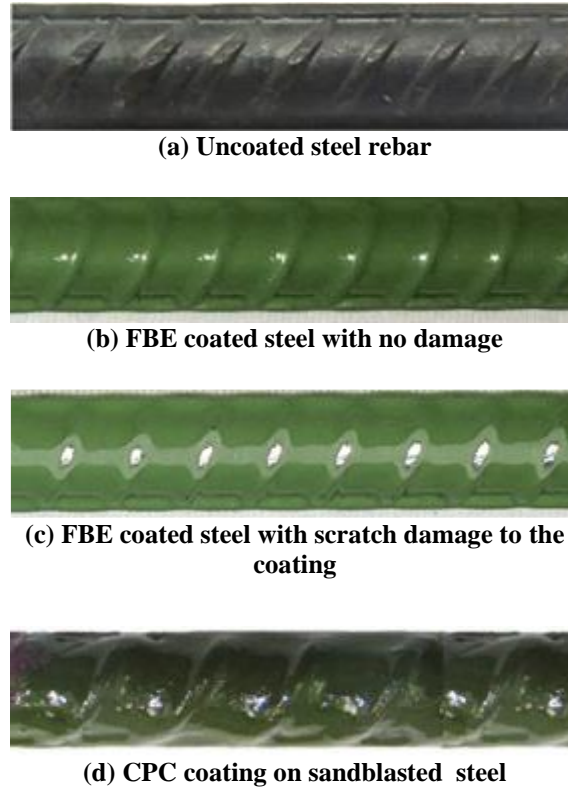
Figure 3.5 Photographs of typical rebars used to prepare 3-bar prism specimens and lollipop specimens

Figure 3.6(a) shows that the three rebars were arranged similar to that specified in ASTM G109(2013). For this, acrylic endplates were fabricated with three holes in them. The rebars were placed at the locations with holes and fastened to 20 mm long screws. After positioning, the prepared rebars were placed in the steel moulds to cast the 3-bar prism specimen. In this study, the mortar was used (instead of concrete) because Cl_{th} is a steel-concrete interface (SCI) property, and it depends on the local characteristics (or microclimate) of the SCI. The microclimate at the SCI can change due to many factors, including the presence of aggregates (Angst et al. 2017). However, the influence of the presence of inert aggregates on Cl_{th} is due to the indirect effect of the change in the microclimate of SCI. To avoid non-uniformities in the physical microclimate at the SCI, the mortar was used to prepare the 3-bar prism specimens. Also, the use of mortar can help to reduce the test duration and the size of the specimens. Many researchers have used mortar to quantify the Cl_{th} of various steel-cementitious systems

(Joseline et al. 2018; Karuppanasamy and Pillai 2017a; b; Rengaraju et al. 2019). Therefore, mortar with cement: sand: w/b of 1: 2.75: 0.5 was used to prepare the 3-bar prism specimens. The Ordinary Portland Cement (53 Grade) with the requirements confirming with IS:12269 (2008) was used to prepare the mortar for the casting of 3-bar prism specimens. The Grade II and Grade III silica sand as per IS:383 (1970) was used in equal proportion by mass (383 1970). Distilled water was used for preparing all the 3-bar prism specimens.

The mortar with cement:sand:water/binder of 1:2.75:0.5 was used. Then, the 3-bar prism specimens were cast and cured in steel moulds for one day. Then, moist cured for another 27 days. Followed by, specimens were kept in the laboratory environment (27 ± 5 °C and 65 ± 5 % relative humidity) for the remaining exposure/testing period. Electrical connections using a 100 Ω resistor were made between the top and bottom rebars [see Figure 3.6(b)]. Silicone sealant was applied on the side faces of the reservoir to enable one-dimensional chloride transport through mortar cover towards the embedded steel rebar. The same specimens were used for the assessment using macrocell corrosion current. Figure 3.6(c) shows the specimens ready for chloride exposure and testing.

.
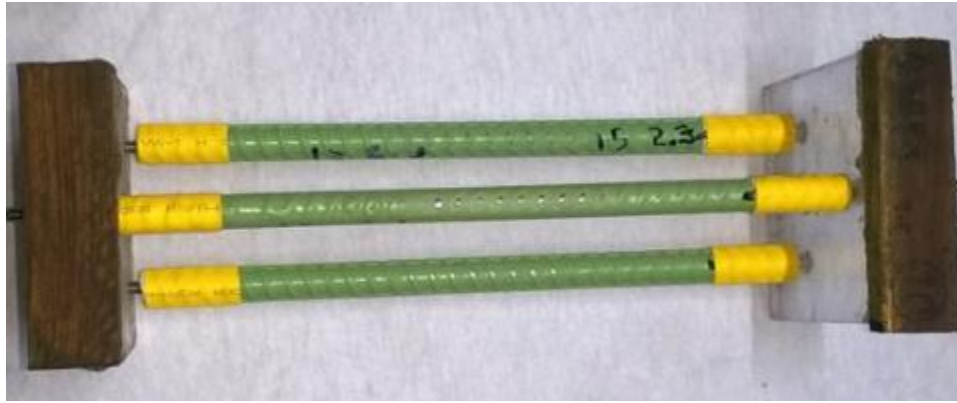
(a) FBEC-SD rebar arrangement before placing them in the mould. The similar arrangement was made for specimens with all other types of steel rebars

Note: All dimensions are in mm.
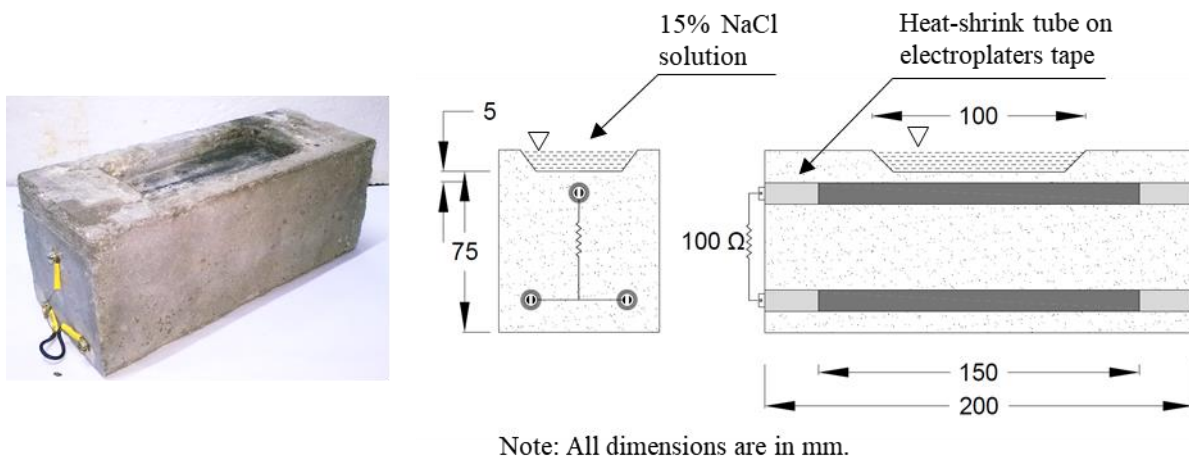
(b) Schematic and photograph of 3-bar prism specimen

(c) 3-bar prism specimens ready for exposure and testing

Figure 3.6 Details on three-bar prism specimens

3.3.1.2   Chloride exposure and an attempt to detect the initiation of corrosion

The specimens were exposed to the cyclic wet-dry regime (two days wet followed by five days dry) using 15% sodium chloride admixed simulated pore solution (0.03% $Ca(OH)_2$ + 2.3% KOH + 1.04% NaOH + 3.5% NaCl + 96.6% of distilled water) solution to accelerate the chloride transport. At the end of each wet regime, the corrosion potentials of top rebars were measured using a Saturated Calomel Electrode (SCE), and potential differences between the top and the bottom rebars were recorded across the 100 Ω resistor. Then, macrocell corrosion current at the end of each cycle and cumulative total corrosion values (total charge passed) were calculated using the trapezoidal rule. As per ASTM G109, when the total corrosion was reached to 150 Coulombs (C), the specimens were defined to have depassivated (ASTM G109-07 2013)

3.3.2   1-bar lollipop specimens for LPR and EIS

3.3.2.1   Specimen preparation

To evaluate the feasibility of LPR and EIS tests, five lollipop specimens of the following types of steel rebars were cast (i) uncoated steel, (ii) FBEC-ND, (iii) CPCC-SB. Figure 3.7 shows the steps adopted for the preparation of lollipop specimens. All the steels were cut to 110 mm length [see Figure 3.7(a)]. Then, one end of all the steel was drilled with a 3.4 mm diameter hole, and a threaded stainless-steel rod was fastened to make the electrical connections for electrochemical tests. The uncoated steel pieces were cleaned and degreased using ethanol and ultrasonic cleaner, and FBE coated steels were degreased using ethanol. Then, to prepare CPC coated steel rebars, uncoated steel rebars were coated with CPC primer and sealant coating per the manufacturers' guidelines. Then, a 5 mm long portion at the end of the coated/uncoated steel rebar was covered with a heat-shrink tube. The heat-shrink tube was extended to about 5 mm to cover the threaded stainless steel.   If any gap was observed between the threaded

stainless-steel rod and the heat-shrink tube, it was filled with was sealed with low viscosity epoxy to avoid entry of moisture or chlorides [see Figure 3.7(c)]. The prepared steel pieces were placed in 110 mm long cylindrical moulds. Mortar (similar to that used in 3-bar prism specimens) with water: binder: sand ratio of 0.5:1:2.75 was placed in moulds to achieve a cover of about 10 mm. Rebars were centered using the plastic cap with a hole in the center [see Figure 3.7(d)]. Then, the specimens were cured in plastic moulds for one day in the laboratory environment (25 ± 2 C and 65 ± 5 % relative humidity). To restrict the exposure to center, except 50 mm mortar at the center of specimens, was covered with three layers of epoxy (see Figure 3.8). This ensures that the chloride ingress will happen only through the 50 mm long uncoated portion at the center. Epoxy coating on mortar on both ends of the specimen can avoid preferential underfilm corrosion of the epoxy-coated end regions of rebars – this was verified after autopsying the specimens at the end of corrosion testing. Each layer of epoxy was cured for two to three hours, as per the manufacturers' guidelines. After curing of epoxy coats, lollipop specimens cured in fog room for 27 days. Then, specimens are ready to expose to chloride solution and testing. Figure 3.8 shows the photograph and schematic of the lollipop specimens.

(a) 110 mm long cut epoxy coated steel rebar

(b) Heat shrink tube applied at the end of FBE coated steel rebar and epoxy filled in the gap between heat shrink tube and stainless steel

(c) Plastic mould with a hole in the plastic cap

(d) Placement of mortar and 3-layer epoxy coating on both ends and a plastic cap placed at the bottom end right after the 3-layer epoxy coating

(e) Lollipop specimens ready for exposure and testing

Figure 3.7 Steps adopted for the preparation of lollipop specimens

Note: All dimensions are in mm
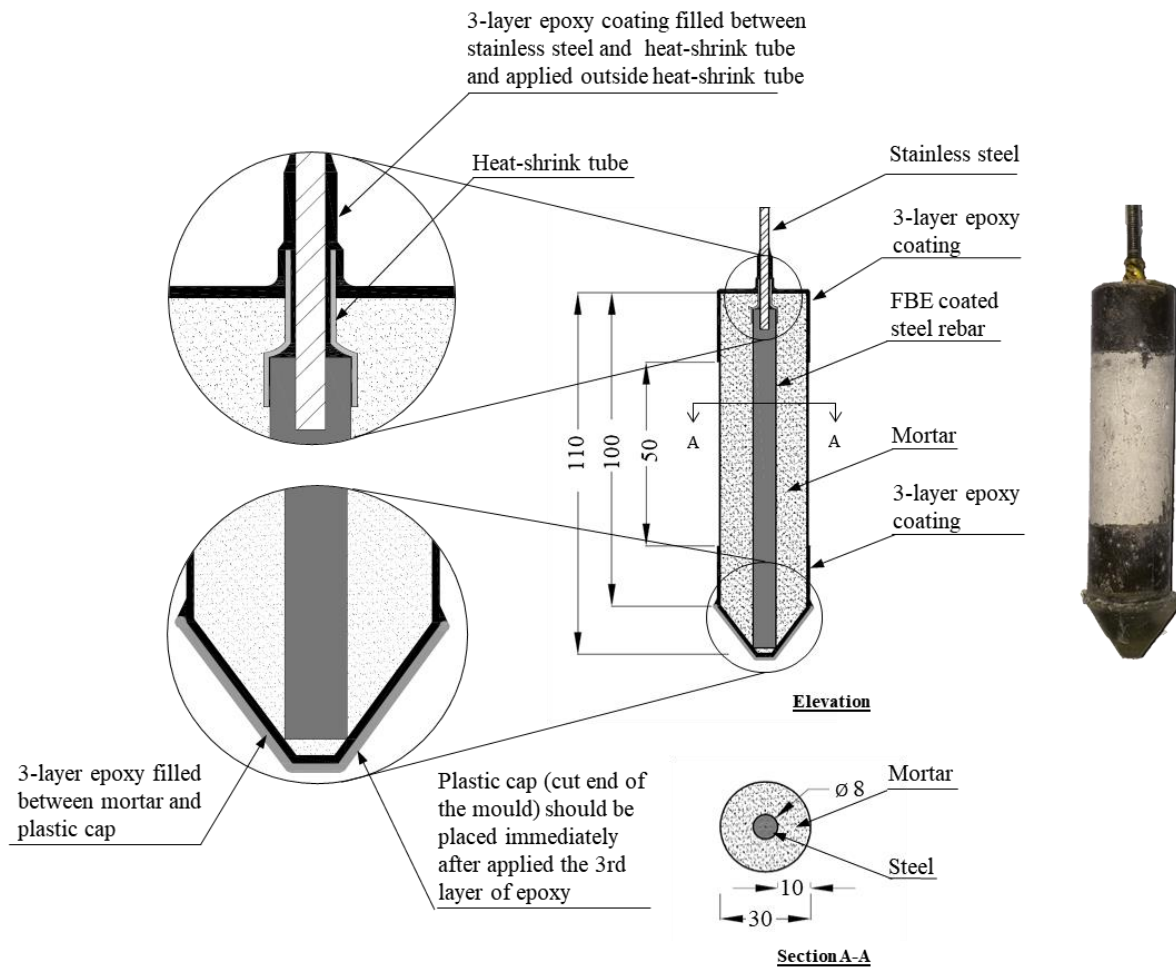
Figure 3.8 Schematic of the lollipop test specimen used for LPR and EIS test

3.3.2.2   Exposure to chlorides and initiation of corrosion

Figure 3.9 shows a three-electrode system used for cyclic exposure, and for LPR and EIS tests. In this, the embedded steel rebar was the working electrode, nickel-chromium mesh placed circumferentially to the lollipop specimen was the counter electrode (not shown in photograph); and saturated calomel electrode was the reference electrode. The simulated concrete pore solution (0.03% $Ca(OH)_2$ + 2.3% KOH + 1.04% NaOH + 3.5% NaCl + 96.6% of distilled water of total volume) contaminated with 3.5% NaCl was used as the immersion solution. LPR tests were performed after every wet period over a scan range of $\pm$ 15 mV with

respect to the HCP at a scan rate of 0.167 mV/s. The LPR curves, which is a plot of instantaneous overvoltage against instantaneous current density, were obtained at the end of every wet period, and the polarization resistance (R_p) was determined.

For the EIS study, the same corrosion cell setup was used. Following input parameters were used for the assessment, An AC potential amplitude ± 10 mV, a frequency range of 10^6 Hz to 0.01 Hz, the DC potential was maintained at HCP, 10 data points per decades were collected. The signal response was analyzed, and resistances offered by each layer (mortar, coating, steel-coating interface) were quantified using the suitable Equivalent Electrical Circuit (EEC), discussed later. Then, resistance offered by the steel-mortar interface (i.e., $1/R_P$) and resistance offered by the coating-steel interface ($R_{P,\ S-C}$) were monitored with respect to the exposure time. When five consecutive values of $1/R_P$ or $1/R_{P,\ S-C}$ lie within a boundary of $\mu \pm 1.3\sigma$, the system was considered to have stabilized (μ - mean; σ - standard deviation). Following this stable state, if two future readings lie above ($\mu \pm 3\sigma$), corrosion is said to have initiated (Karuppanasamy and Pillai 2017a; Rengaraju et al. 2019). Note that HCP, MCC, LPR could detect the initiation of corrosion in specimens with CPC coated steel rebars. As the specimen geometry used for LPR and EIS are the same. Therefore, the testing time required for the initiation of corrosion will be the same. Therefore, CPC coated steel rebars were not assessed using EIS techniques.

Note: Counter electrode (Nickle-Chromium mesh) and solution (SPS) are not shown for the clarity in the photograph and schematic
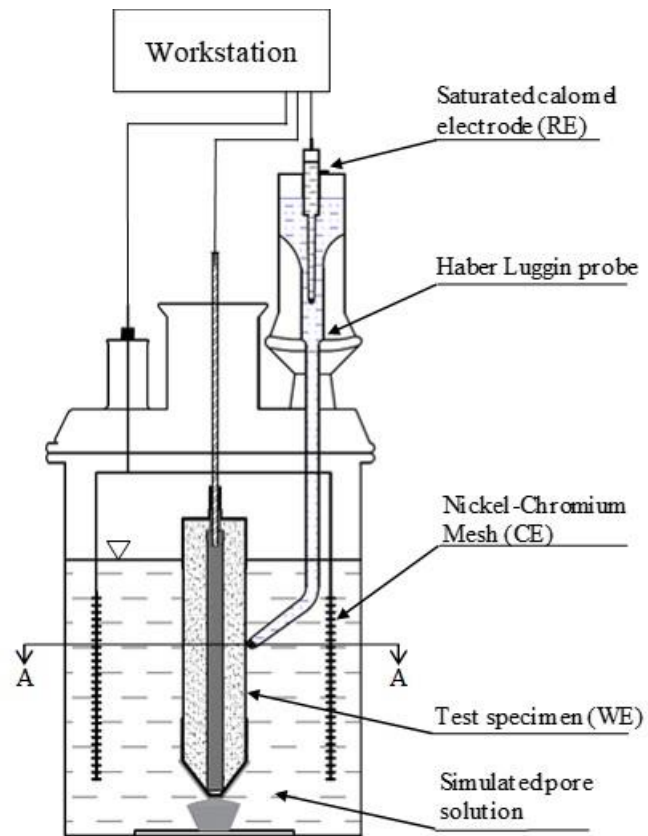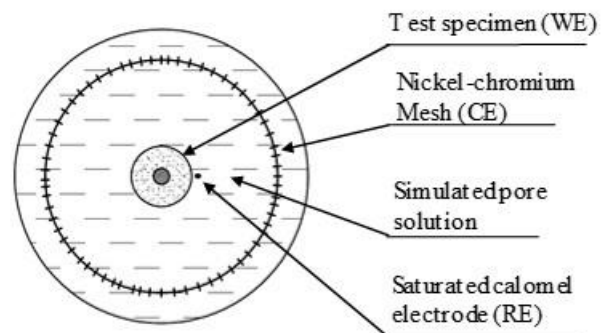
Figure 3.9 The three-electrode corrosion cell test setup for LPR and EIS test

3.4   TEST PROGRAM 2: CORROSION INITIATION OF FBE COATED REBARS

Based on the observations of Test Program 1. It was found that the HCP, MCC, and LPR could not detect the initiation of corrosion in FBE coated steel rebars. Therefore, for this test program, only EIS tests were conducted. For CPC coated steel rebars, tests based on MCC and LPR techniques were performed using 3-bar prism and lollipop specimen, respectively.

3.4.1   Phase 1 - Effect of scratch damage on corrosion initiation

To study the effect of scratch damage on the mechanism of corrosion initiation and chloride thresholds of FBE coated steel rebars, lollipop specimens with following steels were cast: (i) FBE coated steel rebars without any intentional damage or degradation (FBEC-ND) and (ii) FBE coated steel rebars with scratch damage (FBEC-SD). For comparison, lollipop specimens with uncoated steel rebars were cast. The specimens were prepared and exposed to chloride solution, in the same way, was as discussed in Section 3.3.2. For FBE coated steel rebar with damage, the chloride threshold is defined as the chloride concentration at the steel surface at the scratched location, which is required to initiate active corrosion.

Table 3.5 Number and type of specimens used for Phase 1 of Section 3.4.1

Properties	Coating conditions	Type of specimens	Number of specimens
Chloride thresholds	FBEC-ND	Lollipop specimens	5
	FBEC-SD		5
	Uncoated		5
Total number of specimens			**15**

3.4.2 Phase 2 - Effect of exposure to UV/sunlight on coating degradation and corrosion initiation

Tests were conducted to study the mechanisms of coating degradation and initiation of corrosion and to determine the chloride thresholds of FBE coated steel rebars and chloride diffusion coefficient of the coating. Table 3.6 shows the test variables and the number of specimens cast for Phase 2 of this study.

Table 3.6 Test variables and number of samples/specimens used for Phase 2

Properties	Coating conditions	Type of specimens	Number of specimens
Coating integrity	FBE coating without and with UV exposure from 0 to 60 days	5 × 5 mm coating samples	45
Chemical composition	FBEC-ND and FBEC-UV		6
Atomic bonding	FBEC-ND and FBEC-UV		6
Resistance of coating	FBEC-ND and FBEC-UV	Lollipop specimens	Five of each type (total 15)
Chloride thresholds		Coating specimen (extracted from the steel in lollipop specimen after exposure test)	Five of each type (total 15)
Chloride diffusion coefficients			Five of each type (total 10)
Total number of specimens/samples			**100**

3.4.2.1 Exposure to UV rays and coating characteristics

Typical daylight (wavelength of 300 to 340 nm) can be simulated using UVA tube lamps (340 nm), which can be used for accelerated screening tests (Laurence W. McKeen 2006). For this, a UV chamber ($1.5 \times 0.5 \times 0.5$ m) with 12 UVA tube lamps and humidifiers was fabricated, see Figure 3.11 (ASTM G154 2016). Cyclic UV exposure (8 hours with UV lights 'ON' followed by 4 hours of the humid environment with UV lights 'OFF') was maintained using a timer (Liu and Horrocks 2002). For this, the chamber was sealed, and the humidifier was run for 15 minutes at the beginning of the humid period. A total of 45 as-received FBE coated steel rebars with 'no damage or degradation' (denoted as FBEC-ND; each with 8 mm diameter and 50 mm length) were peeled off from the FBE coated steel and kept in the UV chamber for 60 days. Figure 3.10 shows the process adopted for peeling off the coating from steel surface. First, knife cut was made on the coating in a rectangular shape. Then, the steel was bent next to the location of cut. Then, the peeled off coatings were used for the exposure to UV. The cracks due to the process of peeling off of coating was investigated using SEM. No cracks were seen in the area of interest (central region of the coating sample).

(a) Knife cut on coating to peel it off the steel surface

(b) Peeled-off coating samples
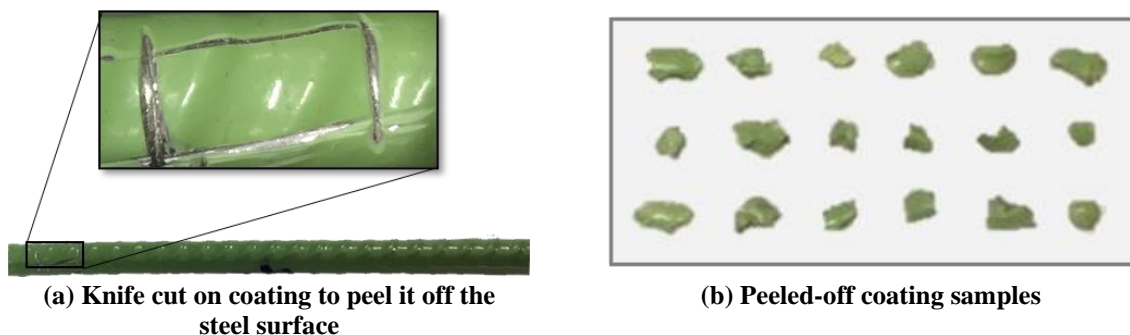
Figure 3.10 Coating samples peeled off from FBE coated steel rebars and ready for UV exposure.

The UV radiation was maintained to be uniform over the length of the tube lamps (as per ASTM G154). The three specimens each were removed after 0, 1, 3, 7, 10, 12, 15, 20, 25, 30, 35, 40,

45, 55, and 60 days of exposure. Then, the specimens were stored in a dark container until tested for changes in coating characteristics. A 5×5 mm size sample of the coating was peeled-off from the exposed surface (i.e., top surface) of each rebar specimen. Micrographs of these samples were obtained using the Scanning Electron Microscope (SEM), and the initiation and widening of cracks as a function of the duration of UV exposure were studied. The chemical composition and atomic bond characteristics of three coating samples (with 0 and 10 days of UV exposure) were obtained from three coating samples of each type using EDX, Fourier Transform – Infra-Red (FT-IR) spectraLiterature report that the epoxy-based coatings can crack between 10 and 15 days of artificial weathering (Asmatulu et al. 2011; Nikafshar et al. 2017). Similar results are observed in the current study using the artificial weathering test method prescribed in ASTM G154 (2016). Also, to obtain the relation between exposure to artificial and natural UV environment, FBE coated rebars were exposed to natural sunlight for about 1.5 months in Summer in Chennai (with temperature ranging from 24 to 39 ^{o}C, relative humidity ranging from 37 to 78%, and average UV index of 10) (Forecast 2020).

(b) Photograph of UV chamber
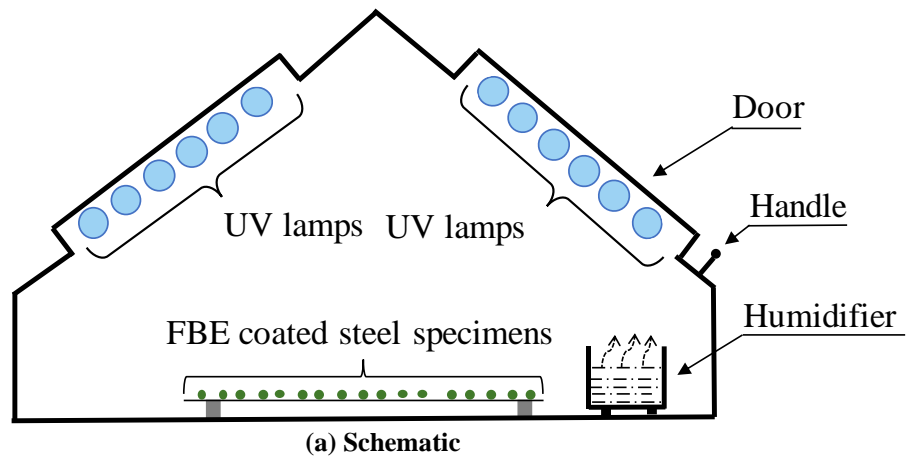
(a) Schematic

Figure 3.11 The UV chamber used for artificial weathering of FBE coated rebars

3.4.2.2 Chloride threshold of FBEC-ND and FBEC-UV

The chloride threshold is defined as the chloride concentration at the steel surface (i.e., at the steel-mortar interface for uncoated rebars and steel-coating interface for FBE coated rebars) that is required to initiate active corrosion. To evaluate the effect of exposure to sunlight/UV rays on corrosion initiation and chloride threshold of FBE coated steel rebar embedded in the cementitious system, five lollipop specimens of each type with the following type of steel reinforcement were cast: (i) Uncoated, (ii) FBE coated steel in as-received condition with 'no

damage or degradation' (FBEC-ND), and (iii) FBE coated steel with ten days of UV exposure (FBEC-UV). For this, five uncoated and ten FBE coated steel rebars of 8 mm diameter and 110 mm long were cut. Then, five FBE coated steel rebars each were placed in the UV chamber for 0 and 10 days, respectively (i.e., for casting five FBEC-ND and five FBEC-UV specimens). Later, the procedure described in Section 3.3.2 was adopted for the preparation of lollipop specimens, and exposure to chloride solution.

Upon initiation of corrosion, a mortar of 0.5 mm depth adjacent to uncoated steel and coated steel was powdered and collected. The chloride concentration in the powdered mortar was determined using the guidelines prescribed in SHRP-330 (SHRP-S-330 1993). For specimens with uncoated steel rebars, this chloride concentration was the chloride threshold. However, chloride concentration at the coating-mortar interface (Cl_{C-M}) do not participate in the corrosion activities of the underlying steel of FBE coated steel rebar. The chloride concentration beneath the coating (i.e., at the steel-coating interface) takes part in the corrosion process; hence, it is considered as the chloride threshold of the FBE coated steel rebars (Trejo 2020).

To determine the chloride concentration at S-C interface, Energy Dispersion X-Ray analysis (EDX) was done along the fractured surface of FBE coating. To avoid cross-contamination of chlorides at various depths at the cross-section of epoxy coating, the coatings for chloride measurements were not cut using a mechanical tool. Instead, the coated steel rebars were cut to half of the cross-section [see Figure 3.12(a)]. Then, the remaining half of the rebar (including coating) was bent and fractured along the cutting plane [see (see Figure 3.12(b)]. Then, chloride concentrations at the steel-coating interface were determined using EDX analysis on the micrograph of FBE coating at Location 6 in the micrograph shown in Figure 3.12(c) is the chloride threshold of FBE coated steel rebars. Note that the chloride concentration was determined at the cross-section of the coating surface, and not beneath the

coating, to avoid the involvement of the chlorides from the unknown depths of the coating. The chloride concentrations determined using this method are in % by weight of the coating. The chloride concentration in the coating, close to the steel-coating interface was determined using EDX analysis and defined as the Cl_{th} of FBE coated steel. During EDX tests, an electron beam with energy 20 keV and working distance was maintained to $\approx$ 10 mm. Note that the measured concentrations are in percentage of chloride by weight of substrate (coating with pores), which represents the local chloride concentration at the location of testing. Therefore, the average of measurements from three locations at the S-C interface was considered (in % by weight of FBE coating). To convert this to % by weight of binder (%bwob), the chloride concentrations in the mortar adjacent to the coating surface (determined as per SHRP 330 (SHRP-S-330 1993)) was considered equal to the chloride concentration in the coating adjacent to the mortar surface (determined using EDX analysis). Similarly, the relative chloride concentrations at the steel-coating interface were determined (in %bwob) from five specimens of each type and was defined as the Cl_{th} of FBE coated steel rebars

3.4.2.3   Chloride diffusion coefficient of FBE coating

As discussed earlier, the FBE coating samples were fractured and chloride concentrations at various depths along the cross-section were obtained using the EDX technique. Similar approach was adopted by (Wang and Gao (2016). Figure 3.12 (c) shows the micrograph and locations to detect the chloride concentration in the cross-section of the FBE coating. Using this framework, the three chloride profiles each from five coating samples were obtained. These chloride profiles and Fick's second law of diffusion was used to determine the chloride diffusion coefficient of the FBE coating without any damage ($D_{cl, coating}$).

Steel cut to about half
of the cross-section

Steel cross-section cut
using mechanical tool

Fractured cross-
section

(a) Steel rebar cur to about half of the cross-section

(b) Half cut and half fractured steel cross-section

Coating-cementitious interface

1
2
3
4
5
6

200 μm

Steel-coating interface

(c) Typical micrograph from fractured FBE coating
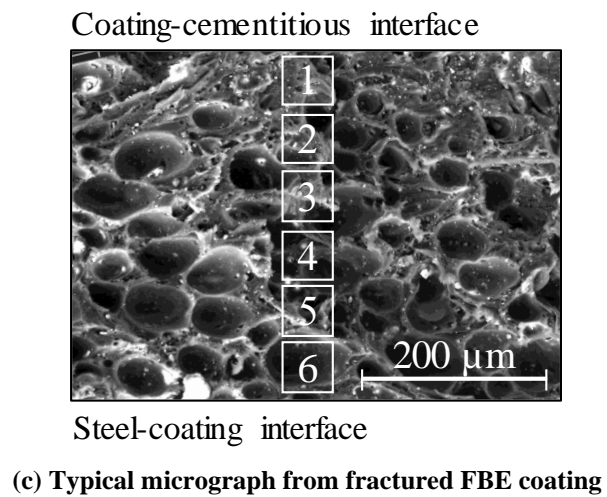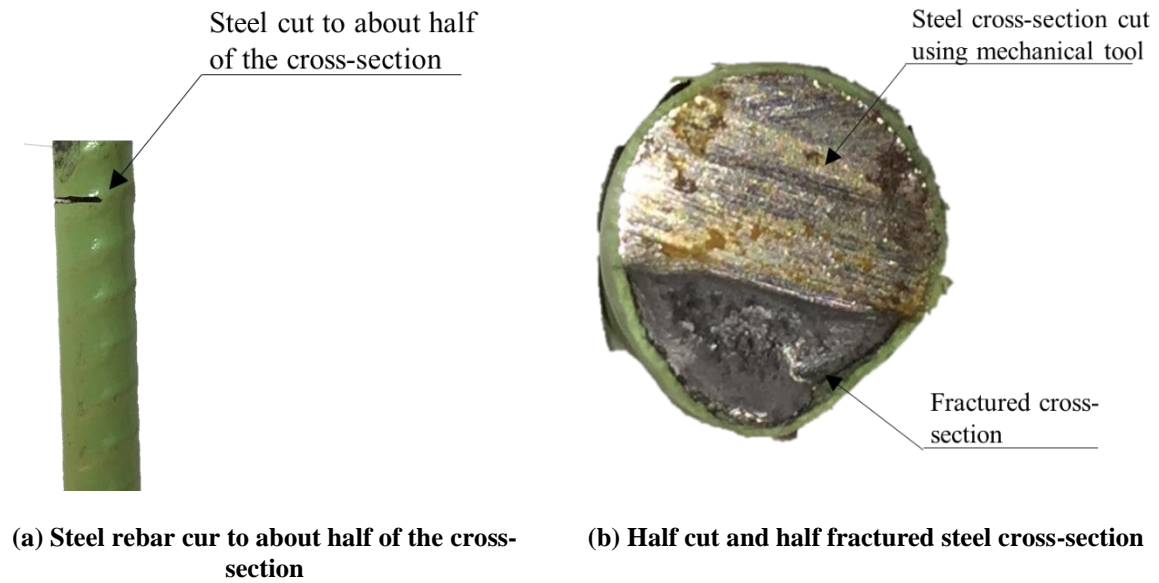
Figure 3.12 Chloride profile and diffusion coefficient of FBE coating

3.4.3 Framework for service life estimation and a case study

Figure 3.13 shows the proposed two-stage chloride diffusion model, where transport of chlorides to steel surfaces takes place through concrete and then coating. An existing service life estimation model (SL-Chlor) was modified by introducing a function for the diffusion of chlorides through the epoxy coating. The coating samples were fractured as discussed as it was done for determining chloride threshold (see Section 3.4.2.3) and then, the chloride profiles were obtained along the cross-section (say, thickness) of the fractured surface of FBE coating. These chloride profiles were used to determine the chloride diffusion coefficients of coating ($D_{cl, \ coating}$) for FBEC-ND and FBEC-UV coatings. Using the maximum chloride concentrations at the surface of concrete, Dcl of concrete, maturity constant (m), concrete cover thickness (x), Cl_{th} of steel, and the $D_{cl, \ coating}$, the service lives of reinforced concrete systems wasere estimated. For this, the MATLAB® program based on Ficks' second law of chloride diffusion through concrete published by (Rengaraju 2019) was modified to accommodate the effect of diffusion of chlorides through the thin epoxy coating (see Equation 1 and 2). For this, chlorides at concrete surface (C_S) were assumed to diffuse through concrete and reach the coating-mortar interface as per Ficks' second law of diffusion (see Equation)

$$C\,(x,t) = \ C_S - (C_s - \ C_i) \times erf\left({}^x\big/\sqrt{(4 \ \times \ D_{cl, \ concrete} \ \times t)}\right) \qquad (3.1)$$

where, '$C(x, t)$' is the chloride concentration measured at depth 'x' from the exposed concrete surface at the exposure time of 't' seconds; 'C_S' is the surface chloride concentration built-up on the exposed concrete surface after exposure time of 't' seconds; 'C_i' is the initial chloride concentration in concrete, which is assumed to be zero in this study; '$D_{cl, \ concrete}$' is apparent chloride diffusion coefficient, and 'erf()' is the mathematical error function. Here, $D_{cl, \ concrete}$ is considered as a time-variant function. Then, for each interval, the chlorides at the coating-mortar interface were considered as the surface chloride concentration of the coating. Then,

using the experimentally determined chloride diffusion coefficient of coating and Ficks' law (Equation 2), the concentration of chloride at the steel-coating interface were determined. When the concentration of chloride was equal to or more than the chloride threshold of the steel-coating interface (reported in this paper), it was defined as the corrosion-free service life (i.e., time taken to initiate corrosion) of RC systems with FBE coated steel rebars. Further details are provided in Appendix C.

$$C\left(x_{epoxy}, t\right) = C_{C-M} - \left(C_{C-M} - C_{i,\ coating}\right) \times erf\left(x_{epoxy} \middle/ \sqrt{(4 \times D_{cl,\ coating} \times t)}\right) \qquad (3.2)$$

Where, $C(x_{epoxy},\ t)$ is the chloride concentration at the depth 'x_{epoxy}' at the time 't' in the epoxy coating. x_{epoxy} is the depth in the epoxy coating from the coating-mortar interface, C_{C-M} is the chloride concentration at the coating-mortar interface, $C_{i,\ coating}$ is the initial chloride concentration in the FBE coating, and $D_{cl,\ coating}$ is the chloride diffusion coefficient of FBE coating, which is determined this study and assumed to be constant throughout the life of the RC systems

Then, as a case study, the t_i for a structural element was estimated, which is discussed later.
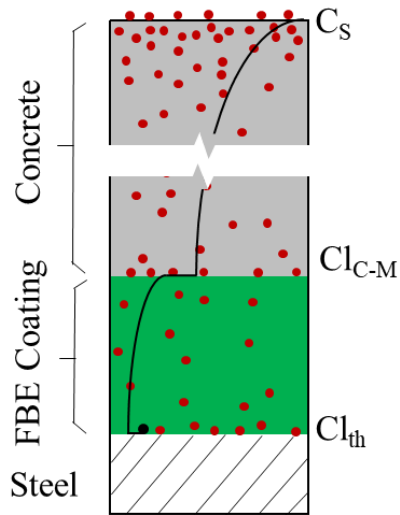
Figure 3.13 Framework for estimation of service life of RC systems with
FBE coated steel rebars

3.5 TEST PROGRAM 3: CORROSION INITIATION AND BOND DEGRADATION OF CPC COATED REBARS

This test program was divided into two phases: Phase 1 described the effect of surface preparation on the chloride threshold, and Phase 2 describes the effect of corrosion on the bond performance of CPC coated steel rebars.

3.5.1 Phase 1 - Effect of surface preparation/sandblasting of steel surface on the chloride threshold

Table 3.7 shows the details of test variables and the number of 3-bar prism and lollipop specimens cast to evaluate the effect of steel surface preparation and CPC coating on the chloride threshold of steel rebars. Following steel surface and coating conditions were studied: (i) 'as-received' steel rebar without coating (AR-woC), (i) 'as-received' steel rebar with CPC coating (CPCC-AR), (iii) 'sand-blasted' steel rebar without coating (SB-woC), and (iv) 'sand-blasted' steel rebar with CPC coating (CPCC-SB). Five 3-bar prism specimens, each with these four types of steel rebars, were prepared (total 20 specimens) and exposed to chlorides until corrosion measurements confirm the initiation of corrosion.

Table 3.7 Test variables and number of specimens for 3-bar prism and 1-bar lollipop specimens

Surface condition	Coating condition	Number of prism specimens	Number of lollipop specimens
As-received (AR)	CPCC	5	5
	woC	5	5
Sand-blasted (SB)	CPCC	5	5
	woC	5	5
Total number of specimens		**20**	**20**

woC – without coating

Figure 3.14 shows the steps to prepare the 3-bar prism specimens with CPC coated steel rebars. To prepare the CPC coated steel, one thin layer of CPC primer was applied on the uncoated steel surfaces (AR and SB) and allowed to dry for a minimum of 30 minutes [Figure 3.14 (a) and (b)]. To avoid the discontinuities in the primer coat, the second layer of CPC primer coat was applied and allowed to dry for 30 minutes. Later, sealant was applied on the primer coated steel surface and allowed to cure for a minimum of 6 hours (as per manufacturer's guideline). The average final coating thickness was measured using an electromagnetic coating thickness gauge. It was ensured that the coating thickness is between the recommended range of coating thickness, i.e., 175 – 300 μm (ASTM A775 2017). Later, the same procedure described in Section 3.3.1.1 to cast the 3-bar prism specimens. It was found that the time required for the initiation of corrosion in these 3-bar prism specimens was about one year. Therefore, lollipop specimens were cast, as per Figure 3.7, and the test procedures based on the LPR technique was adopted to detect the initiation of corrosion. In the case of CPC coated steel rebars, chloride threshold (Cl_{th}) was considered as the minimum chloride concentration required at the steel-coating-concrete interface to initiate active corrosion.

As-received

Sand-blasted

(a) steel surface condition

CPC primer coat

CPC sealer coat
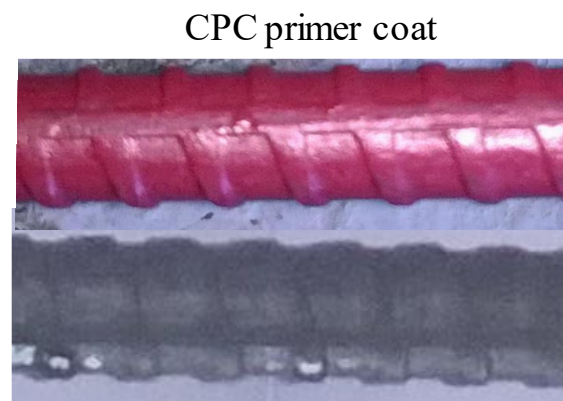
(b) CPC coated steel rebars

(c) uncoated steel rebars arrangement
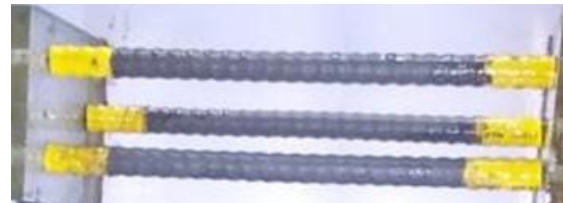
(d) CPC coated steel rebars arrangement

(e) CPC coated rebar cage placed in mould

(f) placement of mortar
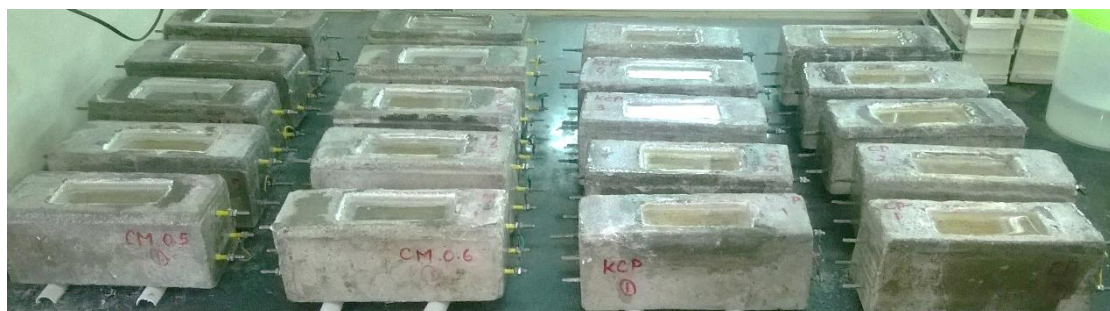
(e) 3-bar prism specimens being exposed to chloride solution

Figure 3.14 3-bar prism specimens with CPC coated steel rebars

The chloride concentration in the mortar-coating interface was considered to be the chloride threshold because the mechanism of corrosion prevention CPC coated steel rebars is based on the passivation provided by CPC coating, and not by the barrier mechanism of the coating. To confirm this, a set of additional/supplementary tests were conducted with different coating thickness (i.e., 100, 300, and 400 µm). It was found that the initiation of corrosion in the specimens were observed statistically at the same time – confirming that the CPC coating doesn't protect steel by barrier mechanism, rather it provides a stable passive film to the steel surface. Table 3.8 shows the number and type of specimens cast to understand the effect of coating thickness on time to corrosion initiation.

Table 3.8 Test variables and number of specimens for lollipop specimens for studying coating thickness and its effects on corrosion initiation

Surface condition	Coating condition	Coating thickness (µm)	Number of lollipop specimens
Cleaned steel	CPC coated	100 ± 20	5
		200 ± 30	5
		450 ± 15	5
Total number of specimens			**15**

3.5.2 Phase 2 - Effect of corrosion on bond strength of CPC coated steel rebars

3.5.2.1 Preparation of pull-out specimens

Table 3.9 shows the test variables and number of specimens cast to investigate the effect of CPC coating and corrosion on the bond performance of uncoated steel rebars. For this, 35 steel rebars of 700 mm length 12 mm diameter were cleaned and degreased using ethanol to avoid the influence of any foreign element (rust layer, oil, grease etc.) on the bond between steel and

concrete. Then they were coated with CPC primer and sealer coats (as per manufacturers guidelines). The total coating thickness for 15 specimens was maintained between 175 – 275 µm (as per IS 13620: 2015 and (ASTM A775 2017)). The coating thickness of five specimens was maintained to 90 ± 15 µm, and for the remaining five, it was maintained between 400 to 450 µm. The pull-out specimens of (150×150×150) mm with 12 mm diameter main steel rebar (MSR) with 70 mm embedded length were cast (as per RILEM TC RC 6, 1983 and (IS-2770 (Part-I) 2007)). The remaining 80 mm of main steel rebar (MSR) was covered with PVC pipe of 14 mm internal diameter. To avoid movement of PVC pipe and to avoid the entry of the cementitious paste or mortar, the double-sided tape was inserted between the gap between MSR and PVC pipe. The spiral steel reinforcement (SSR) was placed around the main reinforcement at about 55 mm away from the MSR to avoid the splitting of concrete due to hoop stresses developed during testing (see Figure 3.17).

Table 3.9 Test variables and number of specimens

Parameter	Uncoated (U)	CPC coated (C)
Compressive strength, f_c (MPa)	30 ±4	30 ±4
Embedment length, L_e (mm)	75	75
Number of specimens	10	25

To study the effect of corrosion on bond performance of uncoated and CPC coated steel specimens, pull-out specimens were cast by embedding MSR (12 mm diameter uncoated and CPC coated steel rebars) in chloride contaminated concrete (2% NaCl by weight of cement) in the removable cylindrical pipe of 100 mm diameter. To avoid chloride contamination of SSR, the space between MSR and PVC pipe was filled with chloride contaminated. The remaining space in the mould (i.e., outside the PVC pipe) was filled with uncontaminated concrete.

Therefore, the SSR remains in contact with uncontaminated concrete, which protects it from corrosion and its influence on the bond strength of MSR and concrete. All the test specimens were cured in steel moulds for one day in laboratory condition (25 ± 2 C and $65 \pm 5\%$ relative humidity) and then cured in fog room (25 ± 2 C and $90 \pm 5\%$ relative humidity).

(a) Section A-A

(b) Front view
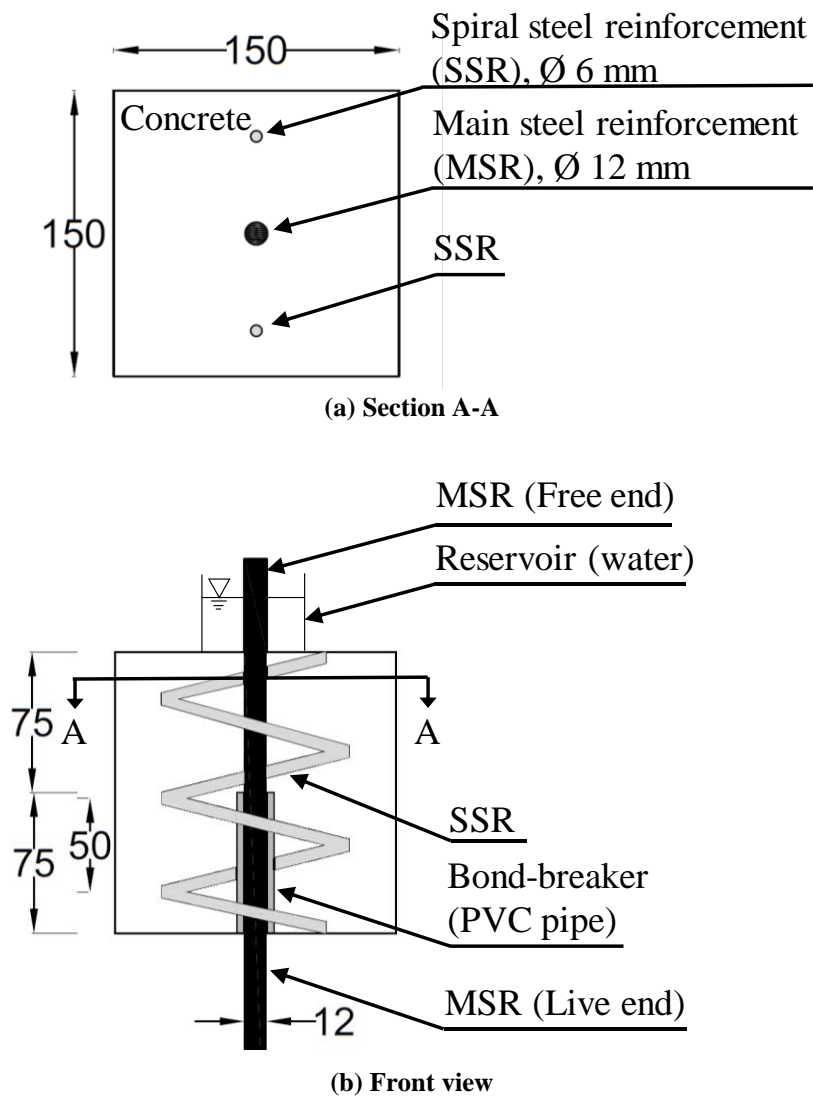
Figure 3.15 Schematic and photograph of pull-out test specimen
(as per RILEM TC RC 6 1983)

114

3.5.2.2 Degree of corrosion/ Corrosion rate measurement

Figure 3.16 shows the pull-out test specimens being exposed to moisture to initiate the corrosion process of MSR. Cyclic 14 days wet and 14 days dry exposure regime was maintained until the corrosion rate was found to be more than 2 mA/m^2 for two consecutive cycles. A handheld corrosion rate meter was used to measure the corrosion rate at the end of each wet regime. Once the corrosion rate of 2 mA/m^2 was observed for two consecutive wet regimes, the exposure to moisture was stopped, and specimens were stored in the laboratory condition until tested. Note that all the specimens were tested at the end of six months after the curing period. All the specimens were stored to avoid the effect of hydration/maturity of concrete and S-C/S-C-C interface properties. Then, the pull-out specimens were tested using the pull-out test setup shown in Figure 3.17 as per IS-2770 (Part-I) 2007.

Figure 3.16 Pull-out specimens with admixed chlorides

3.5.2.3   Pull-out testing

Figure 3.17 shows the pull-out tests setup. A pull-out frame with top and bottom plates connected by four vertical steel pipes was used. The top plate of the frame was connected to a rod with a swivel joint. While testing, this rod was gripped at the edge of the universal testing machine. A hole with a diameter of about 14 mm was provided at the center of the bottom plate, from where the live end of MSR was projected out, and concrete cube was rested on the bottom plate. The live end of MSR was gripped at the bottom edge of the universal testing machine. LVDT was placed at the free end and was connected to MSR and rested on the top of the concrete surface. The LVDT measured the relative displacement between the MSR and concrete surface, which is the slip of MSR with respect to the surrounding concrete. Note that the concrete surface was finished to make the smooth surface for resting the LVDT. The loading to MSR was applied from the live end at a rate of 1 mm/min. The Load-slip response was collected from a data logger. Ten points per second were recorded. The detailed description of the frame used for testing is provided in (Mohandoss 2019). The maximum bond stress was taken as the bond strength of the steel-concrete interface. The slope of the linear portion of the curve before the 0.5 mm slip was considered to be the bond stiffness of the coated/uncoated steel-concrete interface.
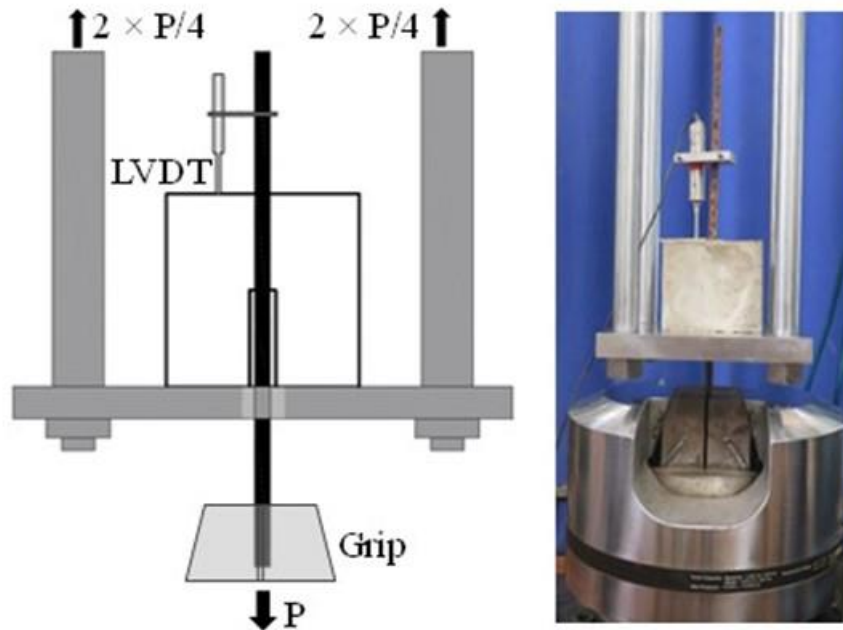
Figure 3.17 Schematic and photograph of the pull-out test setup

3.5.3 Framework for service life estimation and a case study

3.5.3.1 Details of the case study structure

A 6-year old concrete bridge located in the chloride-rich environment (within 2 km from the sea) of a coastal city in India was considered for this study. Figure 3.18(a) shows the schematic showing the girder, pier, pile cap, and pile of this bridge. The bridge experiences around 4 months of heavy rain in a year and the ambient relative humidity ranges between 70 and 85 % during the rest of the year. Therefore, sufficient moisture is expected to be always available at the surface of the embedded rebar. This makes it a favorable condition for the chloride-induced corrosion process (Hussain 2011). The desired service life of the bridge is 120 years. To achieve this long lives, the CPC coated steel rebars were proposed by designers. However, CPC coating was applied on the 'as-received' steel surface. (instead of 'sand-blasted' steel surface). This practice can lead to poor corrosion resistance. Cementitious binders with 25-30 % Class - F fly ash was used in making the M60, M45, M35, and M35 grade concrete for the girders, piers, pile caps, and piles, respectively (see Table 3.10 for mix design).

Table 3.10 Details of the concrete mix used in the bridge

Ingredient	Pile cap and pile (M35), kg	Pier (M45), kg	Girder (M60), kg
Cement (C)	280	390	440
Fly ash (F)	130	145	125
20 mm aggregate	438	0	500
12.5 mm aggregate	605	802	687
Manufactured Sand	737	953	640
Total water	223.6	215.9	183.0
(C+F): FA: CA	1:1.45:2.05	1:1.76:1.48	1:1.13:2.10
Admixture (%bwob)	0.55	0.70	1.10
Retarder (%bwob)	0.10	0.20	0.1

The bridge being in a coastal city, the governing deterioration mechanism could be chloride-induced corrosion. As a conservative practice, service life can be considered as the time to corrosion initiation, t_i, which is defined as the time taken by the chlorides to travel through the cover concrete to reach the steel rebar and initiate the active corrosion. The t_i can be estimated by using the (i) the maximum chloride concentration at the concrete surface (C_{max}), (ii) the chloride diffusion coefficient of cover concrete (D_{cl}), and (iii) the critical chloride threshold of the steel-concrete interface (Cl_{th}) and the Fick's 2nd law of diffusion. To obtain C_{max} and D_{cl}, cylindrical concrete specimens of about 90 mm diameter and 100 mm length were extracted from the girder, pier, pile cap, and pile elements, and laboratory experiments were performed. To determine the Cl_{th}, the as-received and sand-blasted rebars were collected from the bridge site. Then, the CPC coating was applied, and experiments were performed in the laboratory. In this, the effect of surface preparation on the Cl_{th} of rebars was studied. Details on the experimental programs adopted to determine these parameters are discussed next.
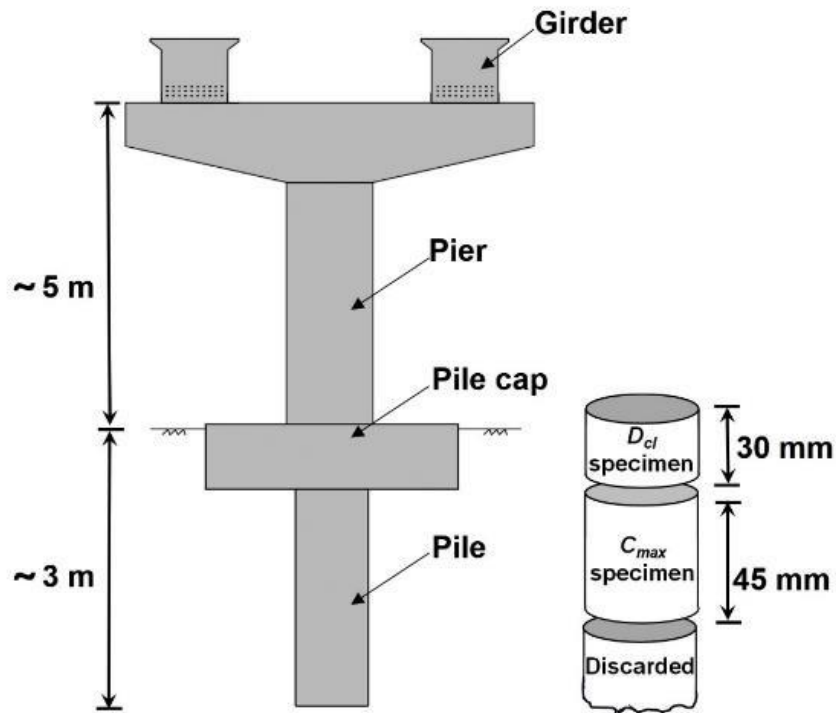
Figure 3.18 Schematics of the bridge elements under study and cylindrical concrete specimens cored from the bridge elements [Not drawn to scale]

3.5.3.2 Maximum chloride concentration at the exposed concrete surface (C_{max})

C_{max} is the maximum chloride concentration that can get accumulated on the exposed surface of the concrete. The C_{max} depends on water-to-binder ratio (w/b), the percentage of fly ash in the cementitious binder, cement content, and the ambient chloride concentration (Shakouri and Trejo 2018). Many literature report that surface chloride concentration increases with the exposure time (Ann et al. 2009; Shakouri and Trejo 2017; Song et al. 2008). Therefore, C_{max} can be determined by long-term exposure (say, several years) of the concrete specimen to the chloride-rich environment. However, such long exposure may not always be possible. Nemecek et al. (2018) and Devi (2012) reported that accelerated testing underestimates the C_{max}, leading to the overestimation of service life (Němeček et al. 2018; Nuralinah 2012). The

aim of this study is to compare the service life of various elements of the bridge with different steel surface conditions. Therefore, rapid migration tests (i.e., NT-build 492) were conducted on concrete specimens extracted from the bridge (NT Build 492 1999). It was experimentally found that the chloride concentration was less than 0.04 %bwob at depths greater than 30 mm from the surface. Hence, a 45 mm thick slice was cut from the extracted cylindrical core specimen for C_{max} study, as shown in Figure 3.18(b). The experimental test setup used for the migration test was the same as that described in NT-build 492. After the completion of the migration test, the average chloride concentration of the 5 mm thick concrete layer in contact with the chloride solution (during the migration test) was determined and defined as C_{max}. Later, this C_{max} was used to determine the time to corrosion initiation.

3.5.3.3   Chloride diffusion coefficient of concrete (D_{cl})

Figure 3.18(b) shows the 30 mm thick test specimen sliced from the extracted core and used to determine D_{cl}. As per ASTM C1556 (2015), chloride profiles up to 25 mm were obtained for each specimen (ASTM C1556 − 11a 2015). Lathe machine and single head diamond dresser tool were used for grinding these concrete specimens. The powdered samples from each layer were collected, and chloride concentrations were determined as per SHRP-S-330 (1993) (SHRP-S-330 1993). Later, these chloride profiles and Fick's second law (Equation 3-1) were used to determine the D_{cl}.

$$C(x,t) = C_s - (C_s - C_i) \times erf\left(\frac{x}{\sqrt{4 \times D_{cl} \times t}}\right) \qquad \textit{3-1}$$

where, $C(x, t)$ is the chloride concentration measured at depth 'x' from the exposed concrete surface at an exposure time of t seconds, 'C_s' is the surface chloride concentration built-up on the exposed concrete surface after exposure time of t seconds, 'C_i' is the initial chloride concentration (assumed to be zero in this study), 'D_{cl}' is the apparent chloride diffusion

coefficient, and *erf*() is the mathematical error function. Here, D_{cl} is considered as a time-variant function and determined by using Equation 3-2,

$$D_{cl}(t) = D_{cl} \times \left(\frac{t_0}{t}\right)^m$$

3-2

where $D_{cl}(t)$ is the chloride diffusion coefficient at time *t*, D_{cl} is the chloride diffusion coefficient of concrete at the age of 28 days, *t* is the age of the bridge in days, 't_0'is age equal to 28 days, and *m* is the decay constant, which was calculated using Equation 3-3 (Bentz 2003).

$$m = 0.2 + 0.4 \left(\frac{\% \ of \ fly \ ash}{50}\right)$$

3-3

3.5.3.4   Chloride threshold and service life of RC systems with CPC coated steel rebars

The chloride threshold (Cl_{th}) is the minimum chloride concentration required at the steel-coating-concrete interface to initiate active corrosion. The Cl_{th} for estimation of service lives of RC elements were determined as explained in Experimental Program 3.5.1. Using these input parameters (C_{max}, D_{cl}, Cl_{th}, *m*, etc.), the service lives of RC elements were estimated using the proposed service life model.

3.6   SUMMARY

This chapter presented the materials used and the methodology adopted for the experimental programs to achieve the objectives defined in Chapter 1. Table 3.11 provides justification for considering various test variables and test methods for each of the objectives of this thesis.

Table 3.11 Summary of test methods for each objective of this thesis

Objectives	Variables/tests considered	Justification for conducting or eliminating the task
Objective 1	FBE coated steel rebars MCC, HCP, LPR, EIS	HCP, MCC, and LPR could not detect the initiation of corrosion. Therefore, the feasibility of the method based on EIS was evaluated.
	CPC coated steel rebars MCC, HCP, LPR	Except for HCP, MCC and LPR could detect the initiation of corrosion. But, MCC was a time-consuming test method. Therefore, short-term test method based LPR was suggested.
Objective 2	Effect of damage to the coating	These inadequate practices were witnessed at many construction sites, and they were not reported in the literature
	Effect of exposure to sunlight	
	Two-stage chloride diffusion to estimate service life	Existing service life models do not consider the diffusion of chlorides through coating. An existing MATLAB® program SL-Chlor was modified to accommodate the diffusion of chlorides through coating
Objective 3	Effect of surface preparation	CPC coatings are applied at the construction sites, and the application of the coating on rusted rebars was found to be a widespread and is a major concern.
	Effect of corrosion on bond	CPC coated steel rebars are newly introduced coated steels. Therefore, literature are not available on the bond performance of RC systems with CPC coated rebars.
	Service life based on bond degradation	The mechanism of corrosion protection was dominated by providing stable passive film and not by chloride transport through the coating. Also, bond degradation was found to be significant after the initiation of corrosion. Therefore, a framework for estimating service life was proposed based on corrosion initiation and bond degradation.

Note: CPC: cement-polymer-composite; EIS: electrochemical impedance spectroscopy; FBE: fusion-bonded-epoxy; HCP: half-cell potential; LPR: linear polarization resistance; MCC: macrocell corrosion current; RC: reinforced concrete

4   RESULTS - FEASIBILITY OF EXISTING TECHNIQUES TO DETECT CORROSION INITIATION OF COATED STEEL REBARS

4.1   INTRODUCTION

This chapter presents the results obtained from the experimental investigation to achieve Objective 1, for which test methods based on techniques such as half-cell potential (HCP), macrocell corrosion current (MCC), linear polarization resistance (LPR), and electrochemical impedance spectroscopy (EIS) are assessed. The challenges associated with each test methodology is discussed. Then, a suitable technique and test methods for FBE and CPC coated steel rebars are suggested.

4.2   FUSION-BONDED-EPOXY (FBE) COATED STEEL REBARS

4.2.1   Half-cell potential (HCP)

Figure 4.2(a) shows the HCP for uncoated steel rebars embedded in 3-bar prism specimens. For each specimen, when the HCP drops below $-270\,\mathrm{mV_{SCE}}$, the embedded steels were confirmed to have the onset of corrosion by visual observation of corroded steel surfaces by autopsying the specimens. Whereas, Figure 4.3(a) shows the HCP for FBE coated steel rebars with no damage (FBEC-ND). Note that ASTM C876 is applicable only to uncoated steel rebars embedded in concrete. However, many researcher tend to use the same for assessment of RC systems with FBE coated steel rebars. HCP measurements of steel in concrete is challenging due to the high resistivity of concrete, the varying relative humidity of concrete, etc. (Elsener et al. 2003). In addition, the large ohmic drop across coating is a challenge for HCP measurements of RC systems with coated steels. The collective effect of these can lead to erroneous interpretation of the measurements of the corrosion potential of underlying steel in coated rebars (Singh and Ghosh 2005). In this study, The HCP measurements for FBEC-ND

123

were found to be unstable throughout the exposure time – indicating that HCP measurements may not reflect the corrosion activities of underlying steels. For FBE coated steel with damage (FBEC-SD), Figure 4.4(a) the HCP measurements were found to be stable after about one week of exposure to chloride solution. The HCP value for FBEC-SD3 and SD5 dropped below −270 mV$_{SCE}$ – indicating the initiation of corrosion, which was confirmed with autopsied 3-bar prism specimen. At the same time, FBEC-SD1 and SD4 were also autopsied, and it was found that the corrosion was initiated at the scratch damage locations in all the rebars. However, initiation of corrosion was not evident from HCP measurements. Figure 4.5(c) shows the corroded steel surface of FBEC-SD4 specimens as the evidence on HCP measurements and interpretation using ASTM C876 may mislead the interpretation. . Here, HCP values of two out of four specimens were found in good agreement with corrosion activities at FBEC-SD steel rebars. The agreement for two specimens can because the saturated calomel electrode (SCE) was placed on the mortar surface right above the location of the damaged coating. In large scale RC systems, the locations of scratch damage are not known. Therefore, the candidate highly recommends not to rely on the HCP measurement for the assessment of structures with FBE coated steel rebars. Figure 4.1 shows that the schematic with HCP measurements on concrete surface with embedded high dielectric FBE coating. Here, R$_{coating}$ >>> R$_{concrete}$. Therefore, there will be significant ohmic drop across the coating and concrete during HCP measurements (Elsener et al. 2003). Therefore, it can be concluded that the HCP measruement and interpretation of results using ASTM C876 (which is meant to be for RC systems with uncoated steel rebars) do not represent the corrosion activity of RC systems with FBE coated steel rebars. However, new interpretation strategy should be developed to use the HCP measurement for RC systems with FBE coated steel rebars, which is out of spope of this thesis.

Note $R_{coating} \ggg R_{Concrete}$
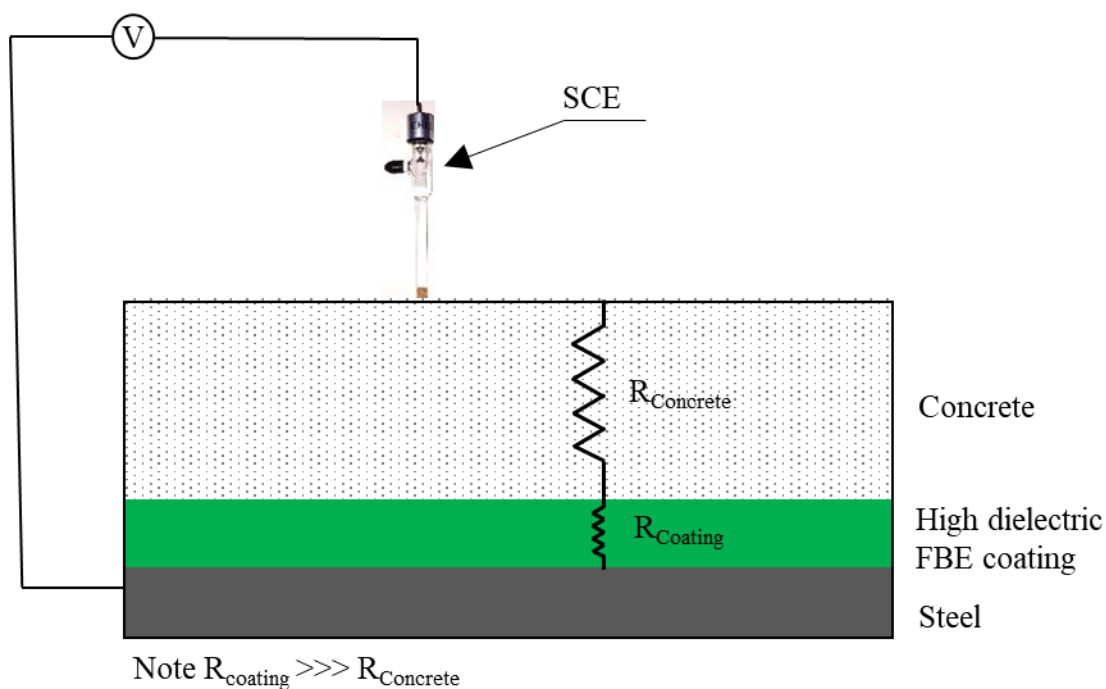
Figure 4.1 Schematic with HCP measurements of RC system with steel rebars coated with high dielectric coating material

4.2.2 Macrocell corrosion current (MCC)

Figure 4.2(b) shows the total corrosion values spiked up to 150 C at the same instance when HCPs reached below -270 mV$_{SCE}$. This indicates the good agreement between initiation of corrosion and criteria prescribed in ASTM G109 and ASTM C876 for specimens with uncoated steel rebars. The initiation of corrosion was confirmed with autopsied 3-bar prism specimens. Figure 4.3 and Figure 4.4 show the total corrosion for 3-bar prism specimens with FBEC–ND and FBEC-SD steels, respectively. Here, very low corrosion or no detectable pattern in the total corrosion was observed even after one year of exposure to 15% NaCl solution. However, the onset of corrosion for specimens with scratch damage to coating was confirmed by visual observation of steel rebars after autopsying the 3-bar prism specimens after about 100 days of exposure. Also, the vertical arrows and dash line represents that the initiation of corrosion was detected when tested using EIS techniques. However, the exposure

of 3-bar prism specimens to chloride solution and testing was continued for more than one year to confirm that HCP and MCC measurements do not show detectable patterns even after prolonged exposure to chloride solution after initiation of corrosion.
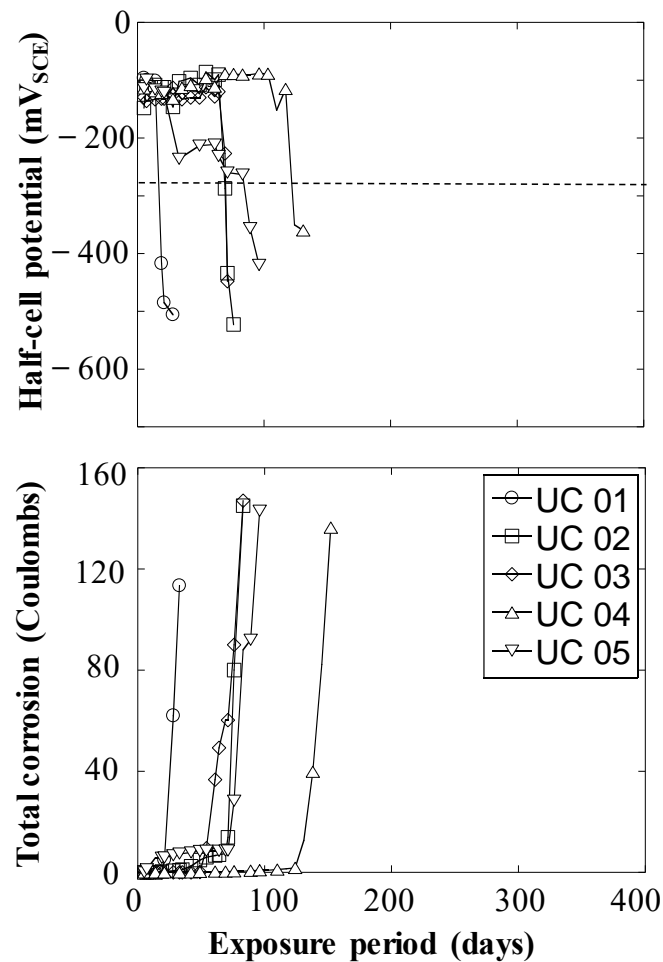
Figure 4.2 Calculated total corrosion and measured half-cell potentials from 3-bar prism specimens with uncoated steel rebars
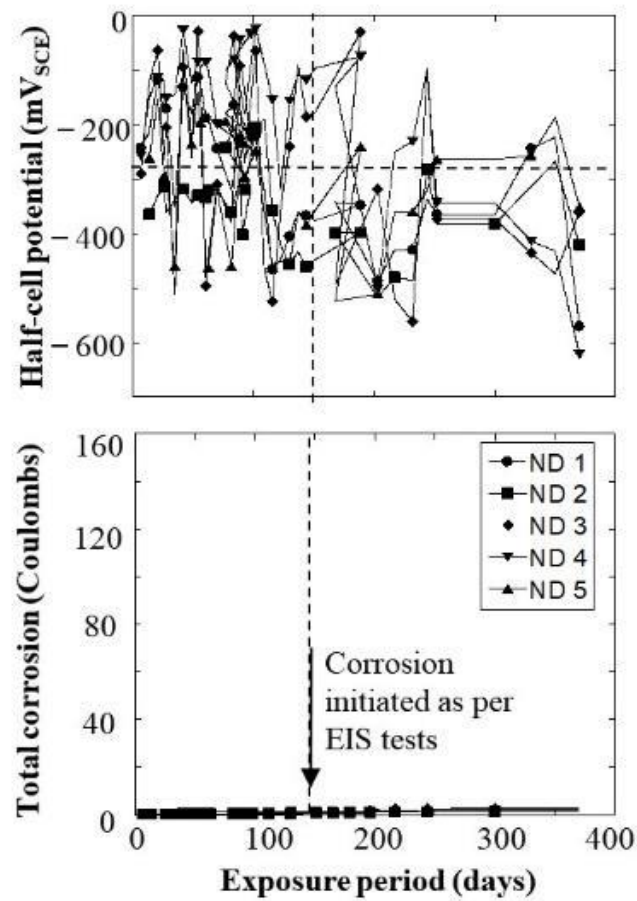
Figure 4.3 Calculated total corrosion and measured half-cell potentials from 3-bar prism specimens with FBE coated steel rebars without damage
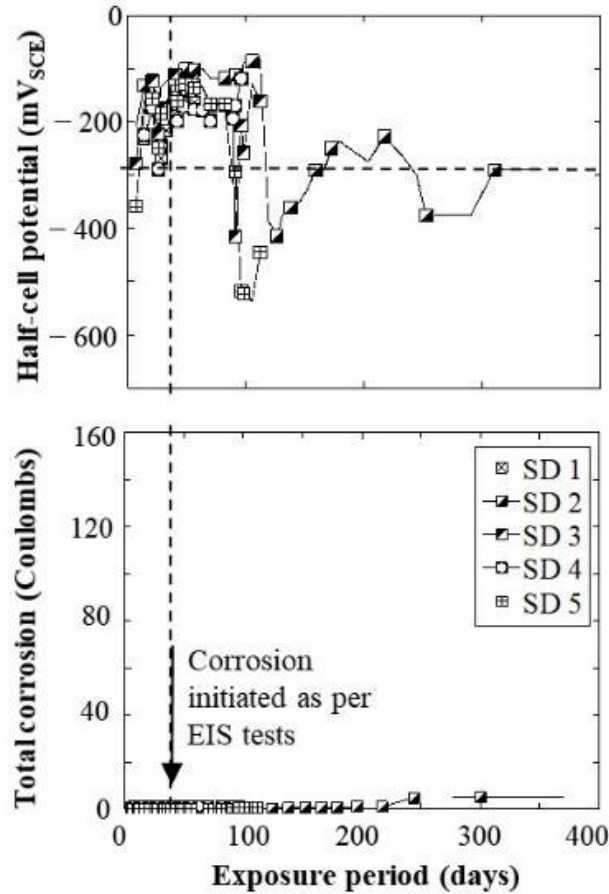
Figure 4.4 Calculated total corrosion and measured half-cell potentials from 3-bar prism specimens with FBE coated steel rebars with damaged coating

Figure 4.5(a) and (b) show the difference in the 3-bar prism corrosion circuits in the case of uncoated and coated steel rebars. Figure 4.5(a) shows that the corrosion cell forms between the top and bottom rebars. The top rebar is close to the reservoir and becomes the anode, and bottom rebars are away from the corrosive environment and are cathode. The formation of corrosion cell between the top and bottom rebar is possible because the resistance offered by the mortar between the top and bottom rebars is significantly low. On the other hand, the resistance FBE coating is significantly high (in this study, $10^3 – 10^4$ $\Omega.cm^2$), and hence, the ionic conduction do not take place between the top and the bottom rebar. Therefore, the corrosion cell forms across various points in the top rebar itself – without the participation of

128

the bottom rebars. Such corrosion may not be reflected in the macro cell corrosion current measurements made across the resistor (see Figure 4.5 (a) and (b)) in MCC tests. Likewise, because of the high ohmic drop across the FBE coating, the HCP measurements made using ASTM C876 did not reflect the true corrosion activities at the steel surface, except when measurements are taken on the damaged coating location, which is not known in RC systems. Figure 4.5(c) shows visible corrosion of steel on the scratches at the center of the rebar – proving the inadequacy of MCC and HCP measurements in detecting the ongoing corrosion in coated rebars. This also shows that only one rebar is required for the assessment of FBE coated steel rebars. Therefore, lollipop specimens were cast to evaluate the feasibility of LPR and EIS [see Section and Figure 3.8].
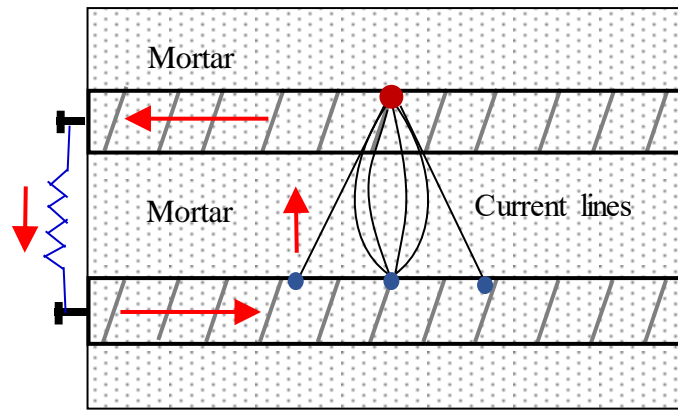
(a) Macrocell corrosion across uncoated steel rebars
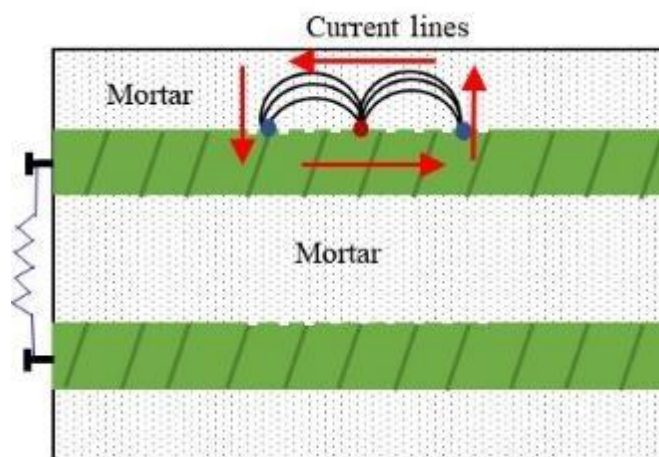
(b) Macrocell on same rebars
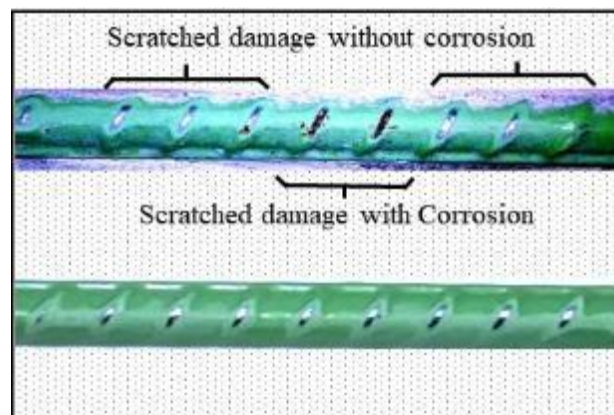
(c) Corrosion mechanism in FBE coated steel rebars with damage

Figure 4.5 Difference in the macrocell corrosion circuits (see arrows) in cases of uncoated and damaged FBE coated steels embedded in mortar/concrete

4.2.3 Linear polarization resistance (LPR)

Figure 4.6 shows a typical LPR response from uncoated steel embedded in the cementitious system. This (E-I) curve is fit to get the resistance to polarization, which is indirectly proportional to the rate of corrosion. Therefore, the higher the resistance to polarization (R_p), the lower is the rate of corrosion. Therefore, when there is a sudden increase in the $1/R_p$ – representing the initiation of corrosion. Figure 4.7 shows the variation of $1/R_p$ for uncoated steel rebars embedded in the cementitious system and exposed to chloride. Note that when corrosion initiates, the rate of corrosion is significantly higher than that in the case when steel is in the passive state. Also, in the case of uncoated steel, rebars embedded in low resistive material do not have a large ohmic drop – resulting in a detectable pattern when corrosion initiates (Kessler and Sagüés 2020; Zhou et al. 2018).
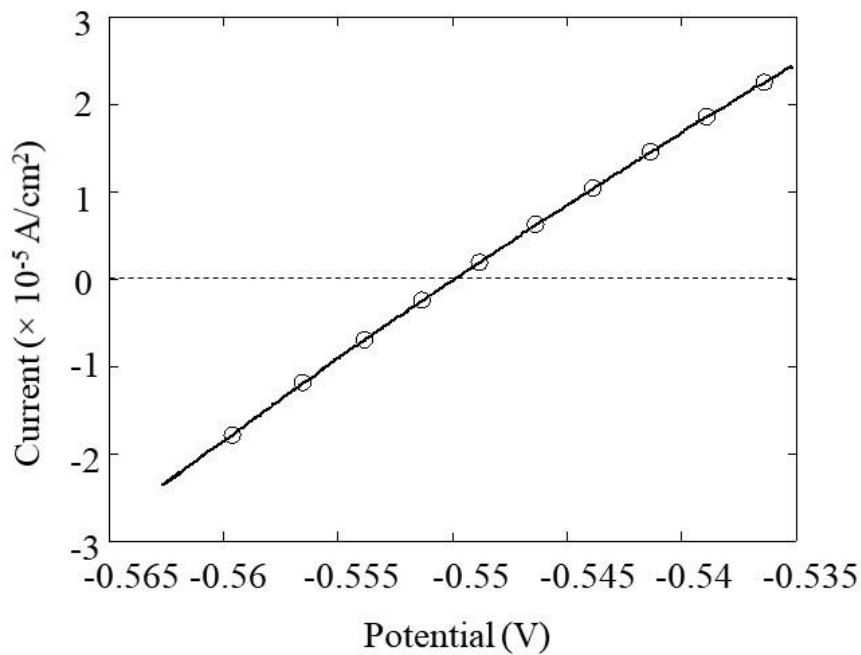
Figure 4.6 Typical linear polarisation resistance curve
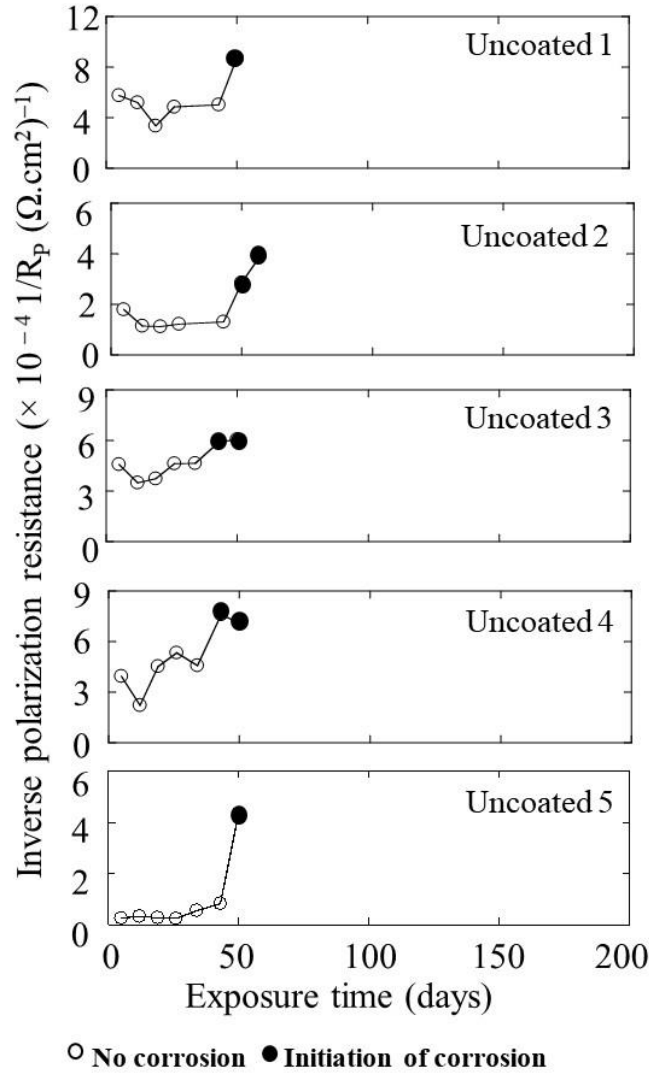
Figure 4.7 variation of $1/R_p$ of uncoated steel rebars embedded in the cementitious system and exposed to chloride

On the other hand, Figure 4.8 shows the variation of $1/R_p$ obtained from lollipop specimens with FBEC-ND steels. Both LPR and EIS data are shown here. Measurements using LPR (circular markers) failed to detect (no rise in $1/R_P$) the initiation of corrosion. Measurements using EIS (square markers) indicated a rise in $1/R_P$ at the time of corrosion initiation. Further details on the efficiency of the EIS technique will be discussed in the next subsection with another set of test specimens. Also, photographs of FBEC-ND steel rebars from lollipop specimens in Figure 4.8 show that the time of autopsy of specimens was not the

time of initiation of corrosion. LPR measurements could detect the corrosion activities only for specimen FBEC-ND4 after the coating was cracked due to expansive force exerted by corrosion products. The cracked locations in the coating can provide conductivity path for electrochemical measurements. In reinforced concrete structures, the location of corrosion, disbondment, and cracking of coating are not known. Also, the high resistance of FBE coating in remaining locations makes it impossible for LPR to get a response from underlying steel rebars, irrespective of ongoing corrosion. In general, resistance to polarization (R_P) using the LPR technique is the combined response from mortar, coating, and steel-coating interface (Fontana 1986; Rengaraju et al. 2019). Therefore, the LPR method provides comprehensive information for the evaluation of the mortar-steel-coating system. A lot of coated systems are highly resistive, and several hundreds of micrometers thick, similar to that used in this study. The LPR method may not work very well due to a large coating resistance (here, $> 10^6 \ \Omega cm^2$). Therefore, the effect of reduction in resistance to the polarization of the steel-coating interface could be significantly less to be detected in the change of total R_P (Fandi and Liu 2016).
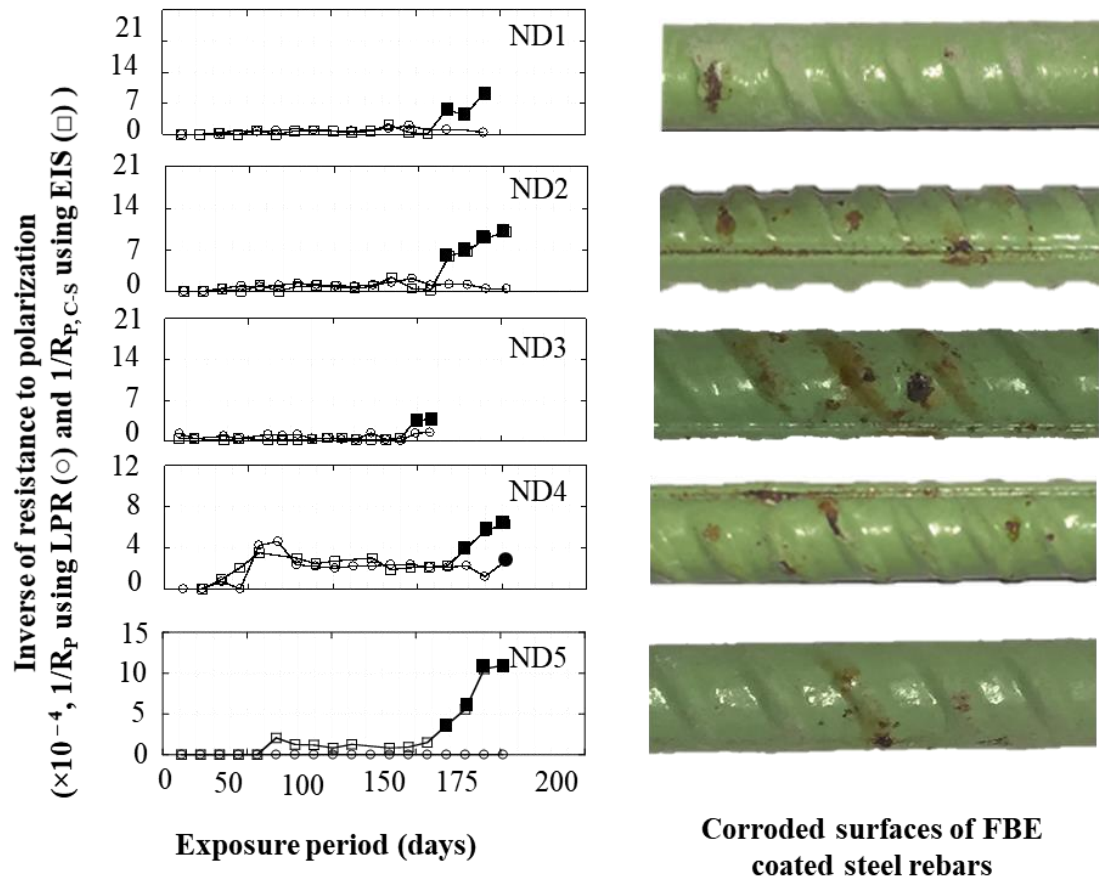
Figure 4.8 LPR and EIS measurements, and photographs of corroded FBE coated steel rebar surfaces after three cycles of detection of the initiation of corrosion using EIS tests

4.2.4 Electrochemical impedance spectroscopy (EIS)

In this section, accelerated corrosion test for coated rebars, cr-ACT, is suggested. For this, specimen design is discussed in Section 3.3.2.1; the exposure condition and testing procedure with input parameters are provided in Section 3.3.2.2. The procedure to adopted to analyze the EIS response, understand the degradation of coating, and initiation of corrosion is discussed next. Note that, EIS technique can captures responses from each element of the working electrode/test specimen (i.e., mortar, coating, and steel-coating interface). Figure 4.9 shows the ideal Nyquist plot from FBEC-ND steel rebar embedded in cementitious systems and the equivalent electrical circuit (ECC) (Lau and Sagüés 2007; Sagues 1988; Wang et al. 2015). As shown, the response has three pure loops, corresponding to mortar, FBE coating, and steel-

134

coating interface (S-C), respectively. The response was analyzed, and resistance offered by each layer (mortar, coating, and steel-coating interface) were quantified using the equivalent electrical circuit shown in Figure 4.9. Here, R_S is the resistance offered by the electrolyte solution; CPE_M and R_M are the capacitance and resistance of the mortar, respectively; CPE_C and R_C are the capacitance and resistance of the coating, respectively. 'W' is the warburg element. Presence of Warburg element indicates the diffusion process of oxygen, chlorides, and other ions (here, chlorides). Depending on the quality of FBE coating, its resistance may reduce as the testing involves continued exposure of the coating to moisture/alkaline environment for many weeks. If it remains high for a long duration, then the ingress of moisture, chloride, and oxygen through the coating will take a long time to reach the steel surface. As the response is obtained from each element of the test specimen. Monitoring of resistance of coating (R_C), resistance to the polarization of steel-coating interface ($R_{P, C-S}$) can reveal the changes in the coating material properties during the exposure to chloride solution. Therefore, R_C was monitored to understand the material properties. Also, $R_{P, C-S}$ was monitored to detect the initiation of corrosion. This enables the monitoring of resistance of coating (R_C), resistance to the polarization of steel-coating ($R_{P, C-S}$), and detecting initiation of corrosion. Therefore, monitoring the response from the steel-coating interface ($R_{P, S-C}$) could detect the initiation of corrosion. The square filled markers in Figure 4.8 show that the specimens with the onset of corrosion. Note that the electrical parameter of solution and mortar (R_S, CPE_M, and R_M) was not monitored as it is out of the scope of this thesis.
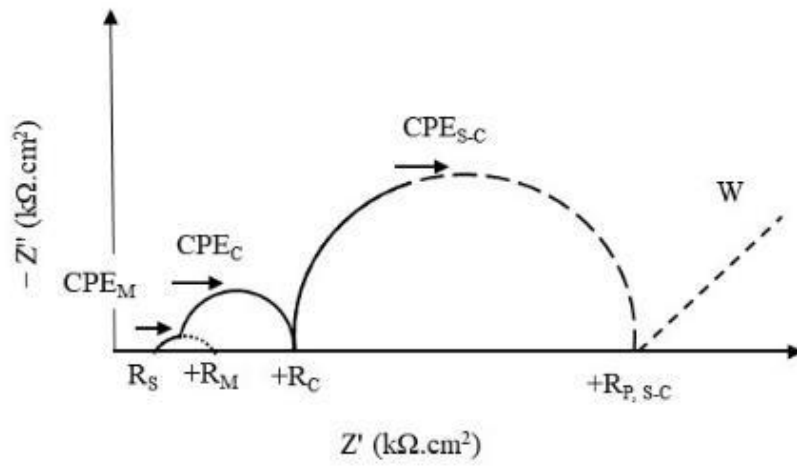
(a) Ideal Nyquist plot
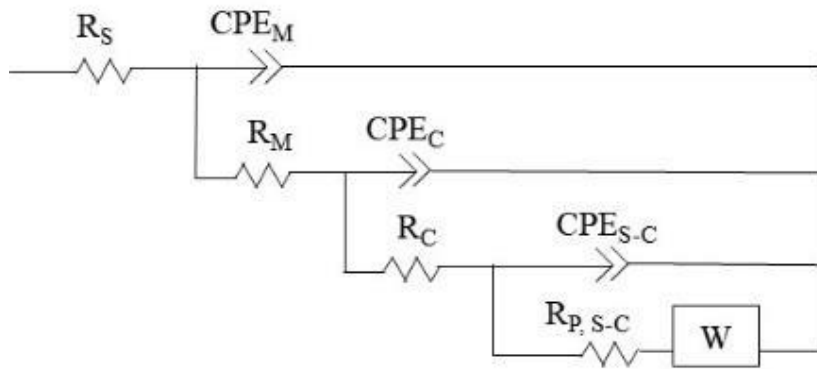
(b) Equivalent electrical circuit (EEC)

Figure 4.9 Ideal EIS response from FBE coated steel rebar embedded in the cementitious system, and corresponding EEC

4.2.4.1 Degradation of FBE coating

EIS response **Coating and corrosion condition**
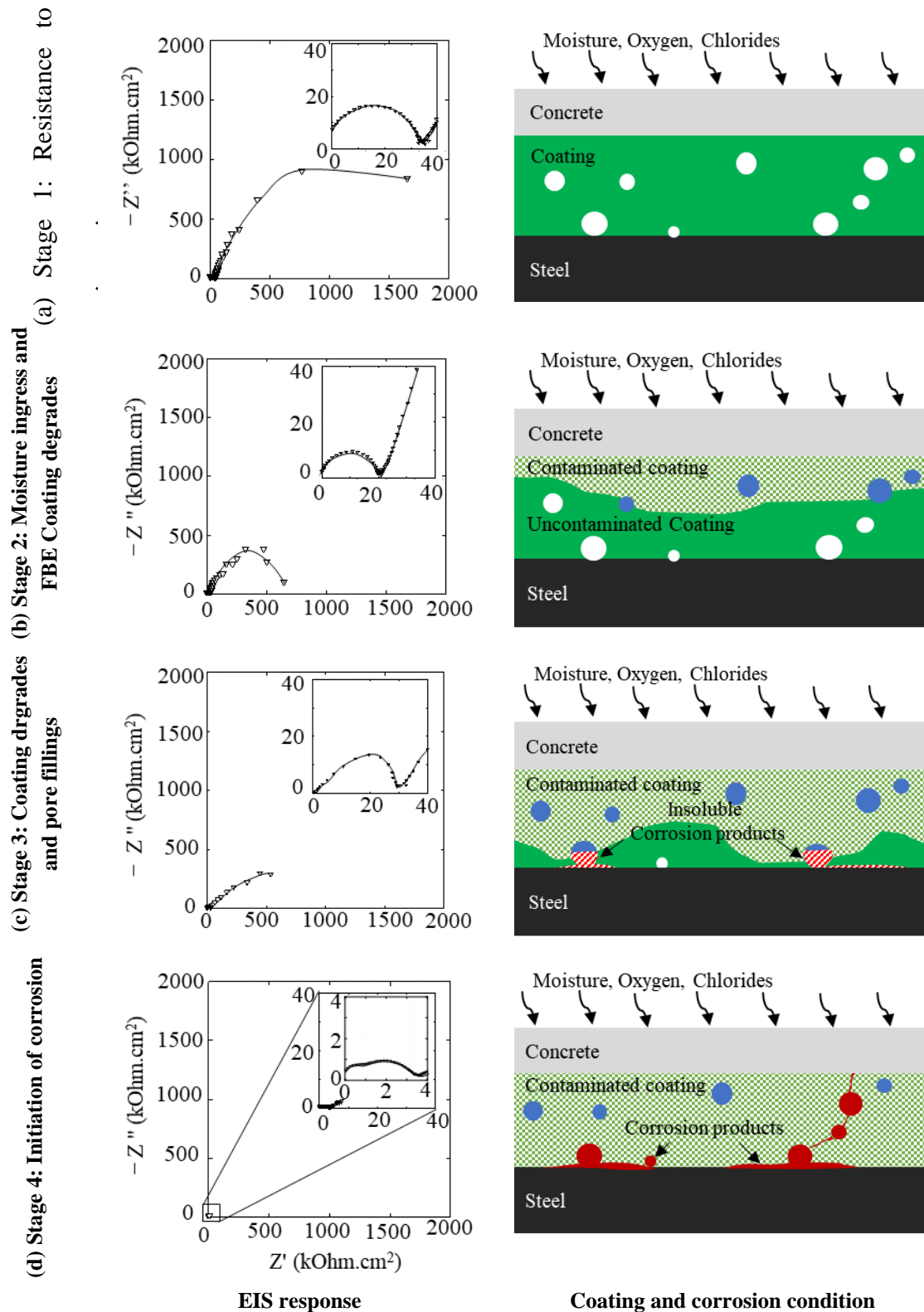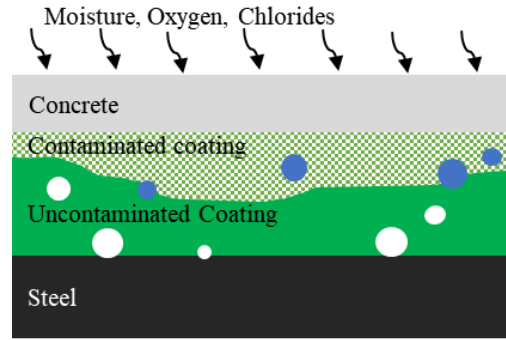
Figure 4.10 shows the typical Nyquist plots obtained from lollipop specimens with FBE coated steel embedded in the cementitious mortar at the following four stages discussed next. Stage 1: resistance to ingress of moisture, oxygen, chlorides, etc. (the initial phase of exposure), Stage

137

2: moisture ingress and degradation of FBE coating, Stage 3: corrosion products are filling the

pores available in the coating at S-C interface, and Stage 4: coating degradation and active

corrosion of steel.

(a) Stage 1: Resistance to
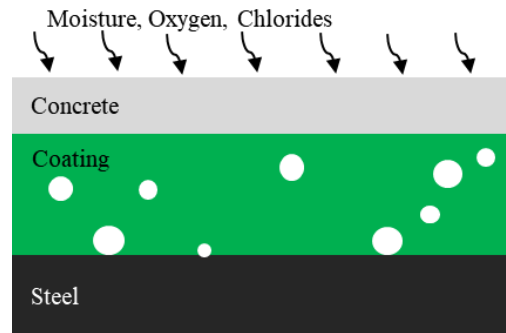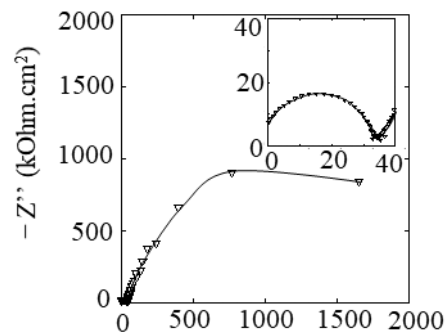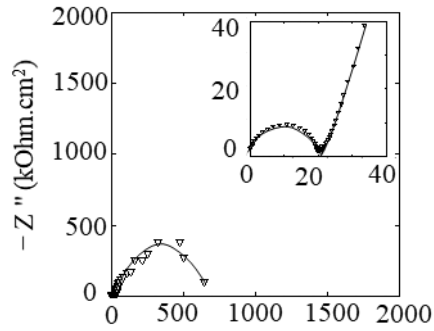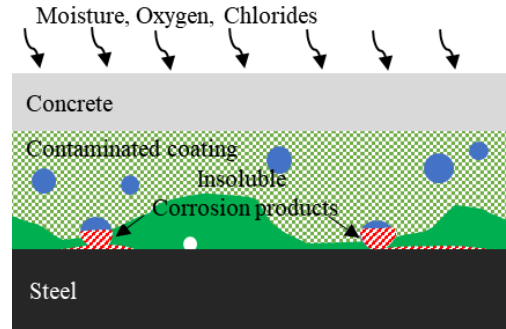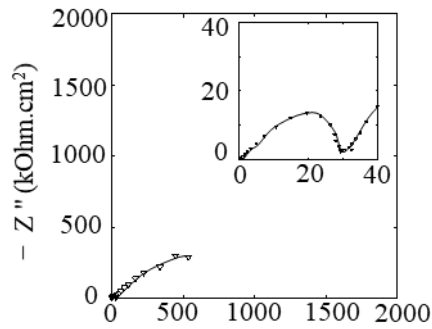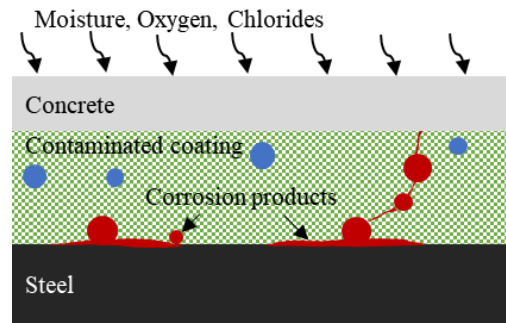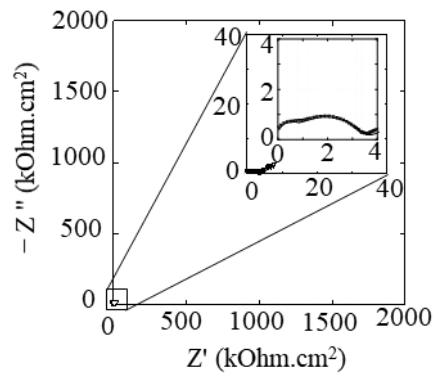
Figure 4.10 (a) shows the Nyquist plot obtained from lollipop specimen with FBE coated steel rebar with an initial exposure period (Stage 1). It consists of three loops (semicircles). The first partial loop corresponds to cementitious mortar; the second pure loop corresponds to FBE coating; the third partial loop corresponds to the steel-coating interface. At this stage, the low-frequency impedance modulus offered by the coating-steel interface was found to be significantly high (10^3 - 10^4 kOhm.cm^2). Therefore, the response from the steel-coating interface is partially recorded due to the chosen operating frequency (i.e., up to 0.01 Hz). Pure loop with high resistance indicates FBE coating acts as a barrier layer and prevents the intrusion

139

of corrosive medium (Tang et al. 2012). Therefore, at this stage, no corrosion activities can

take place. The schematic of steel-coating-concrete (SCC) in

(a) Stage 1: Resistance to
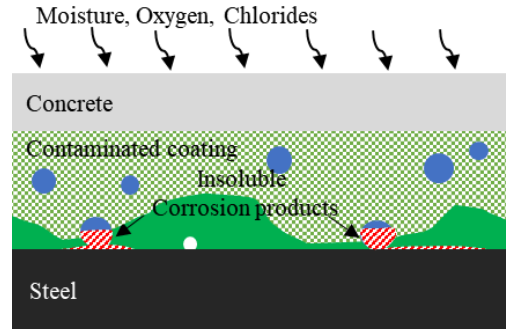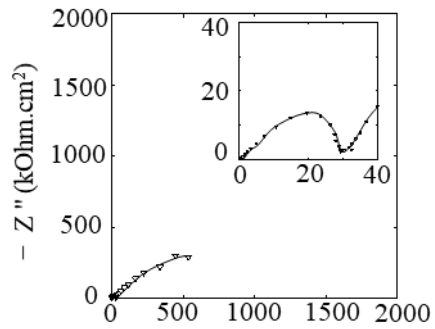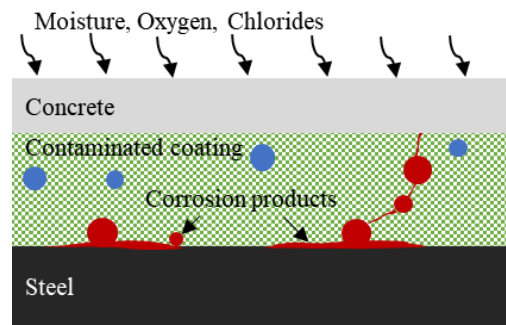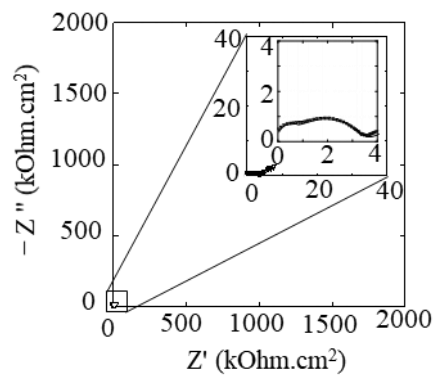
EIS response   **Coating and corrosion condition**

Figure 4.10(a) describes the condition of coating and S-C interface, where the coating is not degraded, and it is able to resist the ingress of pore solution – resulting in no degradation of coating and no corrosion activities at steel surfaces.

(a) Stage 1: Resistance

(b) Stage 2: Moisture ingress and FBE Coating degrades

(c) Stage 3: Coating drgrades and pore fillings

(d) Stage 4: Initiation of corrosion

EIS response

Coating and corrosion condition
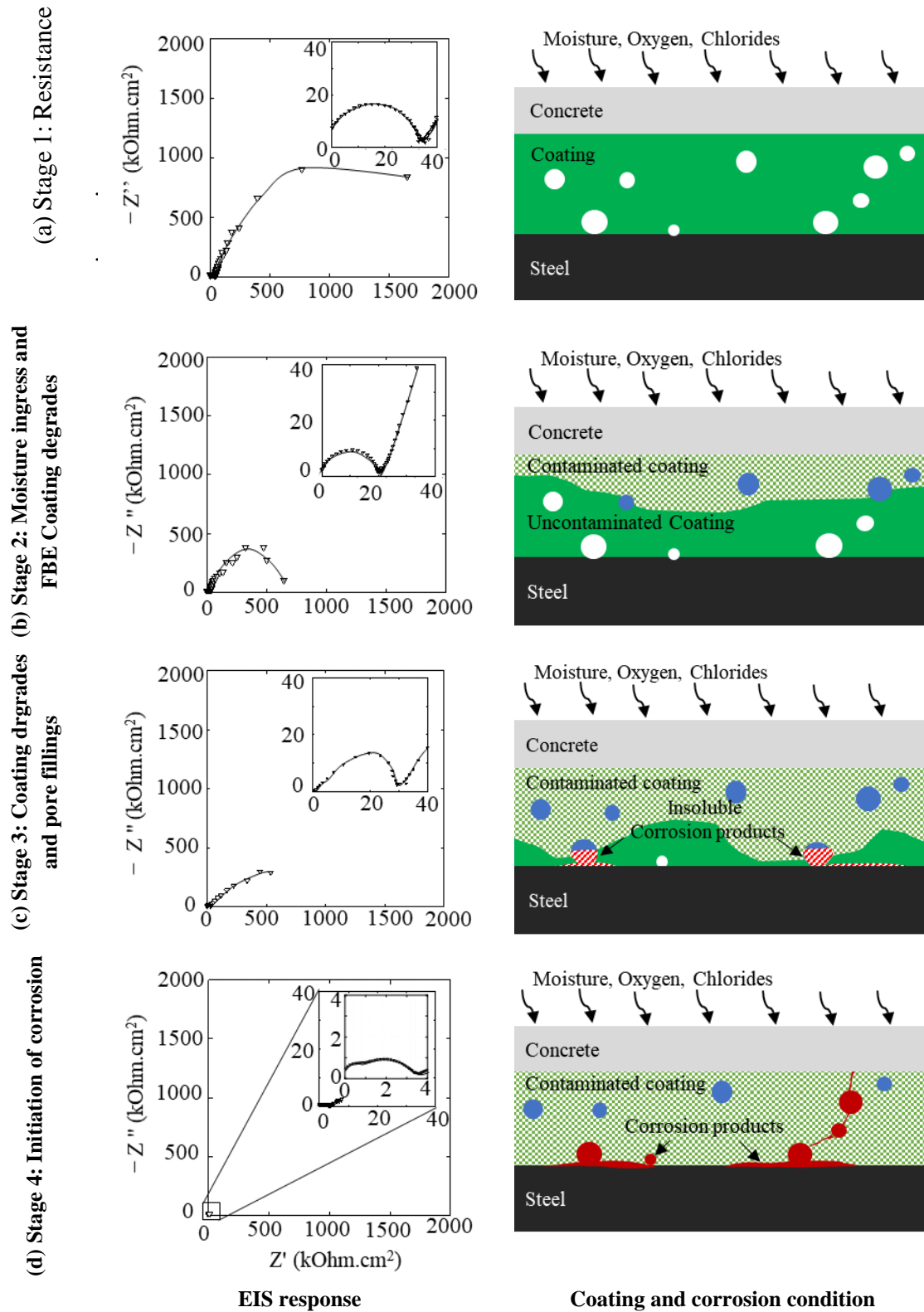
Figure 4.10 (b) shows that the resistance offered by the FBE coating and S-C interface decreases (Stage 2). During this stage, the FBE coating may have degraded due to ingress of moisture/pore solution (Nazarov et al. 2008) and chlorides [see schematic in

(a) Stage 1: Resistance

(b) Stage 2: Moisture ingress and FBE Coating degrades

(c) Stage 3: Coating drgrades and pore fillings

(d) Stage 4: Initiation of corrosion

EIS response

Coating and corrosion condition
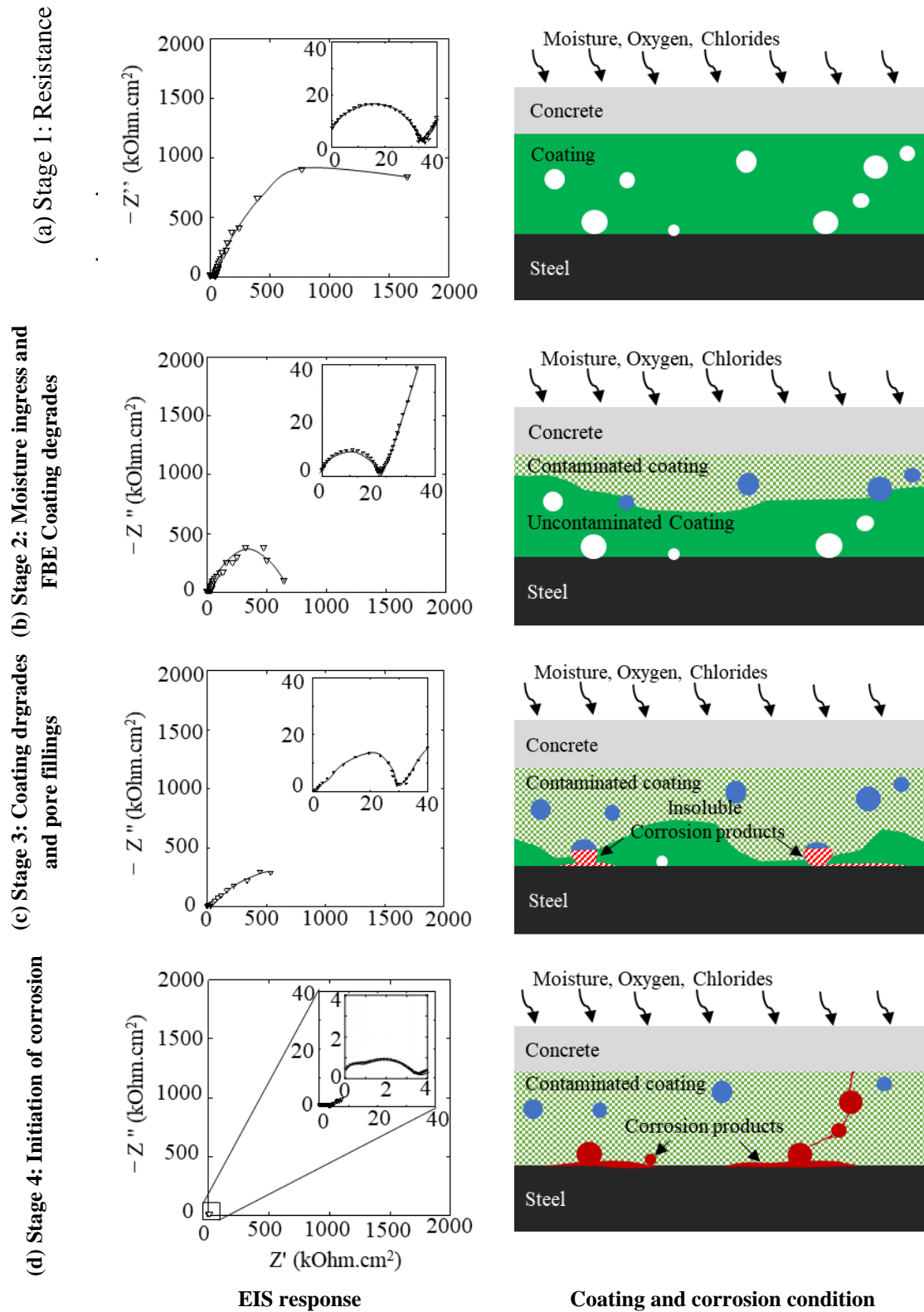
Figure 4.10 (b)].   Therefore, the impedance modulus offered by FBE coating was decreased from $\approx$ 40 kOhm-cm^2 to $\approx$ 20 kOhm-cm^2. The impedance modulus of the steel-coating interface was captured within the operational frequency range (10^6 - 0.01 Hz). Note

that the low-frequency impedance modulus of the S-C interface was still high (10^2–10^3 kOhm-cm^2) – indicating that the steel surface may remain electrochemically inactive due to high resistance to polarization. This high $R_{P, S-C,}$ may be attributed to the unavailability of enough oxygen and moisture at the steel surfaces.


(a) Stage 1: Resistance
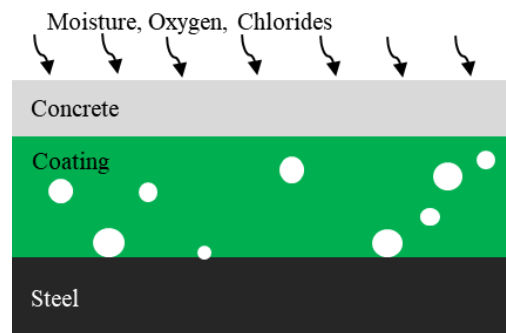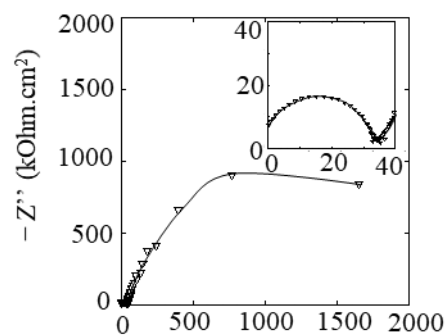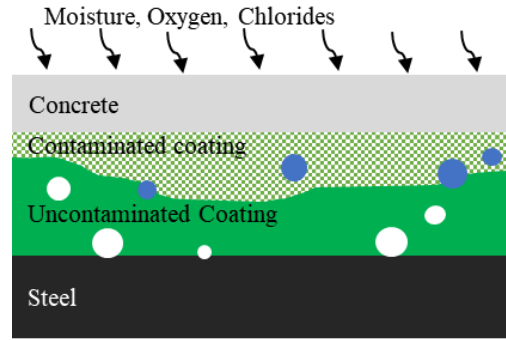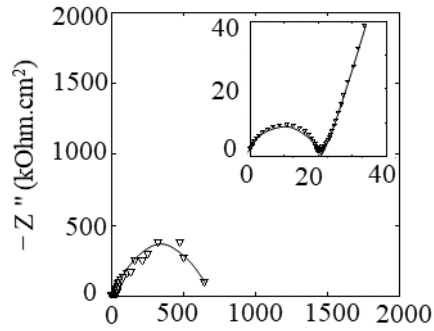
(b) Stage 2: Moisture ingress and FBE Coating degrades

(c) Stage 3: Coating drgrades and pore fillings
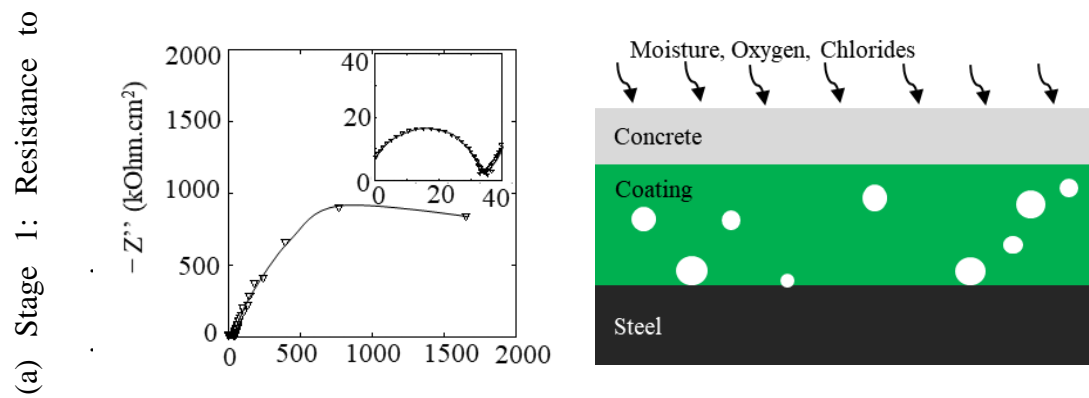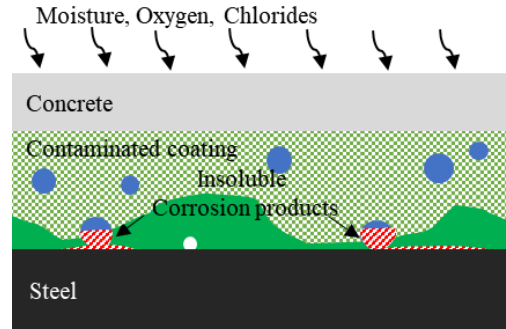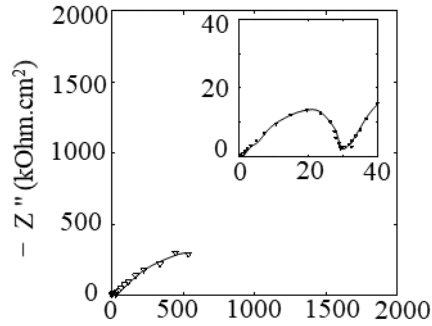
(d) Stage 4: Initiation of corrosion
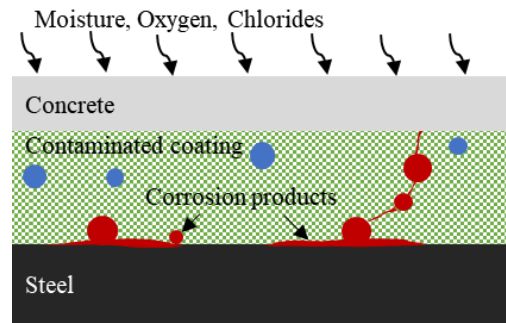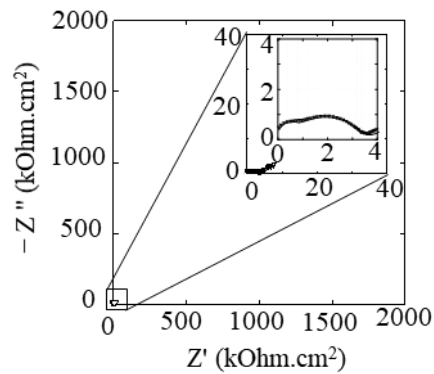
EIS response | Coating and corrosion condition

Figure 4.10 (c) shows that the resistance offered by FBE coating was found to be increasing for a few exposure cycles (Stage 3). This can be attributed to the filling of pores in coating at the S-C interface with insoluble corrosion products (Fe_XO_Y). These insoluble corrosion products may result in more resistance due to its insulating nature (Song et al. 2012; Tang et al. 2012). The formation of Fe_XO_Y corrosion products was justified by obtaining the SE micrograph and EDX response [see Figure 4.11 (a)]. The results from EDX analysis shows that the corrosion products formed at this stage do not have chlorides in them. Therefore, the corrosion products are confirmed to be insoluble and can offer higher resistance.

With further exposure when moisture with chlorides reaches the steel surface, the entrapped corrosion products may move out of pores due to radially outward pressure by the new corrosion products with chloride (Fe_XCl_Y). These corrosion products fill in the available pore space in coating and move out of the thin coating film – resulting in the gradual reduction of resistance of the coating and significant decrease in resistance to the polarization of the S-C interface (i.e., Stage 4).
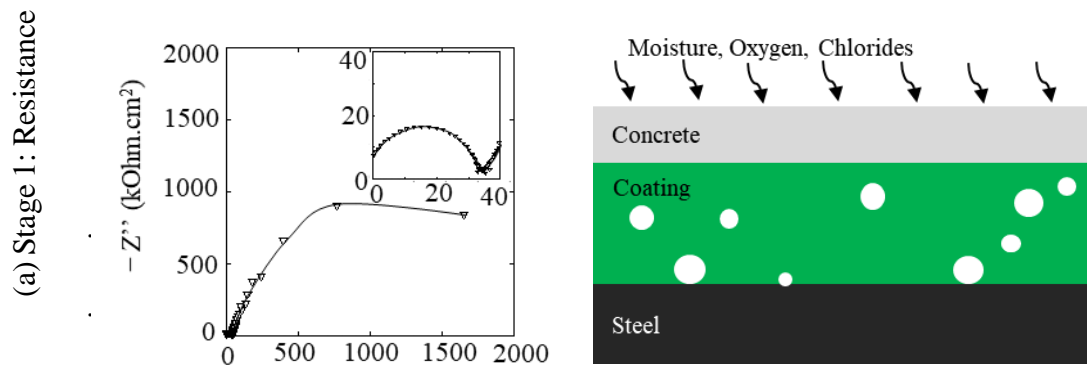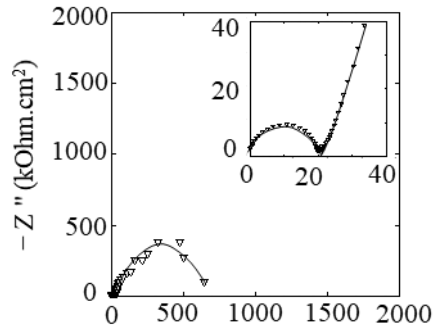
(a) Stage 1: Resistance

(b) Stage 2: Moisture ingress and FBE Coating degrades

(c) Stage 3: Coating drgrades and pore fillings
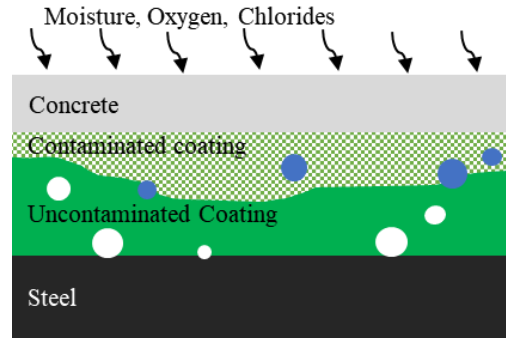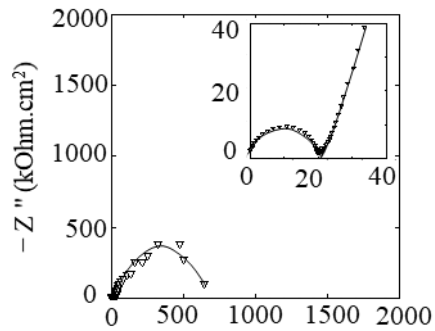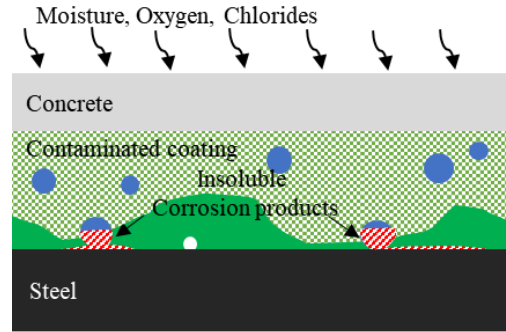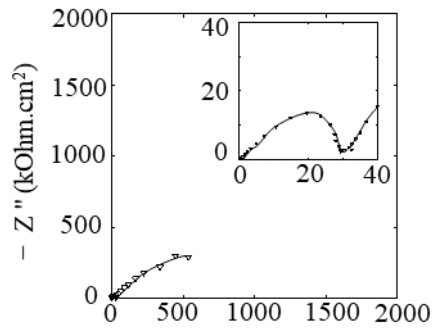
(d) Stage 4: Initiation of corrosion
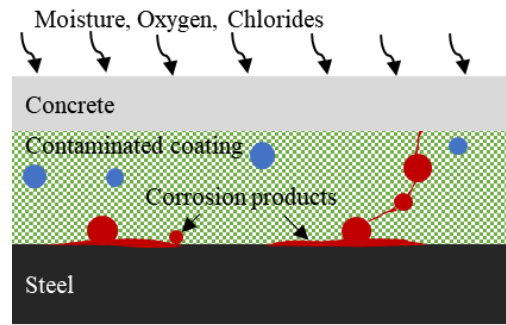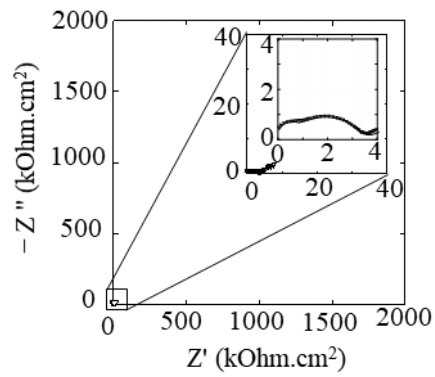
EIS response

Coating and corrosion condition

Figure 4.10 (d) shows the Nyquist plot, where R_C and $R_{P,\,S\text{-}C}$ is significantly low as compared to that obtained in Stage 1, 2, and 3. Schematic is shown in

(a) Stage 1: Resistance
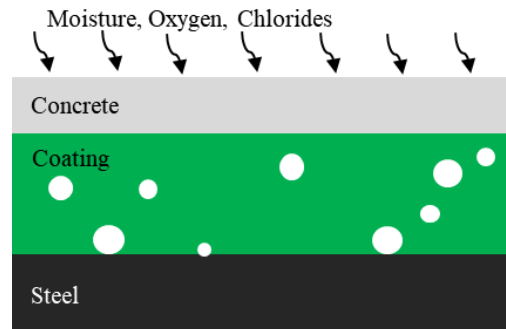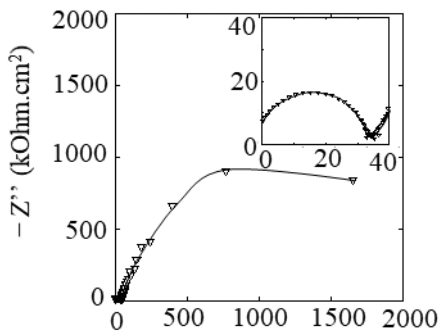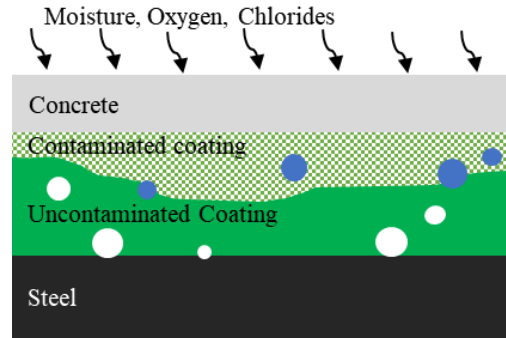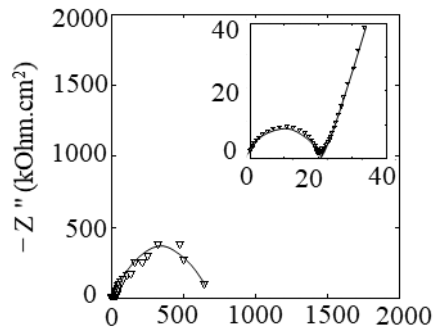
(b) Stage 2: Moisture ingress and FBE Coating degrades

(c) Stage 3: Coating drgrades and pore fillings
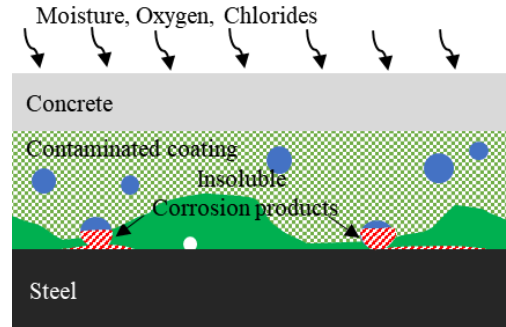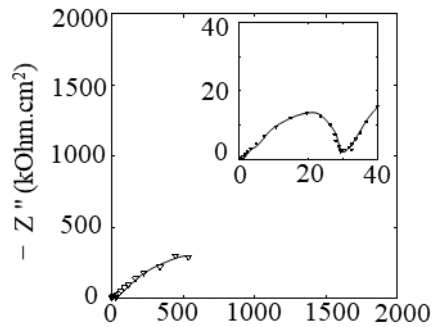
(d) Stage 4: Initiation of corrosion
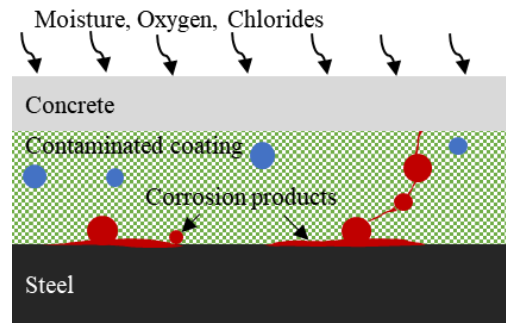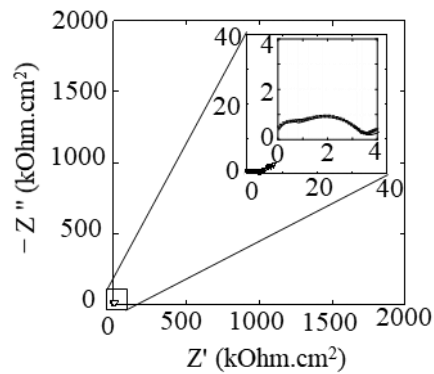
EIS response　　　　**Coating and corrosion condition**

Figure 4.10 (d) shows the coating has significantly degraded, which may allow more moisture, oxygen, and chlorides to steel surface – resulting in the initiation of corrosion due to chlorides at the steel surface. The initiation of corrosion was confirmed by autopsying the lollipop specimen, and the presence of chlorides in corrosion products were confirmed EDX analysis of corrosion products [see Figure 4.11 (b)]. Note that due to the presence of chlorides, the corrosion products will be soluble and conducting in nature - resulting in the flow of corrosion products through the pores in coating and reduced resistance of FBE coating.
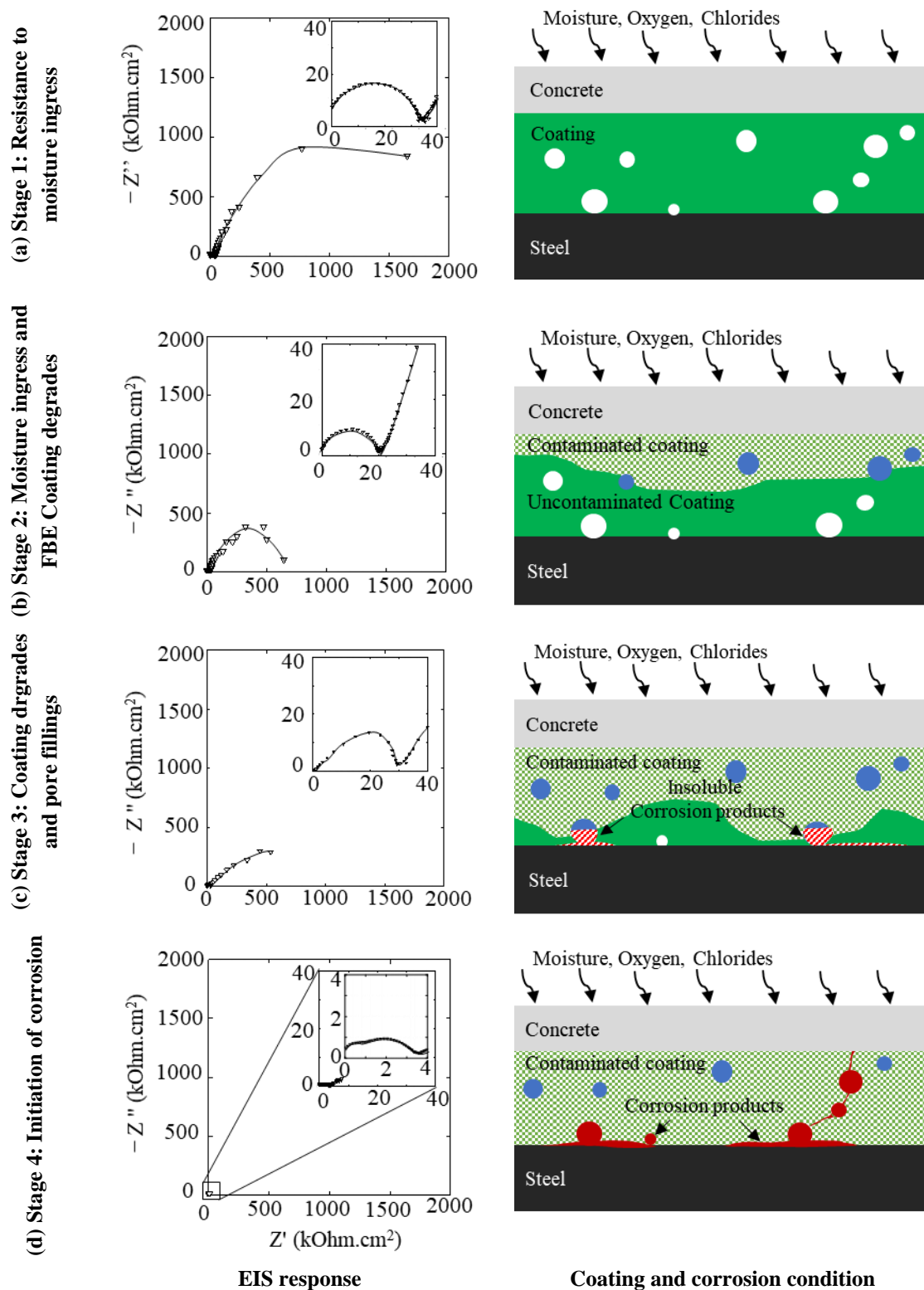
Figure 4.10 EIS response from lollipop specimens with FBE coated steel at various stages during exposure to chloride solution

(a) Insoluble corrosion products (without chlorides) filled in coating – Stage 3

(b) Soluble corrosion products filled in pored in coating – Stage 4
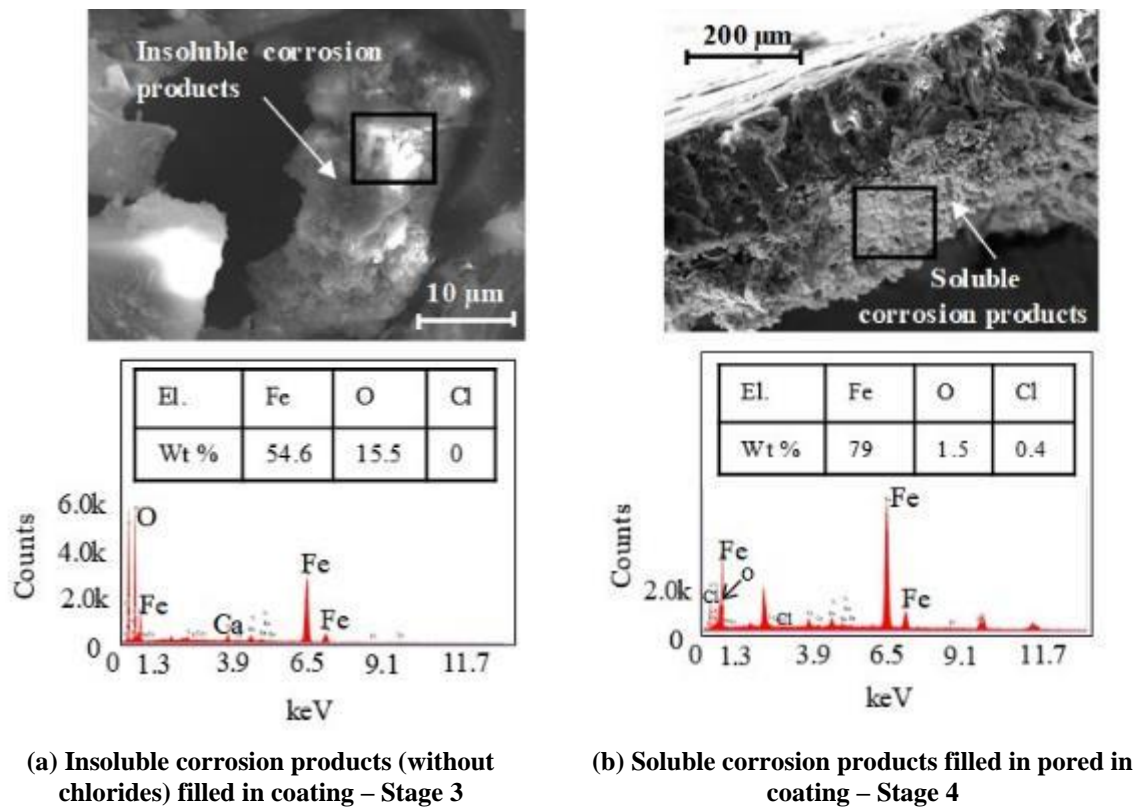
Figure 4.11 Evidence of corrosion products filled in pores of FBE coating

Figure 4.12 shows the variation of coating resistance of FBEC-ND coating, which is discussed in detail earlier (corresponding to

(a) Stage 1: Resistance to moisture ingress

(b) Stage 2: Moisture ingress and FBE Coating degrades

(c) Stage 3: Coating drgrades and pore fillings

(d) Stage 4: Initiation of corrosion

EIS response

Coating and corrosion condition
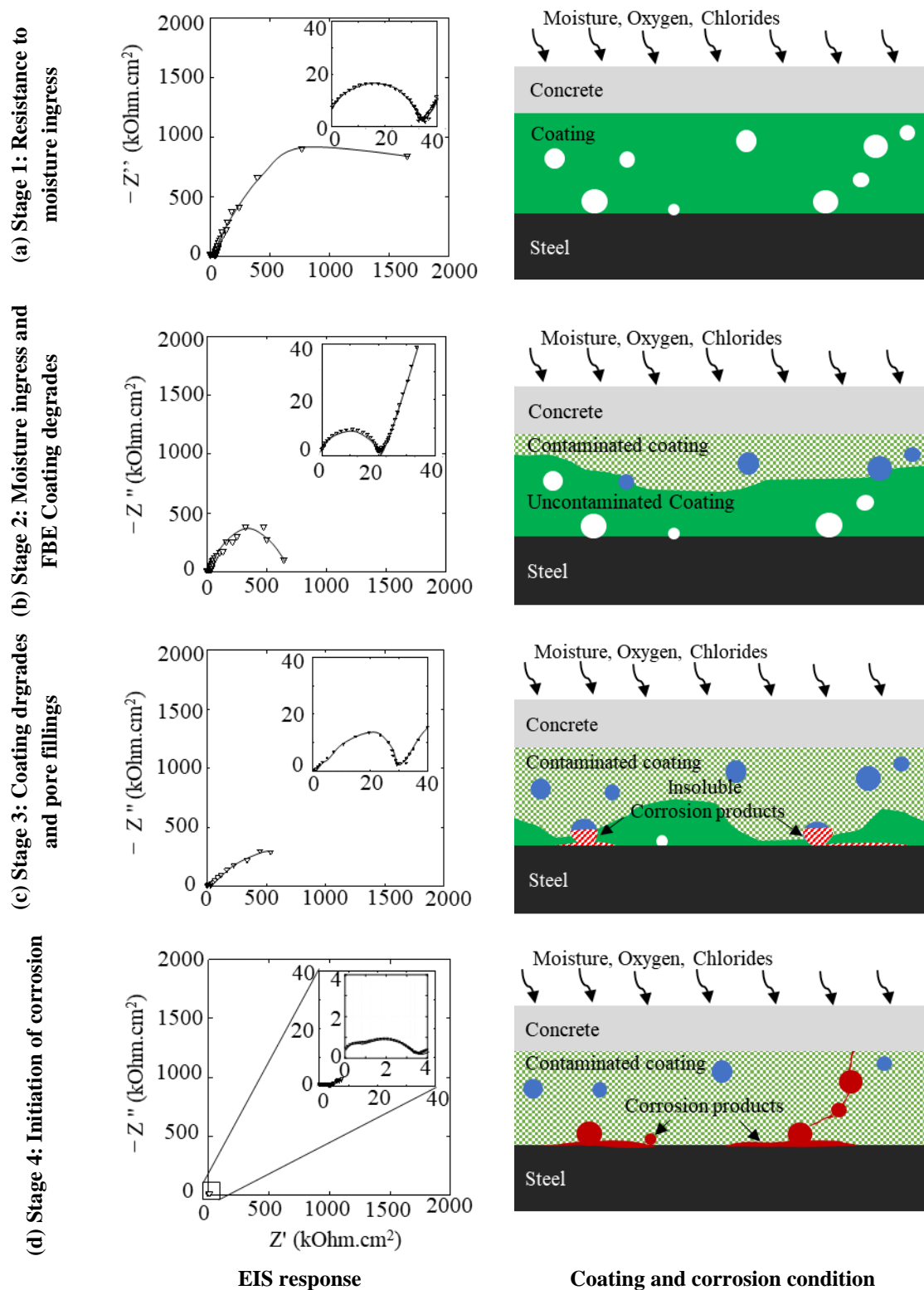
Figure 4.10 and Figure 4.11). Figure 4.13 shows a schematic with the proposed 4-stage

degradation mechanism for FBE coating when exposed to an alkaline solution with chlorides.

Stage 1 is defined when R_C was constant for a few weeks of exposure – indicating that the FBE

coating could resist the ingress of moisture for about three to four weeks. The unfilled elliptical empty pores in the schematic represent that pore solution could not penetrate through the coating. Stage 2 is defined when R_C started to decrease and decreased to about half of the original value of R_C after 1st wet regime. During this stage, the corresponding schematic represents that pore solution (possibly with chlorides) may have penetrated through the FBE coating to some depth of the coating – resulting in the decrease in the R_C of FBE coating. Then, when sufficient moisture and oxygen reach the steel surface, corrosion may initiate, and insoluble corrosion products may fill the pores at the S-C interface. Therefore, Stage 3 is defined with R_C starts to increase due to high electrical resistance offered by filling of insoluble corrosion products in pores of FBE coating (Wang and Gao 2016) [see Figure 4.11 (a)]. Subsequently, with further exposure when pore solution and chlorides reach the steel surface, corrosion may progress due to the solubility of corrosion products due to the presence of chlorides. These corrosion products may exert radial pressure on coating and may result in cracking. Therefore, Stage 4 is defined when R_C continues to decrease due to the increase in the interconnectivity of pores and cracks.
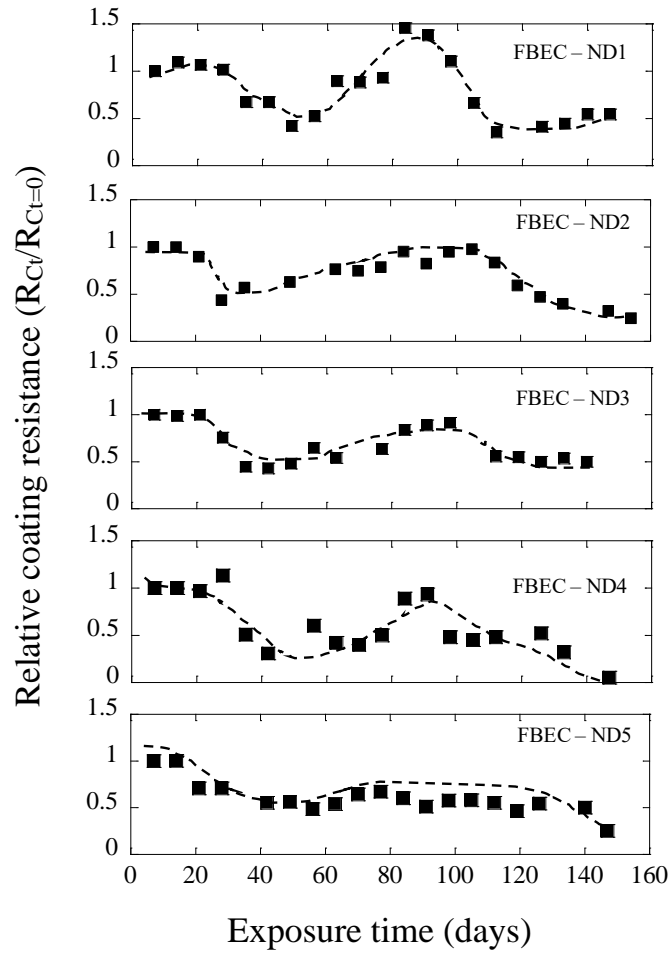
Figure 4.12 Change in relative resistance of coating due to exposure to cement mortar
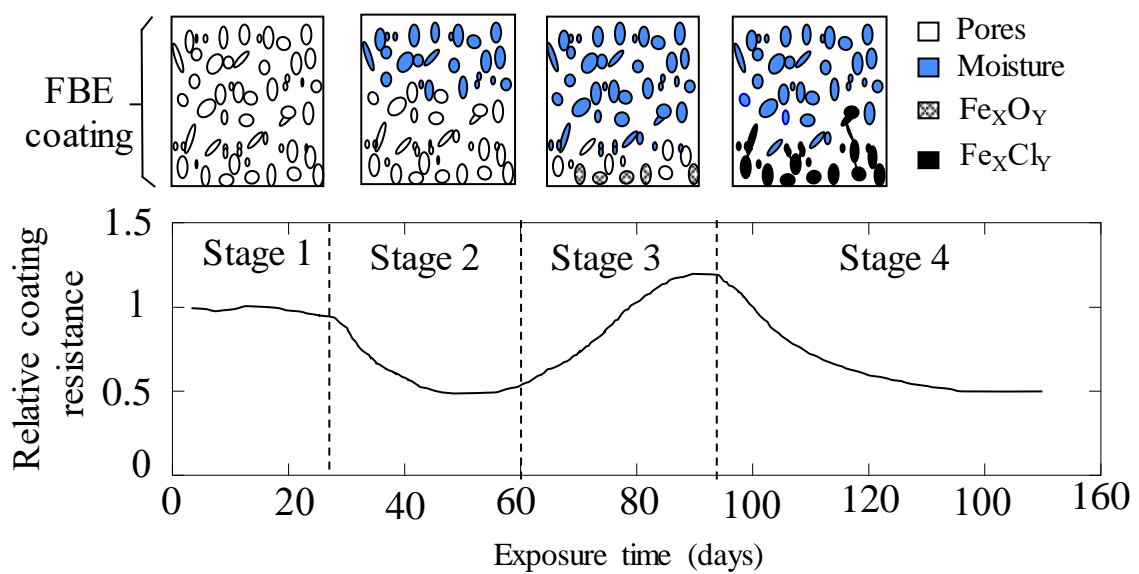
Figure 4.13 Proposed 4-stage coating degradation process

4.2.4.2 Initiation of corrosion

Figure 4.14 shows the typical impedance spectra (Nyquist and Bode plot) from FBEC- ND and FBEC-SD specimens at initial exposure period, at intermediate exposure period, and post-initiation of corrosion. For FBEC-ND,, Figure 4.14 shows that the slope of the tail of the Nyquist plot at initiatial exposure cycles (here, third wet cycle, W3) is more than 45° - indicating significantly high $R_{P, S-C}$. Similarly, the Bode plot at the end of W3 shows that at low frequencies, the magnitude of the impedance is inversely proportional to the square root of the frequency. This behavior can be encountered in systems where the electrochemical processes are under diffusion control [42] – indicating that the corrosion process in FBEC-ND steel rebars are governed by diffusion of deleterious elements such as chlorides. The similar response with slightly lower inverse relation between frequency and impedance modulus was observed during intermediate exposure period (here, W10). The slow change in the behaviour of Bode plot indicates that the diffusion through FBE coating is a slow process. However, once the corrosion was initiated, the magnitude of impedance at low frequencies are constant, indicating that the corrosion process is independent of the diffusion of deleterious elements. Therefore, after this stage, corrosion can continue in the same micro-environment without further diffusion of chlorides.
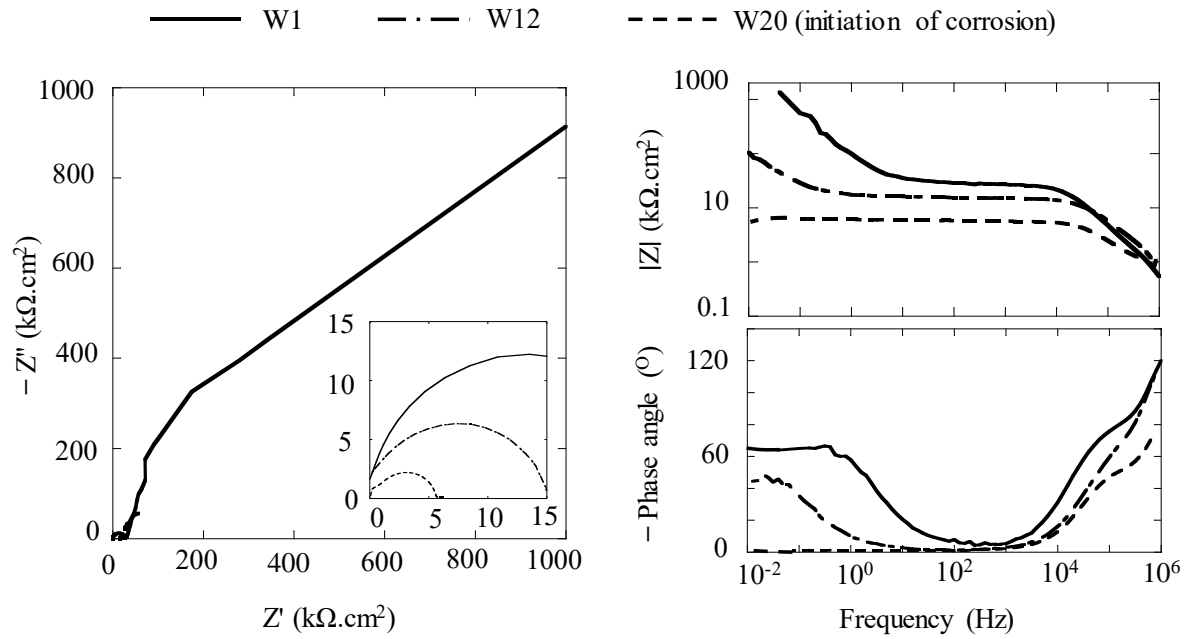
Figure 4.14 Typical impedance spectra at OCP obtained from FBE coated steel before and after initiation of corrosion

Figure 4.15 shows the variation of $1/R_{P, S-C}$ for FBEC-ND specimens. Note that $1/R_{P, S-C}$ for values for FBEC-ND, showed a spike up for all the specimens at around 40 days of exposure. This can be attributed to the formation of the oxide/passive layer (Fe_XO_Y) on the steel surface. However, once these insoluble corrosion products are formed, steel rebars remain passive until the chlorides reach to the rebar surface. The large clearly visible spikes in the $1/R_{P, S-C}$ data represents the initiation of corrosion (here, represented with the filled markers). Upon initiation of corrosion was confirmed using statistical analysis of $1/R_{P, S-C}$, the specimens were autopsied and visually inspected. For FBEC-ND steels, the surface of coated steel did not show visible corrosion [see Figure 4.16(a)]. Then, the coated steel rebars from lollipop specimens were cut at various locations. The initiation of corrosion was confirmed by visible underfilm corrosion in the coated steels. Figure 4.16 shows the zoomed image of the cross-sections with corrosion under the coating.

155
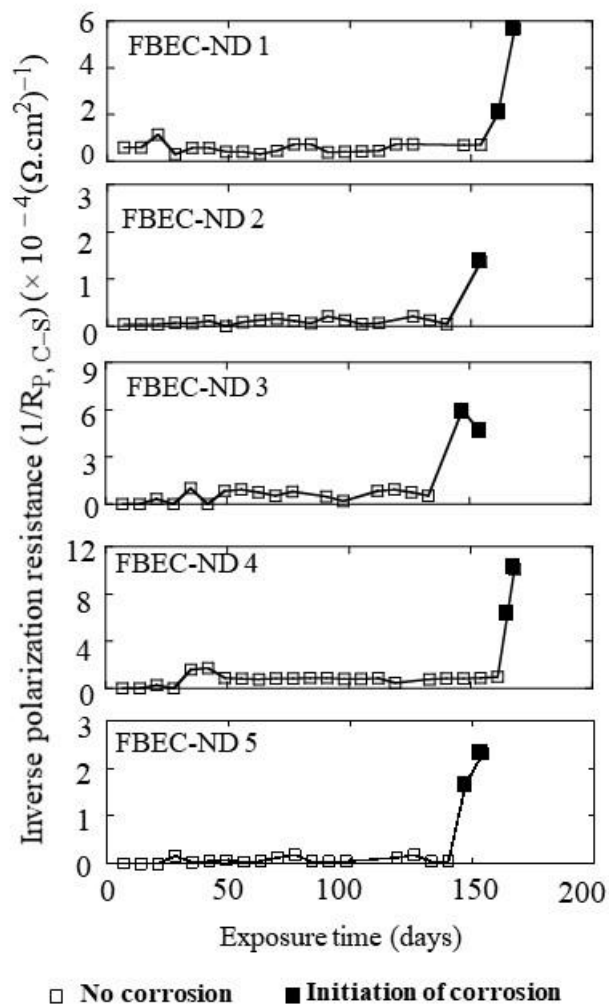
Figure 4.15 Detection of initiation of corrosion (unfilled and filled markers indicate passive and active corrosion measurements, respectively))

(a) Coated rebar

(b) Close-up of cut section

Corrosion products
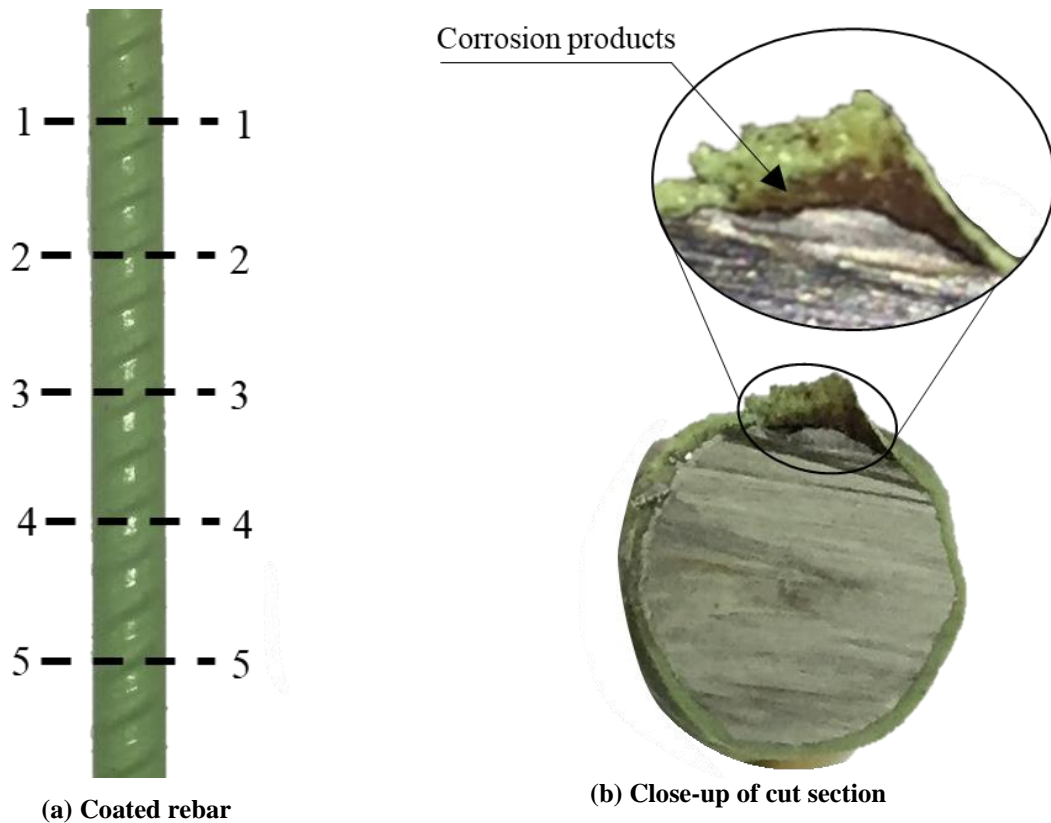
Figure 4.16 FBE coated steel rebar extracted from a lollipop specimen after initiation of corrosion has been detected using EIS tests(a) Surface of FBE coated steel showing no evidence of ongoing underfilm corrosion (b) Cross-section of FBE coated steel with evidence of ongoing underfilm corrosion.

4.3 CEMENT-POLYMER-COMPOSITE (CPC) COATED STEEL REBARS

4.3.1 Half-cell potential (HCP)

Figure 4.17 shows the variation of HCP obtained from 3-bar prism specimens with CPCC-SB steel rebars. Note that the HCP values start to show the disturbance after about 75 days of exposure to chloride solution. For two out of five specimens, the HCP measurements were dropped below $-$ 275 mV$_{SCE}$. However, for the remaining three specimens, HCP measurements did not show the detectable pattern for the initiation of corrosion. Therefore, the exposure to these specimens was continued and autopsied when MCC values also showed the pattern for the initiation of corrosion. Note that HCP for all the specimens did not show the detectable pattern to confirm the initiation of corrosion. This can be because of the high electrical resistance offered by the air entrapped between the steel rebars and CPC coating. A few iterature report the HCP as a suitable technique for detecting the initiation of corrosion (Pei et al. 2017). However, the time of detection of corrosion using HCP may not be the time to corrosion initiation. This was justified by the visual inspection of corrosion steel specimens from this study and reported in the literature (Pei et al. 2017).. Therefore, the candidate does not recommend HCP measurements for detecting the initiation of corrosion.
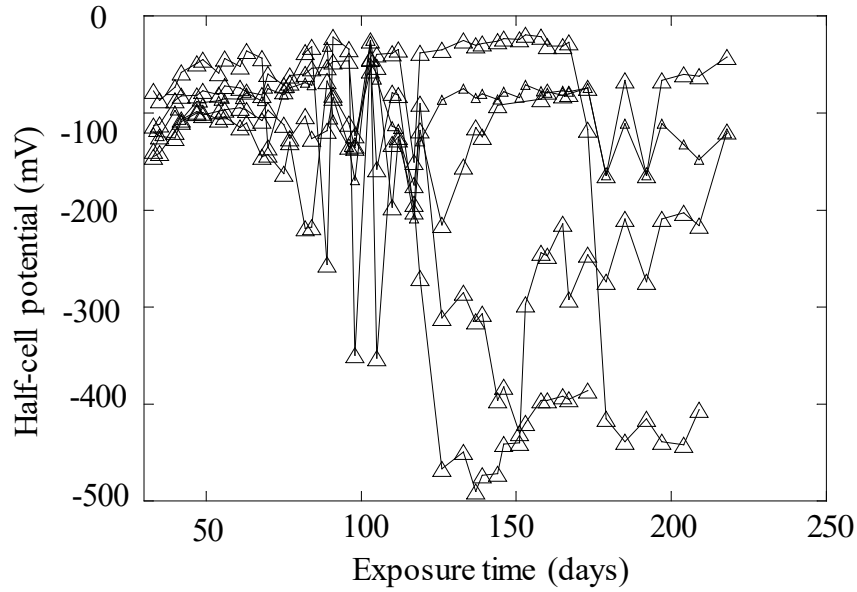
Figure 4.17 variation of half-cell potential during the exposure time

4.3.2 Macrocell corrosion current (MCC)

Figure 4.18 shows the variation of MCC for CPC coated steel. In the initial exposure period, the MCC was low (< 10 C). After exposure to chlorides for about 175 days the MCC for the 3-bar prism specimens started to show the spikes – indicating the initiation of corrosion. In this study, the corrosion initiation criteria similar to that prescribed in ASTM G109 was adopted. The initiation of corrosion was confirmed by visual observation by autopsying the specimens when the initiation of corrosion was detected (see Figure 4.18). The MCC measurements could detect the initiation of corrosion because the resistance offered by the CPC coating is significantly less (Mohammed et al. 2014; Vedalakshmi et al. 2000) (in this study (0.2 $k\Omega.cm^2$). Note that the time taken for detecting the initiation of corrosion with MCC using 3-bar prism specimens is more than six months. The assessment of such coated systems with 3-bar prism specimens can be time-consuming. Therefore, the assessment of CPC coating was investigated with lollipop specimens.
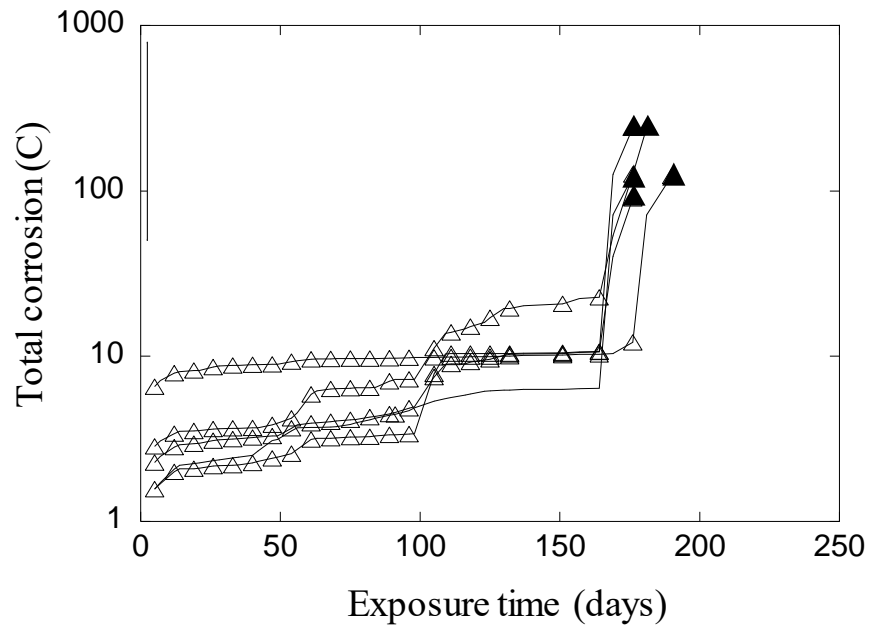
(a) Variation of total macrocell corrosion current during exposure time
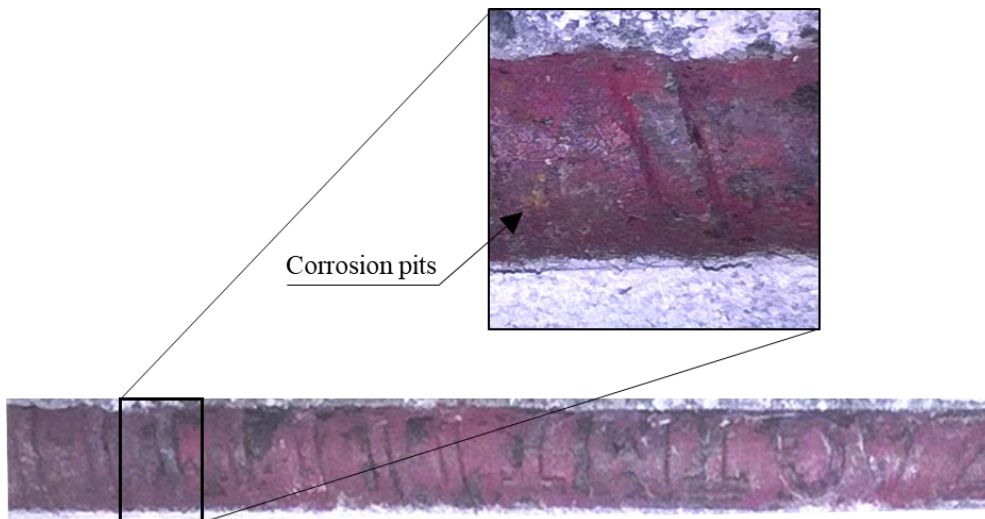
Corrosion pits

(b) Steel rebar with negligible corrosion after autopsying the 3-bar prism specimens after the corrosion was detected using MCC technique

Figure 4.18 Total macrocell corrosion current and corroded steel rebar from 3-bar prism specimens

4.3.3   Linear polarization resistance (LPR)

Figure 4.19 shows the variation of resistance to the polarization of CPC coated steel rebars embedded in mortar. Spikes in *1/R$_P$* values indicate the initiation of corrosion. Note that the initiation of corrosion was detected for all the specimens between 50 and 100 days of exposure to chloride solution. The initiation of corrosion was confirmed by visual observation of steel rebars by autopsying the specimens when the initiation of corrosion was detected by statistical analysis by the procedure suggested in 3.3.2.2. Also, the initiation of corrosion was detected within 100 days. The LPR could detect the initiation of corrosion because the test methods based on LPR works well for systems with low resistance of electrolyte (Rengaraju et al. 2019). Here, resistance offered by CPC coating is significantly less 0.2 kΩ.cm^2 (Vedalakshmi et al. 2000). Therefore, the assessment of CPC coated steel rebars is recommended with lollipop specimens using LPR technique.
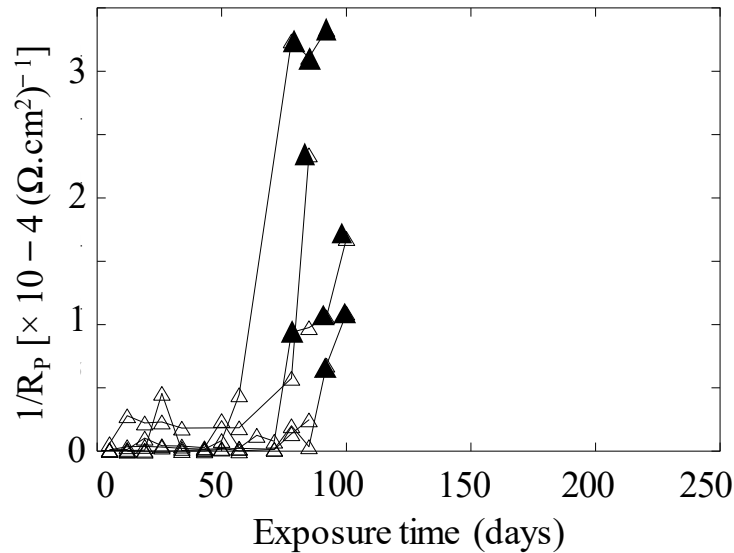
Figure 4.19 Variation of 1/Rp for CPC coated steel rebars and initiation of corrosion

4.4   RECOMMENDATIONS

Based on results and detailed data analysis, it is recommended not to adopt HCP, MCC, and LPR techniques and to adopt the EIS technique to detect corrosion initiation of FBE coated rebars. It is also recommended not to use HCP and MCC and to use either LPR or EIS techniques to detect corrosion initiation of CPC coated rebars. Table 4.1 summarizes these recommendations.

Table 4.1 Summary of major findings from Objective 1

Steel surface conditions	Test methods based on techniques to detect corrosion initiation	Justification/Remarks
Uncoated	MCC, HCP, LPR, EIS	Works in low resistive cementitious cover
FBE coated	EIS	Work effectively even if the resistivity of FBE coating is high ($1000\,\mathrm{k\Omega cm^2}$)
CPC coated	LPR, EIS	Resistivity of CPC coating is relatively low ($20\text{-}200\ \Omega\mathrm{cm^2}$)

4.5   SUMMARY

Assessment of RC systems with coated steel rebars is challenging due to the unavailability of the standard test method. For this, conventional test methods based on techniques such as half-cell potential (HCP), macrocell corrosion current (MCC), linear polarization resistance (LPR), and electrochemical impedance spectroscopy (EIS) were assessed.

5 RESULTS – CORROSION INITIATION OF

FUSION-BONDED-EPOXY (FBE) COATED STEEL REBARS

5.1 INTRODUCTION

This chapter presents the effect of inadequate construction practices on the coating characteristics, initiation of corrosion, chloride threshold, and service life of RC systems with FBE coated steel rebars. For this, as-received FBE coated steel with no damage (possible with pinholes), and the inadequate construction practices such as scratch damage to coating and exposure of FBE coating to UV rays were mimicked in the laboratory and assessed with test methodology based on EIS, as suggested in Chapter 4. Later, the frameworks were developed to determine the parameters such as chloride thresholds, diffusion coefficients of coating for estimation of service lives of the RC system with FBE coated steel rebars. The framework for the estimation of service lives was also proposed. Using the proposed frameworks, the differences in chloride diffusion coefficients, chloride thresholds, and estimated service life for inadequate construction practices were quantified. The studies were conducted in two phases – Phase 1 on scratch damage and Phase 2 on UV degradation and subsequent service life studies.

5.2 PHASE 1 - EFFECT OF SCRATCH DAMAGE TO FBE COATING

5.2.1 Chloride-induced initiation of corrosion

The Section 4.2.4.2 highlighted that the corrosion in FBE coated steel rebars with no damage to coating is a result of slow diffusion process. On the other hand, for FBEC-SD

specimens,
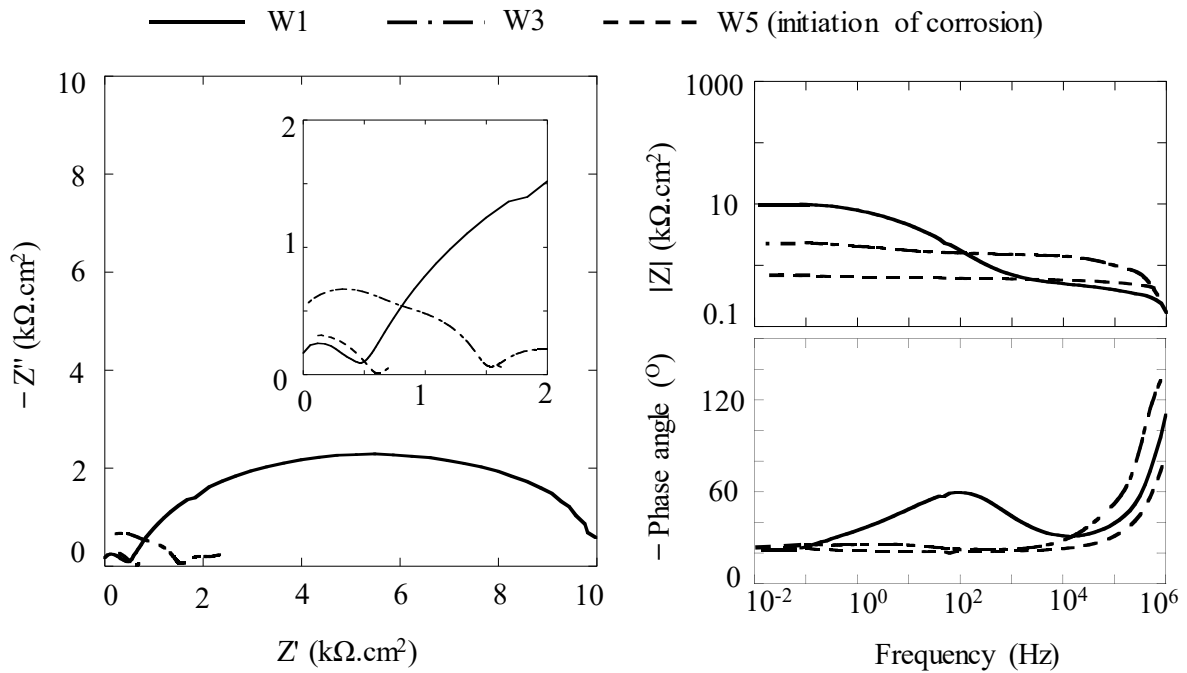
Figure 5.1(b) shows that the magnitude of impedance at low frequencies are constant from the beginning of the exposure (i.e., from first exposure cycle, W1) – indicating the pure resistive behavior of RC systems with damaged FBE coated steel rebars (Oliveira and Ferreira 2003a). In addition, the magnitude of the impedance of FBE coated steel rebars were significantly less than that of undamaged FBE coated steel – indicating that the corrosion can initiate even without chlorides at steel surfaces (Tang et al. 2012). With further exposure, within three to five exposure cycles (W3 and W5),the magnitude of impedance modulus was found to be decreasing – indicating that the rate of corrosion was increasing with an increase in the chloride concentration at the steel surface .
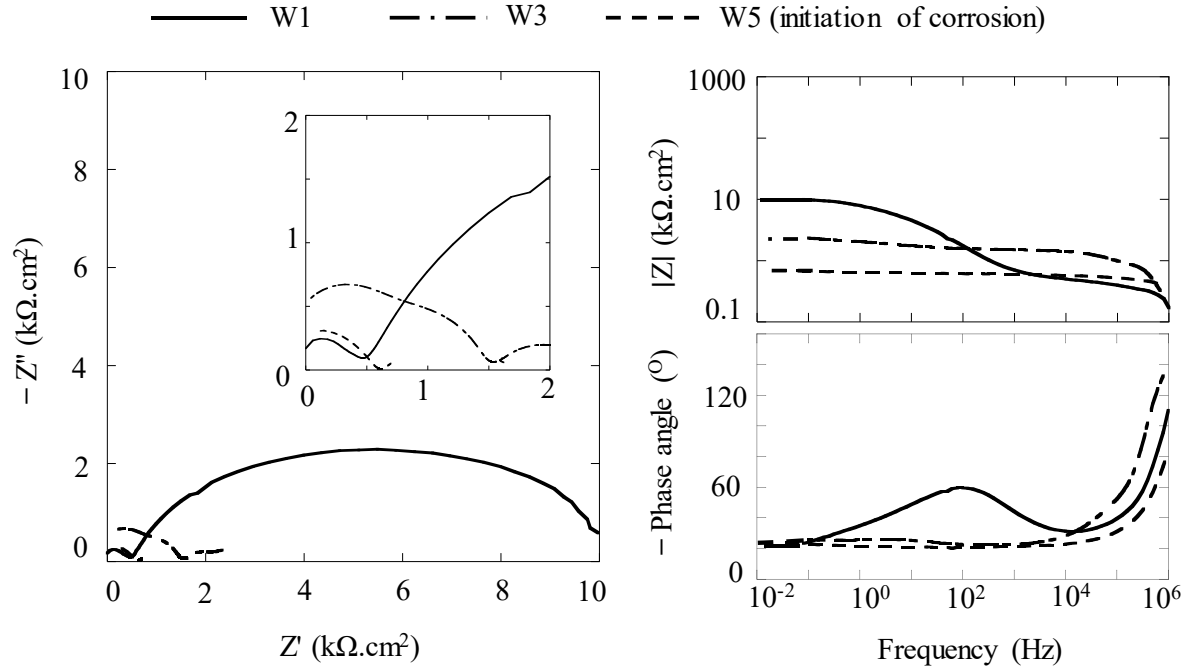
Figure 5.1 Typical impedance spectra at OCP obtained from FBE coated steel before and after initiation of corrosion [W1: 1st wet cycle, W3: 3rd wet cycle, and W5: 5th wet cycle]

Figure 5.2 shows the variation of $1/R_{P, S-C}$ for FBEC-ND, and FBEC-SD specimens, respectively. For FBEC-ND, upon initiation of corrosion was detected using statistical analysis of $1/R_{P, S-C}$, the initiation of corrosion was confirmed by visual inspection after autopsying the specimens (Liu et al. 2009). For FBEC-ND steels, the surface of coated steel did not show visible corrosion [see Figure 4.16(a)]. Then, the coated steel from lollipop specimens were cut at various locations. The initiation of corrosion was confirmed by visible underfilm corrosion in the coated steels with corrosion under the coating shown in Figure 4.16.

Similarly, Figure 5.2(b) shows that the initiation of corrosion for specimens with FBEC-SD steel was detected within 40 days of exposure. The rate of corrosion for these specimens were high from the beginning of the exposure – indicating that chlorides may not be required for corrosion to progress in case of FBE coated steel with scratch damage (Tang et

al. 2012). Also, when lollipop specimens with FBEC-SD steel rebars were autopsied, many

corrosion pits were visible on the steel surface at scratch damage location [see
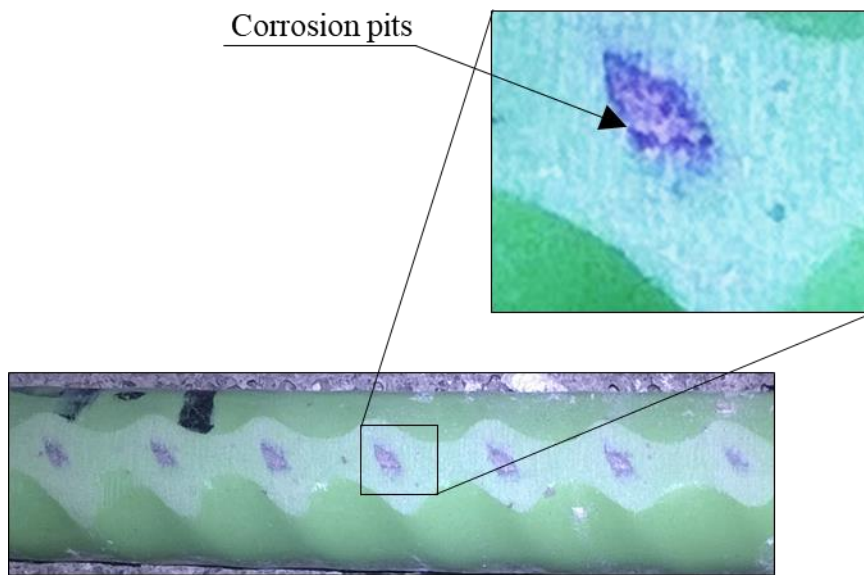
Figure 5.3(c)]. Therefore, proposed EIS based methodology can be used as a to detect

the initiation of corrosion in FBE costed steel rebars embedded in the cementitious system at

the early stage. The image analysis of the coating interface revealed that an average of 25% of

the total volume of coating are voids, which was also confirmed by water uptake calculation

suggested by (Singh and Ghosh 2005). Similar pore volumes were also reported by (Zhao et

al. 2019). If the underlying steel rebars are uniformly corroding, then about 1% of steel cross-

sectional loss is required for corrosion stains to be visible on the coating surface. In the case

of RC systems, there is additional confinement due to concrete. Therefore, more corrosion

products may be required to crack the coating. Then, additional corrosion products will be

required to exert pressure on the concrete surface – indicating that by the time corrosion stains

are visible on the concrete surface; a significant steel cross-sectional loss has already occurred

to the steel rebars. Note that the corrosion in FBE coated steel rebars is primarily localized

corrosion. Therefore, corrosion stains on the coating or concrete surface will be visible only

after considerable cross-section loss of steel rebars.
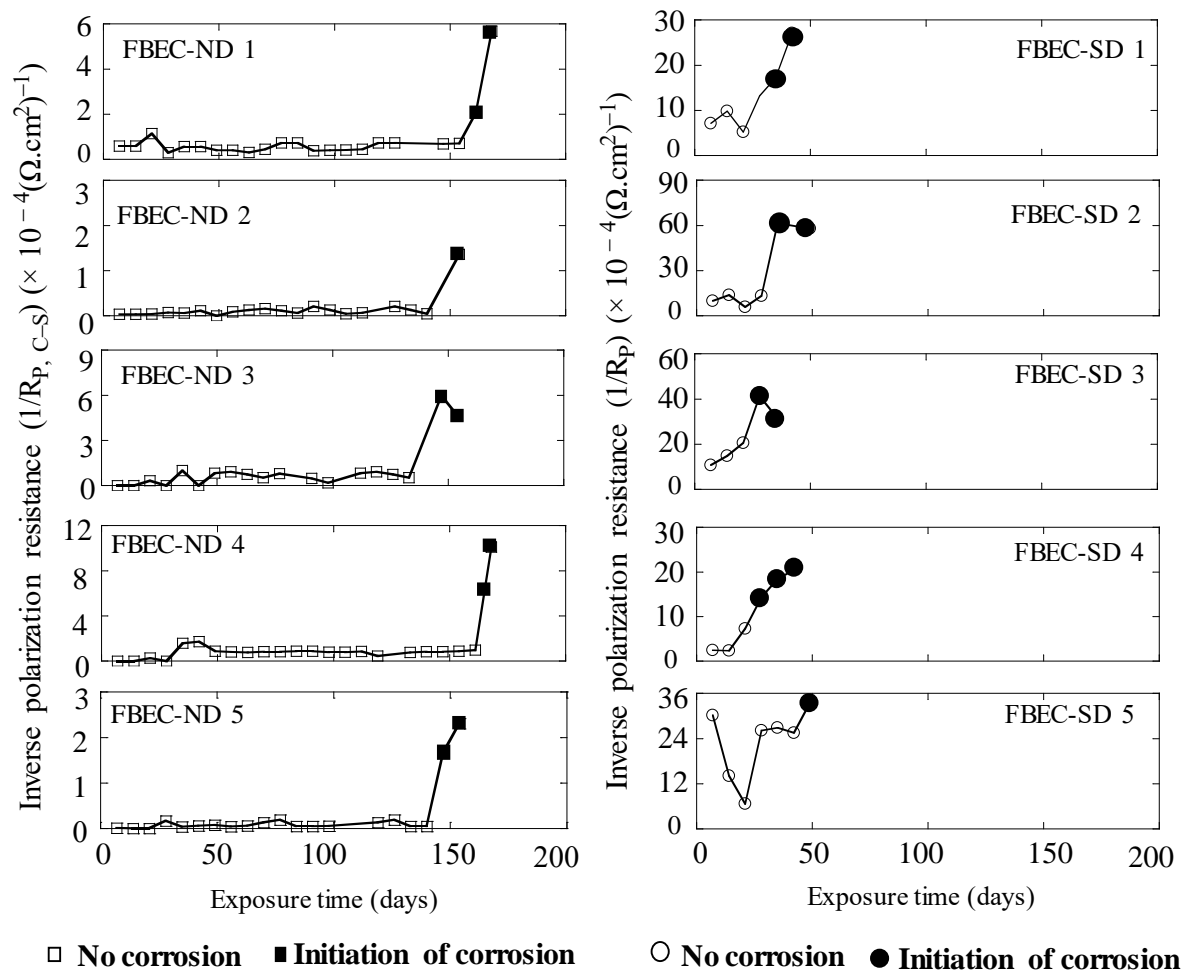
Figure 5.2 Detection of initiation of corrosion (unfilled and filled markers indicate passive and active corrosion measurements, respectively)
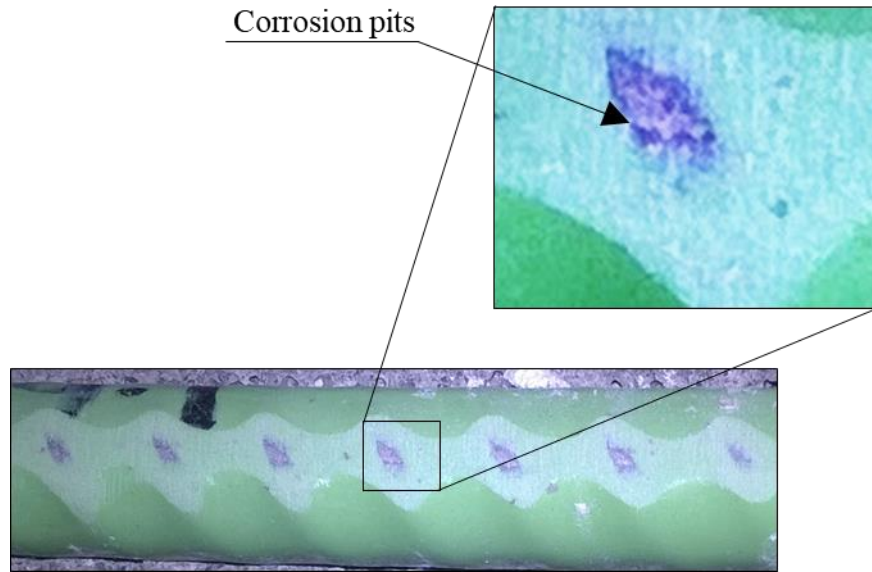
Figure 5.3 FBE coated steel rebar extracted from a lollipop specimen after initiation of corrosion has been detected using EIS-based tests

5.2.2 Chloride thresholds

Figure 5.4 shows the average chloride threshold of uncoated, FBEC-ND, FBEC-SD type specimens were found to be 0.4, 0.12, and 0.22 %bwob. Also, literature shows that the chloride thresholds of damaged FBE coated steel rebars are $1 - 5$ Cl$^-$/OH (Kessler et al. 2015), which is in agreement with the chloride thresholds of FBEC-SD steel rebars embedded in mortar. Kessler et al. (2015) also highlighted that the chloride threshold of FBEC-SD steel depends on the defect size of the scratches. In this research, only one defect size is considered, i.e., 0.6% by surface area of coated steel rebars. It was also reported that the propagation time depends on the available sites for cathodic reactions. In the case of FBE coated steel rebars with limited damage to the coating, the cathodic sites can be limited. Therefore, the propagation of corrosion may be slower than uncoated steel rebars. However, in reality, the coating on coated steel rebars are severely damaged before embedding them in concrete. Therefore, the cathodic sites

can be easily available – resulting in fast propagation of corrosion. Therefore, propagation time is not considered for the estimation of service life.

Here, the Cl_{th} for FBE coated steel with no damage (FBEC-ND) and FBE coated steel with scratch damage (FBEC-SD) was found to be 70% and 50% less than the Cl_{th} of uncoated steel rebars, respectively. Note that the Cl_{th} of FBEC-ND is less than FBEC-SD because the Cl_{th} for FBEC-ND was determined from the chloride concentration in the coating interface at the steel-coating interface, as explained in Section 3.4.2.2. On the other hand, for FBEC-SD, chloride threshold was the chloride concentration in the mortar, which was in contact with the damaged locations.
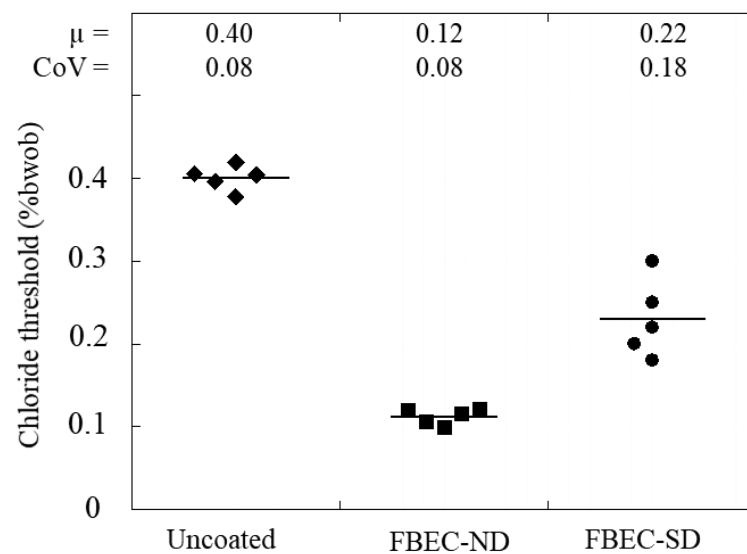
Figure 5.4 Chloride thresholds of uncoated, and FBE coated steel rebars with and without damage to the coating

5.3   PHASE 2 - EFFECT OF PROLONGED EXPOSURE TO SUNLIGHT/UV RAYS

5.3.1   Effect of UV exposure on coating characteristics

Figure 5.5(a)-(l) show the scanning electron micrographs (SEMs) obtained from the surface of epoxy coating samples at 0, 10, 12, 15, 20, 25, 35, 40, 50, 55, and 60 days of cyclic exposure in UV chamber. Figure 5.5(a) is from a FBEC-ND specimen and Figures (b) through (l) are from FBEC-UV specimens with specific days of exposure, as mentioned in the images. The photo-stabilizers (i.e., TiO_2 and ZnO) could prevent disintegration/microcracking of the coating until 10 days of UV exposure in the laboratory. Figure 5.6 summarizes the crack widths shown in these SEMs and shows the increase in crack width as a function of the duration of UV exposure. As per Figure 5.5(a)-(l) and Figure 5.6, the microcracking initiated at about 10 days of exposure to UV radiation in laboratory. This cracking can be due to the deficiency of photo-stabilizers on the surface of the epoxy coating, which in turn exposes the bulk material and allows its disintegration. The crack width was increasing up to 25 days of exposure to UV radiation. Then, the crack width was stabilized for the next about 25 days of exposure; this can be due to the presence of photo-stabilizers in the bulk coating, which is relatively better protected by the outer layers of coating (i.e., typical sigmoid curve as seen in shrinkage behavior of materials). The evidence of this shrinkage-induced cracking is discussed later in this section. With further exposure, the crack width was found to increase rapidly at about 50 days in the UV chamber (i.e., from about 0.5 to 1 mm) – indicating the rupturing of coating.

The coating started to crack after 10 days in the UV chamber (see Figure 5.5(c)), which is equivalent to about 1.5 months of exposure to sunlight. To validate this, Figure 5.7 shows the micrographs of coating in three cases: (a) without exposure to UV radiation, (b) with 10 days of exposure to UV radiations in the laboratory, and (c) with 45 days of exposure to natural environment/sunlight at Chennai, India with UVI > 8. The latter two cases resulted in

170

significant long and wide cracks. Therefore, 10 days of exposure in the UV chamber is considered for studies on chloride thresholds of FBE coated steel rebars.
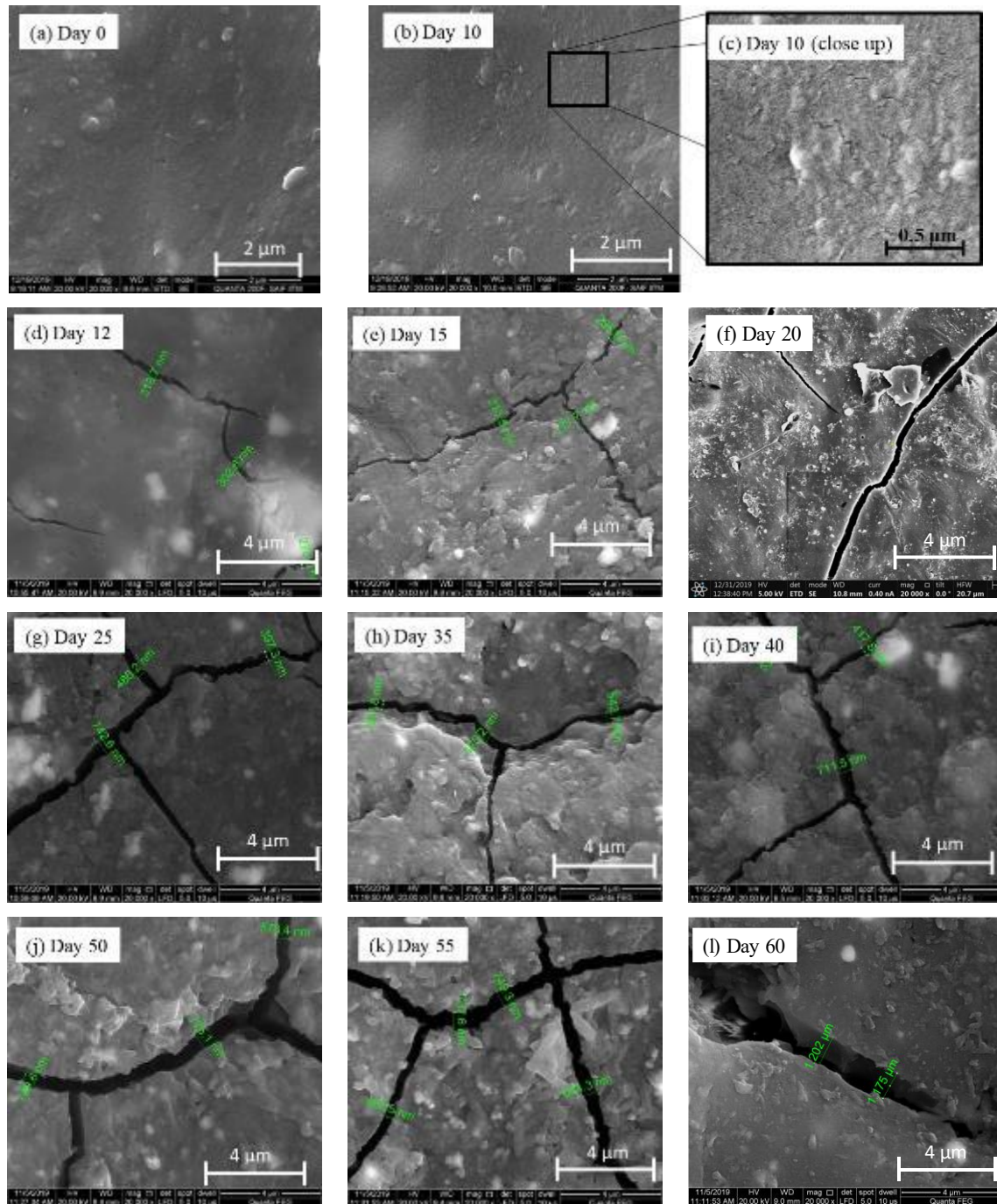
Figure 5.5 Micrographs showing crack evolution on epoxy coating exposed to UV rays
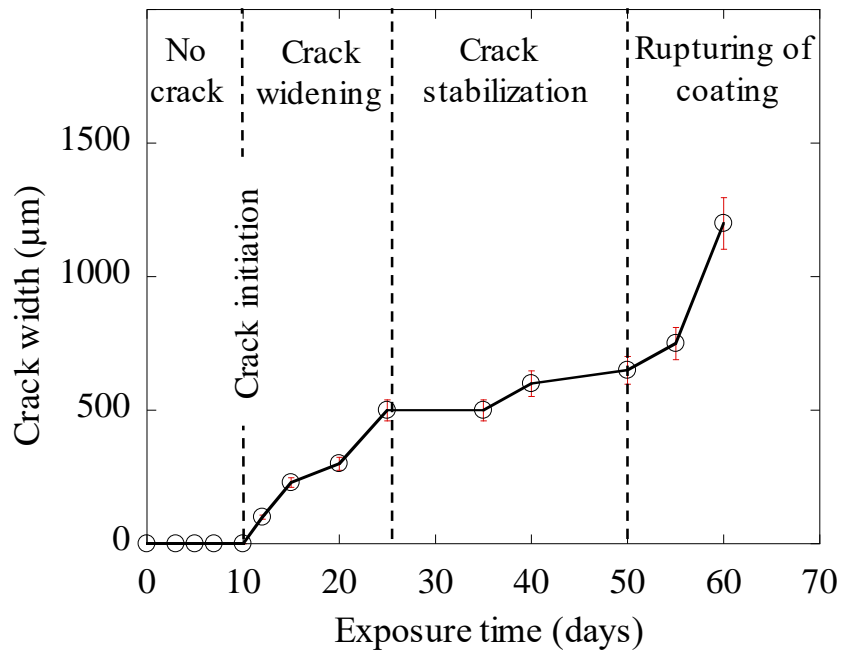
Figure 5.6 Effect of ultraviolet exposure on crack width on the FBE coating surface
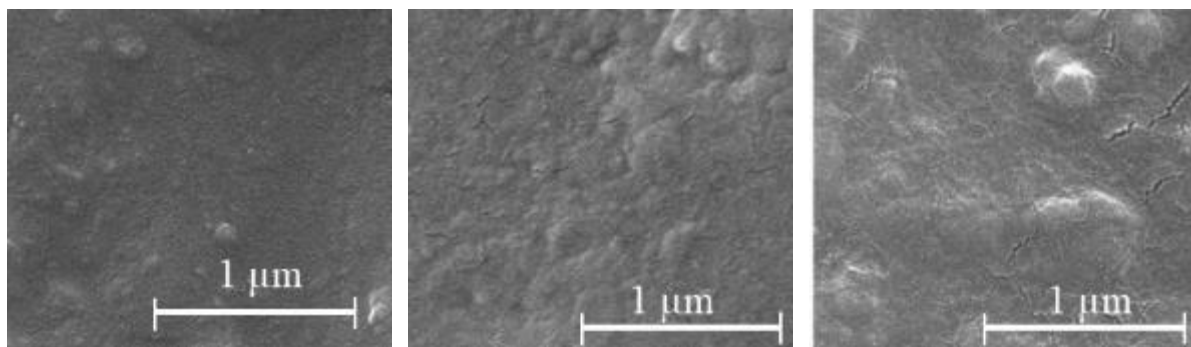
(a) Without exposure to UV rays (no cracks)

(b) At 10 days of exposure in UV chamber in the laboratory (crack initiation)

(c) At 45 days of exposure in natural sunlight/UV rays (long and wide cracks)

Figure 5.7 Cracks on FBE coatings formed due to UV/sunlight exposure

To investigate the reason for cracking, FT-IR spectra (for the range of 600 cm^{-1} to 4000 cm^{-1}) were obtained from epoxy coating samples subjected to 0 and 10 days of UV exposure in the laboratory (see Figure 5.8). The first, second, third, and fourth regions shown in the spectra range from 600 to 1500, 1500 to 2000, 2000 to 2500, and 2500 to 4000 cm^{-1}, respectively. The first region contains characteristic peaks for the individual bonds such as -C-O and -C-H in the epoxy coating (Baker et al. 2015). After exposure to UV rays, the intensity of peaks between 1000 and 1200, and at 2932 cm^{-1} decreased – indicating the breakage of -C-H bonds (Suliga et al. 2018; Wang et al. 2017). In addition, the peaks at 1231, 1296, and 1463 cm^{-1} disappeared after exposure to UV rays – indicating the breakage of bonds in CH$_2$. In the case of FBEC-ND samples, peaks were observed at 860 and 970 cm^{-1} – indicating the presence of benzene. When exposed to UV rays, an additional peak was observed at 1508 cm^{-1} – indicating that the benzene did not undergo photodegradation until 10 days of UV exposure in the laboratory – in agreement with the literature (Wang et al. 2017). The FT-IR spectra obtained from the FBEC-ND and FBEC-UV samples show that the hydroxyl groups are the weakest bonds in the epoxy coating used in this study. The available sites after the breakage of hydroxyl bonds can get oxidized. The decrease in the area under the curve between 1550 to 1750 cm^{-1} (between the two vertical dashed lines in Figure 5.8) indicates the formation of the carbonyl group. The formation of the carbonyl group is the result of the photodegradation process of epoxy polymer, which can result in shrinkage-induced cracking of coatings (Nikafshar et al. 2017; Woo et al. 2007). This observation on carbonyl group formation justifies the shrinkage-induced cracking phenomenon proposed earlier in this section (i.e., the sigmoid curve until about 50 days followed by a rapid increase in crack width) discussed in Figure 5.6.
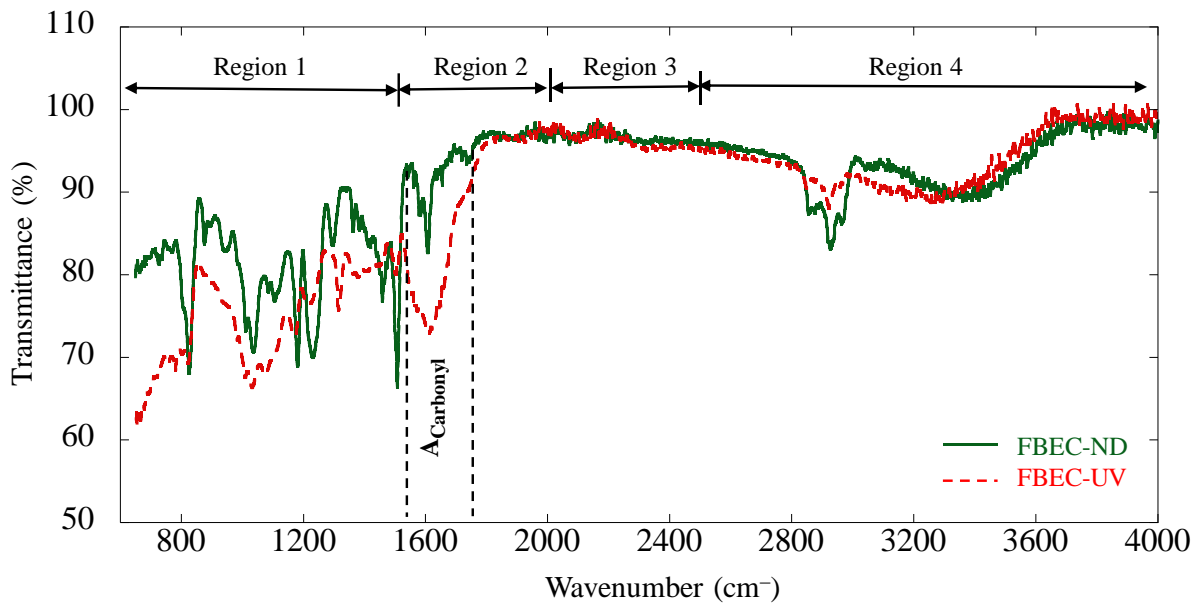
Figure 5.8 FT-IR spectra of FBE coating with and without exposure to UV rays

In addition, the chemical composition from the coating samples were collected before and after the exposure to UV rays to understand why the cracking initiated at some specific locations? Figure 5.9 shows that the various chemicals are used for the manufacturing of epoxy resin used for coating the steel rebars. A huge variation of concentration was found for each of the elements. Here, a few of the elements (C, Ba, etc.) are found to have the coefficient of variations (CoV) of concentration more than 0.5. Also, a few of the elements such as S, Cl, Ca, Fe, Zn, etc. are found to have CoV more than 1 – indicating that the distribution of each of the elements is not uniform on the surface of the coating. Note that the concentration of each of the elements can influence the corrosion, mechanical, and interface properties of FBE coating. For example, inappropriate quantities of $BaSO_4$ can result in more voids, crazes, microcracks, and low bonding between steel and coating (Wang et al. 2008). Addition of curing agent lesser or more than required concentration can result in reduction in crosslinking, density, and resistance of coating (Monetta et al. 1993). Therefore, the control on the

concentration and its distribution is essential to achieve the desired properties. Here, the effect of nonuniform distribution of photo stabilizers such as TiO_2 and ZnO is discussed next.

Table 5.1 provides the chemical composition at the surface of the epoxy coating extracted/peeled-off from three locations on the FBEC-ND and FBEC-UV samples using EDX analysis. It shows that the concentrations of Ti and Zn on the three FBEC-ND specimens vary significantly, which can be attributed to the variation in the concentration of photo-stabilizers (i.e., TiO_2 and ZnO) on the surface of epoxy coating – possibly a manufacturing defect. Also, it was found that the concentrations of TiO_2 and ZnO were negligible at cracks on the surface of FBEC-UV samples – indicating that with the deficiency of TiO_2 and ZnO, the epoxy coating can get degraded and microcracks can form within ten days of laboratory expos due to UV (340 nm) rays (see Table 5.1). The regions with depletion of photo-stabilizers such as TiO_2 and ZnO can also undergo photodegradation (Ghasemi-Kahrizsangi et al. 2015a). On the other hand, barium and Sulphur were found in the bulk of epoxy coating – indicating that barium sulfate ($BaSO_4$) was added to the epoxy material - probably to enhance the bond between steel and epoxy coating (Cheng et al. 2007). However, the addition of barium sulfate can increase the brittleness, which in turn can lead to cracking of coating when the bar is bent, and the epoxy coating at the outer surface of the bent gets elongated (Kamde and Pillai 2017).
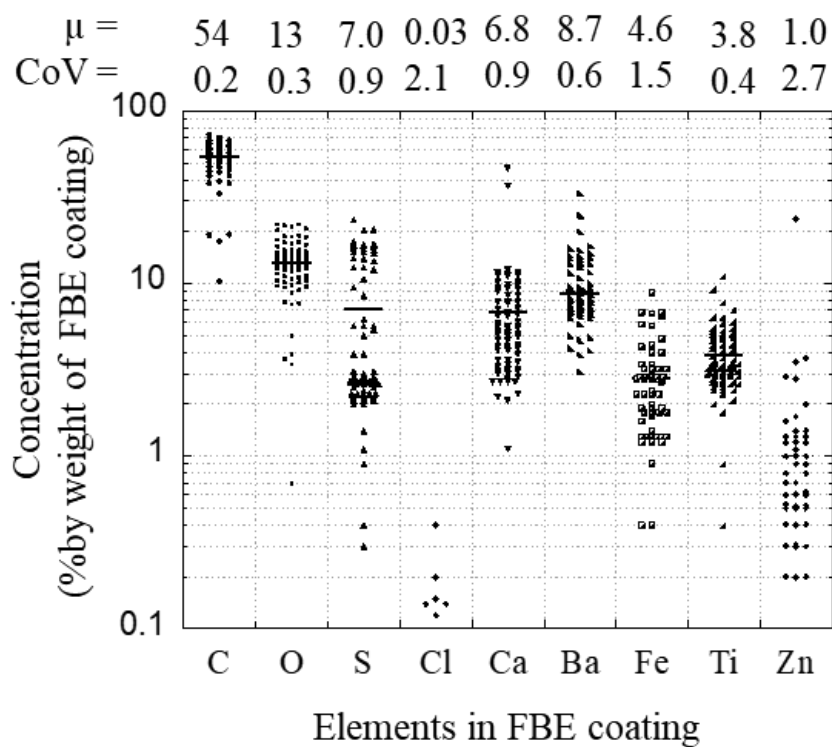
Figure 5.9: Variation in the chemical composition of FBE coating

Table 5.1 Chemical composition of FBE coating specimen*

Element	FBEC-ND		FBEC -UV				
			away from cracks		at crack		μ2 - μ3
	μ1	CoV	μ2	CoV	μ3	CoV	
C	42.4	0.57	49.3	0.3	42.2	0.3	7.1
N	3.4	1.7	0.5	1.4	3.1	1.2	-2.6
O	9	5.6	11.2	0.4	14.3	0.2	-3.1
Mg	1.5	0.5	0.5	1.6	0.4	1.5	0.1
Si	3.3	0.7	3.1	0.5	2.0	0.7	1.2
Ca	3.7	0.94	2.8	0.8	1.7	1.5	1.1
S	22.4	1.0	13.1	1.6	20.5	0.5	-7.4
Ba	12.13	1.8	1.5	1.2	14.0	0.5	-12.5
Ti	4.65	1.7	8.6	1.2	0.3	1.5	8.3
Zn	0.9	1.1	2.0	0.5	0.3	1.2	1.7

*Weight percentage

Figure 5.10 shows the Nyquist plots of the FBEC-ND and FBEC-UV specimens. The resistance of coating (R_C) from FBEC-UV specimens with significant cracking exhibited a resistance of ≈ 5 kΩ-cm^2, which was significantly less than that of FBEC-ND specimens (i.e., ≈ 30 kΩ-cm^2). This indicates that the type of cracks formed in such coatings can provide easy pathways for deleterious elements such as moisture, oxygen, chlorides, etc. to reach the steel surface (Liu et al. 2009). Therefore, the candidate suggests that FBE coated steel rebars should not be exposed to sunlight for more than one month (including storage and construction stages).
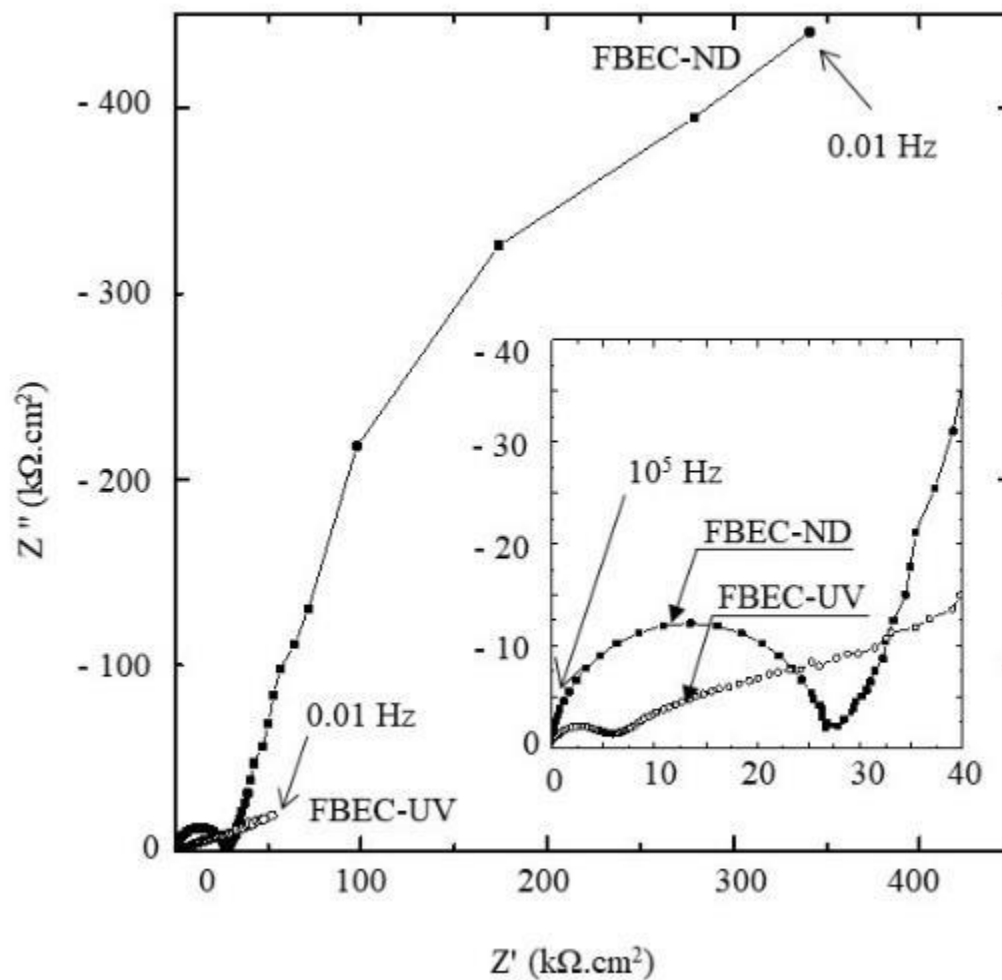
Figure 5.10 EIS response from FBE coated steels - with and without UV exposure and then embedded in mortar

177

5.3.2 Coating degradation and corrosion initiation

5.3.2.1 FBEC-ND

Figure 5.11 show the degradation of FBEC-ND and FBEC-UV systems in terms of the change in coating resistance, R_C. Figure 5.11(a) show the 4-stage degradation process of FBEC-ND coating in cement mortar (alkaline in nature) [also discussed in detail in Section 4.2.4.1]. Figure 5.12(a) shows the drawing with the proposed 4-stage degradation process for FBEC-ND systems. Stage 1 is defined as the period when the resistance of coating (R_C) embedded in mortar is constant (say, during the first few weeks of exposure) – indicating that the coating could resist the entry of alkaline pore solution and moisture for about three to four weeks. Stage 2 is defined as the period when the R_C decreases. Typically, R_C decreases to about half the original value after 1st wet period. Similar responses were also presented by Zayed and Sagues (1990) (Abla M. Zayed 1990). During this time, the alkaline pore solution and moisture (probably chlorides as well) could have partially penetrated the undamaged coating and reduced the R_C. Then, when sufficient moisture and oxygen are available at the steel surface, corrosion might initiate and propagate. Stage 3 is defined as the period when R_C increases, which can be attributed to the additional resistance offered by pores in the inner layer of coating (i.e., near the steel surface) that are densely filled with corrosion products (Wang and Gao 2016). This filling of pores at the inner layer of epoxy coating with corrosion products was confirmed by microanalytical analysis (SEM and EDX analysis) of the pores. This can obstruct the further entry of oxygen and delay the corrosion process. In Stage 4, the corrosion products continue to build-up, resulting in increased expansive stresses and cracking of coating, which in turn increases the interconnectivity of pores/holidays/cracks and allows the entry of more pore solution, moisture, and chlorides. The coating with interconnected pores/pinholes/cracks filled with moist corrosion products can exhibit a low coating resistance.

5.3.2.2   FBEC – UV

Figure 5.11 shows the monitoring data from five of the specimens used for assessment. Figure 5.12(b) show the schematic for the 2-stage fast degradation process of FBEC-UV coating in cement mortar exposed to chlorides. The first five plots indicate the data collected from five specimens during the exposure of lollipop specimens with FBEC-UV steel rebars. The resistance of the coating was found to be constant for about $1 - 2$ cycles of exposure -indicating that the FBEC-UV coating could resist the penetration of moisture/chloride during this time. With further exposure, the resistance of FBEC-UV coating was found to be significantly decreasing. The last drawing shows the degradation process of FBEC-UV coating. Stage 1 is defined as the initial period when R_C offered by the coating was significantly high. Stage 2 is defined as the period when R_C decreases significantly. Unlike Stage 3 in the case of FBEC-ND, the FBEC-UV specimens did not exhibit an increase in R_C. The corrosion products formed in the case of FBEC-UV rebars can exert the expansive pressure and diffuse and permeate out through the cracks in FBE coating that can form within 10 days of exposure in UV chamber (see Figure 5.5). With further exposure, R_C continued to decrease, mainly because of the presence of chlorides and the formation of soluble corrosion products filling the space available in the coating.

(a) Proposed four-stage coating degradation process in FBEC-ND specimens

(b) Proposed two stage coating degradation process in FBEC- UV specimens
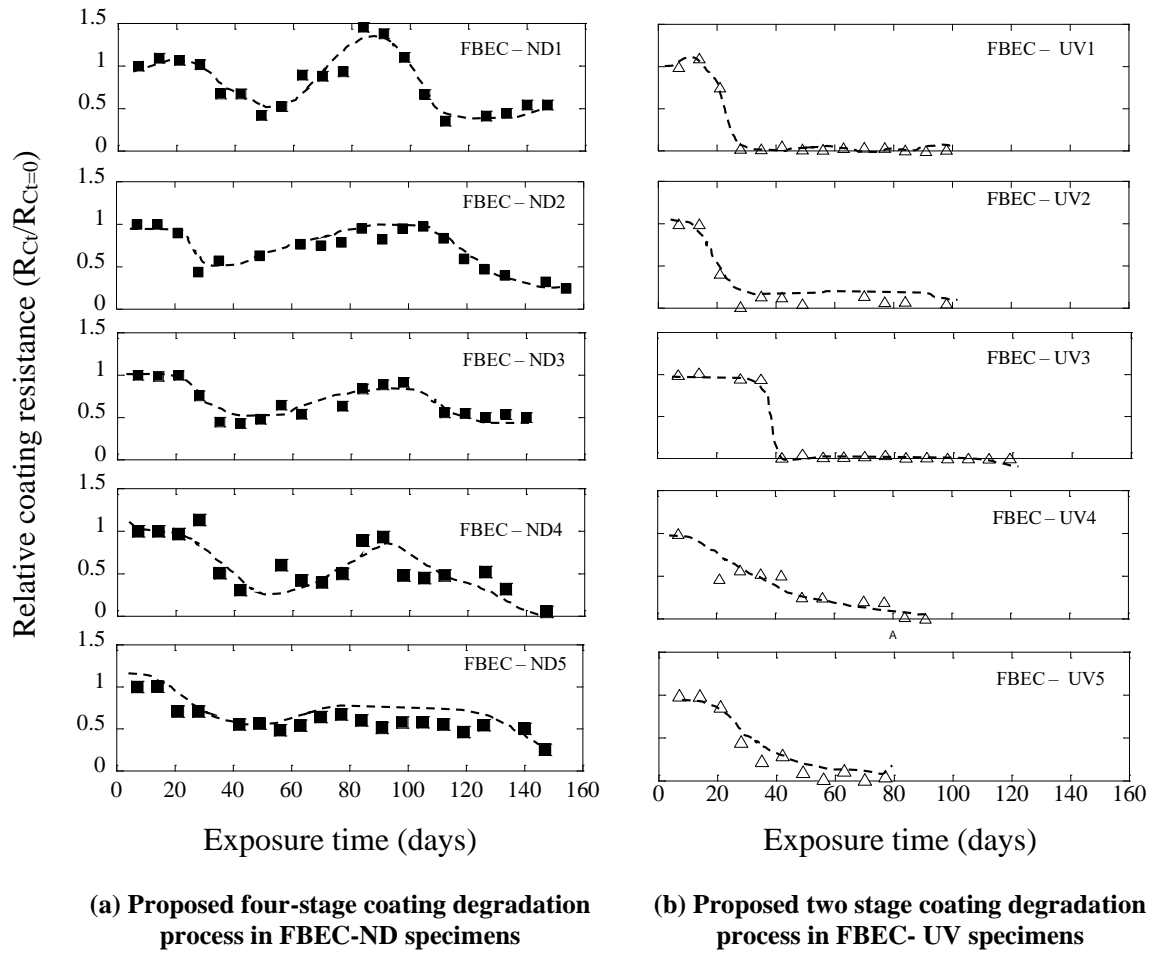
Figure 5.11 Change in relative resistance of coating due to exposure to cement mortar
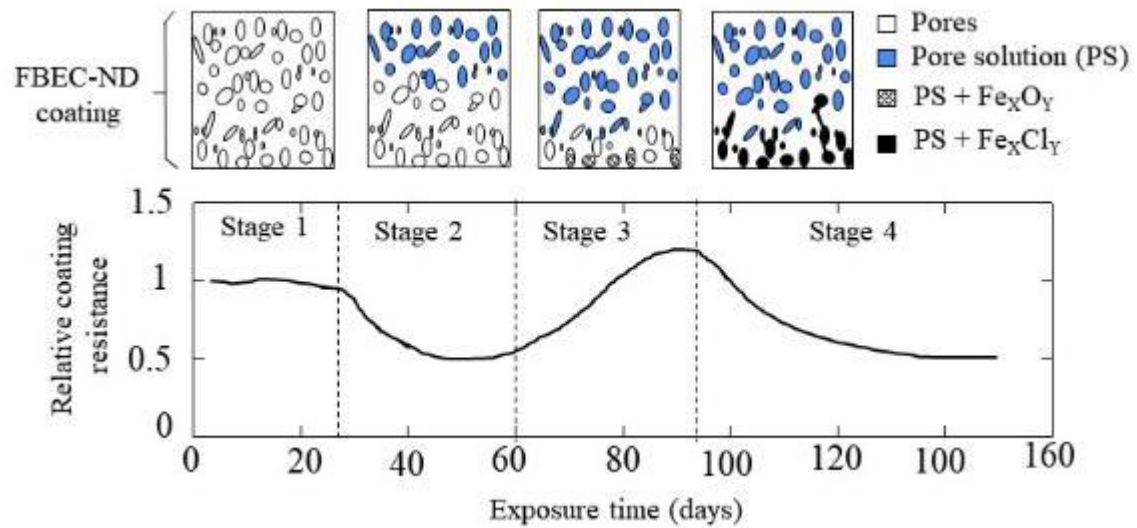
(a) Mechanism of degradation of FBEC-ND coating
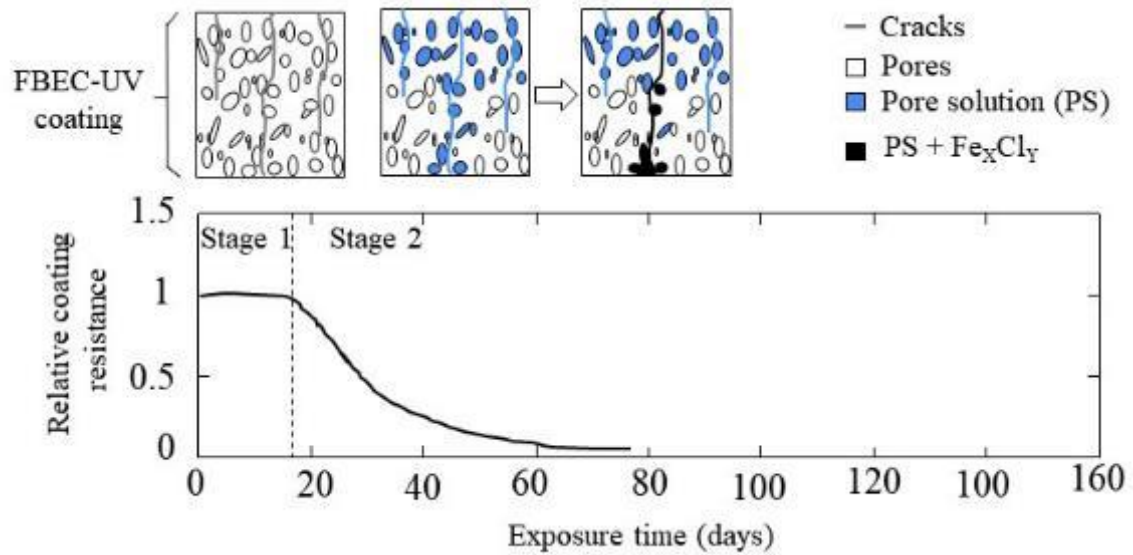
(b) Mechanism of degradation of FBEC-UV coating

Figure 5.12 Schematic and proposed mechanism for coating degradation for FBEC-ND and FBEC-UV coatings and leading to initiation of corrosion

Figure 5.13(a) shows the proposed mechanisms for the initiation of corrosion in concrete with FBE coated steel rebars exposed to sunlight/UV rays. Note that all the shown cracks are not of the same depth. As shown, the metal surface below one of the deep cracks can act as an anode and another crack with moisture can provide a least resistive path (for ionic conduction), and the steel surface below can act as cathode. The micrograph in Figure 5.13(b) shows such cracks formed in FBE coating. Also, such cracks can facilitate the transport of oxygen, moisture, and chlorides to the steel surface. Figure 5.13(c) shows a schematic of the propagation of underfilm corrosion and the associated mechanisms. In this case, if the bond between steel and coating cannot resist the expansive forces, the coating disbondment will occur – resulting in further propagation of underfilm corrosion (Wan et al. 2017), which is evident from Figure 5.13(d). Micrograph reveals that the corrosion progresses under the coating and corrosion products first fill the pores in the inner layer of FBE coating. To confirm this, the lollipop test specimens were autopsied, and the coating surface and the steel surface (after removing the mortar cover) were visually inspected. Figure 5.13(e) shows a photograph and schematic of corroded FBEC-UV steel rebar with localized corrosion spots and underfilm corrosion. Therefore, for the structures that are already built with FBE coated steel rebars, it is essential to form preventive maintenance strategies to delay the initiation of corrosion in RC systems. For future construction, it is essential to prevent FBE coated steel rebars from getting exposed sunlight/UV rays before placing them in concrete systems so that the coating can work effectively in resisting chloride attack.
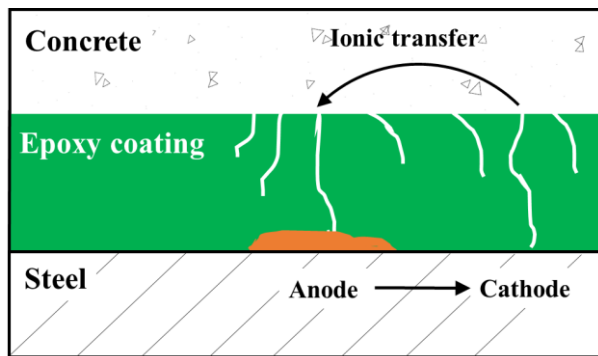
(a) Corrosion initiation mechanism
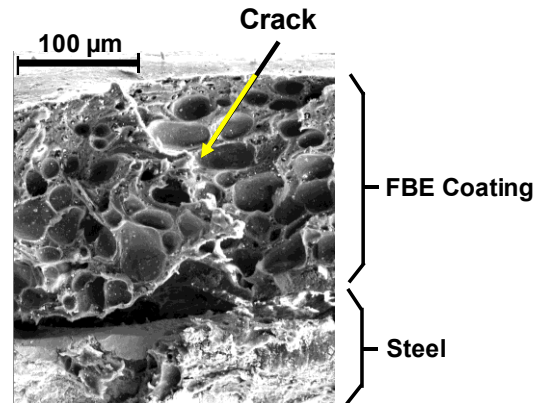
(b) Crack in FBE coating
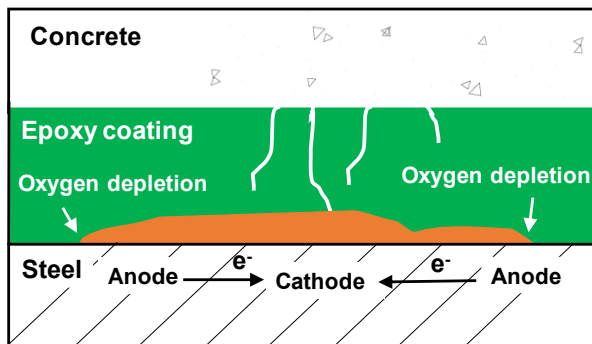
(c) Corrosion propagation mechanism
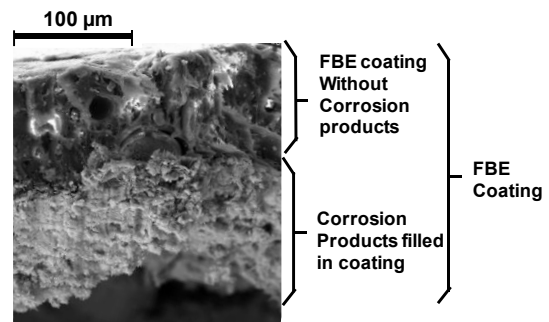
(d) FBE coating partially filled with underfilm corrosion products

■ **Corrosion spots (UV-induced crack locations)**　　■ **Underfilm corrosion products**
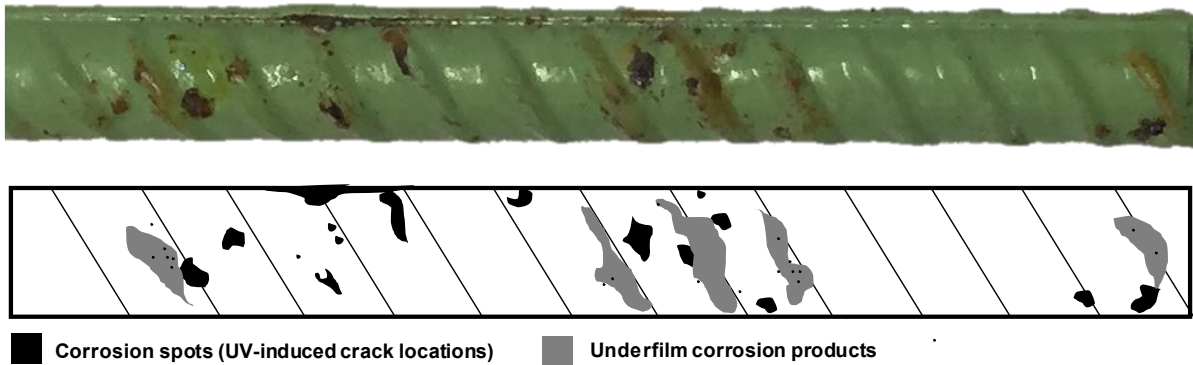
(e) FBEC – UV steel rebar showing the oozing out of underfilm corrosion products through cracks

Figure 5.13 Proposed corrosion mechanisms of FBE coated steel exposed to UV/sunlight and then embedded in concrete

5.3.3 Chloride threshold of steel (uncoated, ND and UV)

The comparison of the polarization resistance of the steel or steel-coating interface (R_P or $R_{P,\ S-C}$) can be used as a short-term test for screening the steel rebars. However, evaluation based on chloride threshold (Cl_{th}) is a more rational approach to define the corrosion performance and service life of coated or uncoated steel rebars in cementitious systems. Figure 4.15(a) shows the variation of inverse polarization resistance (i.e., $1/R_P$) for uncoated rebars as a function of exposure time. Figure 4.15(b) and (c) show the variation of inverse polarization resistance (i.e., $1/R_{P,\ S-C}$) for FBE coated rebars without and with UV exposure. The filled markers represent the points of active corrosion (i.e., after the initiation of corrosion). The specimens with uncoated steel rebars exhibited the initiation of corrosion at about 50 days of cyclic wet-dry exposure to SPS solution with chlorides; whereas, FBEC-ND and FBEC-UV specimens exhibited initiation of corrosion between 150 and 170 days and between 50 and 80 days of cyclic wet-dry exposure, respectively. The delay in the initiation of corrosion in FBEC-ND specimens can be attributed to its low chloride diffusion coefficient. On the other hand, the early initiation of corrosion in FBEC-UV specimens can be attributed to the easy ingress of chlorides through the cracked coating.
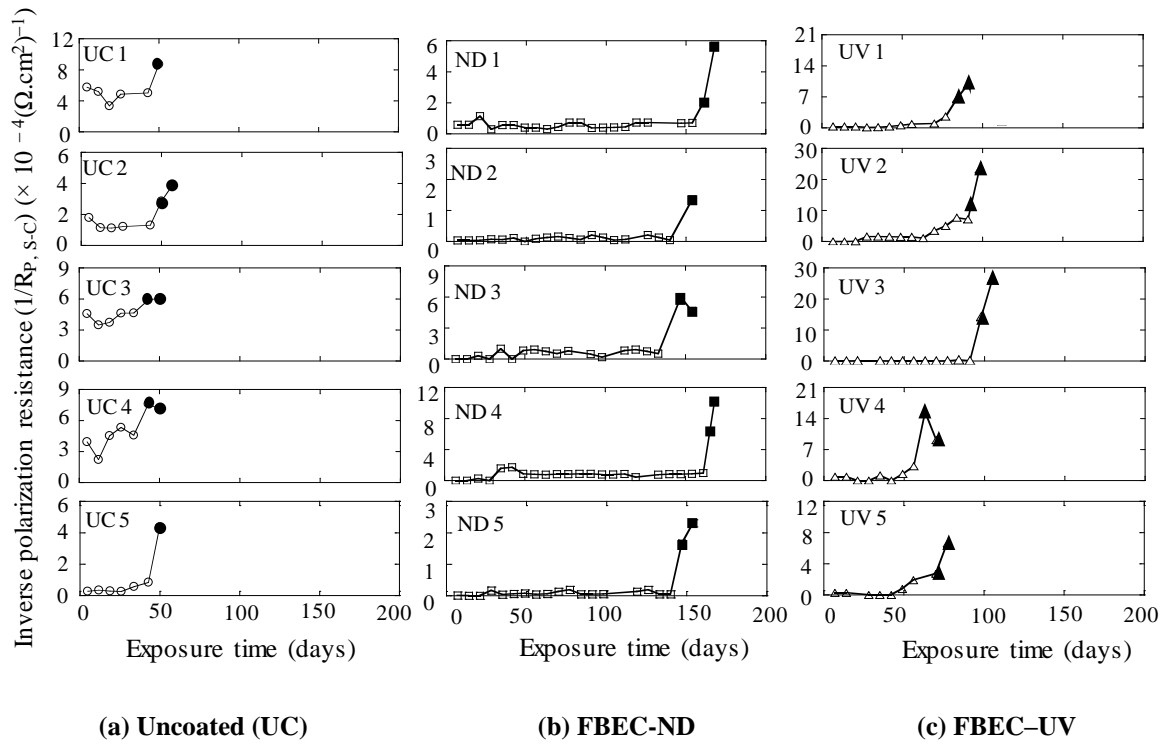
Figure 5.14 Detection of initiation of corrosion in lollipop specimens using the EIS technique (unfilled and filled markers indicate passive and active corrosion measurements, respectively)

See Figure 5.15 for the mean and coefficient of variation of Cl_{th} observed for uncoated, FBEC-ND, and FBEC-UV specimens. The chloride threshold (Cl_{th}) of uncoated steel was found to be 0.42 %bwob with a coefficient of variation of 0.1. The average chloride concentrations on the coating surface (at the coating-mortar interface) were found to be 0.75 and 0.53 %bwob. Similarly, literature suggest the chloride threshold of FBE coated steel rebar as 1 - 2 % by weight of cement (Cortés 1998; Darwin et al. 2014), which is significantly higher than the chloride threshold of uncoated steel rebars (i.e., $\approx$ 0.4 % by weight of cement) (Rengaraju 2019). However, these values are determined based on half-cell potential measurements, macrocell corrosion current, and linear polarization resistance, which may not be valid for RC systems with FBE coated steel rebars. However, these chlorides in mortar do

not participate in the corrosion process at the steel-coating interface because they are separated by a physical barrier (i.e., FBE coating). Therefore, chlorides at the innermost layer of FBE coating (at the steel-coating interface) were determined and defined as Cl_{th}. In this manner, the average Cl_{th} for the FBEC-ND and FBEC-UV steel rebars were found to be 0.12 and 0.07 % bwob, respectively. This is about 1/4th of the Cl_{th} of uncoated steels. This significant difference in Cl_{th} of uncoated and coated steel rebars can be attributed to the differences in the pH of mortar (i.e., 12 ± 1) and of FBE coating (i.e., 6 ± 1) in contact with uncoated and coated steel rebars, respectively (Mundra et al. 2017). Also, the difference in the size of cracks in coatings can lead to differences in the microclimate at the steel-coating interface (i.e., the concentration of oxygen and moisture). As discussed, exposure of FBE coating to UV rays can crack the coating, which can allow more oxygen and moisture to the steel surface – resulting in the alteration of microclimate at the steel surface (Séverine Marie Noëlle Cambier 2014).which in turn can lead to the difference in Cl_{th} between the uncoated, FBEC-ND, and FBEC-UV cases.

μ =	0.42	0.12	0.08
CoV =	0.10	0.08	0.12
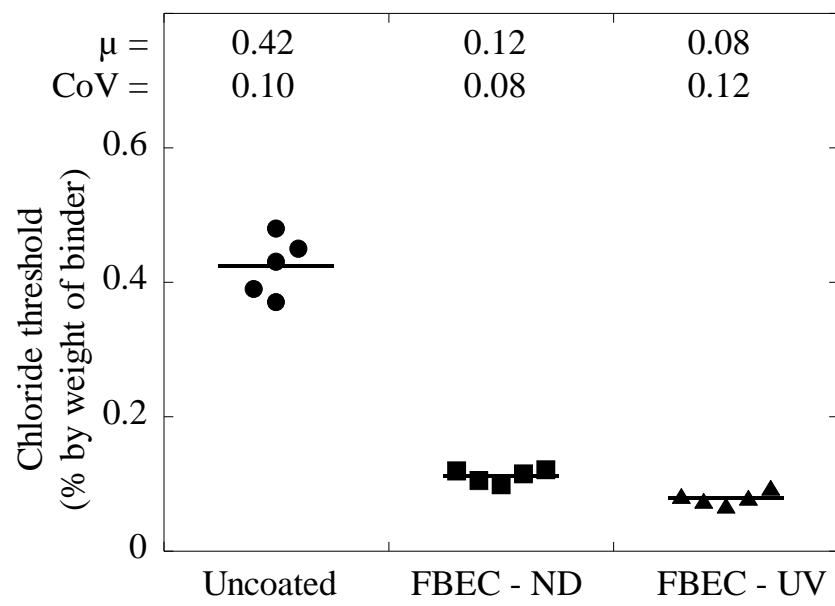
Figure 5.15 Chloride thresholds of uncoated and coated steels

5.3.4 Chloride diffusion coefficient of FBE coating

Figure 5.16 shows that the chloride profiles for FBEC-ND and FBEC-UV coatings. Note that, in FBEC-ND coatings, the chloride concentrations at first few micrometers away from the surface is significantly lower than that at the surface. This can be attributed to the closely packed microstructure of the FBEC-ND coating surface (Javidparvar et al. 2016). For the remaining depth, the chloride concentration is similar. In case of FBEC-UV coatings, the chloride concentrations were found to be gradually decreasing as a function of the distance from the exposed coating surface (till the steel-coating interface). This can be attributed to the microcracking of FBE coating due to exposure to UV radiations and corresponding faster ingress of chlorides. The average $D_{cl, coating}$ for FBEC-ND and FBEC-UV coating specimens were found to be 1.6×10^{-20} and 8.7×10^{-18} m^2/s, with a cov of 0.2 and 0.36, respectively. This significant difference between D_{cl} of ND and UV coatings indicate that the exposure to UV rays can severely degrade the coating – leading to faster ingress of chlorides. The $D_{cl, coating}$ in this study is found to be in the order of 10^{-18} to 10^{-20} m^2/s, which is in agreement with the results reported by Singh and Ghosh (2005). On the other hand, for concrete, many literature report the D_{cl} is more than 10^{-12} m^2/s (Pillai et al. 2019; Zhang et al. 2018)
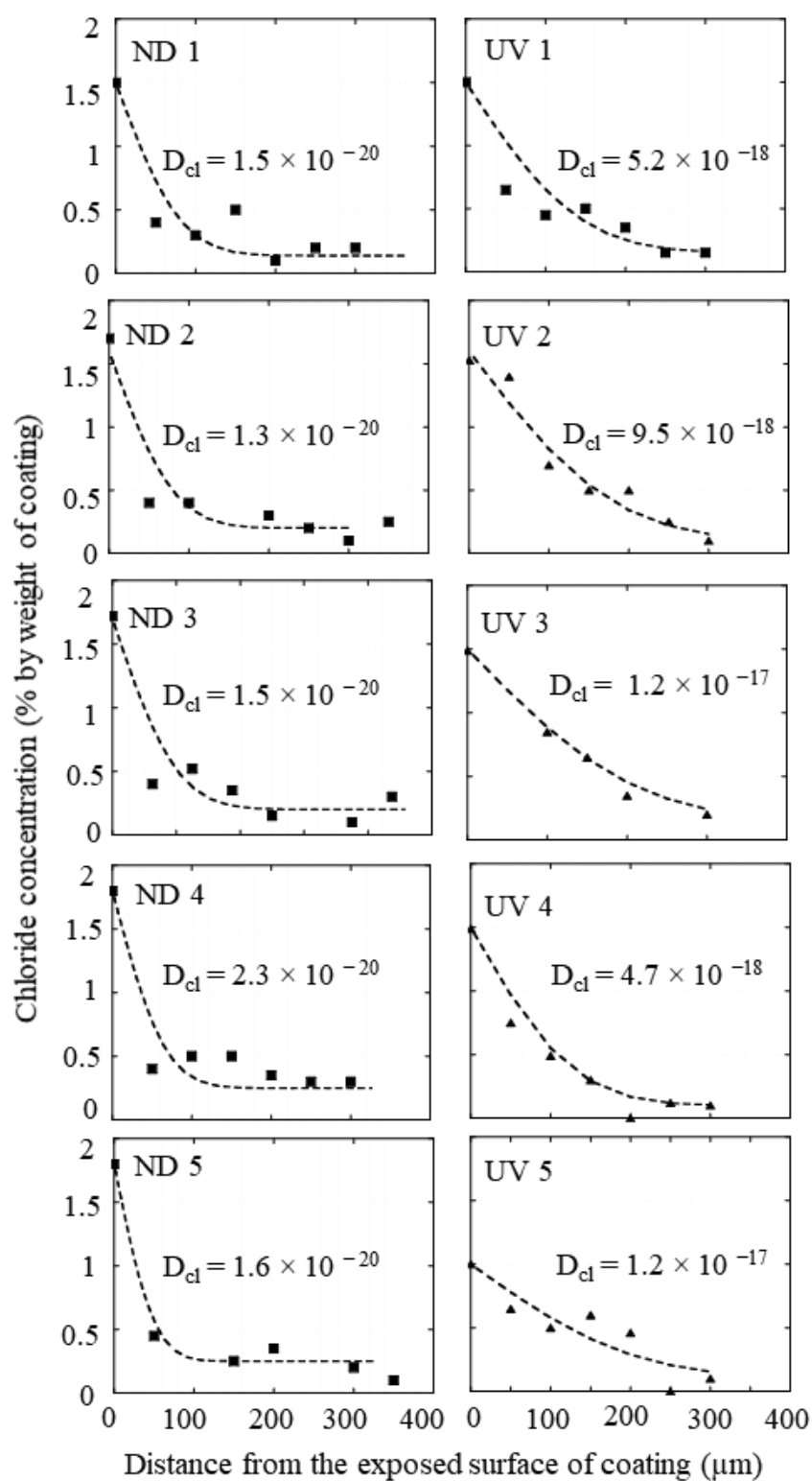
Figure 5.16 Chloride profile in coating at the time of corrosion initiation (obtained using EDX technique)

5.4 PROPOSED FRAMEWORK AND SERVICE LIFE ESTIMATION

5.4.1 Proposed framework for service life estimation

Figure 5.17 shows the schematic of proposed framework for the estimation of service lives of RC systems with FBE coated steel rebars. The concept is to introduce the with two-stage diffusion of chlorides: first, through concrete; then, FBE coating. Figure 5.17(b) shows that at age = t_0 of RC systems, the chloride concentration at the concrete surface is zero. At this stage, the chloride concentrations at the coating surface are also zero. Therefore, chlorides do not diffuse through the coating. Later, at age = t_1, the accumulated chloride concentration at the concrete, coating, and steel surfaces are $C_{S, t1}$, $Cl_{C-M, t1}$, and C_{t1}. Therefore, as a result of chloride concentration gradient at concrete, coating, and steel surface, chlorides diffuse through the concrete and coating materials. At this stage, the chloride concentration at the steel surface is less than the chloride threshold of FBE steel rebars. Therefore, the corrosion of steel does not take place. Later, at age = t_i, the accumulated chloride concentration at the steel surface is equal to the chloride threshold of FBE coated steel rebars, results in the initiation of corrosion. The time required for the chlorides to reach the steel surface through concrete and chloride to the concentration equal to the chloride threshold is defined as the service life of RC systems with FBE coated steel rebars. To estimate the service life of such RC systems, the following input parameters were used maximum surface chloride concentrations of concrete, D_{cl} of concrete, maturity constant (m) of concrete, concrete cover thickness (x), coating thickness, $D_{cl, coating}$, and Cl_{th} of coated steel rebars. A MATLAB® program based on diffusion of chlorides through concrete published by Rengaraju (2019) was modified to accommodate the diffusion of chlorides through FBE coating. Details on the procedure to estimate the service life is provided in Appendix C.

(a) Instantaneous chloride concentrations at various locations in a coated rebar system

(b) Time-dependent changes in chloride profile
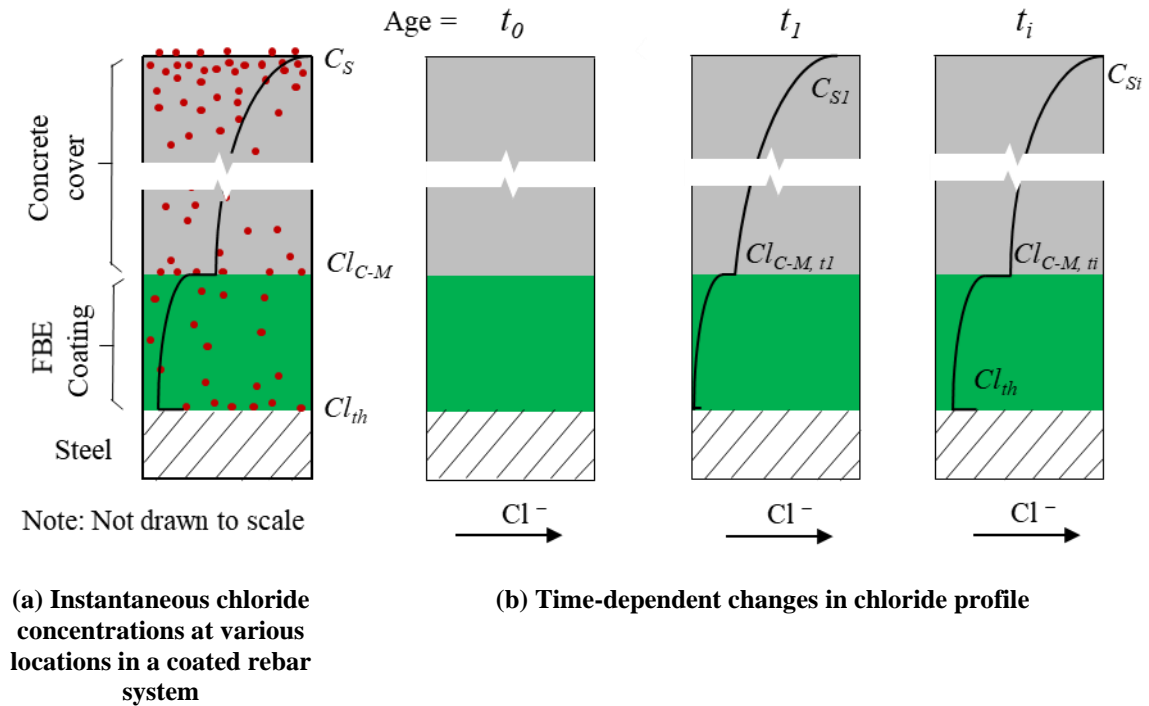
Figure 5.17 Proposed framework for service life estimation of FBE coated steel in cementitious systems

5.4.2 Effect of scratch damage and UV degradation on service life

As a case study, the determined $D_{cl, coating,}$ and Cl_{th} values were used to estimate the service life of a typical reinforced concrete system with FBE coated steel rebars. Figure 5.18 shows the cumulative distribution functions for the time to initiation of corrosion [traditionally defined as service life (t_i)] of reinforced concrete systems with uncoated, FBEC-ND, and FBEC-UV steel rebars. The input parameters used to obtain the cumulative distribution function are presented along with the cumulative distribution function. This case study shows that allowing FBE-coated rebars to get exposed to sunlight/UV for about a month can reduce the average expected service life from about 120 years to 75 (by about 40%). Also, the t_i of element with FBEC-UV steel rebars was found to be about 20% less than that with the systems

with uncoated steel rebars. Therefore, the use of FBE coated steel is not beneficial if exposure to sunlight/UV cannot be avoided during various stages of transportation storage and construction. Note that the results presented in this thesis are for FBE coated steel rebars exposed to UV rays for about one month. It was observed that the cracks were widened with further exposure to UV rays (see Figure 5.6). More than one month of exposure to sunlight can result in higher D_{cl} of FBE coating and lower t_i than what is presented here. Similarly, t_i for RC systems with FBEC-SD steel was found to be about 40% less than the t_i for RC systems uncoated steel rebars, which is about 70% less than the t_i with FBEC-ND steel rebars. The service life predictions presented here do not include all type of damages of epoxy-coated reinforcement. Thus, the real service life could be significantly less than presented here.

$$
\begin{array}{lcl}
D_{cl,\,concrete} & = & LN\,(1.7,\,0.35) \times 10^{-11}\,m^2/s \\
C_{max} & = & LN\,(1.2,\,0.03)\,\%bwob \\
x & = & LN\,(50,\,0.2)\,mm \\
m & = & 0.3 \\
D_{cl,\,FBEC\text{-}ND} & = & LN\,(1.6,\,0.20) \times 10^{-20}\,m^2/s \\
D_{cl,\,FBEC\text{-}UV} & = & LN\,(8.6,\,0.36) \times 10^{-18}\,m^2/s \\
Coating\ thickness & = & 200\,\mu m
\end{array}
$$
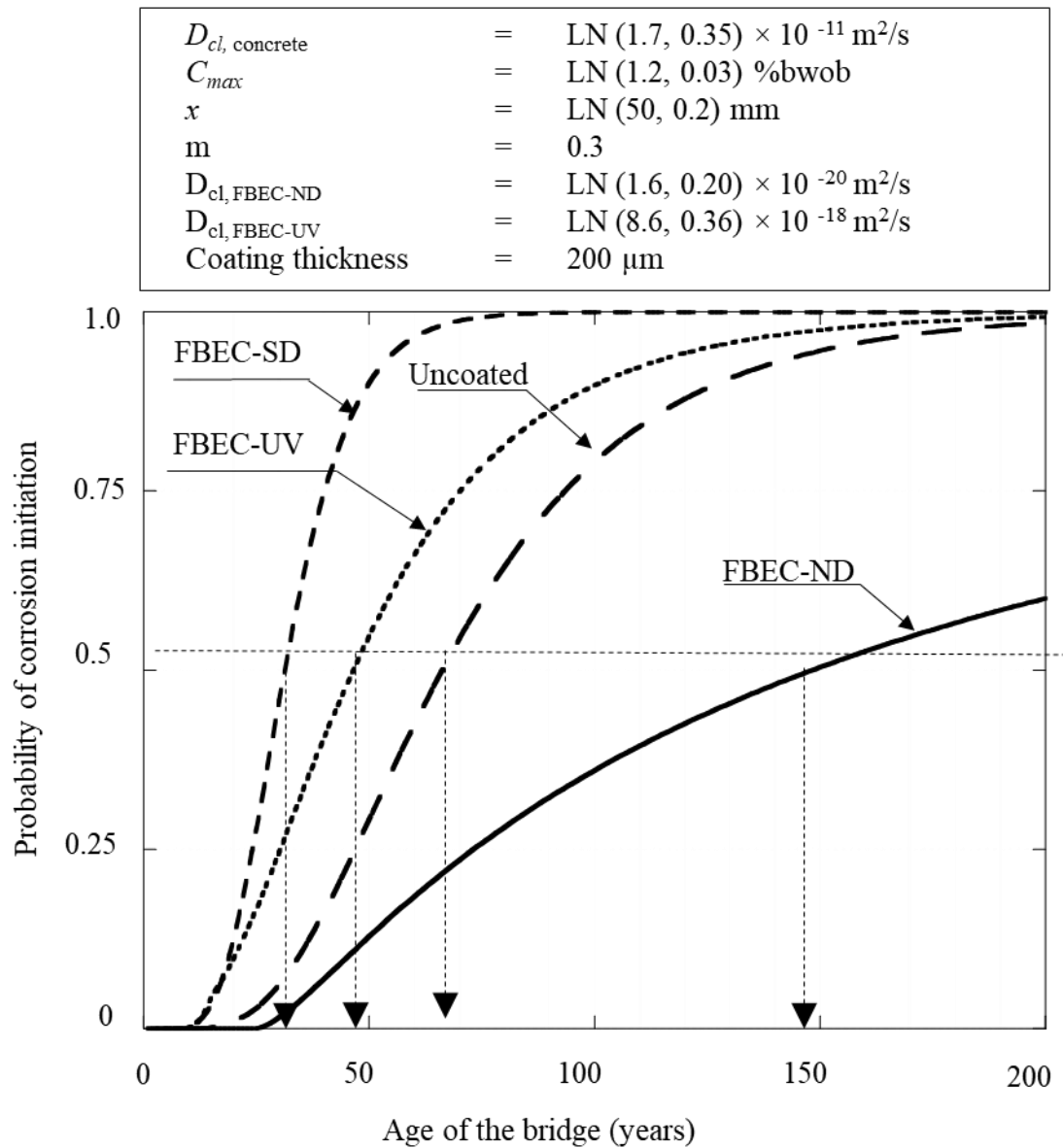
Figure 5.18 Cumulative distribution function for time to corrosion initiation

5.4.3 Effect of coating thickness on service life

Figure 5.19 shows the photographs of coated steel rebars from a 100 mm long FBE coated steel rebar used in lollipop specimens to evaluate the feasibility of the LPR technique. The specimens were exposed to chloride solution for about four weeks after the initiation of corrosion was detected using EIS technique. Therefore, the surfaces of coated steel rebar were

193

severely corroded at a specific location. To investigate this, the coating thickness profile was obtained from these specimens by using an electromagnetic coating thickness gauge. The horizontal line LLI represents the lower limit of CT as specified by IS 13620 (2015). The horizontal line LLA represents the lower limit of CT specified by ASTM A775 (2017). The horizontal line UL represents the upper limit of CT specified by IS 13620 (for rebars with all diameters) and ASTM A775 (for rebars with diameter less than 16 mm). The line with the unfilled circular markers represents the measured CT on the FBE coated steel rebars at locations between two ribs and on the top of ribs. It was found that the CTs were nonuniform throughout the length of the FBE coated steel rebars. In most of the locations, the CT was found to be more than the CT specified by any of the standard [IS 13620 (2015) and ASTM A775(2017)], which can result in a reduction in bond strength between steel and concrete (Kobayashi and Takewaka 1984; Miller et al. 2003), which is out of the scope of this thesis. In some locations, CT was found to be less than 175 µm, and severe corrosion activities were observed at these locations. Therefore, the candidate recommends modifying the current specifications in IS 13620 (2005) to increase the lower limits of CT to 200 µm. Also, the statement from ASTM A775 (2017) "the average of all recorded coating thickness measurements shall not be less than the specified minimum thickness or more than the specified maximum thickness." Should be modified to "Individually recorded coating thickness shall not be less than the specified coating thickness, and the average value of coating thickness value should not be more than the specified maximum limits." in ASTM A775 and added to IS 13620.
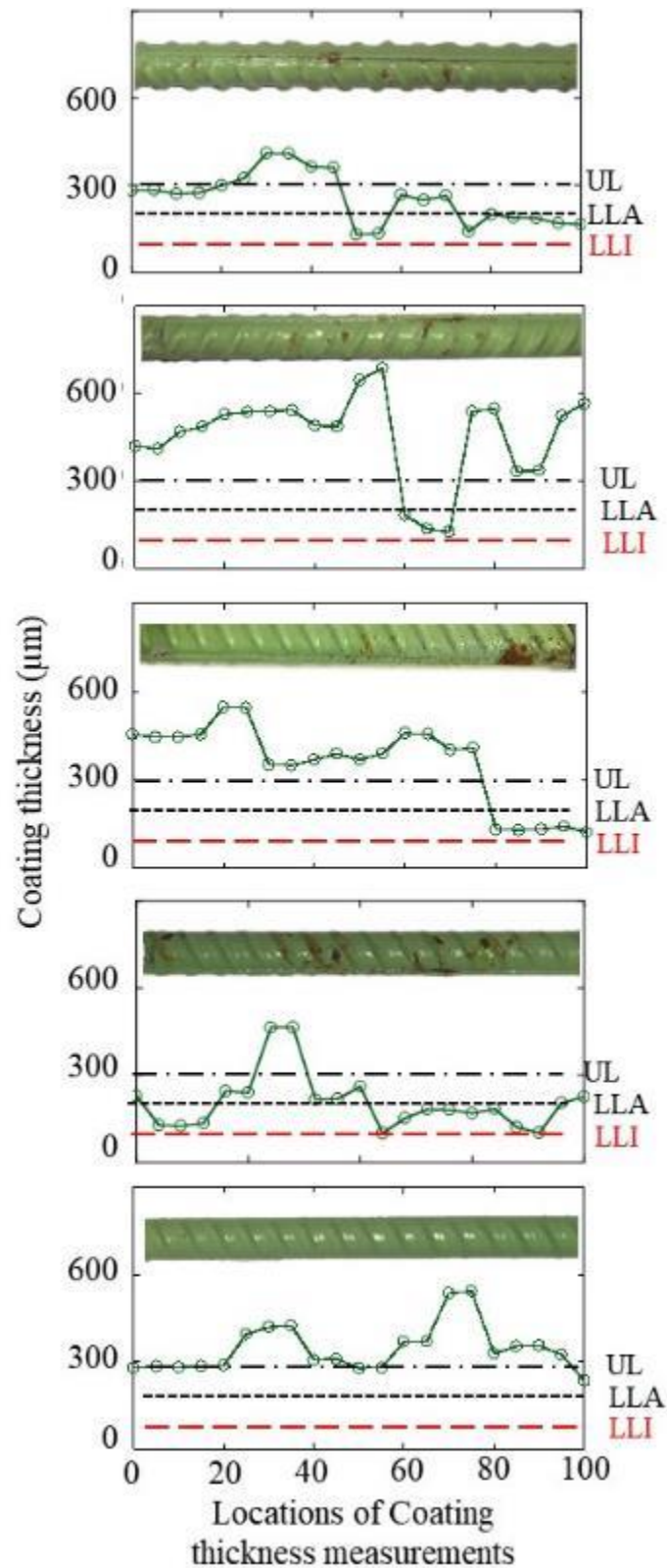
Figure 5.19 Coating thickness profile and location of corrosion activities (UL: upper limit of CT as per ASTM A775 & IS 13620; LLI: Lower limit of CT as per IS 13620; LLA: Lower limit of CT as per ASTM A775)

195

Figure 5.20 shows the cumulative distribution function for the time to corrosion initiation of RC systems with uncoated, FBEC-SD, and FBEC-ND steel rebars with a coating thickness of 300 µm, 200 µm, and 100 µm. It was found that the service life for RC systems with FBEC-ND steel rebars with $t_{coating}$ of 200, and 100 µm was about 30 and 50% less than the service life of RC systems with FBE coated steel rebars with $t_{coating}$ of 300 µm, respectivey. Note that the service life of RC system with FBE coated steel rebars with $t_{coating}$ of 100 µm was only about 20% more than that of t_i with RC systems with uncoated steel rebars. Note that the coating of the coated steel rebars gets damaged due to poor construction practices. Therefore, the service life for RC systems with FBEC-SD rebars was found to be 35% less than the service life of RC systems with uncoated steel rebars.
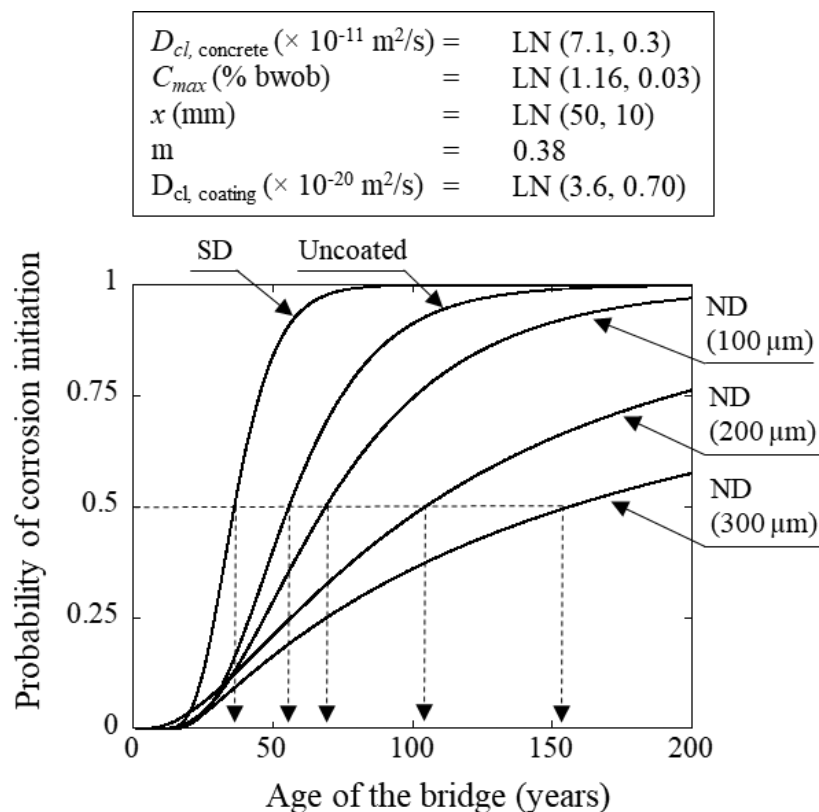
Figure 5.20 Effect of coating thickness and damage to the coating on the service lives of RC systems with FBE coated steel rebars

Photographic evidence from various construction sites are available, showing that the coatings are damaged before embedding them in the concrete. Also, manufacturing defects such as varying and inadequate coating thickness are widespread due to inefficient standard specification and poor-quality management at the manufacturing units. Based on the various tests and detailed investigation of results, it is recommended to check the changes in the characteristics of epoxy coating and the chloride threshold of FBE coated steels. The tests must be performed on coated steel samples that have been exposed to UV rays in the laboratory for 10 days to represent the typical field exposure to sunlight/UV rays and compare with the performance of uncoated steels.

Based on the experimental results and detailed analysis, candidate recommends the following prescriptive and performance guidelines/specifications for the use of FBE and CPC coated steel rebars for new constructions and existing structures. A few remedial measures are also suggested for the existing structures with FBE and CPC coated steel rebars. Then, the scope for future research in continuation to this thesis is discussed.

5.5   RECOMMENDATIONS

5.5.1   For new constructions with FBE coated steel rebars

Based on the results from microanalytical tests (SEM, EDX, FTIR) on 45 coating samples and electrochemical tests on 30 3-bar prism specimens, 35 1-bar lollipop specimens, it is recommended to check the changes in the characteristics of epoxy coating and the chloride threshold of FBE coated steels. The tests must be performed on coated steel samples that have been exposed to UV rays in the laboratory for 10 days to represent the typical field exposure to sunlight/UV rays and compared with the performance of uncoated steels. In addition to the coating requirements prescribed in ASTM A775, the following prescriptive and performance specifications are recommended

- The number of cracks = zero: No cracks should appear on micrographs obtained at a magnification of 20,000.

- The concentration of Ti and Zn on the coating surface > 5% and > 2% by weight of the coating, respectively

- Assessment of RC systems with FBE coated steel rebars should be conducted by using test methodology based on EIS technique. One of such test methodology is suggested in this thesis.

- Chloride diffusion coefficient of FBEC-UV coating should not be more than 1.2 times that of the chloride diffusion coefficient of FBEC-ND coating

- Average Cl_{th} (FBEC-ND) $\approx$ average Cl_{th} (FBEC-UV)

- Service life concrete systems with FBE coated steel rebars must be assessed using both the chloride threshold and chloride diffusion coefficients of concrete cover and FBE coating and must be greater than the desired service life.

- Change the clause, "…to less than two months." in the ASTM 775 (2017) to "FBE coated steel rebars must be covered with opaque polyethylene sheeting to protect it from sunlight, salt spray and weather exposure to minimise the total duration of sunlight/UV exposure to less than a month. The total duration of exposure includes the time during transportation, storage, and various construction stages until the coated steel rebars are embedded in concrete.

- Modify the text "the average of all recorded coating thickness measurements shall not be less than the specified minimum thickness or more than the specified maximum thickness." in ASTM A775 to "Individually recorded coating thickness shall not be less than the specified coating thickness and the average value of coating thickness value should not be more than the specified maximum

limits." The modified statements can be added or replaced in other standards or guidelines.

➢ The allowable damage level in coating = zero; no damage to coating should be acceptable

➢ The text in ASTM A775 "…No single recorded coating thickness measurement shall be less than 80 % of the specified minimum thickness or more than 120 % of the specified maximum thickness." should be modified to "…No single recorded coating thickness measurement shall be less than 175 µm or more than 120 % of the specified maximum thickness."

➢ Bending of rebars should be done before the application of the coating. Add subnote "This Table is provided only to check the flexibility of FBE coating. Bending of FBE coated steel is not recommended" to Table 1 in ASTM A775.

➢ The $R_{P,S\text{-}C}$ of FBE coated steel rebars embedded in concrete and saturated for more than two days $> 5 \times 10^7$ kΩ.cm^2

➢ Urgently ban or place a moratorium on the use of FBE coated steel rebars unless the construction sites ensure that the FBE coated steel rebars are not mechanically damaged (scratch/pinched) and they are not exposed to sunlight (UV rays) for more than two weeks

5.5.2 For existing structures with FBE coated steel rebars

➢ Inspect the RC structures with FBE coated steel rebars with test methodology with EIS techniques at regular intervals. Monitor the degradation of the coating.

➢ The regular monitoring of $R_{P,\ C\text{-}S}$ can help to estimate the service lives of RC systems with FBE coated steel and plan the remedial measures for these structures

(for more details, refer Sections 4.2.4, 5.3.2, and 5.3.3)(Kamde and Pillai 2020b; c)

➤ Extensive research is needed to evaluate the feasibility of a suitable repair strategy. As these coatings are dielectric in nature or they have significantly high resistance, the electrochemical repair techniques such as cathodic protection (sacrificial anodes or impressed current), chloride extraction may not work due to the lack of interconnectivity of rebars, and limited steel surface for ionic conduction. A few of these techniques may result in cathodic disbondment of the coating. Therefore, the authors recommend coating the concrete surface by an insulating material such as epoxy, which will restrict the ingress of further chlorides.

Figure 5.21 shows the conceptualized repair strategy for RC systems with FBE coated steel rebars. Where if the concrete surface is coated with epoxy or any other nonpermeable coating, the further ingress of chlorides can be restricted. Here, the effectiveness of repair of RC systems is discussed with respect to the age at which the coating to concrete surface is applied. For example, if the concrete surface is coated at the time of corrosion initiation or when sufficient chlorides are available within the concrete, the corrosion of steel rebars will continue, and the repair using concrete coating may not be useful. Therefore, soon the damage level in such systems will significantly increase.

If the concrete surface is coated at the age = t_1, the chloride concentrations within the concrete is low. Therefore, the rate of the diffusion process of chloride will reduce due to no further exposure to chlorides – resulting in a significant delay in the initiation of corrosion and damage level to the RC systems. If the concrete surfaces are coated at the early stages (say, t_0), when no chlorides in the concrete, the corrosion initiation time can be significantly delayed.

Hence, surface coating is recommended if the chloride concentration in concrete is significantly lower than the chloride required to initiate the corrosion.

(a) Suggested repair strategy

(b) Effect of early repair on damage level of structure (conceptualized)
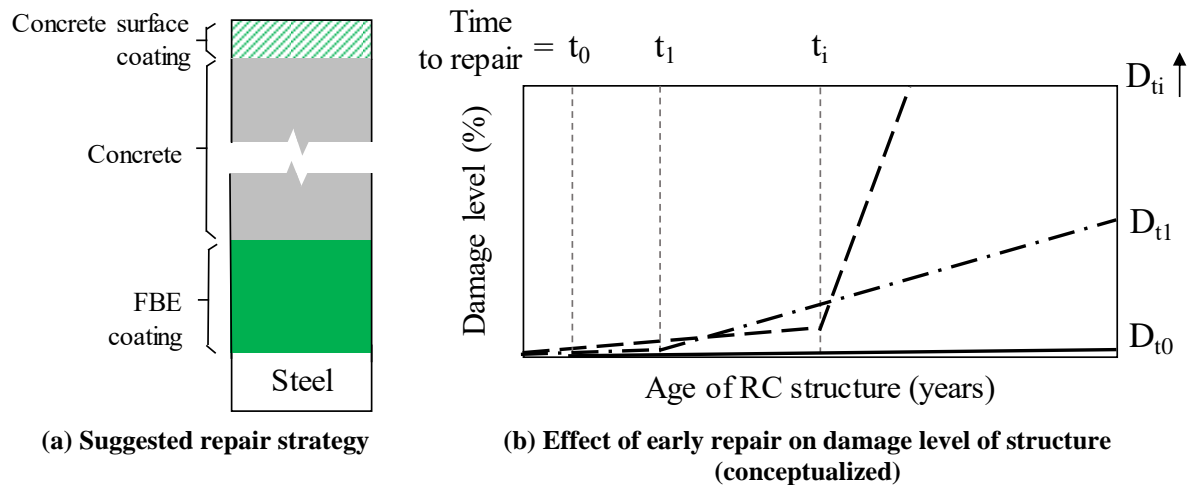
Figure 5.21 Suggested remedial measure for existing structures with FBE coated steel rebars

5.6   SUMMARY

In Subsection 5.2, the effect of damage to FBE coating on corrosion initiation was investigated. Also, the corrosion mechanism for the same was proposed. Then, in Section 5.3, the effect of prolonged exposure of fusion-bonded-epoxy (FBE) coated steel rebars to sunlight/ultraviolet (UV) rays was investigated. A comprehensive laboratory study was conducted to understand the effect of exposure to UV rays on the coating characteristics, corrosion initiation characteristics, and the service life of concrete systems. The recommendations are suggested for new constructions and existing structures with CPC coated steel rebars are proposed

6 RESULTS – CORROSION INITIATION AND BOND DEGRADATION OF CEMENT-POLYMER-COMPOSITE (CPC) COATED STEEL REBARS

6.1 INTRODUCTION

This chapter presents the effect of inadequate application of CPC coating on the corrosion initiation, chloride threshold, and service life of RC systems. For this, steel-mortar specimens were assessed with test methodology suggested in Chapter 3 with MCC and LPR techniques. After that, the effect of corrosion on bond characteristics were quantified. Then, a framework was described considering the effect of corrosion initiation and bond characteristics to estimate the service life of RC systems with CPC coated steel rebars. Then, the differences in the service lives of RC systems adequate and inadequate construction practices were quantified.

6.2 PHASE 1 - EFFECT OF SURFACE PREPARATION ON CHLORIDE THRESHOLD

Figure 6.1(a) and (b) show that the schematic of adequately and inadequately coated CPC steel rebars, respectively. Inadequate application of CPC coating can result in premature initiation of corrosion, which is experimentally investigated in this Section.

(a) Coating applied on sandblasted steel surface   (b) Coating applied on the rusted steel surface
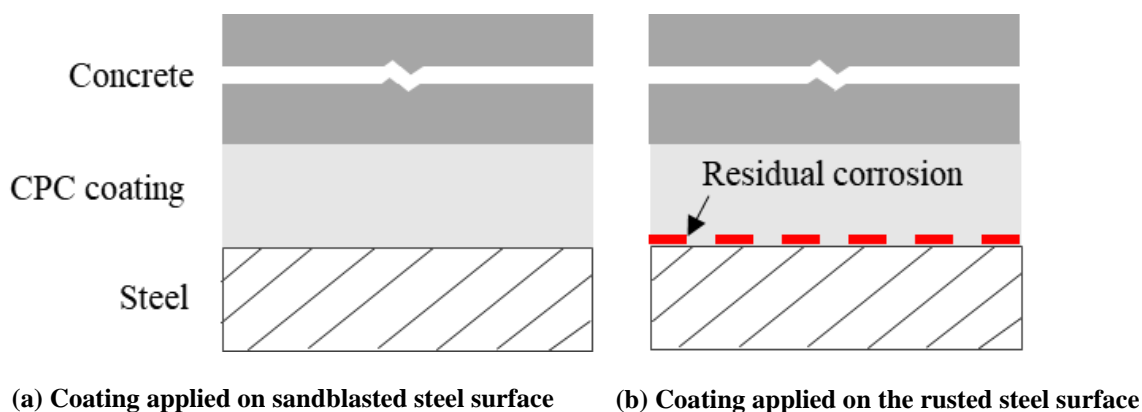
Figure 6.1 Schematic diagrams of CPC coated steel rebars

Figure 6.2 to Figure 6.5 show the total corrosion (in Coulombs) for AR-woC, SB-woC, CPCC-AR, and CPCC-SB 3-bar macrocell specimens (with two cases in each graph). In this study, corrosion is defined to initiate when the total corrosion reached 150 C (ASTM G109-07 2013). As shown in Figure 6.2, the AR-woC and SB-woC specimens exhibited corrosion initiation at about 50 and 70 days of cyclic exposure, respectively. This delay in the onset of corrosion for SB-woC specimens can be attributed to the formation of a uniformly thick and dense passive layer that is well-adhered to the SB steel surface with high surface energy (Ding et al. 2018). On the other hand, the passive layer on the as-received steel surface may not exhibit uniform thickness and may be porous due to the presence of rust and dust particles on the steel surface (Ding and Poursaee 2017).
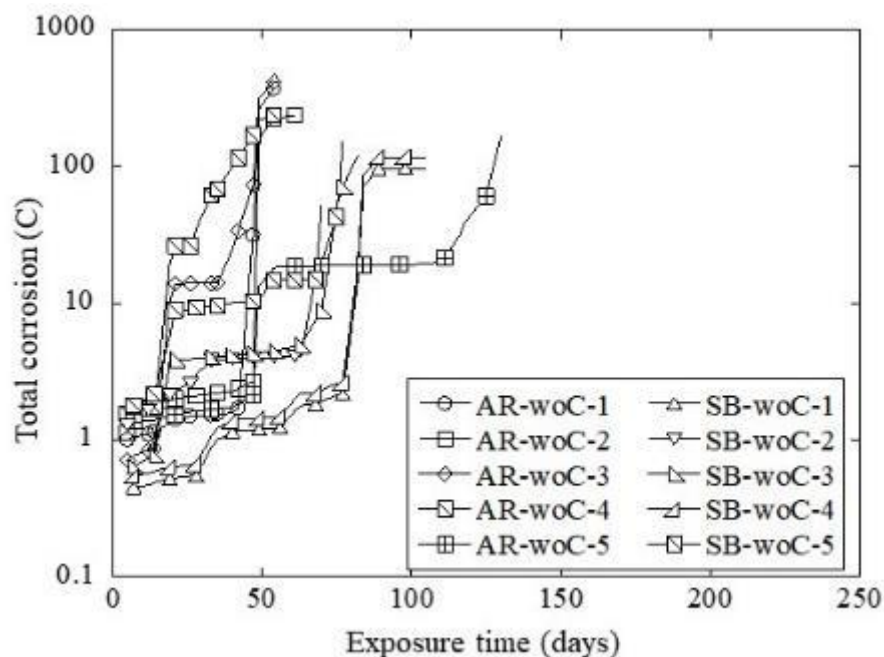
Figure 6.2 Effect of sandblasting on corrosion initiation of uncoated steel rebars

Figure 6.3 shows that the AR-woC and CPCC-AR specimens exhibited corrosion initiation at the same time. The effect of the coating is not realized due to the inadequacy in the

preparation of the steel surface before the application of CPC coating. For example, two CPCC-AR specimens exhibited corrosion along with all the AR-woC specimens at about 60 days of cyclic exposure. The candidate observed that the rust on the steel surface offered traction during the application of the coating. As a result, the intermittent microcracks were observed between the steel and CPC coating (see Figure 6.6 (a)). It was experimentally found that the CPC coating can absorb about [mean:25, standard deviation: 1.33] % moisture by weight of the coating material. If the coating does not adhere to the steel surface, it may not be able to provide the stable passive film to the steel surface, and chlorides with moisture can penetrate through the coating and lead to localized and premature corrosion. In addition, the rust layer might absorb the moisture and maintain a corrosive environment between the steel and coating. This moist rust layer can provide a low resistance path for ionic transfer and lead to premature corrosion, even with low chloride levels. It can be concluded that the CPC coating exhibits no improvement in corrosion resistance when applied on the AR surface (see Figure 6.8).

Figure 6.4 shows that the SB-woC and CPCC-SB specimens exhibited corrosion initiation at about 70 and 200 days of exposure, respectively. Therefore, there is a significant improvement in corrosion resistance when the coating is applied to clean/sand-blasted steel surface. This is mainly due to the physical barrier provided by the coating, which is well-adhered to the steel surface. Many site personnel have the wrong perception that the CPC coating can perform well even without sandblasting or cleaning of steel surface. To address this, Figure 6.5 (d) provides evidence that the AR specimens with CPC coating exhibited corrosion initiation between 50 and 100 days of exposure. This large scatter could also be attributed to the variation in the quality of coating when applied on the as-received steel surface.

204
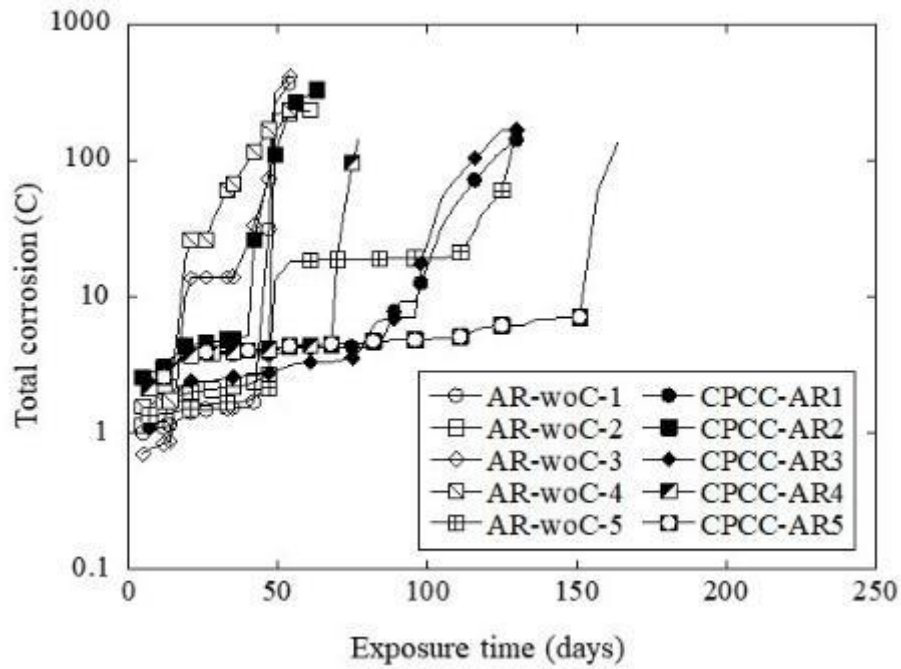
Figure 6.3 Effect of CPC coating on 'as-received' steel surface on corrosion initiation

On the other hand, the CPCC-SB specimens exhibited corrosion only after 200 days of cyclic exposure - indicating the highest corrosion resistance among the cases studied. The average time to corrosion initiation for AR-woC, CPCC-AR, SB-woC, CPCC-SB was found to 68, 88, 80, and 200 days, respectively. The system with sandblasting and coating (CPCC-SB) could significantly delay the corrosion initiation process to approximately twice the duration observed in the case of CPCC-AR. This is because when CPC coating is applied on the SB surface, it can provide (i) high resistance to chloride penetration due to better continuity of the CPC coating, ii) reduced ionic transfer, iii) good adherence between the steel and CPC coating and iv) limited availability of oxygen to the steel substrate.
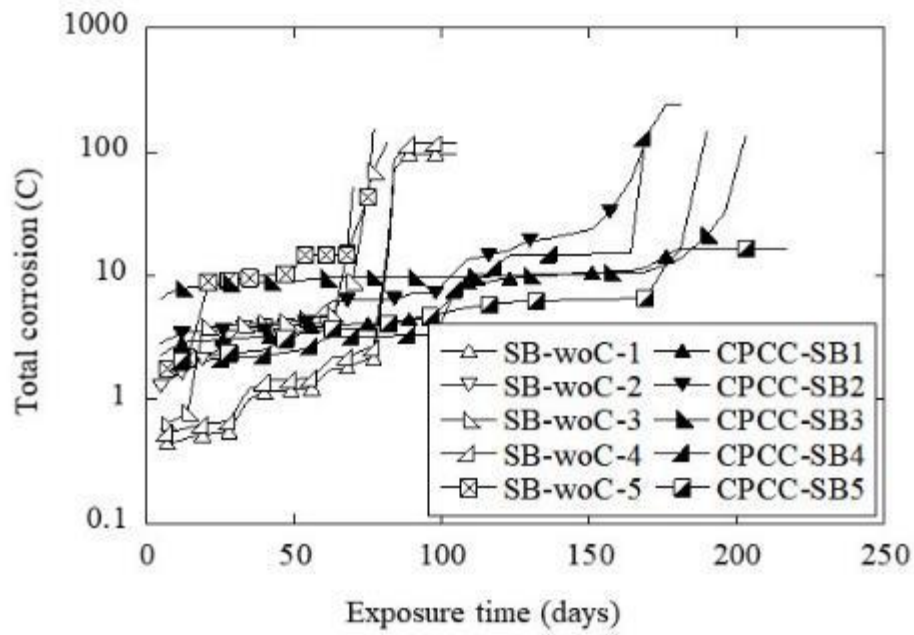
Figure 6.4 Effect of CPC coating on sandblasted steel surface on corrosion initiation
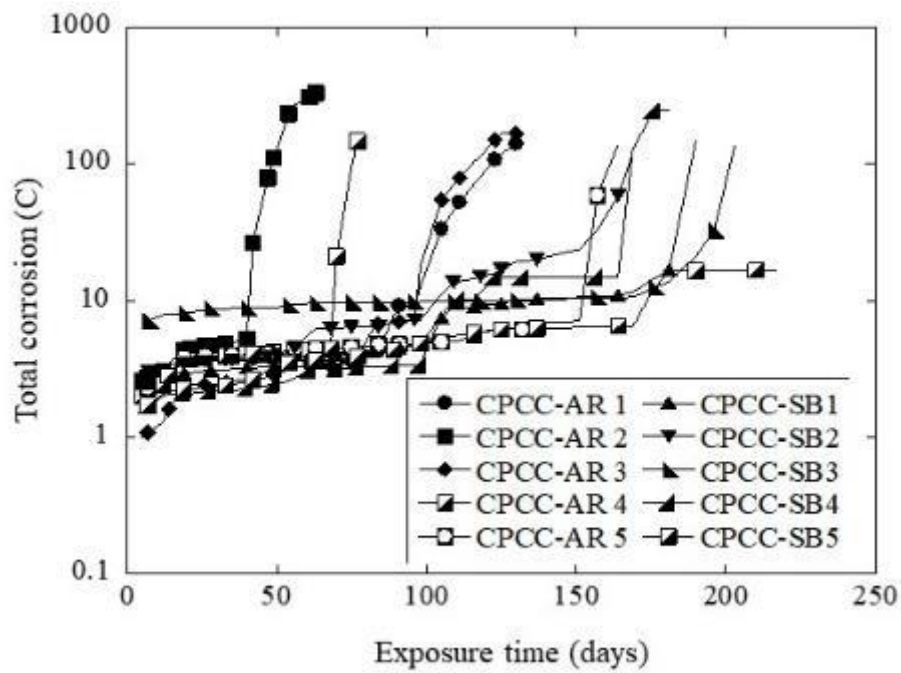
Figure 6.5 Effect of surface initiation on corrosion initiation of CPC coated steel rebars

(a) CPCC-AR   (b) CPCC-SB
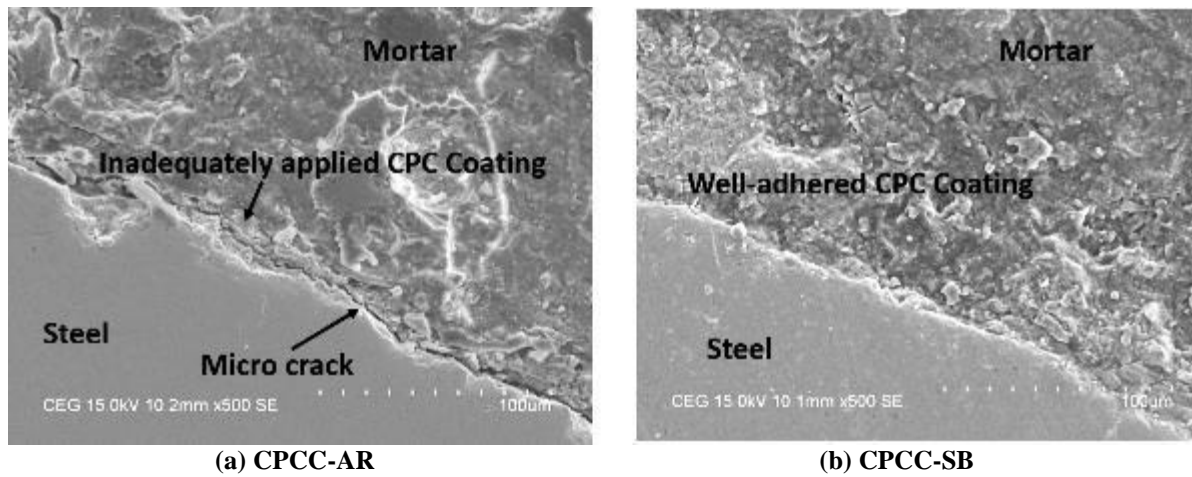
Figure 6.6 SE micrographs of the steel-coating-mortar interface

Similarly, all four cases (AR-woC, AR-CPCC, SB-woC, and SB-CPCC) were investigated using a short-term test method based on the LPR technique using the lollipop specimen. Results for corrosion initiation were similar to those obtained from 3-bar prism specimens.
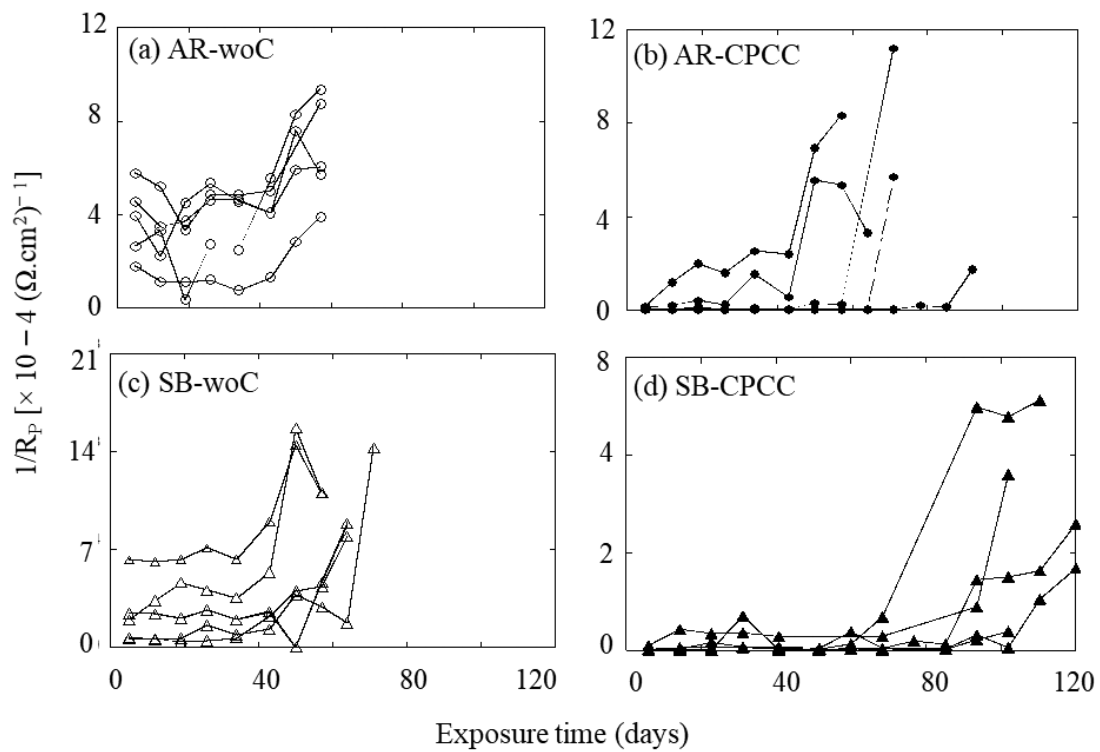
Figure 6.7 Effect of surface preparation on corrosion initiation of CPC coated steel rebars

Upon corrosion initiation, the 3-bar prism and lollipop specimens were autopsied. The powdered mortar samples were collected from the mortar adjacent to the top rebar. The chloride concentrations in the collected powder were determined using the guidelines given in SHRP-330 (1993) and defined as Cl_{th}. Figure 6.8(a) shows that the statistical distributions of Cl_{th} [expressed as ~LN(μ, COV) %bwob] of AR-woC, CPCC-AR, SB-woC, and CPCC-SB specimens were ~LN (0.4, 0.03), ~LN (0.5, 0.07), ~LN (0.6, 0.12), ~LN (0.9, 0.08) %bwob, respectively; and Figure 6.8(b) shows the statistical distributions of Cl_{th} of AR-woC, CPCC-AR, SB-woC, and CPCC-SB specimens were ~LN (0.40, 0.08), ~LN (0.45, 0.12), ~LN (0.45, 0.18), ~LN (0.88, 0.18) %bwob, respectively.
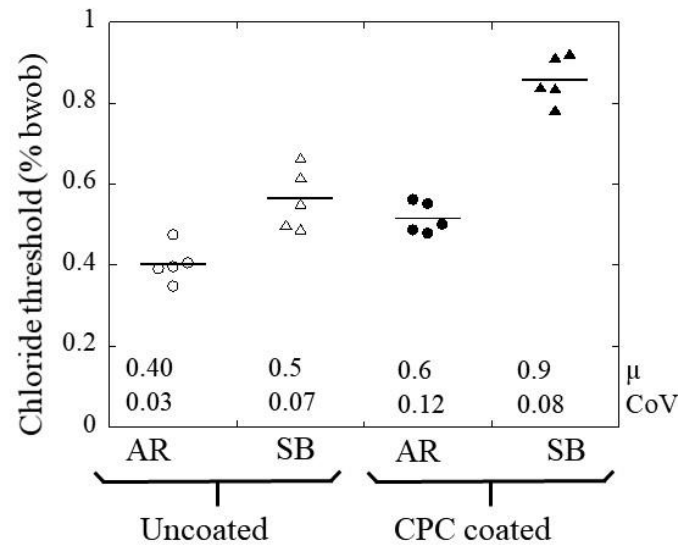
(a) Chloride threshold: 3-bar prism specimens
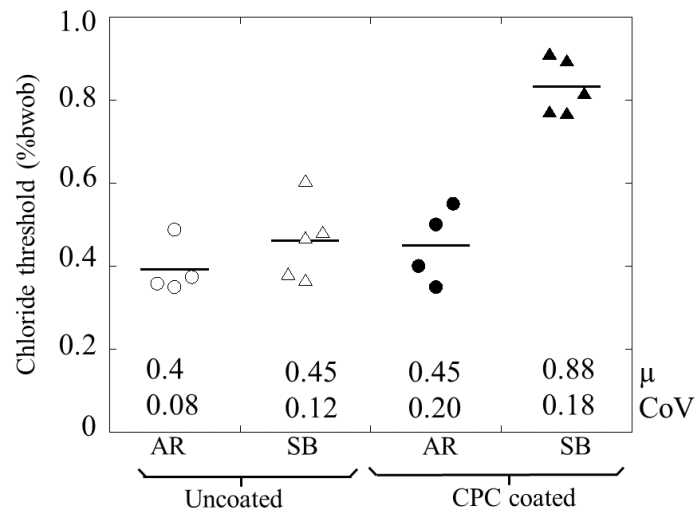
(b) Chloride threshold: Lollipop specimens

Figure 6.8 Chloride thresholds of uncoated and CPC coated steels

The corrosion for all lollipop specimens with various coating thicknesses (100, 300, and 400 µm) were found to at the same time (between 100 to 130 days) – indicating that the corrosion protection of steel is due to the passivation provided by CPC coating and not due to barrier mechanisms. The average Cl_{th} of CPCC-SB specimens was found to be (i.e., 0.9% bwob) than the other cases. This indicates that the full potential of CPC coating can be exploited only when it is applied on the SB steel surface. The comparison of chloride threshold

from 3-bar prism and lollipop specimens indicates that the test methodology based on the LPR technique with lollipop specimens can be used for determining the Cl_{th} of CPC coated steel rebars.

The corroded steel surfaces of all the specimens were visually observed and photographs were taken. Figure 6.9 (a)-(d) show sketches of various types of steel specimens showing the regions with corrosion and/or debonded coating. The dark-shaded regions in Figure 6.9(a) shows that the large surface area of rebars in AR-woC specimens was corroded; whereas, for SB-woC type specimen, corrosion was limited to a smaller surface area [see Figure 6.9(b)]. This is evidence of the formation of a stable and uniform passive layer on SB-woC steel specimens. Figure 6.9(c) shows the corroded surface of CPCC-AR specimens, where a larger area of rebar surfaces was found to be corroded, and a significant coating was disbonded from the steel surface – indicating the under-film corrosion. This is because of the low resistance path offered by the possible moist rust layer between the steel substrate and CPC coating (see the typical long and continuous microcrack in Figure 6.6 (a)). However, as shown in Figure 6.9(d), when sandblasting is done prior to the application of CPC coating, limited corrosion was observed. This indicates that the CPC coating was continuous and well-adhered to the sand-blasted steel surface – resulting in limited entry of chlorides. Also, once the corrosion was initiated, the ionic conduction was reduced due to the limited steel surface available as cathode – resulting in minimal under film/crevice corrosion. Therefore, it is suggested to use CPC coated rebar only when the steel surface is clean.

(a) As-received steel rebars without coating	
(b) sandblasted steel rebars without coating	
(c) As received steel rebars with CPC coating	
(d) Sandblasted steel rebars with the coating	

Corrosion spots　　**Coating debonding**
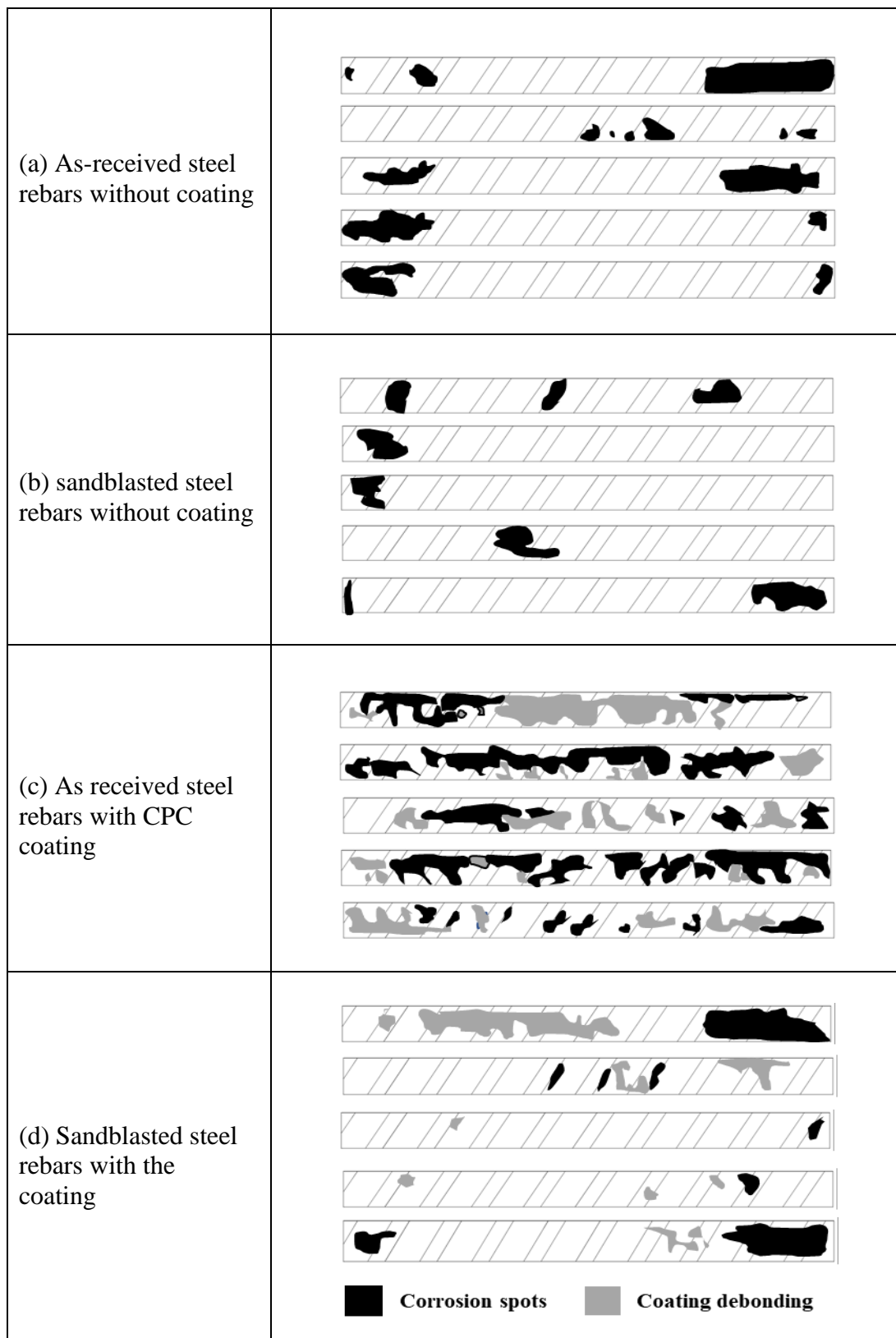
Figure 6.9 Schematic of corroded surfaces of uncoated and CPC steel rebars

at the end of the test

6.3   PHASE 2 - EFFECT OF CORROSION INITIATION ON BOND PERFORMANCE

6.3.1   Bond stress-slip behaviour and disbondment

Figure 6.10(a) shows that the negligible corrosion does not affect the bond stress-slip response of uncoated steel rebars. The zoomed τ-slip curves in Figure 6.10(a) confirmes that the low degree of corrosion does not affect the τ-slip behavior of RC systems with uncoated steel rebars. Whereas, Figure 6.10(b) shows that the post-peak response of CPC coated specimens with negligible corrosion (C2) follows a wavy pattern. The wavy pattern can attributed to the increase in the stress due to accumulation of compressed concrete and coating at the ribs (resulting in an increase in the bond stress); followed by a slip at every rib (resulting in the reduction in bond stress).   This proposed mechanism was confirmed by visual observation of accumulated concrete and coating at the ribs of the MSR from autopsied specimens of Case C1, which is discussed later.

Stress-slip reponse from Case C2 (CPC coated steel rebars with negligible corrosion) was found to be similar to the case C1. However, following differences were observed: (i) the slope of the pre-peak response was lower than the slope observed in Case C1 and much less than the Case U1 and U2 [see the zoom-in image in Figure 6.10(a) and (b)]. The decrease in the slope indicated that the CPC coated steel rebars systems can undergo significant slip with negligible corrosion. (ii) Pre-peak response was found to follow sigmoidal curve, which indicates the initial slip occurs due to a less/negligible adhesion and frictional force between steel and concrete [see second zoomed image in Figure 6.10(b)]. Later, when mechanical interlocking comes in action, the bond stress was found to be increasing. (iii) In post-peak response, the wavy pattern with increased amplitude of crests and throughs were observed as compared to that with Case C1. The increased amplitude of crests are due to the accumulation of a larger

amount of CPC coating at the steel ribs due to the disbonding of CPC coating from the steel surfaces. Once the CPC coating and concrete are accumulated on the steel rib, the deeper throughs are observed due to larger slips, due to reduced rib face angle. These τ-slip curves were used to determine the τ_b and bond stiffnesses of S-C and S-C-C interfaces with and without corrosion.

This proposed mechanism was confirmed by visual observation of MSR from autopsied specimens of Case C1. Photographs in Figure 6.14 (c) indicated the accumulation of compressed concrete and coating on the ribs. Such a phenomenon is not observed in the specimens with uncoated steel rebars, where once the maximum bond stress was attained, further slip occurred at lower bond stresses, and no increase in τ was observed [see Figure 6.10(a)]. Photographs in Figure 6.14 (a) indicated shear failure in the concrete phase of U1 type specimens due to the formation of concrete piping. Similarly, when specimens with uncoated steel rebars and negligible corrosion (U2) were tested, the τ-slip response similar to Case U1 was observed. Also, shear failure due to concrete piping was observed when autopsied specimens were visually investigated [see photograph in Figure 6.14 (b)].

On the other hand, when specimens with CPC coated steel rebars with negligible corrosion were tested, the bond stress-slip response was found to be similar to the case C1. However, the following differences were observed: (i) the slope of the pre-peak response was lower than the slope observed in Case C1 and much less than the Case U1 and U2 [see the zoom-in image in Figure 6.10(a) and (b)]. The decrease in the slope indicated that the CPC coated steel rebars systems with negligible corrosion can undergo significant slip even with very less applied bond stress; (ii) the pre-peak response was found to follow the sigmoidal curve, which indicates the initial slip occurs due to a less/negligible adhesion and the frictional force between steel and concrete [see the second zoomed image in Figure 6.10(b)]. Later, when mechanical interlocking comes into action, the bond stress was found to be increasing.

(iii) In post-peak response, the wavy pattern with increased amplitude of crests and throughs were observed as compared to that in Case C1. The increased amplitude of crests are due to the accumulation of a larger amount of CPC coating at the steel ribs due to the disbondment of CPC coating from the steel surface. Once the CPC coating and concrete are accumulated on the steel rib, the deeper throughs are observed due to larger slips, due to reduced frictional forces. These τ-slip curves were used to determine the τ_b and bond stiffnesses of S-C and S-C-C interfaces with and without corrosion. Figure 6.11 shows that the CPC coated steel rebars have significant bond loss with initiation or negligible corrosion. Therefore, this confirms that the change in bond stress-slip behavior is the result of negligible corrosion. The effect of negligible corrosion and resulting coating disbondment is discussed next.

(a) Uncoated steel

(b) CPC coated steel rebar
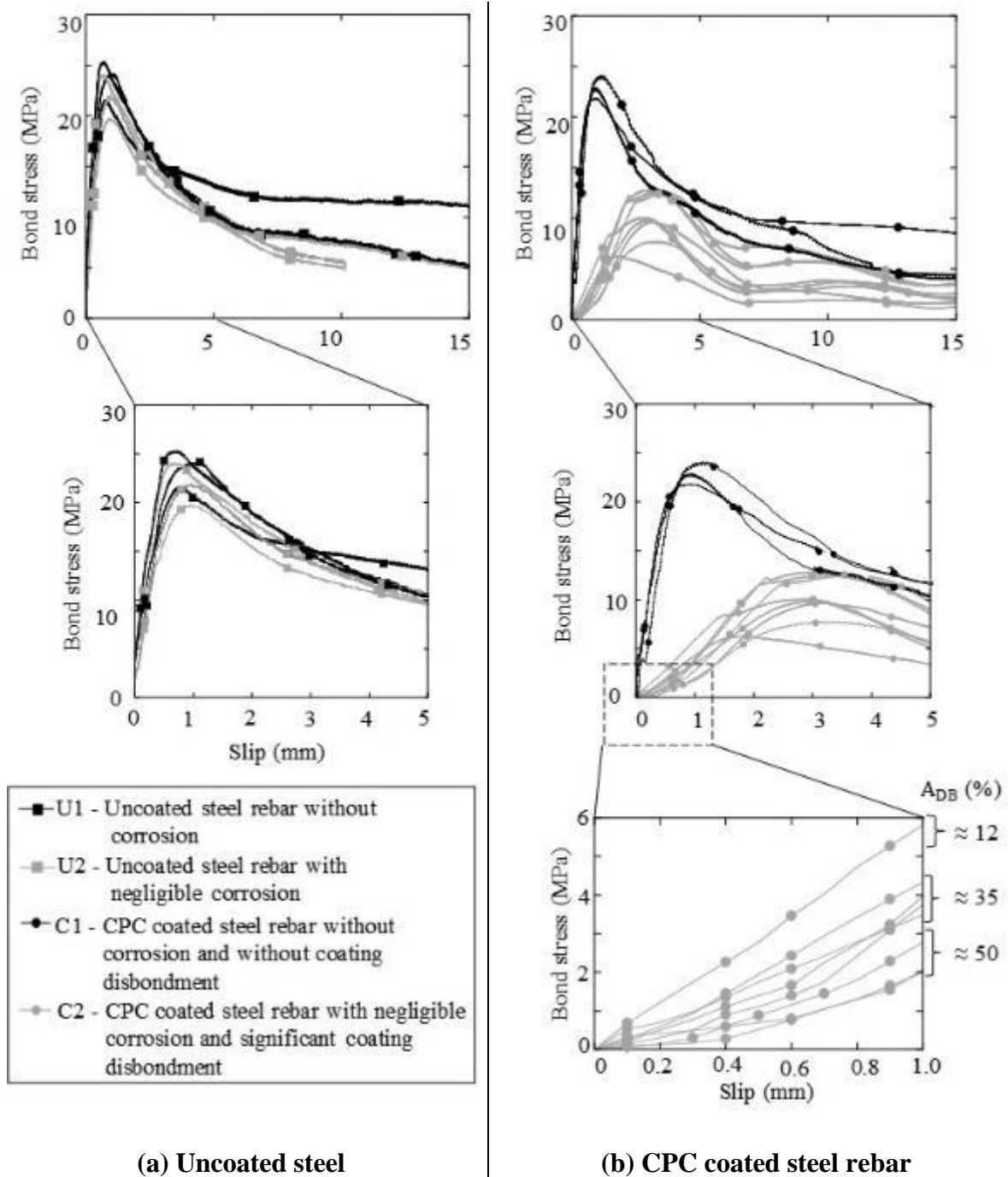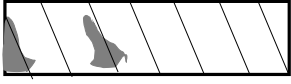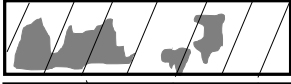
Figure 6.10 Effect of the initiation of corrosion and/or disbondment of coating on the bond stress-slip response

| Specimen ID | Photograph and sketches of disbonded area | A_{DB} (%) |

Figure 6.11 Area of disbondment along the embedded length (A_{DB}) after the pull-out test of 'C2' specimens

216

6.3.2 Effect of corrosion initiation on bond strength and stiffness

Figure 6.12(a) shows a dot plot of τ_b (i.e., the peak value of bond stress) in each case. The average τ_b of specimens U1 and U2 were found to be about ≈ 23 MPa. Note that there is no change in the bond strength due to negligible corrosion. The presence of negligible corrosion was justified by visual inspection of MSR by autopsying the specimens. The specimens C1 and C2 exhibited average τ_b of ≈ 17 and ≈ 10 MPa, respectively. These are about 20 and 70% less than the τ_b of Case U1 or U2, respectively. The τ_b of C2 systems with negligible corrosion and significant coating disbondment ($A_{DB} \approx 50\%$) was found to be about 80% lower than that of specimens with uncoated steel rebar (U1 and U2). Note that not much literature are available on the effect of corrosion on bond performance CPC coated steel rebars. (Natarajan et al. 2005) report that the after initiation of corrosion, the bond strength between CPC coated steel and concrete was found to be 9% more than the bond between uncoated steel and concrete. However, the degree of corrosion (%mass loss of steel) or degree of coating disbondment was not reported. Also, the mechanisms responsible for increase in bond strength are not reported. The results reported in this thesis are contradicting with the results reported by (Natarajan et al. 2005) can be due to the method adopted for corrosion. (Natarajan et al. 2005) used the voltage application for inducing the corrosion. That can alter the steel-concrete interface, which may not happen in natural exposure (Choi et al. 2014; Ihekwaba et al. 1996).

Figure 6.12(b) summarises the stiffnesses of RC systems with and without corrosion in uncoated and CPC coated steel rebars. The average stiffnesses of U1 and U2 were found to be ≈ 1.6 MPa – indicating that the negligible corrosion do not affect the stiffness of RC systems with uncoated steel rebars. Whereas, the average stiffnesses of CPC coated steel rebars and concrete without and with negligible corrosion was found to be ≈ 1.4 MPa and 0.6 MPa, respectively. The stiffness of RC system with the CPC coated steel rebars was found to be reduced by 10%. The stiffness of C2 was $\approx 60\%$ of the stiffness of Case C1. The significant

reduction in stiffness can be attributed to reduction in the adhesion and cohesion/frictional force at the steel-coating-concrete interface (Jorge et al. 2012). The significant reduction in the stiffness of RC system indicates that the structures may experience the large slip even when small bond stresses are applied. Therefore, Figure 6.12(c) shows that the bond stress required for 0.025 mm slip for case U1, U2, C1, and C2 are 5.2, 5.1, 2.4, and 0.5 MPa. Note that for C1 and C2, about 40% and 60% less stress is required to attain the same slip than for U1 and U2– indicating that the bond stiffness a sensitive parameter for slips. Photographs in Figure 6.11 confirms that these changes are the result of negligible corrosion and significant disbonding.
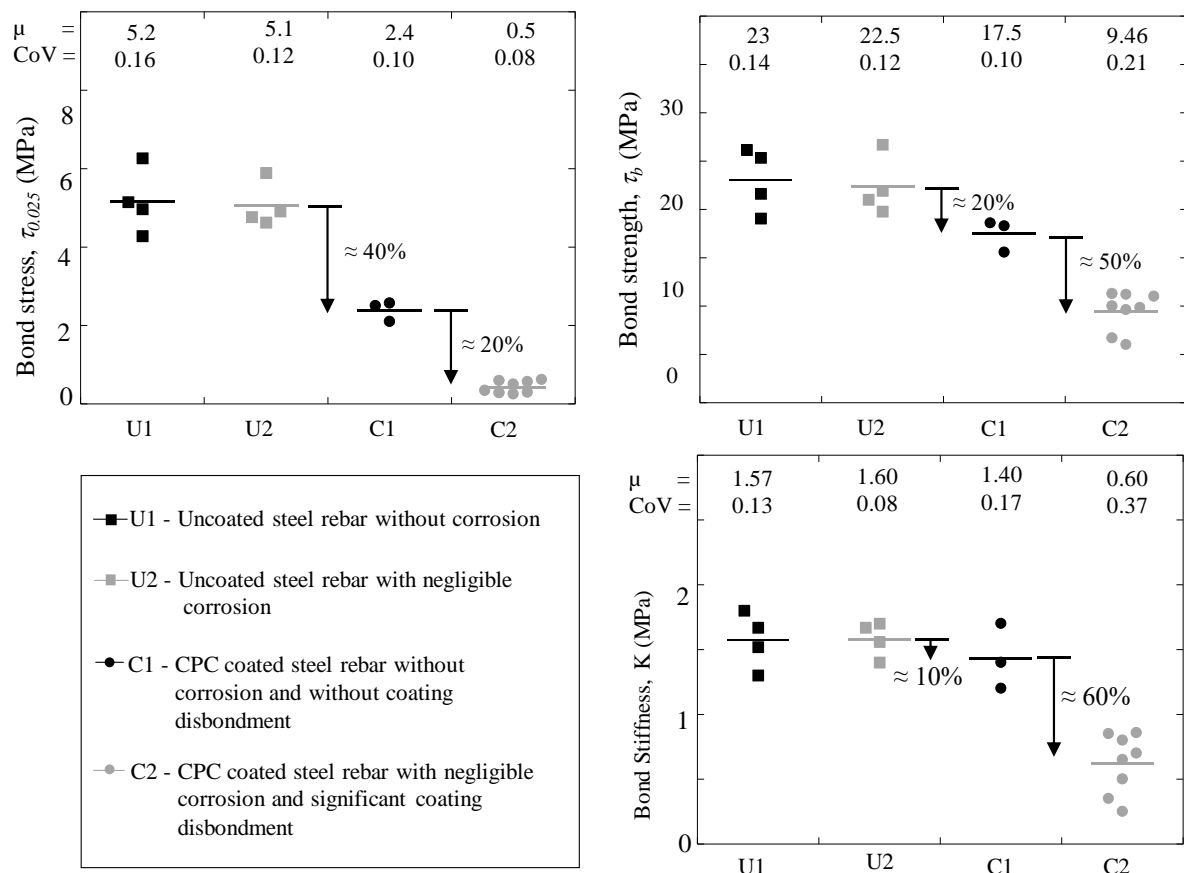
Figure 6.12 Effect of negligible corrosion and/or coating disbondment on (a) bond stress at 0.025 mm slip, (b) bond strength, and (c) stiffnesses of S-C/S-C-C interfaces

Figure 6.13 shows that the decrease in τ_b can result in an increase in the required development length. In the case of CPC coated steel rebars, negligible corrosion can result in about 40 to 80% reduction of τ_b ($\tau_{b,\,C1}$). This reduction in bond strength can result in an additional requirement of about $2 - 5$ times more development length (L_d). Note that the requirement of additional L_d is for the existing structures, for which these structures are not designed. Therefore, the structures with CPC coated steel rebars can undergo sudden failure due to the inability to satisfy the additional requirement of L_d.

Unlike CPC coated steel rebars, RC systems with uncoated steel rebars with corrosion level up to steel mass loss of about 1% do not experience the reduction in bond strength. Therefore, the RC structure with uncoated steel rebars are expected to have propagation time ($t_{p,\,U}$) of about 6-10 years (Bentz 2003). Whereas, for CPC coated steel RC structures may experience a sudden reduction in the bond strength capacity. Therefore, propagation time for CPC coated steel rebars ($t_{p,\,C}$) can be negligible (≈ 0 years).
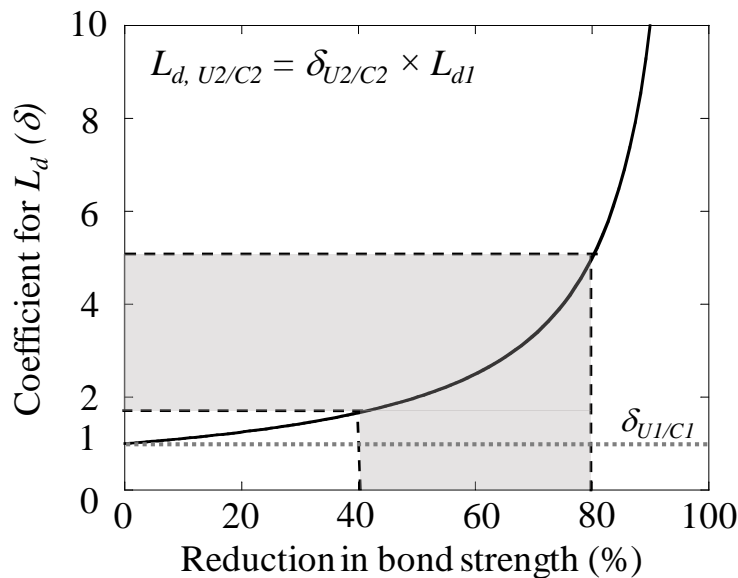
Figure 6.13 Effect of degradation of bond strength on the required development length of CPC coated steel embedded in concrete

6.3.3   Mechanisms of bond stress – slip behaviour

Figure 6.14 (a), (b), (c), and (d) show the photographs of the embedded region of MSR for Case U1, U2, C1, and C2 after the pullout testing, respectively. In the case of uncoated steel rebars without and with negligible corrosion, it was found that the failure was due to the formation of concrete piping in the bulk concrete phase – probably due to the good chemical adhesion and the frictional force between steel and concrete, and good resistance from the ribs contributing to the interlocking mechanism. Hence, the bond strength will be the result of chemical adhesion (A), frictional resistance (F), and mechanical interlocking (M) between steel and concrete. Figure 6.14 (a) and (b) demonstrate the action of forces has been demonstrated in FBD of Cases U1 and U2.

In the case of CPC coated steel rebars, the photograph revealed that the CPC coating and concrete were compressed at the steel ribs during the pullout testing – indicating that the chemical adhesion and frictional forces are not high as the Case U1 and U2. However, note that the CPC coating was not disbonded from the steel surface – indicating that the bond failure took place at the coating-concrete interface. Therefore, the adhesion between steel and coating was more than the adhesion between coating and concrete. Therefore, the slip in the case of C1 is governed by the weak chemical adhesion and the frictional force between the coating-concrete interface. In addition, the accumulation of coating and concrete was observed at the ribs will result in the mechanical interlocking with a lower rib face angle due to accumulated concrete and coating. Therefore, the bond strength for CPC coated steel rebars without corrosion is governed by the chemical adhesion and friction at the CPC coating-concrete interface, and mechanical interlocking at the S-C-C interface with relatively lower rib face

angles generated by accumulated by coating and concrete. Based on this, Figure 6.14(c) shows the Freebody diagram for the Case C1 with relatively low A, F, and M.

Figure 6.14(d) shows the photograph of embedded MSR of Case C2, where a large portion of CPC coating is disbonded from steel surface – indicating that the chemical adhesion and frictional forces are negligible between steel and coating. Therefore, the slip takes place at the steel-coating interface. However, during slip, when CPC coating and concrete gets compressed at the steel ribs, the mechanical interlock starts to dominate the τ-slip response. Later, when more bond stress is applied, the resultant resistance is due to mechanical interlock and the frictional force between S-C-C interface. Note that the mechanical interlock in the case of C1 & C2 is less than the mechanical interlock in the case of U1 & U2 due to the equivalent rib face angle in Case C1 and C2, which is smaller than the actual rib face angle of steel. When coating and concrete get compressed at the steel ribs, the resultant rib face angle is due to the equivalent rib face angle formed due to these compressed materials. Therefore, Figure 6.14(c) shows the free body diagram for Case C2, where C and F are negligible, and only M acts on the S-C-C.

Figure 6.14(a) to (d) shows the mechanisms for the slip between steel and concrete for S-C and S-C-C interfaces. The stiffness of S-C and S-C-C affect the slip mechanism. Higher the interface stiffness, lower is the slip observed. Therefore, the least slip is observed in the case of U1 and U2. As the acting forces get altered due to CPC coating, the stiffness of S-C-C is reduced, and slip observed in the case of C1 is higher than U1 and U2.

Similarly, when corrosion altered the S-C-C interface, the stiffness was significantly reduced, which resulted in a larger slip than that for the Case C1 (i.e., CPC coated steel without corrosion). A generalized τ-slip behavior for CPC coated steel rebars without and with corrosion are discussed next. Also, based on the results, a service life model is proposed next.

A: Adhesion; F Frictional; M: Mechanical Interlock; S-C: Steel-Concrete Interface; S-C-C: Steel-Coating-Concrete Interface; K_{U1}: Stiffness of S-C interface of Case U1; K_{U2}: Stiffness of S-C interface of Case U2; K_{C1}: Stiffness of S-C-C interface of Case C1; K_{C2}: Stiffness of S-C-C interface of Case C2; s_{U1}: Bond slip corresponding to Case U1; s_{U2}: Bond slip corresponding to Case U2; s_{C1}: Bond slip corresponding to Case C1; s_{C2}: Bond slip corresponding to Case C2

Photographs			
Free-body diagrams for S-C/S-C-C			
Interface stiffness and slips			
(a) U1 - Uncoated steel without corrosion	**(b) U2 - Uncoated steel with negligible corrosion**	**(c) C1 - CPC coated steel without corrosion and without coating disbondment**	**(b) C2 - CPC coated steel with negligible corrosion and significant coating disbondment**
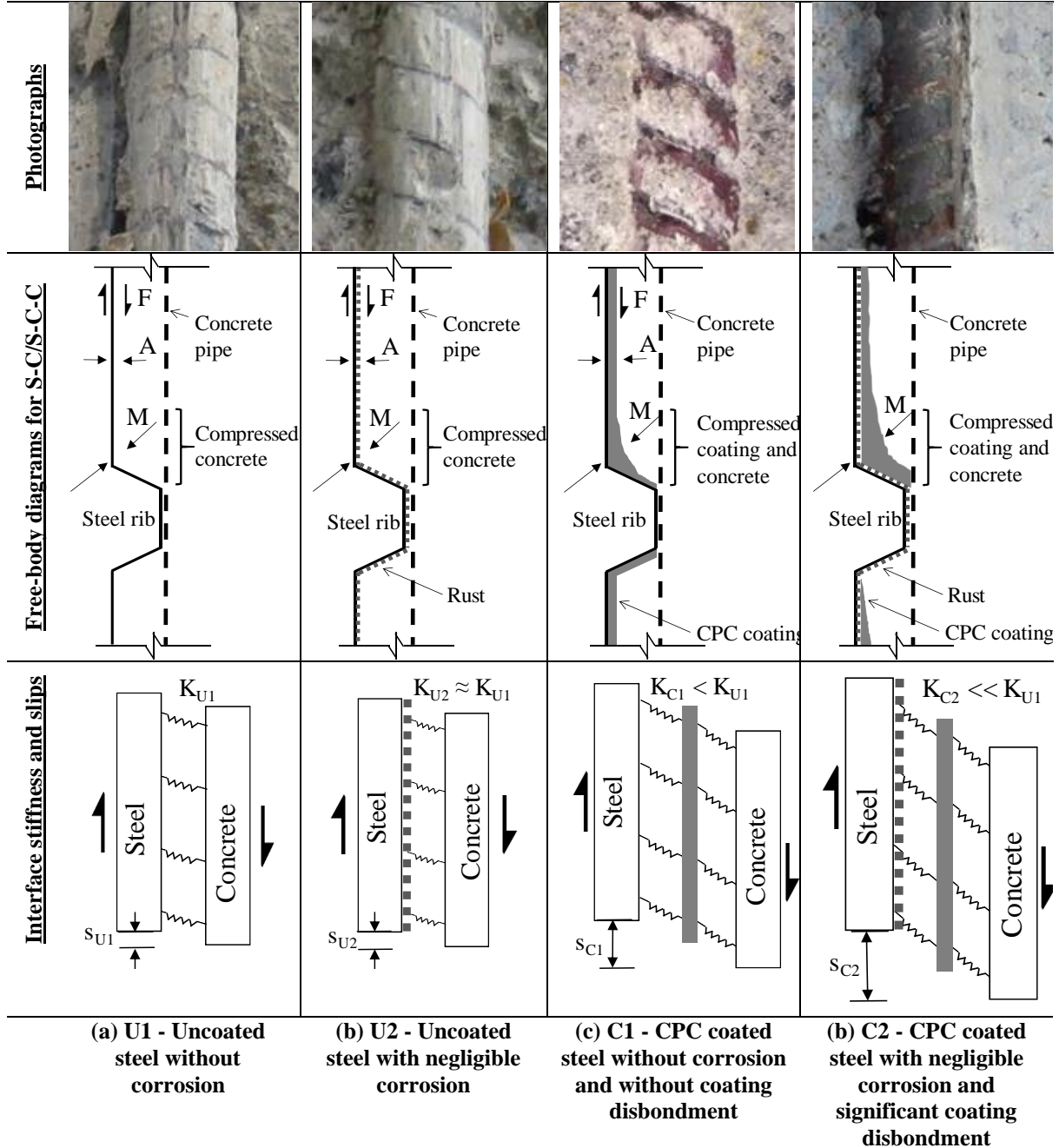
Figure 6.14 Mechanisms of bond stress-slip between concrete and uncoated and CPCcoated steel with and without corrosion and disbondment

6.4 PROPOSED FRAMEWORK AND SERVICE LIFE ESTIMATION FOR CPC COATED SYSTEMS

6.4.1 Proposed bond stress – slip behaviour

Figure 6.15 shows the proposed τ-slip behavior of RC systems with CPC coated steel rebars without and with negligible corrosion. For comparison, τ-slip behavior of RC systems with uncoated steel rebars is also presented. Note that the slope of the τ-slip curve for uncoated steel rebars with and without corrosion ($\theta 1$) is higher than CPC coated steel rebars without ($\theta 2$) and with corrosion ($\theta 3$) [$\theta 1 > \theta 2 \gg \theta 3$]. As the stress level is increased, Case U1, U2, and C1 continue to have the linear response between τ and slip, until $\tau_{b, U1}$, $\tau_{b, U2}$, and $\tau_{b, C1}$, respectively [$\tau_{b, U1} \approx \tau_{b, U2} > \tau_{b, C1}$]. Whereas, the response from case C2 was found to follow the sigmoidal curve, where the slope of τ-slip curve was found to be increased after the initial slip of about 0.5 mm. This increase in slope can be attributed to the involvement of mechanical interlocking after sufficient CPC coating and concrete are accumulated at the steel ribs. Later, the τ was increased until $\tau_{b, C2}$, which was significantly lower than $\tau_{b, U1}$, $\tau_{b, U2}$, and $\tau_{b, C1}$. The significant low value to $\tau_{b, C2}$ can be attributed to negligible chemical adhesion and friction and lower mechanical interlocking due to a reduction in the equivalent rib angle. Later this stage, uncoated steel experienced the formation of concrete piping and shear failure in the concrete phase. Shear failure in the concrete phase resulted in a gradual decrease in τ and increase in the slip between steel and concrete. Whereas, Case C1 and C2 experienced wavy pattern after peak stress ($\tau_{b, C1}$, and $\tau_{b, C2}$). This indicates the accumulation of concrete and coating at the ribs (resulting in an increase in the bond stress) followed by a slip at every rib (resulting in the reduction in bond stress).

U1 – Uncoated steel rebar without corrosion
U2 – Uncoated steel rebar with negligible corrosion
C1 – CPC coated steel rebar without corrosion and without coating
      disbondment
C2 – CPC coated steel rebar with negligible corrosion and
      significant coating disbondment
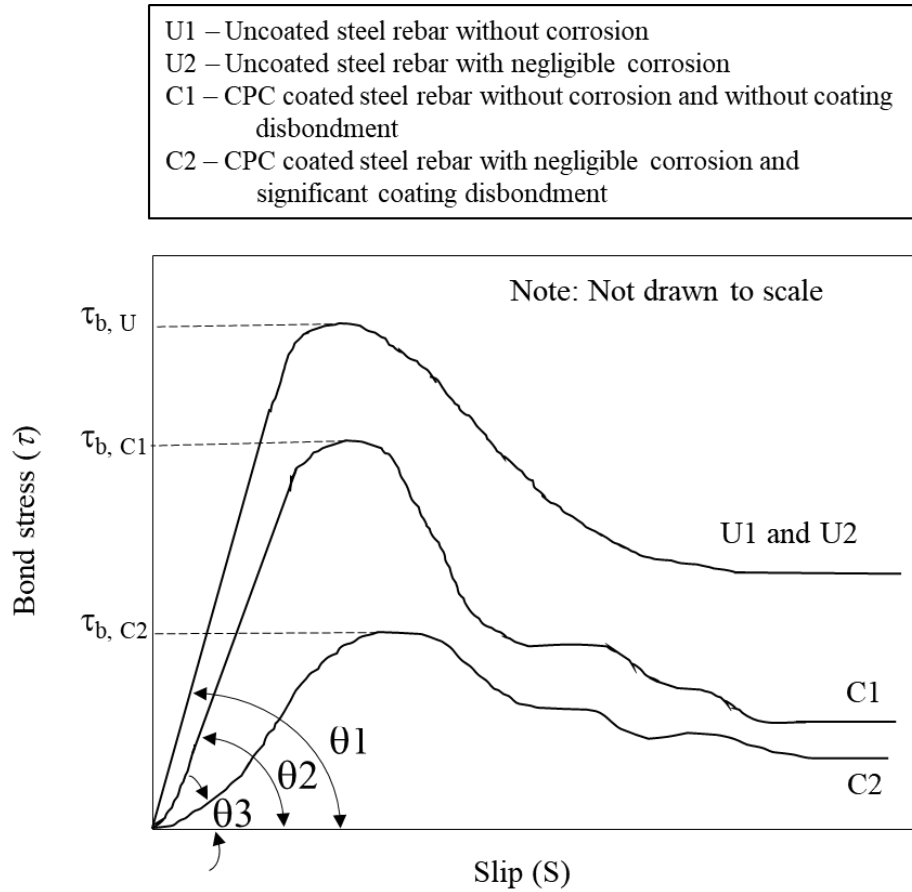
Figure 6.15 Proposed bond stress-slip model for CPC coated steel rebars with and without disbonded coating

6.4.2   Proposed service life model

Figure 6.16 shows the proposed service life model for RC systems with CPC coated steel rebars. Here, the bond strength of RC systems with uncoated steel rebars was found to be increasing after the initiation of corrosion in RC systems with coated steel rebars ($t_{i, U}$). Therefore, once the corrosion is initiated, the rebars experience the reactionary confinement and do not show adverse effects on the structural capacity of RC systems until the corrosion mass loss is more than about 1%. Therefore, the time for the first repair of RC systems with uncoated steel rebars can be considered as the time when the bond strength goes below the required bond strength of RC systems ($t_{i, U}$). On the other hand, for RC systems with CPC

224

coated steel rebars, the bond strength was found to decrease by about 50-70% than the bond strength of RC systems with the initiation of corrosion (see Figure 6.12). Therefore the time to corrosion initiation for RC systems with CPC coated steel rebars ($t_{P, C}$) can be considered as the time of the end of service life. Therefore, the time to corrosion propagation for RC systems with CPC coated steel rebars ($t_{P, C}$) is approximately zero. Therefore candidate recommends for preventive maintenance of RC systems with CPC coated steel rebars. One case study was considered to demonstrate the effect of inadequate application of CPC coating on the service lives of RC systems with CPC coated steel rebars, and the same is presented next.
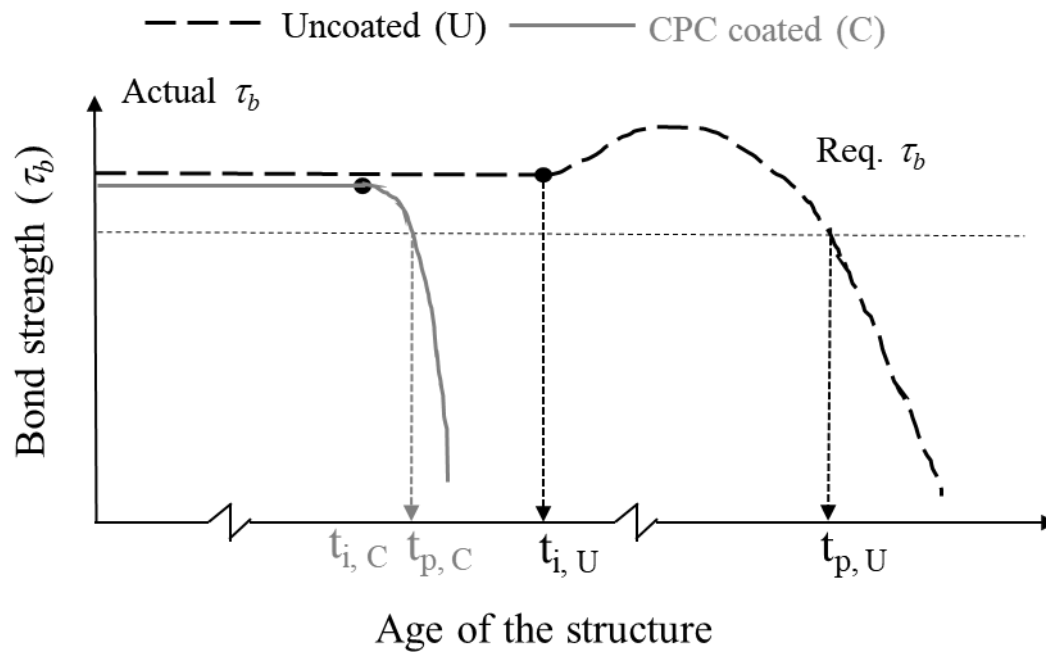
Figure 6.16 Proposed service life model based on bond loss for RC structures

6.4.3 A case study

A 6-year old concrete bridge located in the chloride-rich environment (within 2 km from the sea) of a coastal city in India was considered for this study. To obtain C_{max} and D_{cl}, cylindrical concrete specimens of about 90 mm diameter and 100 mm length were extracted from the girder, pier, pile cap, and pile elements, and laboratory experiments were performed.

6.4.3.1 Maximum chloride concentration at the concrete surface (C_{max})

Table 6.2 shows that the average C_{max} of concrete specimens obtained from the girder, pier, pile cap, and pile were 1.16, 1.17, 1.29, and 2.94 % by weight of binder (%bwob), respectively. The time required to build the C_{max} on the concrete surface (*time_C_{max}*) depends of the porosity and the ion-exchange phenomenon at the near-surface concrete and the exposure conditions. Here, each element of the bridge is made of different concretes and exposed to different exposure conditions. For example, the girders and piers are exposed to airborne chlorides; whereas, the pile caps and piles are exposed to moist soil with chlorides. The average surface chloride concentrations (C_s) at 6 years of exposure were found to be 0.1, 0.2, 0.9, and 2.6 %bwob for girder, pier, pile cap, and pile, respectively. Based on this, the rate of growth of C_s was determined assuming a linear increase. The *time_C_{max}* for the girder, pier, pile cap, and pile was estimated to be 65, 36, 10, and 6.5 years, respectively.

6.4.3.2 Chloride diffusion coefficient of concrete (D_{cl})

Figure 6.17(a) to (j) show the chloride profiles of the concrete specimens obtained from girders, piers, pile caps, and piles. Due to the significant variations in the leaching/chloride-ion exchange phenomenon near the concrete surface, the chloride concentrations in the 5 mm thick layer near the concrete surface was not considered for determining the D_{cl} (Shakouri and Trejo 2017). These chloride profiles and Fick's second law were used to determine the D_{cl} for each

specimen. Note that these diffusion coefficients are determined at the age of 6 years. Hence, D_{cl} at 28 days were calculated by estimating the decay constant, m, from Equation 3. As shown in Figure 6.17 (k), the average D_{cl} (at 28 days) after the construction of the girder, pier, pile cap, and pile were estimated to be 1.71, 1.9, 2.4, and 2.7×10^{-11} m^2/s, respectively. Then, these diffusion coefficients were used for further assessment. The quality and uniformity in the construction practices (say, mixing, placement, compaction, curing, etc. of concrete) can significantly influence the variation in the transport properties of concrete. Higher the coefficients of variation (COV) of D_{cl}, the larger will be the uncertainty in the estimated t_i. In this study, the uncertainty in the t_i due to the D_{cl} of girder and pile caps were assessed using the COV of 36% and 7%, as exhibited by the three values of D_{cl} obtained. In the case of piers and piles, only two specimens could be obtained and tested for D_{cl}, for which the COV was assumed to be 25%.

6.4.3.3   Chloride threshold

Table 6.1 shows that the statistical distributions of Cl_{th} [expressed as $\sim$LN(μ, COV) %bwob] of AR-woC, CPCC-AR, SB-woC, and CPCC-SB specimens were $\approx$ LN(0.4, 0.03), $\approx$ LN(0.5, 0.07), $\approx$ LN(0.6, 0.12), $\approx$ LN(0.9, 0.08) %bwob, respectively, as determined in Section 6.2.

Table 6.1 Chloride threshold used in cased study (determined in Section 6.2)

Steel surface condition	Coating condition	Chloride threshold
AR	woC	$\approx$ LN(0.4, 0.03)
	CPCC	$\approx$ LN(0.5, 0.07)
SB	woC	$\approx$ LN(0.6, 0.12)
	CPCC	$\approx$ LN(0.9, 0.08)
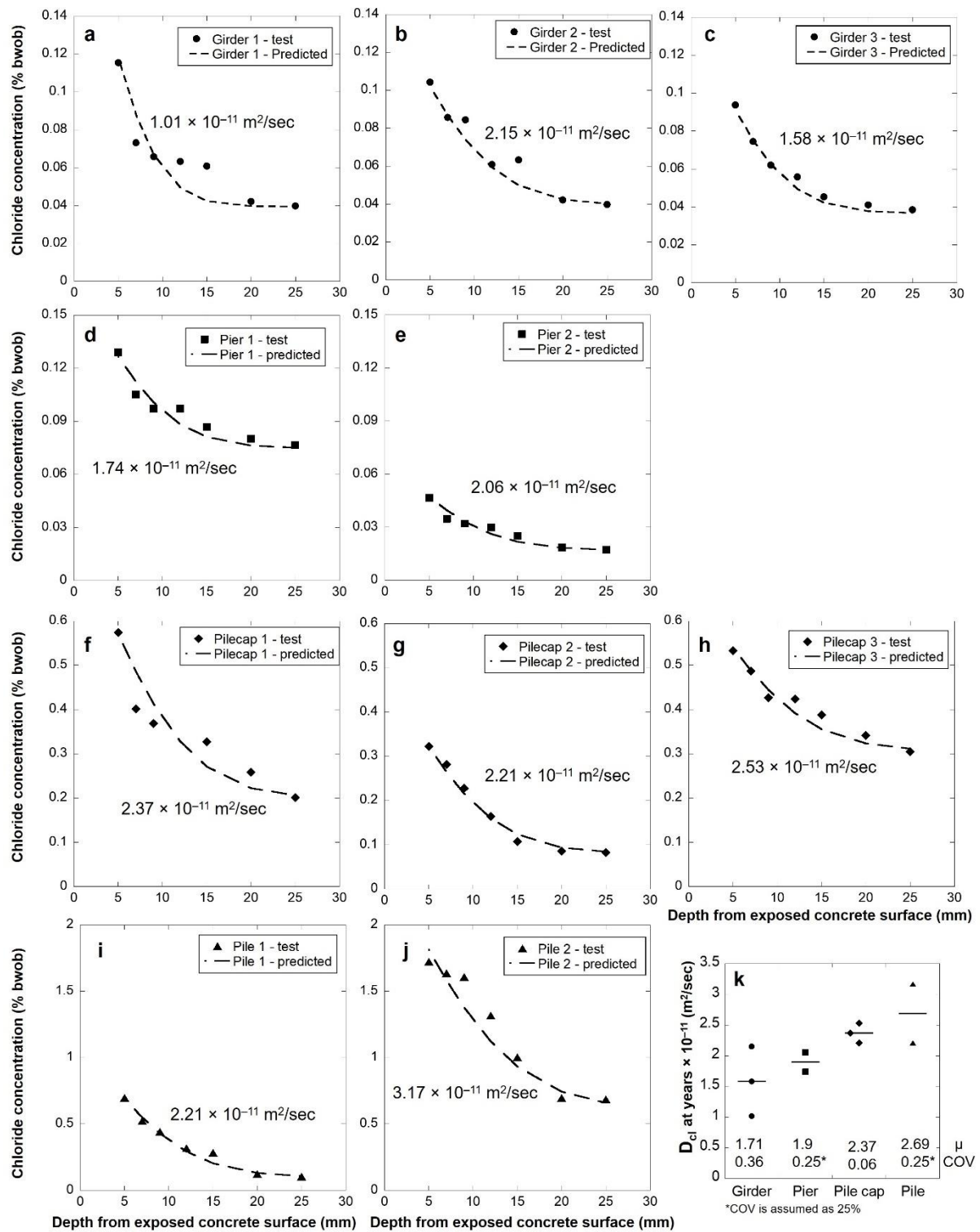
Figure 6.17 Chloride profiles and diffusion coefficients for various concrete specimens cored from the bridge elements

Table 6.2 Chloride transport properties of concrete for different structural elements

Structural element	m	D_{cl} (m²/s)	Cs (% bwob)	C_{max} (% bwob)	time_C_{max} (years)
Girder (M60)	0.38	1.71×10^{-11}	0.1	1.16	65
Pier (M45)	0.42	1.90×10^{-11}	0.2	1.17	36
Pile cap (M35)	0.45	2.37×10^{-11}	0.9	1.29	10
Pile (M35)	0.45	2.69×10^{-11}	2.6	2.94	6.5

6.4.3.4   Service life estimates

Figure 6.18(a) to (d) shows the Cumulative Distribution Function (CDF) of t_i for the girder, pier, pile cap, and pile elements, respectively. The probability of 50 % of corrosion initiation was the end of service life. The input parameters, such as D_{cl}, C_{max}, concrete cover (x), and m for each case are given adjacent to the respective CDFs. In each case, t_i for CPCC-AR specimens was found to be at least 50% less than CPCC-SB specimens. The estimated t_i for the best case (CPCC-SB) of pile caps and piles was found 90 and 40 years, respectively, which is significantly shorter than the original design life of 120 years. It should be noted that the pile cap and pile elements are underground, where availability of oxygen is limited, and therefore, the corrosion rate of rebars could be less (Azoor et al. 2019). However, sufficient oxygen can be available for 1 to 2 meters below the ground level, and the corrosion rate within this region for pile cap and pile could be high when sufficient chlorides are available – leading to premature corrosion of these elements (Azoor et al. 2019).
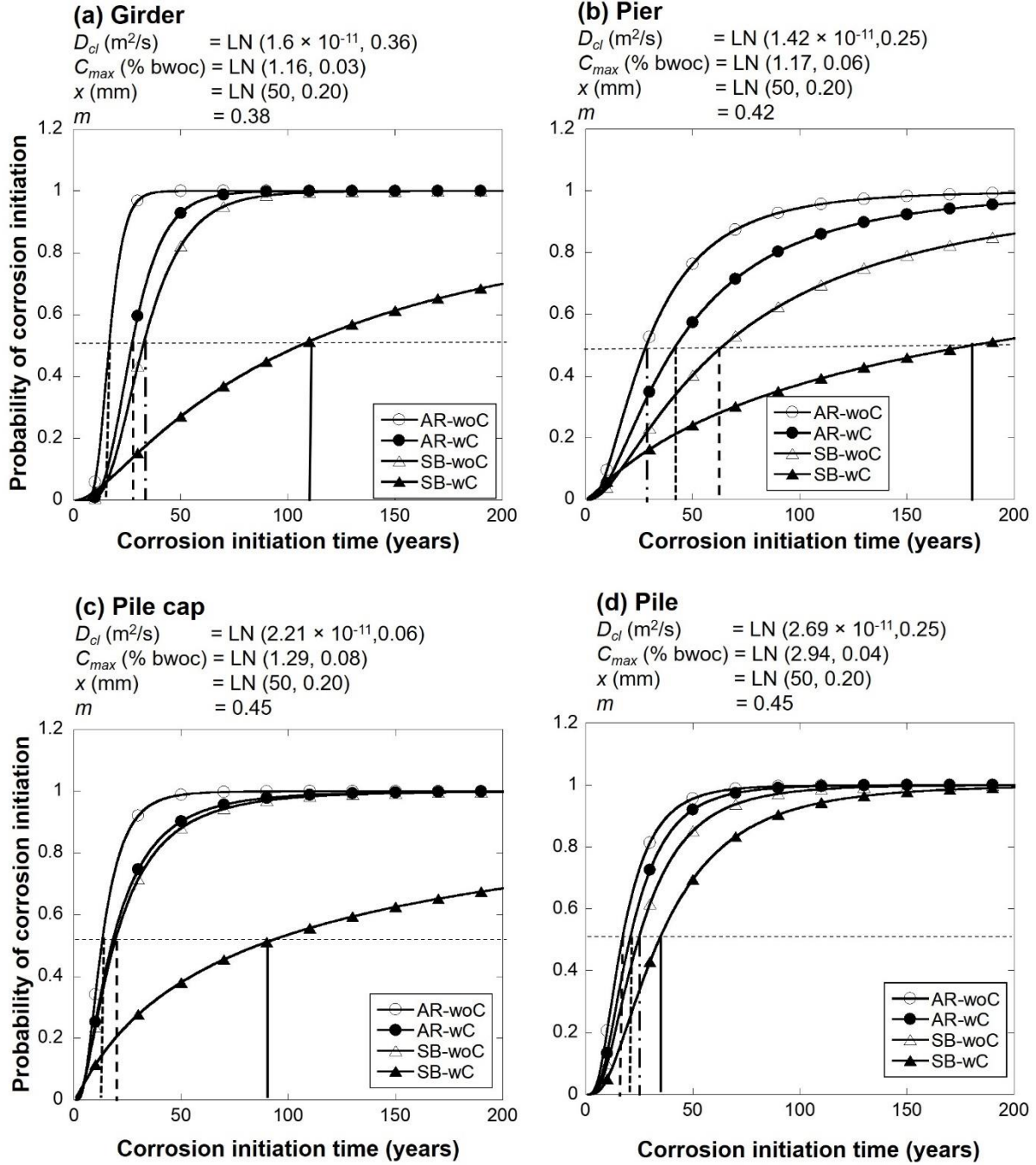
Figure 6.18 CDF of corrosion initiation time for (a) girder, (b) pier, (c) pile cap, and (d) pile

6.5   RECOMMENDATIONS

6.5.1   For new constructions with CPC coated steel rebars

➢ Considering the poor performance of CPC coating when applied on rusted/as-received steel surface, candidate recommends to avoid using the CPC coating when the coating on sand-blasting of steel rebar is not possible (for more details, refer Kamde and Pillai 2020a).

➢ Urgently ban or place a moratorium on the use of CPC coated steel rebars unless the construction sites ensure that the CPC coating will be applied on the cleaned/sandblasted steel rebars.

6.5.2   For existing structures with CPC coated steel rebars

➢ Inspect the RC structures with CPC coated steel rebars at regular interval and estimate the residual service life (for more details, refer Kamde and Pillai 2020b).

➢ As the resistance of CPC coating is low (20 - 200 Ω). Therefore, the cathodic prevention systems using galvanic anodes could be installed to delay the onset of corrosion. However, the feasibility of the application of SACP on RC systems with CPC coated steel rebars should be investigated.

➢ A small investment of about 3% of the total project cost before the onset of corrosion can significantly delay the initiation of corrosion (Byrne et al. 2016). Once corrosion starts, it is more difficult and expensive to install an efficient cathodic protection system – hence, cathodic prevention is recommended.

➢ Urgently ban or place a moratorium on the use of CPC coated steel rebars unless the construction sites ensure that the coating is done on sand-blasted steel surface (not later than three hours).

6.6 SUMMARY

Recently, many infrastructure systems (railways/highways) have been constructed using Cement-Polymer-Composite (CPC) coated steel rebars. Many of them are constructed with poor quality coatings. To quantify the differences in the chloride threshold (Cl_{th}) of coated and uncoated as-received (AR) and sand-blasted (SB) steel specimens, 3-bar prism, and lollipop specimens were cast and tested. Then, To assess the effect of CPC coating and/or negligible corrosion on bond stress-slip response of RC systems, pull-out specimens of $(150 \times 150 \times 150)$ mm with 12 mm diameter rebar with 70 mm embedded length were cast and tested. With negligible corrosion, the τ_b can significantly reduce by about 50-70%. Similar reductions were also observed in the stiffnesses of S-C and S-C-C interfaces. Based on the results, bond stress-slip mechanisms are proposed for CPC coated steel rebar without and with corrosion. Also, a service life model for RC structures with CPC coated steel rebars are also offered. Then, one such bridge was considered, where CPC coating material was applied on as-received steel rebar with a layer of rust (instead of the clean sand-blasted surface). To assess the quality of concrete used, cylindrical concrete specimens were extracted from the various elements on the bridge. Experiments were performed to determine surface chloride concentrations (C_s), maximum surface chloride concentrations (C_{max}), and diffusion coefficients (D_{cl}). Service lives were estimated using the SL-Chlor MATLAB program. The recommendations are suggested for new constructions, and existing structures with CPC coated steel rebars are proposed.

7   CONCLUSIONS AND RECOMMENDATIONS

7.1   INTRODUCTION

This thesis is based on a comprehensive experimental program on the electrochemical response from coated steel rebars embedded in cementitious systems. First, the feasibility of conventional test methodologies such as half-cell potential (HCP), macrocell corrosion current (MCC), linear polarization resistance (LPR), and electrochemical impedance spectroscopy (EIS) were evaluated. Following this, the test methodology suggested by Rengaraju (2019) was modified to cr-ACT and used for assessment of RC systems with FBE coated steel rebars, and lr-ACT technique was adopted for RC systems with CPC coated steel rebars. Following this, the effect of inadequate construction practices were evaluated on corrosion initiation, chloride threshold, and service life of RC systems with FBE and CPC coated steel rebars. The major findings and conclusions are presented in this chapter. This chapter is divided in three subsections:(i) Conclusions, (ii) Major contributions, and (iii) Recommendations for future research.

7.2   CONCLUSIONS

7.2.1   Objective 1 - Feasibility of existing techniques to assess the coated steel rebars embedded in cementitious systems

> ➢   Conventional test methods that are used for assessment of RC systems with uncoated steel rebars such as test methods based on half-cell potential (HCP), macrocell corrosion current (MCC), and linear polarization resistance (LPR) failed to detect the initiation of corrosion in RC systems with FBE coated steel rebars.

➤ Only EIS-based tests are able to detect corrosion initiation of FBE coated steel rerbars in cementitious systems

➤ Both LPR and EIS based are able to detect corrosion initiation of CPC coated steel rebars in cementitious systems

➤ Table 7.1 summarises the testing techniques suggested for various steel rebars.

Table 7.1 Summary of test methods for uncoated and coated steel rebars

Steel surface conditions	Suitable techniques to detect corrosion initiation	Justification/Remarks
Uncoated	MCC, HCP, LPR, EIS	Works in low resistive cementitious cover
FBE coated	EIS	Work effectively even if the resistivity of FBE coating is high ($1000\,k\Omega cm^2$)
CPC coated	LPR, EIS	The resistivity of CPC coating is relatively low (20-$200\ \Omega cm^2$)

➤ A four-stage FBE coating degradation mechanism is proposed; the degradation of FBE coating involves following stages: (i) Resistance to moisture ingress, (ii) Moisture ingress and degradation of coating, (iii) Pore filling due to the formation of insoluble corrosion products, (iv) Moisture/chloride ingress, coating degradation, and initiation of corrosion.

7.2.2 Objective 2 – Performance of FBE coated steel rebars

➢ Micro-analytical results (FTIR/XRD/SEM/EIS) showed that about one month of UV exposure could result in shrinkage-induced cracking of the coating.

➢ FBE coating without any damage/degradation (FBEC-ND) and (FBEC-UV) undergoes a 4-stage slow degradation and 2-stage fast degradation when exposed to cement mortar and chlorides.

➢ Mechanisms of initiation of corrosion of FBEC-UV and FBEC-SD steel rebars embedded in concrete and exposed to chlorides are proposed.

➢ The chloride threshold (Cl_{th}) of FBE coated steels is about 1/4th the chloride threshold of uncoated steels. Exposure to UV rays can further decrease the Cl_{th}. Also, scratch damage to coating can result in Cl_{th} half of the uncoated steel rebars.

➢ The chloride diffusion coefficient of coating ($D_{cl,\ coating}$) can increase by about 40 times when exposed to sunlight/UV rays.

➢ A framework to estimate the service life of RC structure with FBE coated steel rebars was proposed – considering the 2-stage transport of chloride (i.e., diffusion of chlorides through concrete and coating), and Cl_{th} of coated steel rebars.

➢ The following performance indicators were found to be dominating in ensuring the desired performance of FBE coating: (i) electrical resistance of the coating (R_C), (iii) chloride thresholds of the steel-coating interface (Cl_{th}), (iii) chloride diffusion coefficient of coating ($D_{cl,\ coating}$). It was found that a high R_C of epoxy coating was a good indicator of its performance in resisting the ingress of moisture/water and chlorides. Also, the Cl_{th} and $D_{cl,\ coating}$ of FBE coated steel-concrete systems, is found to vary significantly due to abrasion/scratching at sites and exposed to sunlight for longer than one month. Hence, such tests must be

done on rebar specimens reflecting the true field conditions and the expected deviations in Cl_{th} and $D_{cl,\ coating}$ must be accounted for estimating their service life.

➢ The coating thickness of less than 200 µm resulted in about 50% reduction in the service lives than expected. The service lives of RC systems with FBEC-SD and FBEC-UV steel rebars were found to be 75% and 65% less than the service lives of RC systems with FBEC-ND steel rebars.

7.2.3   Objective 3 – Performance of CPC coated steel rebars

➢   Application of CPC coating on as-received steel surface can result in a thin, long, and continuous crack at the steel-coating interface. This crack can act as a reservoir and provide a low resistive path for the corrosion process.

➢   Experimental results show that the lack of cleaning/sandblasting prior to the application of CPC coating can lead to 50% reduction of the Cl_{th} of adequately CPC coated steel rebars.

➢   In the case of CPC coated steel rebars, the bond stress - slip behavior is governed by the adhesion, frictional, and mechanical interlocking forces at steel-coating or coating-concrete interfaces, whichever is less. With negligible corrosion, chemical adhesion and friction forces were found to be diminished between steel and coating, and bond strength was the result of only mechanical interlocking.

➢   CPC coating was found to reduce the bond strength by about 20% of the bond strength of uncoated steel rebars. With negligible corrosion, the bond strength of RC systems with CPC coated steel rebar was reduced by about 40-80% of the initial bond strength, which can result in the 2-5 times additional development length.

➢   A service life model for RC systems with CPC coated steel rebars is proposed considering the initiation of corrosion and immediate loss in bond strength between steel and concrete.

➢   The service lives of RC systems with inadequately CPC coated steel rebars were found to be at least 40% less than the service lives of RC systems with adequately CPC coated steel rebars.

7.2.4   Limitations

➢   Validity of the proposed test methods is not verified on large scale RC systems.

➢   Diffusion coefficients of FBE coating were considered to be constant throughout the service life, which can increase due to degradation of coating with time. Therefore, the decay constant of FBE coating should be determined and used for the estimation of service lives of RC systems with FBE coated steel rebars.

➢   For FBE and CPC coated steel rebars, the service lives of RC systems may get affected due to many other inadequate practices such as discontinuity in the coating, combination of scratch damage, and degradation due to exposure to sunlight, and other environmental factors, which is not studied in this thesis.

➢   The bond strength is determined using pullout specimens, which does not represent the flexural member of RC systems. Therefore, the results from the bond characteristics study can be used for the qualitative assessment.

7.3   MAJOR CONTRIBUTIONS

➢   EIS and LPR based test methods are proposed to detect the initiation of corrosion of FBE and CPC coated steel rebars, respectively, embedded in cementitious systems.

➢   Mechanism of UV-induced chemical changes, shrinkage, and cracking of FBE coating, and the resulting steel corrosion are proposed.

➢   4-stage slow degradation and 2-stage fast degradation mechanisms for undamaged and UV-damaged FBE coatings, respectively, are proposed when exposed to alkaline plus chloride environment.

➤ Mechanisms of bond degradation for RC systems with CPC coated steel rebars with and without corrosion are proposed.

➤ A framework for the determination of diffusion coefficient of coating, chloride thresholds, and estimation of service life of RC systems with FBE and CPC coated steel rebars are proposed.

➤ Sufficient database on chloride thresholds and estimated service lives are generated to make necessary changes in IS 13620, ASTM 775, and other guidelines.

➤ Prescriptive and performance specifications for new constructions and remedial measures for existing structures are suggested.

➤ The major recommendations from this study for practical applications are provided in Sections 4.4, 5.5, and 6.5.

7.4 RECOMMENDATIONS FOR FUTURE RESEARCH

➤ The validity of test methodologies suggested in this thesis can be evaluated for the assessment of the large scale RC systems with FBE and CPC coated steel rebars.

➤ A study to evaluate the effect of degree of corrosion on bond strength between FBE coated steel and concrete should be conducted, especially for the case when FBE coated steel rebars are exposed to sunlight for more than one month.

➤ The effect of long-term exposure to the alkaline environment on the FBE coating characteristics such as coating integrity, diffusion coefficients should be evaluated.

➤ The relation between the performance indicators should be developed to eliminate the regeourous process of estimating the residual service life. For example, the

relation between electrical resistance of coating (R_C) and chloride diffusion coefficient of coating ($D_{cl,\,coating}$) can help to estimate $D_{cl,\,coating}$ without the tests involving log-term exposure and EDX analysis.

➢ R_C can be used to estimate the present condition of coating in concrete. A detailed investigation and database on R_C and coating condition will help in investigation of RC systems with FBE coated steel rebars.

➢ Worldwide, many structures are built with FBE and cementitious coated steel rebars with inadequate practices, which might experience premature initiation of corrosion. As these coatings are dielectric, conventional repairs techniques may not be successful in controlling the corrosion in these RC structures. Therefore, research should be carried out to identify a suitable/feasible repair strategy. The feasibility of cathodic protection with sacrificial anodes and coating on concrete surface (suggested in this thesis) should be investigated further.

➢ The industry needs a more reliable solution for the durable life of RC structures. Metallic coated steel rebars are promising the robustness in their performance. More research on their long-term performance is required to validate the durability claims of these steel rebars. Also, their manufacturing and use should be standardized to avoid experiences similar to FBE and CPC coated steel rebars.

This page is intentionally left blank

8   REFERENCES

Ababneh, A. N., Sheban, M. A., and Abu-Dalo, M. A. (2012). "Effectiveness of Benzotriazole as Corrosion Protection Material for Steel Reinforcement in Concrete." Journal of Materials in Civil Engineering, 24(2), 141–151.

ACI Committee 222 (2001). Protection of Metals in Concrete Against Corrosion. ACI222R-01, Farmington Hills.

ACI Committee 408 (2003). ACI 408R-03 Bond and Development of Straight Reinforcing Bars in Tension. American Concrete Institute.

Al-Amoudi, O. S. B., Maslehuddin, M., and Ibrahim, M. (2004). "Long-term performance of fusion-bonded epoxy-coated steel bars in chloride-contaminated concrete." ACI Materials Journal, 101(4), 303–309.

Alexander, M., and Beushausen, H. (2019). "Durability, service life prediction, and modelling for reinforced concrete structures – review and critique." Cement and Concrete Research, Elsevier, 122(February), 17–29.

Almusallam, A. A., Al-Gahtani, A. S., and Aziz, A. R. (1996). "Effect of reinforcement corrosion on bond strength." Construction and Building Materials, 10(2), 123–129.

Amleh, L., and Mirza, S. (1999). "Corrosion influence on bond between steel and concrete." ACI Structural Journal, 96(3), 415–423.

Angst, U. (2011). "Chloride induced reinforcement corrosion in concrete - Concept of critical chloride content – methods and mechanisms." Concept of Critical Chloride Content—Methods and mechanisms, Norwegian University of Science and Technology.

Angst, U. M., Geiker, M. R., Michel, A., Gehlen, C., Wong, H., Isgor, O. B., Elsener, B., Hansson, C. M., François, R., Hornbostel, K., Polder, R., Alonso, M. C., Sanchez, M., Correia, M. J., Criado, M., Sagüés, A., and Buenfeld, N. (2017). "The steel–concrete interface." Materials and Structures, 50(2), 143.

Ann, K. Y., Ahn, J. H., and Ryou, J. S. (2009). "The importance of chloride content at the concrete surface in assessing the time to corrosion of steel in concrete structures." Construction and Building Materials, Elsevier Ltd, 23(1), 239–245.

Assaad, J. J., and Issa, C. A. (2012). "Bond strength of epoxy-coated bars in underwater concrete." Construction and Building Materials, 30, 667–674.

ASTM A1096M (2016). "Standard Test Method for Evaluating Bond of Individual Steel Wire" , Indented or Plain, for concrete reinforcement, American Society of Testing and Materials, West Conshohocken

ASTM A775-19 (2017). Standard Specification for Epoxy-Coated Steel Reinforcing Bars 1. American Society of Testing and Materials, West Conshohocken.

ASTM C1556-11a. (2015). 1556,"Standard Test Method for Determining the Apparent Chloride Diffusion Coefficient of Cementitious Mixtures by Bulk Diffusion," Annual

Book of ASTM Standards, ASTM, West Conshohocken, USA.

ASTM C204-18. (2019). "Standard Test Methods for Fineness of Hydraulic Cement by Air-Permeability." ASTM Standard Book, West Conshohocken, USA.

ASTM C305. (2015). Standard Practice for Mechanical Mixing of Hydraulic Cement Pastes and Mortars. ASTM Standard Book, West Conshohocken, USA.

ASTM C876. (2015). Astm C876: Standard Test Method for Half-Cell Potentials of Uncoated Reinforcing Steel in Concrete. ASTM Standard Book, West Conshohocken, USA.

ASTM G109-07. (2013). Standard Test Method for Determining the Effects of Chemical Admixtures on the Corrosion of Embedded Steel Reinforcement in Concrete Exposed to Chloride Environments. Americal Society of Testing and Materials, West Conshohocken, USA.

ASTM G154-16 (2016). "Standard Practice for Operating Fluorescent Ultraviolet (UV) Lamp Apparatus for Exposure of Nonmetallic Materials", ASTM Standard Book, West Conshohocken, USA,.

Auyeung, Y., Balaguru, P., and Chung, L. (2000). "Bond behavior of corroded reinforcement bars." ACI Structural Journal, 97(2), 214–220.

Azoor, R. M., Deo, R. N., Birbilis, N., and Kodikara, J. (2019). "On the optimum soil moisture for underground corrosion in different soil types." Corrosion Science, Elsevier Ltd., 10.1016/j.corsci.2019.108116

Baker, M. J., Trevisan, J., Bassan, P., Bhargava, R., Butler, H. J., Dorling, K. M., Fielden, P. R., Fogarty, S. W., Fullwood, N. J., Heys, K. A., Hughes, C., Lasch, P., Martin-Hirsch, P. L., Obinaju, B., Sockalingum, G. D., Sulé-Suso, J., Strong, R. J., Walsh, M. J., Wood, B. R., Gardner, P., and Martin, F. L. (2014). "Using Fourier transform IR spectroscopy to analyze biological materials." Nat Protoc.9(8), 1771–1791, doi:10.1038/nprot.2014.110.

Barbucci, A., Delucchi, M., Goretta, L., and Cerisola, G. (1998). "Electrochemical and physico-chemical characterization of fluorinated organic coatings for steel and concrete protection: Influence of the pigment volume concentration." Progress in Organic Coatings, 33(2), 139–148.

Bentz, E. C. (2003). "Probabilistic modeling of service life for structures subjected to chlorides." ACI Materials Journal, (100), 391–397.

Bhaskar, S., Bharatkumar, B. H., Gettu, R., and Neelamegam, M. (2010). "Effect of corrosion on the bond behaviour of OPC and PPC concretes." Journal of Structural Engineering (Madras), 37(1), 37–42.

Bhattacharjee, B. (2012). "Some issues related to service life of concrete structures." The Indian Concrete Journal, (January), 23–29.

Bhattacharya, R., PAL, S., BHOUMICK, A., and BARMAN, P. (2012). "Annual Variability and Distribution of Ultraviolet Index Over India Using Temis Data."

International Journal of Engineering Science and Technology, 4(11), 4577–4583.

Bi, H., and Sykes, J. (2016). "Cathodic delamination of unpigmented and pigmented epoxy coatings from mild steel." Progress in Organic Coatings, Elsevier B.V., 90, 114–125.

Bíaz, B., Nóvoa, X. R., Pérez, C., and Pintos, A. (2018). "EIS study of epoxy resin applied on carbon steel using double-cylinder electrolyte cell." Progress in Organic Coatings, Elsevier, 124(December 2017), 275–285.

Biegafiska, B., Zubielewicz, M., and Qmiesze, E. (1988). "Influence of barrier pigments on the performance of protective coatings." Progress in Organic Coatings, 16, 219–229.

Brown, M. C., Weyers, R. E., and Sprinkel, M. M. (2006). "Service life extension of virginia bridge decks afforded by epoxy-coated reinforcement." Journal of ASTM International, 3(2), 1–13.

Byrne, A., Holmes, N., and Norton, B. (2016). "State-of-the-art review of cathodic protection for reinforced concrete structures." Magazine of Concrete Research, 68(13), 664–677.

Cabrera, J. G. (1996). "Deterioration of concrete due to reinforcement steel corrosion." Cement and Concrete Composites, 18(1), 47–59.

Cambier, S. M., Posner, R., and Frankel, G. S. (2014). "Coating and interface degradation of coated steel, Part 1: Field exposure." Electrochimica Acta, Elsevier Ltd, 133, 30–39.

Cao-Paz, A., Covelo, A., Farina, J., Nóvoa, X. . R., Pérez, C., and Rodríguez-Pardo, L. (2010). "Progress in Organic Coatings Ingress of water into organic coatings : Real-time monitoring of the capacitance and increase in mass." 69, 150–157.

Castel, A., François, R., and Arliguie, G. (2000). "Mechanical behaviour of corroded reinforced concrete beams - Part 2: experimental study of corroded beams." Materials and Structures/Materiaux et Constructions, 33(233), 539–544.

Castel, A., Vidal, T., and François, R. (2007). "Serviceability model of corroded reinforced concrete based on the CEB-FIP model code." Structural Concrete, 8(3), 139–146.

Central Electrochemical Research Institute Karaikudi. (1993). "Cement Polymer Composite Coating system for corrosion protection of reinforcing and prestressing steel."

Chen, X., Ebert, W. L., and Indacochea, J. E. (2017). "Electrochemical corrosion of a noble metal-bearing alloy-oxide composite." Corrosion Science, Elsevier, 124(June 2018), 10–24.

Cheng, K. C., Lin, C. M., Wang, S. F., Lin, S. T., and Yang, C. F. (2007). "Dielectric properties of epoxy resin-barium titanate composites at high frequency." Materials Letters, 61(3), 757–760.

Choi, Y. S., Yi, S. T., Kim, M. Y., Jung, W. Y., and Yang, E. I. (2014). "Effect of corrosion method of the reinforcing bar on bond characteristics in reinforced concrete specimens." Construction and Building Materials, Elsevier Ltd, 54, 180–189.

Chung, L., Kim, J. J., and Yi, S. (2008). "Cement & Concrete Composites Bond strength prediction for reinforced concrete members with highly corroded reinforcing bars." 30, 603–611.

Cividanes, L. S., Simonetti, E. A. N., Moraes, M. B., Fernandes, F. W., Thim, G. P., and Tecnol, I. (2014). "Influence of Carbon Nanotubes on Epoxy Resin Cure Reaction Using Different Techniques : A Comprehensive Review." Polymer Engineering and Science, 2461–2469.

Cortés, E. V. (1998). "Corrosion Performance of Epoxy-Coated Reinforcement in Aggressive Environments." The University of Texas at Austin.

Cox, G. L., and Roetheli, B. E. (1931). "Effect of Oxygen Concentration on Corrosion Rates of Steel and Composition of Corrosion Products Formed in Oxygenated Water." Industrial and Engineering Chemistry, 23(9), 1012–1016.

Criado, M., Sobrados, I., Bastidas, J. M., and Sanz, J. (2016). "Progress in Organic Coatings Corrosion behaviour of coated steel rebars in carbonated and chloride-contaminated alkali-activated fly ash mortar." Progress in Organic Coatings, Elsevier B.V., 99, 11–22.

Criado, M., Sobrados, I., and Sanz, J. (2014). "Progress in Organic Coatings Polymerization of hybrid organic – inorganic materials from several silicon compounds followed by TGA / DTA , FTIR and NMR techniques." Progress in Organic Coatings, Elsevier B.V., 77(4), 880–891.

Cunat, P. (2004). "Alloying Elements in Stainless Steel and Other Chromium-Containing Alloys." International Chromium Development Association.

Darwin, A. B., and Scantlebury, J. D. (2002). "Retarding of corrosion processes on reinforcement bar in concrete with an FBE coating." Cement & Concrete Composites, 24, 73–78.

David Trejo. (2020). "Personal discussion with Prof. David Trejo." Oregon State University, Chennai.

Dhanya, B. S. (2015). "Study of the influence of supplementary cementitious materials on selected durability parameters of concrete." Indian Institute of Technology Madras.

Dhole, G. S., Gunasekaran, G., Naik, R., Ghorpade, T., and Vinjamur, M. (2020). "Fluorescence based corrosion detecting epoxy coating." Progress in Organic Coatings, Elsevier, 138(October 2019), 105425.

Ding, L., and Poursaee, A. (2017). "The impact of sandblasting as a surface modification method on the corrosion behavior of steels in simulated concrete pore solution." Construction and Building Materials, Elsevier Ltd, 157, 591–599.

Ding, L., Torbati-sarraf, H., and Poursaee, A. (2018). "Surface & Coatings Technology The in fl uence of the sandblasting as a surface mechanical attrition treatment on the electrochemical behavior of carbon steel in di ff erent pH solutions." Surface & Coatings Technology, Elsevier, 352(May), 112–119.

Dong, S., Zhao, B., Lin, C., Du, R., Hu, R., and Xiaoge, G. (2012). "Corrosion behavior of epoxy / zinc duplex coated rebar embedded in concrete in ocean environment." Construction and Building Materials, Elsevier Ltd, 28(1), 72–78.

Egorov, M. D., Sapozhnikov, Y. L., and Shakhnazarov, Y. V. (1989). "Effect of carbon content on the structure, hardness, and thermal stability of boron-chromium cast steels." Strength Properties, 5(December), 61–64.

Elbusaefi, A. A. (2014). "the effect of steel bar corrosion on the bond strength of concrete manufactured with cement replacement materials." Cardiff University, Cardiff University.

Elsener, B., Andrade, C., Gulikers, J., Polder, R., and Raupach, M. (2003). "Half-cell potential measurements - Potential mapping on reinforced concrete structures." Materials and Structures/Materiaux et Constructions, 36(261), 461–471.

Fang, C., Lundgren, K., Chen, L., and Zhu, C. (2004). "Corrosion influence on bond in reinforced concrete." Cement and Concrete Research, 34(11), 2159–2167.

Fanous, F., and Wu, H. (2005). "Performance of Coated Reinforcing Bars in Cracked Bridge Decks." Journal of Bridge Engineering, 10, pp 255-261.

FHRA. (1976). Interim Report No. 2 - NEEP No. 16 Coated Reinforcing Steel for Bridges. Washington D.C.

FIB Model Code. (2010). Lausanne, Switzerland.

Fontana, M. G. (1986). Corrosion Engineering. McGraw-Hill Book Company, Singapore.

Forecast, L. weather. (2020). "Weather Atlas." web, <https://www.weather-ind.com/en/india/chennai-long-term-weather-forecast>.

Fountoulakis, I., Zerefos, C. S., Bais, A. F., Kapsomenakis, J., Koukouli, M. E., Ohkawara, N., Fioletov, V., De Backer, H., Lakkala, K., Karppinen, T., and Webb, A. R. (2018). "Twenty-five years of spectral UV-B measurements over Canada, Europe and Japan: Trends and effects from changes in ozone, aerosols, clouds, and surface reflectivity." Comptes Rendus - Geoscience, Academie des sciences, 350(7), 393–402.

Gergely, P., and Lutz, L. A. (1967). "Maximum Crack Width in Reinforced Concrete Flexural Members." American Concrete Institute SP20, 87–117.

Ghasemi-Kahrizsangi, A., Shariatpanahi, H., Neshati, J., and Akbarinezhad, E. (2015a). "Degradation of modified carbon black/epoxy nanocomposite coatings under ultraviolet exposure." Applied Surface Science, Elsevier B.V., 353, 530–539.

Ghasemi-Kahrizsangi, A., Shariatpanahi, H., Neshati, J., and Akbarinezhad, E. (2015b). "Corrosion behavior of modified nano carbon black/epoxy coating in accelerated conditions." Applied Surface Science, Elsevier B.V., 331, 115–126.

Griffith, A., and Laylor, H. M. (1999). Epoxy Coated Reinforcement Study. Oregon Department of Transportation Research, Oregon.

Guadagno, L., Raimondo, M., Vittoria, V., Vertuccio, L., Naddeo, C., Russo, S., Vivo, B. De, and Lamberti, P. (2014). "RSC Advances aeronautics and aerospace †." Royal Society Chemistry Advances, (4), 15474–15488.

Hamad, B. S. (1995). "Comparative Bond Strength of Coated and Uncoated Bars with Different Rib Geometries." ACI Material Journal, (85), 579–590.

Hansson, C. M., Haas, R., Green, R., Evers, R. C., Gepraegs, O. K., and Al-Assar, R. (2000). Corrosion Protection Strategies for Ministry Bridges. University of Waterloo.

Heberlein, C., Bournay, E., Foster, H., Bennett, J., Dearing, J. A., Curlin, J. S., Gonin, E., Lemmet, S., Shende, R., Bisset, R., Clark, E., Fenner, A., Gobert, S. De, Natarajan, B., Sharma, K. M., and Williams, M. (2008). "Vital ozone graphics 2.0 climate link." UNEP DTIE, RRID-Arendal.

Huang, C.-H. (2014). "Effects of Rust and Scale of Reinforcing Bars on the Bond Performance of Reinforcement Concrete." Journal of Materials in Civil Engineering, 26(4), 576–581.

Hussain, R. R. (2011). "Effect of moisture variation on oxygen consumption rate of corroding steel in chloride contaminated concrete." Cement and Concrete Composites, Elsevier Ltd, 33(1), 154–161.

Hussain, S. E., Rasheeduzzafar, Al-Musallam, A., and Al-Gahtani, A. S. (1995). "Factors affecting threshold chloride for reinforcement corrosion in concrete." Cement and Concrete Research, 25(7), 1543–1555.

Idun, E. K., and Darwin, D. (1999). "Bond of Epoxy-Coated Reinforcement : Coefficient of Friction and Rib Face Angle." ACI Materials Journal, 96(March), 609–616.

Ihekwaba, N. M., Hope, B. B., and Hanssont, C. M. (1996). "PULL-OUT AND BOND DEGRADATION OF STEEL REBARS IN ECE CONCRETE." Cement and Concrete Research, 26(2), 267–282.

Indian Standards. (1988). "IS: 4031-1988." Bureau of Indian Standards.

IS 13620 (2015) "IS 13620: FUSION BONDED EPOXY COATED REINFORCING BARS- SPECIFICATION." Bureau of Indian Standards.

IS 383(1970) "Concrete, specification for coarse and fine aggregates from natural sources for." Bureau of Insian Standard.

IS-2770 (Part-I). (2007). "Methods of Testing Bond in Reinforced Concrete Part 1 pull-out test" Bureau of Indian Standards, New Delhi.

IS 2386- Part I. (1963). "Method of test for aggregate for concrete. Part I - Particle size and shape." Bureau of Indian Standards, New Delhi, India, (Reaffirmed 2002).

IS 383 (2002). "Specification for coarse and fine aggregates from natural sources for concrete" Bureau of Indian Standards, New Delhi, India, (Reaffirmed 2002).

Jalili, M. M., Moradian, S., and Hosseinpour, D. (2009). "The use of inorganic conversion

coatings to enhance the corrosion resistance of reinforcement and the bond strength at the rebar/concrete." Construction and Building Materials, Elsevier Ltd, 23(1), 233–238.

Javidparvar, A. A., Ramezanzadeh, B., and Ghasemi, E. (2016). "Effects of surface morphology and treatment of iron oxide nanoparticles on the mechanical properties of an epoxy coating." Progress in Organic Coatings, Elsevier B.V., 90(January), 10–20.

Jiang, C., Wu, Y. F., and Dai, M. J. (2018). "Degradation of steel-to-concrete bond due to corrosion." Construction and Building Materials, Elsevier Ltd, 158, 1073–1080.

Jolivet, D., Bonen, D. M., and Shah, S. P. (2007). "The corrosion resistance of coated steel dowels determined by impedance spectroscopy." Cement and Concrete Research, 37(7), 1134–1143.

Jorge, S., Dias-da-Costa, D., and Júlio, E. N. B. S. (2012). "Influence of anti-corrosive coatings on the bond of steel rebars to repair mortars." Engineering Structures, Elsevier Ltd, 36, 372–378.

Joseline, D., Kamde, D., Rengaraju, S., and Pillai, R. G. (2018). "Residual Service Life Estimation and its Importance for Pretensioned Concrete (PTC) Bridges in Coastal Cities." Sixth International Conference on the Durability of Concrete Structures, 800–806.

Kahhaleh, K. Z., Vaca-cortés, E., Jirsa, J. O., Wheat, H. G., and Carrasquillo, R. L. (1998). Corrosion performance of epoxy-coated reinforcement – macrocell tests. Texas, USA.

Kamde, D. K., and Pillai, R. G. (2017). "Comparison of Corrosion of Damaged Fusion-Bonded-Epoxy- Coated (FBEC) and Uncoated Steel Rebars." ICACMS.

Kamde, D. K., and Pillai, R. G. (2018). "Effect of the degree of corrosion on bond performance of Cement-polymer-composite (CPC) Coated steel rebars." ICCRRR, 3–7.

Kamde, D. K., and Pillai, R. G. (2020a). "Effect of surface preparation on corrosion of steel rebars coated with cement-polymer-composites (CPC) and embedded in concrete." Construction and Building Materials, Elsevier Ltd, 237(117616), 1–11.

Kamde, D. K., and Pillai, R. G. (2020b). "Chloride-induced corrosion of Fusion- Bonded-Epoxy coated steel rebars in concrete and its effects on service life." Materials and Corrosion.

Kamde, D. K., and Pillai, R. G. (2020c). "Effect of sunlight/ultraviolet exposure on the corrosion of fusion bonded-epoxy (FBE) coated steel rebars in concrete." Corrosion (Houston).

Karuppanasamy, J., and Pillai, R. G. (2017a). "A short-term test method to determine the chloride threshold of steel – cementitious systems with corrosion inhibiting admixtures." Materials and Structures, Springer Netherlands, 50(4), 1–17.

Karuppanasamy, J., and Pillai, R. G. (2017b). "Statistical Distributions for the Corrosion Rates of Conventional and Prestressing Steel Reinforcement Embedded in Chloride

Contaminated Mortar." Corrosion Journal, 73(9), 1119–1131.

Kearsley, E. P., and Joyce, A. (2014). "Effect of corrosion products on bond strength and flexural behaviour of reinforced concrete slabs." Journal of the South African Institution of Civil Engineering, 56(2), 21–29.

Kessler, S., Angst, U., Zintel, M., Elsener, B., and Gehlen, C. (2016). "Epoxy-coated reinforcement in concrete structures: Results of a Swiss pilot project after 24 years of field exposure." Materials and Corrosion, 67(6), 631–638.

Kessler, S., Zintel, M., and Gehlen, C. (2015). "Defects in epoxy-coated reinforcement and their impact on the service life of a concrete structure A study of critical chloride content and macro-cell corrosion." Structural Concrete, (3), 398–405.

Kim, G. R., Lee, S. H., Song, H. Y., Han, J. M., and Shipbuilding, D. (2007). "Paper No. 07013." NACE CORROSION Conference and Expo, (07013), 1–13.

Kivell, A., Palermo, A., and Scott, A. (2011). "Effects of Bond Deterioration due to Corrosion in Reinforced Concrete." (081), 1–8.

Kobayashi, K., and Takewaka, K. (1984). "Experimental studies on epoxy coated reinforcing steel for corrosion protection." International Journal of Cement Composites and Lightweight Concrete, 6(2), 99–116.

Kranc, S. C., and Alberto A. Sagues. (2001). "Detailed modeling of corrosion macrocells on steel reinforcing in concrete." Corrosion Science, Paper N#13(43), 1355–1372.

Larnach, W. J. (1952). "Changes in bond strength caused by re-vibration of concrete and the vibration of reinforcement." Magazine of Concrete Research, 4(10), 17–21.

Latif, J., Khan, Z. A., and Stokes, K. (2020). "Structural monitoring system for proactive detection of corrosion and coating failure." Sensors and Actuators, A: Physical, Elsevier B.V., 301, 111693.

Lau, K., and Sagüés, A. A. (2007). "Coating Condition Evaluation of Epoxy-Coated Rebar." The electrochemical society, 3(13), 81–92.

Laurence W. McKeen. (2006). "Measurement of Coating Properties and Performance." Fluorinated Coatings and Finishes Handbook, William Andrew Publishing, 175–196.

Ldun, E. K., and Darwin, D. (1999). "Bond of epoxy-coated reinforcement: Coefficient of friction and rib face angle." ACI Structural Journal, 96(4), 609–615.

Lee, H.-S., Noguchi, T., and Tomosawa, F. (2002). "Evaluation of the bond properties between concrete and reinforcement as a function of the degree of reinforcement corrosion." Cement and Concrete Research, 32(8), 1313–1318.

Li, C.-Q., Yang, S. T., and Saafi, M. (2014). "Numerical Simulation of Behavior of Reinforced Concrete Structures considering Corrosion Effects on Bonding." Journal of Structural Engineering, 140(12), 1–10.

De Lima, H. M. L. F., Tavares, S. S. M., Martins, M., and Araújo, W. S. (2019). "The

effect of copper addition on the corrosion resistance of cast duplex stainless steel." Journal of Materials Research and Technology, Brazilian Metallurgical, Materials and Mining Association, 8(2), 2107–2119.

Lin, H., and Zhao, Y. (2016). "Effects of confinements on the bond strength between concrete and corroded steel bars." Construction and Building Materials, Elsevier Ltd, 118, 127–138.

Liu, B., Fang, Z. G., Wang, H. Bin, and Wang, T. (2013). "Effect of cross linking degree and adhesion force on the anti-corrosion performance of epoxy coatings under simulated deep sea environment." Progress in Organic Coatings, Elsevier B.V., 76(12), 1814–1818.

Liu, M., and Horrocks, A. R. (2002). "Effect of Carbon Black on UV stability of LLDPE films under artificial weathering conditions." Polymer Degradation and Stability, 75, 485–499.

Löf, D., Hamieau, G., Zalich, M., Ducher, P., Kynde, S., Midtgaard, S. R., Parasida, C. F., Arleth, L., and Jensen, G. V. (2020). "Dispersion state of TiO2 pigment particles studied by ultra-small-angle X-ray scattering revealing dependence on dispersant but limited change during drying of paint coating." Progress in Organic Coatings, Elsevier, 142(November 2019), 105590.

Lyon, S. B., Bingham, R., and Mills, D. J. (2017). "Progress in Organic Coatings Advances in corrosion protection by organic coatings : What we know and what we would like to know." Progress in Organic Coatings, Elsevier B.V., 102, 2–7.

Mahltig, B., Bottcher, H., Rauch, K., Dieckmann, U., Nitsche, R., and Fritz, T. (2005a). "Optimized UV protecting coatings by combination of organic and inorganic UV absorbers." Thin Solid Films, 485, 108–114.

Mahltig, B., Böttcher, H., Rauch, K., Dieckmann, U., Nitsche, R., and Fritz, T. (2005b). "Optimized UV protecting coatings by combination of organic and inorganic UV absorbers." Thin Solid Films, 485(1–2), 108–114.

Malik, A. U., Andijani, I., Ahmed, S., and Al-Muaili, F. (2002). "Corrosion and mechanical behavior of fusion bonded epoxy (FBE) in aqueous media." Desalination, 150(3), 247–254.

Malik, A. U., Mayan Kutty, P. C., Siddiqi, N. A., Andijani, I. N., and Ahmed, S. (1992). "The influence of pH and chloride concentration on the corrosion behaviour of AISI 316L steel in aqueous solutions." Corrosion Science, 33(11), 1809–1827.

Mangat, P. S., and Elgarf, M. S. (1999). "Bond characteristics of corroding reinforcement in concrete beams." Materials and Structures, 32(March), 89–97.

Manning, D. G. (1996). "Corrosion performance of epoxy-coated reinforcing steel: North American experience." Construction and Building Materials, 10(5), 349–365.

Mansfeld, F., and Tsail, C. H. (1991). "Determination of coating deterioration with EIS. I. Basic relationships." Corrosion, 47(12), 958–963.

Marcos-Meson, V., Solgaard, A., Fischer, G., Edvardsen, C., and Michel, A. (2020). "Pull-out behaviour of hooked-end steel fibres in cracked concrete exposed to wet-dry cycles of chlorides and carbon dioxide – Mechanical performance." Construction and Building Materials, Elsevier Ltd, 240, 117764.

Marsh, J., Scantlebury, J. D., and Lyon, S. B. (2001). "The effect of surface / primer treatments on the performance of alkyd coated steel." CORROSION SCIENCE, Elsevier Ltd, 43(5), 829–852.

Mayne, J. E. O. (1973). "The mechanism of the protection of iron and steel by paint." Anti Corrosion, (October), 3–8.

McDonald, D. (2009). "Epoxy-Coated Reinforcing Steel Bars in Northern America." (November).

McDonald, D. B. (2010). "Use and Performance of Epoxy-Coated Reinforcing Steel Over 37 Years." International Bridge Conference, (August).

McDonald, D. B. (2016). "Corrosion of Steel in Concrete." Corrosion of Steel in Concrete Structures, 277.

McHattie, J. S., Perez, I. L., and Kehr, J. A. (1996). "Factors Affecting Cathodic Disbondment of Epocy Coatings for Steel Reingorcing Bars." Cement and Concrete Composites, 18/(95), 93–103.

Miller, G. G., Kepler, J. L., and Darwin, D. (2003). "Effect of epoxy coating thickness on bond strength of reinforcing bars." ACI Structural Journal, 100(3), 314–320.

Miszczyk, A., and Darowicki, K. (2018). "Water uptake in protective organic coatings and its re fl ection in measured coating impedance." Progress in Organic Coatings, Elsevier, 124, 296–302.

Mitsuba. (2016). "Mitsuba's Rebar Coating Equipment- Epoxy Spray Guns For Rebar Coating." Mitsuba Systems, <https://www.youtube.com/watch?v=_Rp_hpforbI>.

Mohammed, M. S. H. S., Raghavan, R. S., Knight, G. M. S., and Murugesan, V. (2014). "Macrocell Corrosion Studies of Coated Rebars." Arabian Journal for Science and Engineering, 39(5), 3535–3543.

Mohandoss, P. (2019). "Assessment of transmission length and bond strength of pretensioned concrete systems with seven-wire strands." Indian Institute of Technology Madras.

Montes, P., Bremner, T. W., and Kondratova, I. (2004). "Eighteen-year performance of epoxy-coated rebar in a tunnel structure subjected to a very aggressive chloride-contaminated environment." Corrosion, 60(10), 974–981.

Mundra, S., Criado, M., Bernal, S. A., and Provis, J. L. (2017). "Chloride-induced corrosion of steel rebars in simulated pore solutions of alkali-activated concretes." Cement and Concrete Research, Elsevier, 100(October 2016), 385–397.

Nair, S. A. O., and Pillai, R. (2017). "' TM-Ring Test ' - A quality control test for TMT (or

QST) steel reinforcing bars used in reinforced concrete systems." ICI journal, (April), 1–9.

Nair, S. A. O., and Pillai, R. G. (2020). "Microstructural and corrosion characteristics of Quenched and Self-Tempered (QST) steel reinforcing bars." Construction and Building Materials, Elsevier Ltd, 231, 117109.

Natarajan, C., Jayabalan, P., Begum, N. A., and Rajaraman, A. (2005). "Corrosion protection by coatings on prestressed steel." Corrosion, 61(12), 1189–1193.

Nazarov, A., Prosek, T., and Thierry, D. (2008). "Application of EIS and SKP methods for the study of the zinc/polymer interface." Electrochimica Acta, 53(25), 7531–7538.

Němeček, J., Kruis, J., Koudelka, T., and Krejčí, T. (2018). "Simulation of chloride migration in reinforced concrete." Applied Mathematics and Computation, 319, 575–585.

Nikafshar, S., Zabihi, O., Ahmadi, M., Mirmohseni, A., Taseidifar, M., and Naebe, M. (2017). "The effects of UV light on the chemical and mechanical properties of a transparent epoxy-diamine system in the presence of an organic UV absorber." Materials, 10(2), 1–18.

Nóvoa, X. R., Pérez, C., and Rodríguez-pardo, L. (2010). "Ingress of water into organic coatings: Real-time monitoring of the capacitance and increase in mass." Progress in Organic Coatings journal, 69, 150–157.

NT Build 492. (1999). Concrete, mortar and cement-based repair materials: Chloride migration coefficient from non-steady-state migration experiments. NORDTEST, FINLAND, 1–8.

Nuralinah, D. (2012). "Laboratory test and numerical analysis of chloride ingress into concrete subjected into airborne salt." Ph.D. Thesis, Nagaoka University of Technology, Nagaoaka, Niigata, (June).

Parhizkar, N., Shahrabi, T., and Ramezanzadeh, B. (2017). "A new approach for enhancement of the corrosion protection properties and interfacial adhesion bonds between the epoxy coating and steel substrate through surface treatment by covalently modified amino functionalized graphene oxide film." Corrosion Science, Elsevier, 123(April), 55–75.

Pathania, A., Arya, R. K., and Ahuja, S. (2017). "Crosslinked polymeric coatings : Preparation , characterization , and diffusion studies." Progress in Organic Coatings, Elsevier B.V., 105, 149–162.

Peddamallu, N., Sridharan, K., Nakayama, T., and Sarathi, R. (2019). "Understanding the fundamental properties of epoxy molybdenum disulfide nanocomposites." Polymer Composites, 40(4), 1556–1563.

Pei, X., Noël, M., Fam, A., and Green, M. (2015). "Development length of steel reinforcement with corrosion protection cementitious coatings." Cement and Concrete Composites, Elsevier Ltd, 60, 34–43.

Pei, X., Noël, M., Green, M., Fam, A., and Shier, G. (2017). "Cementitious coatings for improved corrosion resistance of steel reinforcement." Surface and Coatings Technology, Elsevier B.V., 315, 188–195.

Perini, N., Prado, A. R., Sad, C. M. S., Castro, E. V. R., and Freitas, M. B. J. G. (2012). "Electrochemical impedance spectroscopy for in situ petroleum analysis and water-in-oil emulsion characterization." Fuel, 91(1), 224–228.

Phares, B. M., Fanous, F. S., Wipf, T. J., Lee, Y.-S., and Jolley, M. J. (2006). Evaluation of corrosion Resistance of Different Steel Reinforcement Types.

Pianca, F., Schell, H., and Cautillo, G. (2005). "The performance of epoxy coated reinforcement : experience of the Ontario ministry of transportation." 23, 286–308.

Pillai, R. G., Gettu, R., and Santhanam, M. (2020). "Use of supplementary cementitious materials (SCMs) in reinforced concrete systems – Benefits and limitations." Revista ALCONPAT, 10(2), 147–164.

Pyc, W. A. (1998). "Field performance of epoxy-coated reinforcing steel in virginia bridge decks." Virginia Polytechnic Institute and State University.

Pyć, W. A., Weyers, R. E., Weyers, M., Mokarem, D. W., and Zemajtis, J. (2000). "FIELD PERFORMANCE OF EPOXY-COATED REINFORCING STEEL IN VIRGINIA BRIDGE DECKS." Virginia Department of Transportation.

Rajagopalan, N., Gupta, S. C., Krishna, K., Srira, P., Srinivasan, S., and A. K., H. (2001). "Coatings For Steel And Concrete." Durability of concrete structures, 247–262.

Rajitha, K., Mohana, K. N. S., Mohanan, A., and Madhusudhana, A. M. (2020). "Evaluation of anti-corrosion performance of modified gelatin-graphene oxide nanocomposite dispersed in epoxy coating on mild steel in saline media." Colloids and Surfaces A: Physicochemical and Engineering Aspects, Elsevier, 587(November 2019), 124341.

Rao, G. A. (2014). "Parameters Influencing Bond Strength of Rebars in Reinforced Concrete." International Journal of Applied Engineering and Technology, 4(1), 2277–212.

Ray, A., Mukerjee, D., Sen, S.K., Bhattacharya, A., Dhua, S.K., Prasad, M.S., Banerjee, N., Popli, A.M., Sahu, A.K. (1997) "Microstructure and properties of thermomechanically strengthened reinforcement bars: A comparative assessment of plain-carbon and low-alloy steel grades.", Journal of Materials Engineering and Performance, 6 (3), pp. 335-343.

Rengaraju, S. (2019). "Electrochemical Response and Chloride Threshold of Steel in Highly Resistive Concrete Systems." Indian Institute of Technology Madras.

Rengaraju, S., Neelakantan, L., and Pillai, R. G. (2019). "Investigation on the polarization resistance of steel embedded in highly resistive cementitious systems e An attempt and challenges." Electrochimica Acta, Elsevier Ltd, 308, 131–141.

Rodriguez, J., Ortega, L. M., and Casal, J. (1997). "Load carrying capacity of concrete

structures with corroded reinforcement." Construction and Building Materials, 11(4), 239–248.

Roger, M. J., EJames, O. J., and Dalel, F. L. (1980). "The effect of moisture on the physical and mechanical integrity of epoxies." JOURNAL OF MATERIALS SCIENCE 15, 15, 751–764.

Ryou, J., Voigt, T., Konsta-Gdoutos, M. S., Varacalle, D. J., Mason, T., and Shah, S. P. (2005). "Corrosion resistance of functionally graded coatings on plain steel rebars." Journal of Advanced Concrete Technology, 3(1), 69–75.

Sagues, A. A. (1988). "Technical Note: Equivalent Circuits Representing the Impedance of a Corroding Interface." Corrosion, 44(8), 555–557.

Sagüés, A. A., Lau, K., Powers, R. G., and Kessler, R. J. (2008). "Corrosion of epoxy-coated rebar in marine bridges - A 30 year perspective." 17th International Corrosion Congress 2008: Corrosion Control in the Service of Society, 5(6), 2812–2828.

Sagüés, A. A., and Zayed, A. M. (1991). "Low-Frequency Electrochemical Impedance for Measuring Corrosion of Epoxy-Coated Reinforcing Steel in Concrete." Corrosion, 47(11), 852–859.

Sajedi, S., and Huang, Q. (2017). "Load-deflection behavior prediction of intact and corroded RC bridge beams with or without lap splices considering bond stress-slip effect." Journal of Bridge Engineering, 22(1), 1–15.

Scannell, W. T., and Clear, K. C. (1990). "Long-Term Outdoor Exposure Evaluation of Concrete Slabs Containing Epoxy-Coated Reinforcing Steel." RANSPORTATION RESEARCH RECORD, 70–78.

Selvaraj, R., Selvaraj, M., and Iyer, S. V. K. (2009). "Studies on the evaluation of the performance of organic coatings used for the prevention of corrosion of steel rebars in concrete structures." Progress in Organic Coatings, 64(4), 454–459.

Sergi, G. (2018). "Corrosion Control and Cathodic Protection of Steel Reinforcement: Past Present and Future." CORCON 2018.

Séverine Marie Noëlle Cambier. (2014). "Atmospheric corrosion of coated steel; relationship between laboratory and field testing." Ohio State University, The Ohio State University.

Shakouri, M., and Trejo, D. (2017). "A time-variant model of surface chloride build-up for improved service life predictions." Cement and Concrete Composites, 84.

Shakouri, M., and Trejo, D. (2018). "A study of the factors a ff ecting the surface chloride maximum phenomenon in submerged concrete samples." 94(December 2017), 181–190.

Shang, H., Ren, G., Hou, D., Zhang, P., and Zhao, T. (2019). "Bond behaviour between steel bar and concrete under sustained load and dry-wet cycles." Magazine of Concrete Research, 71(13), 700–709.

Sharma, N. P., Bhattarai, B. K., Sapkota, B., and Kjeldstad, B. (2012). "Ground based comparison of solar UV index in Kathmandu, Pokhara and Biratnagar." Atmospheric Environment, Elsevier Ltd, 60, 428–435.

SHRP-S-330. (1993). "Standard Test Method for Chloride Content in Concrete Using the Specific Ion Probe." Strategic Highway Research Program, National Research Council, Washington, DC.

Singh, D. D. N., and Ghosh, R. (2005). "Unexpected Deterioration of Fusion-Bonded Epoxy-Coated Rebars Embedded in Chloride- Contaminated Concrete Environments." Corrosion, 61(8), 815–829.

Singh, S., Lodhi, N. K., Mishra, A. K., Jose, S., Kumar, S. N., and Kotnala, R. K. (2018). "Assessment of satellite-retrieved surface UVA and UVB radiation by comparison with ground-measurements and trends over Mega-city Delhi." Atmospheric Environment, Elsevier, 188(August 2017), 60–70.

Song, H.-W., Lee, C.-H., and Ann, K. Y. (2008). "Factors influencing chloride transport in concrete structures exposed to marine environments." Cement and Concrete Composites, 30(2), 113–121.

Song, J., Wang, L., Zibart, A., and Koch, C. (2012). "Corrosion protection of electrically conductive surfaces." Metals, 2(4), 450–477.

Startsev, V. O., Lebedev, M. P., Khrulev, K. A., Molokov, M. V, Frolov, A. S., and Nizina, T. A. (2018). "Effect of outdoor exposure on the moisture diffusion and mechanical properties of epoxy polymers." Polymer Testing, 65(August 2017), 281–296.

Subramanian, N. (2005). "Development length of reinforcing bars - Need to revise Indian codal provisions." Indian Concrete Journal, 79(8), 39–46.

Suliga, A., Jakubczyk, E. M., Hamerton, I., and Viquerat, A. (2018). "Analysis of atomic oxygen and ultraviolet exposure effects on cycloaliphatic epoxy resins reinforced with octa-functional POSS." Acta Astronautica, Elsevier Ltd, 142(October 2017), 103–111.

Swamy, R. N., and Koyama, S. (1989). "Epoxy Coated Rebars The Panacea for Steel Corrosion in Concrete." Construction and Building Materials, 3(2), 86–91.

Tait, W. S. (2012). "Corrosion Prevention and Control of Chemical Processing Equipment." Handbook of Environmental Degradation of Materials: Second Edition, Elsevier Inc., 863–886.

Tan, R., Hendriks, M. A. N., Geiker, M., and Kanstad, T. (2020). "Analytical calculation model for predicting cracking behavior of reinforced concrete ties." Journal of Structural Engineering (United States), 146(2), 1–17.

Tang, F., Bao, Y., Chen, Y., Tang, Y., and Chen, G. (2016a). "Impact and corrosion resistances of duplex epoxy/enamel coated plates." Construction and Building Materials, Elsevier Ltd, 112, 7–18.

Tang, F., Chen, G., and Brow, R. K. (2016b). "Chloride-induced corrosion mechanism and

rate of enamel- and epoxy-coated deformed steel bars embedded in mortar." Cement and Concrete Research, Elsevier Ltd, 82, 58–73.

Tang, F., Chen, G., Brow, R. K., and Koenigstein, M. L. (2014a). "Electrochemical Characteristics and Equivalent Circuit Representation of Mortar-Coating-Steel Systems by EIS." Corrosion conference, 1–10.

Tang, F., Chen, G., Brow, R. K., and Koenigstein, M. L. (2014b). "Corrosion resistance of a sand particle-modified enamel coating applied to smooth steel bars." Materials, 6(9), 6632–6645.

Tang, F., Chen, G., Brow, R. K., Volz, J. S., and Koenigstein, M. L. (2012). "Corrosion resistance and mechanism of steel rebar coated with three types of enamel." Corrosion Science, Elsevier Ltd, 59, 157–168.

Tang, F., Chen, G., Volz, J. S., Brow, R. K., and Koenigstein, M. L. (2013). "Cement-modified enamel coating for enhanced corrosion resistance of steel reinforcing bars." Cement and Concrete Composites, Elsevier Ltd, 35(1), 171–180.

Tastani, S. P., and Pantazopoulou, S. J. (2013). "Reinforcement and Concrete Bond: State Determination along the Development Length." Journal of Structural Engineering, 139(9), 1567–1581.

Trejo, D., and Pillai, R. G. (2004). "Accelerated chloride threshold testing - Part II: Corrosion-resistant reinforcement." ACI Materials Journal, 101(1), 57–64.

Tuutti, K. (1982). "Corrosion of steel in concrete." LUND University.

Vaca-cortes, E., Kahhaleh, K. Z., Jirsa, J., Harovel, G., Carrasquillo, R. L., Herman, R. S., and Miguel, A. (1998). Corrosion Performance of Epoxy-Coated Reinforcement- Summary, Findings, and Guidelines.

Vedalakshmi, R., Kumar, K., Raju, V., and Rengaswamy, N. S. (2000). "Effect of prior damage on the performance of cement based coatings on rebar: Macrocell corrosion studies." Cement and Concrete Composites, 22(6), 417–421.

Venkatesan, P., Palaniswamy, N., and Rajagopal, K. (2006a). "Corrosion performance of coated reinforcing bars embedded in concrete and exposed to natural marine environment." 56, 8–12.

Venkatesan, P., Palaniswamy, N., and Rajagopal, K. (2006b). "Corrosion performance of coated reinforcing bars embedded in concrete and exposed to natural marine environment." Progress in Organic Coatings, 56(1), 8–12.

Vera, R., Venegas, R., Carvajal, A. M., Corvo, F., and Pérez, T. (2012). "Performance of carbon steel and galvanized steel in reinforced concrete structures after accelerated carbonation." International Journal of Electrochemical Science, 7(11), 10722–10734.

Walsh, M., and Sagues, A. (2016). "Steel Corrosion in Submerged Concrete Structures - Part 1: Field Observations and Corrosion Distribution Modeling." Corrosion, 1945.

Wan, H., Song, D., Li, X., Zhang, D., Gao, J., and Du, C. (2017). "Failure mechanisms of

the coating/metal interface in waterborne coatings: The effect of bonding." Materials, 10(4), 1–15.

Wang, K., Liu, Z., Wang, Z., and Yang, W. (2014a). "Study on Polymer Modified Cement-Based Coating with Healing Effect on Rusty Carbon Steel." 2014.

Wang, S., Liu, D., Du, N., Zhao, Q., Liu, S., and Xiao, J. (2014b). "Relationship between dissolved oxygen and corrosion characterization of X80 steel in acidic soil simulated solution." International Journal of Electrochemical Science, 10(5), 4393–4404.

Wang, X. H., Chen, B., Gao, Y., Wang, J., and Gao, L. (2015). "Influence of external loading and loading type on corrosion behavior of RC beams with epoxy-coated reinforcements." Construction and Building Materials, Elsevier Ltd, 93, 746–765.

Wang, X. H., and Gao, Y. (2016). "Corrosion behavior of epoxy-coated reinforced bars in RC test specimens subjected to pre-exposure loading and wetting-drying cycles." Construction and Building Materials, Elsevier Ltd, 119, 185–205.

Wang, Z., Liu, F., Li, J., He, C., and Peng, X. (2017). "Effect of Ultraviolet Absorber on Photo-Degradation of Epoxy Coating Studied by Slow Positron Beam." ACTA Physica Polonica A, 132(5), 1523–1526.

Weyers, R. E., Ryan, M., Mokarem, D. W., Jerzy Zemajtis, Michael M. Sprinkel, and John G. Dillard. (2000). "Field performance of epoxy-coated reinforcing steel in virginia bridge decks." Environmental Engineering, (Final Report).

Wilkins, R. J. (1951). "Some experiments on the load distribution in bond tests." Magazine of Concrete Research, 2(5), 65–72.

Woo, R. S. C., Chen, Y., Zhu, H., Li, J., Kim, J., and Leung, C. K. Y. (2007). "Environmental degradation of epoxy – organoclay nanocomposites due to UV exposure . Part I : Photo-degradation." Composite Science and Technology, 67, 3448–3456.

Wu, C., Chen, G., Volz, J. S., Brow, R. K., and Koenigstein, M. L. (2013). "Global bond behavior of enamel-coated rebar in concrete beams with spliced reinforcement." Construction and Building Materials, 40, 793–801.

Xue, X., Yang, J., Zhang, W., Jiang, L., Qu, J., Xu, L., and Zhang, H. (2015). "The study of an energy efficient cool white roof coating based on styrene acrylate copolymer and cement for waterproofing purpose — Part I : Optical properties , estimated cooling effect and relevant properties after dirt and accelerated exposures." Construction and Building Materials journal, 98, 176–184.

Yalciner, H., Eren, O., and Sensoy, S. (2012). "Cement and Concrete Research An experimental study on the bond strength between reinforcement bars and concrete as a function of concrete cover , strength and corrosion level." Cement and Concrete Research, Elsevier Ltd, 42(5), 643–655.

Yeih, W., Huang, R., Chang, J. J., and Yang, C. C. (1997). "Pullout test for determining interface properties between rebar and concrete." Advanced Cement Based Materials, 5(2), 57–65.

Zayed, A. M., and Sagues, A. A. (1990). "Corrosion at surface damage on an epoxy coated reinforcing steel." Corrosion Science, 30(10), 11125–11144.

Zemajtis, J., Weyers, R. E., and Sprinkel, M. M. (1998). "An Evaluation of the Performance of Epoxy-Coated Reinforcing Steel in Concrete Exposure Specimens." Final contract report by Virginia Transportation Research Council, 147 p.

Zemajtis, J., Weyers, R. E., Sprinkel, M., and McKeel, W. T. (1996). Epoxy-coated reinforcement - A historical performance review.

Zhang, D., Qian, H., Wang, L., and Li, X. (2016). "Comparison of barrier properties for a superhydrophobic epoxy coating under different simulated corrosion environments." Corrosion Science, Elsevier Ltd, 103, 230–241.

Zhang, R., Castel, A., and François, R. (2009). "Serviceability Limit State criteria based on steel-concrete bond loss for corroded reinforced concrete in chloride environment." Materials and Structures/Materiaux et Constructions, 42(10), 1407–1421.
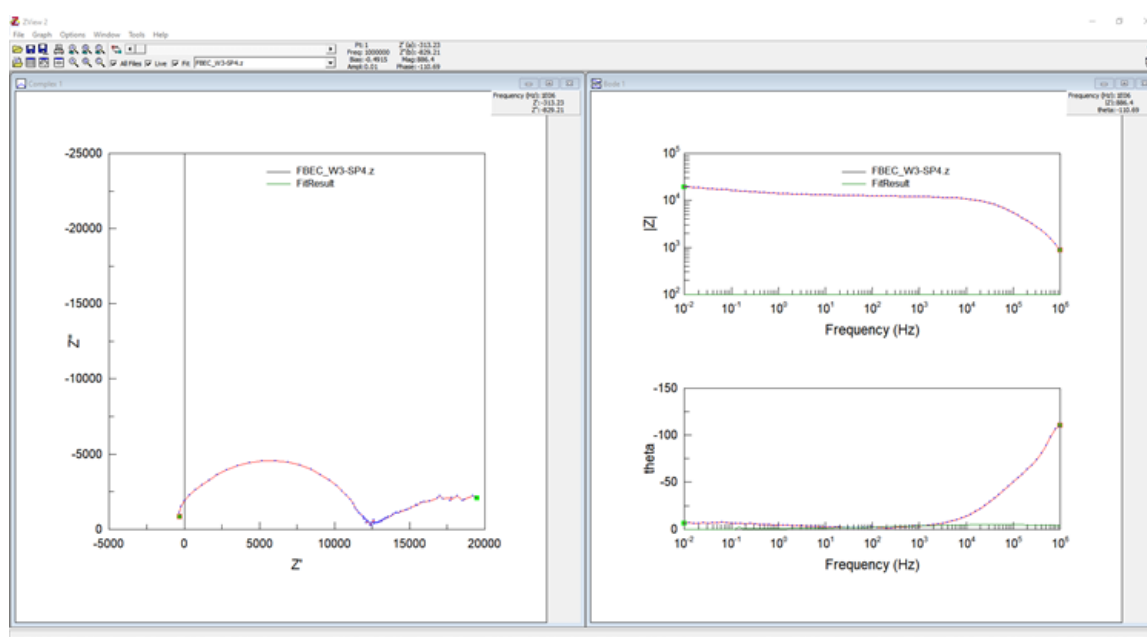
This page is intentionally left blank

APPENDIX A - PROCEDURES TO FIT EIS RESPONSE TO

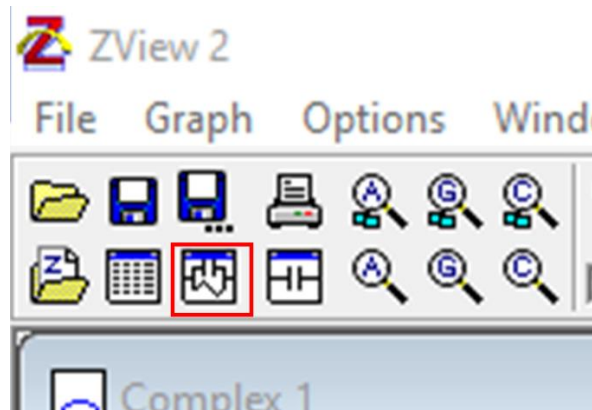# EQUIVALENT ELECTRICAL CIRCUIT

INTRODUCTION

This Appendix describes how to fit electrochemical impedance spectra to an equivalent electrical circuit.

FITTING OF ELECTROCHEMICAL IMPEDANCE SPECTRA TO THE

ELECTRICAL EQUIVALENT CIRCUIT

    i)   Open EIS file to fit

ii)   In Zview, click on the equivalent circuit tool

iii)   The screen shown below will appear
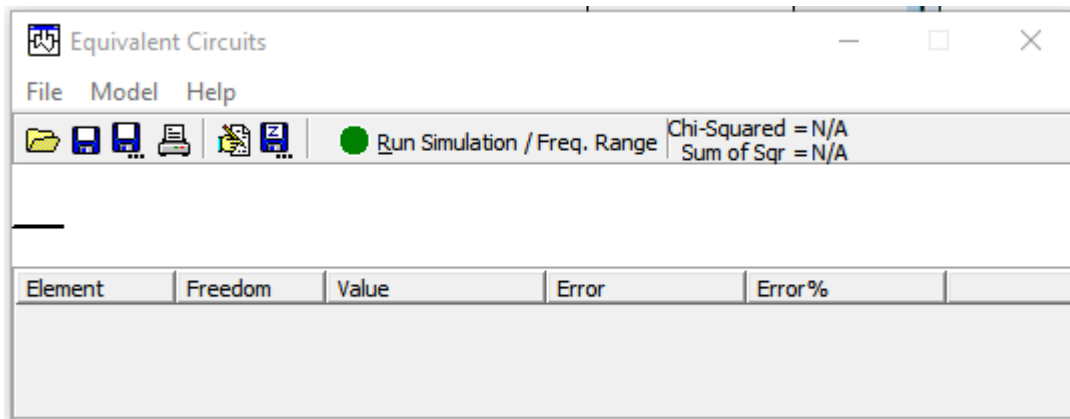
iv)   Construct the equivalent circuit. The equivalent circuit can be adapted or modified from the EEC available in literature. The modification should be done based on the physical understanding of the system. A few examples for modifications are given below
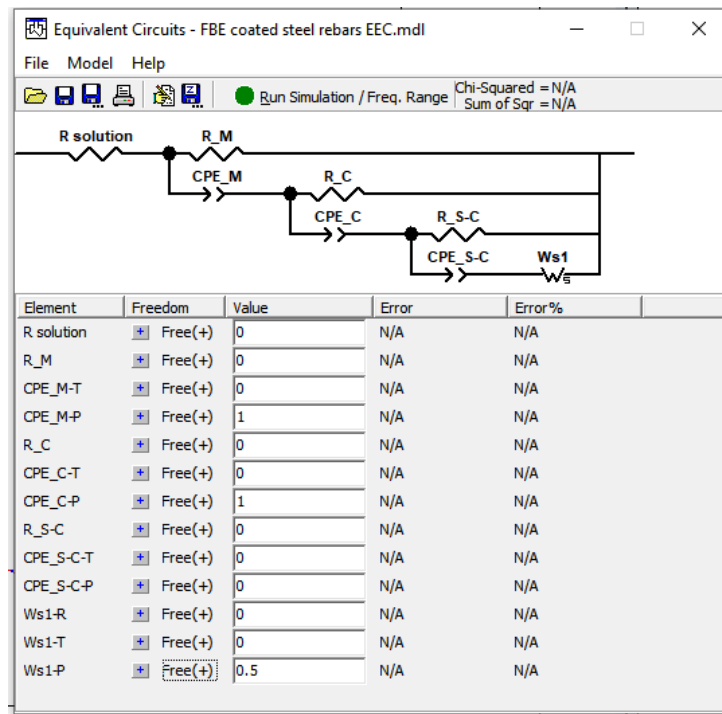
v)   Give nonzero values to all the elements. Note that all the CPE component should be less than 1. And save the circuit

vi)   Choose the EIS file to run the simulation. A fit will be generated with a large error in each component. For the optimized fitting, use an instant fit option. For that, cho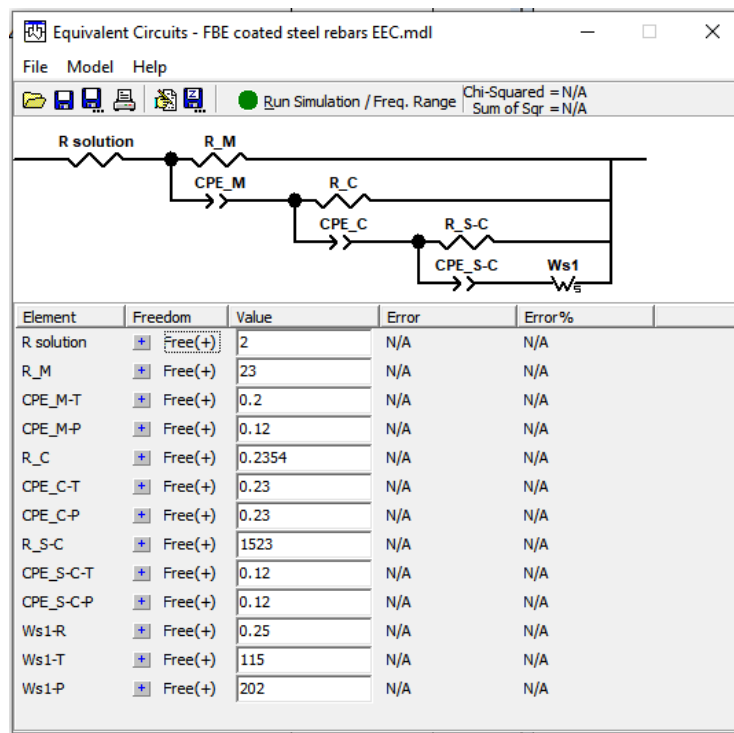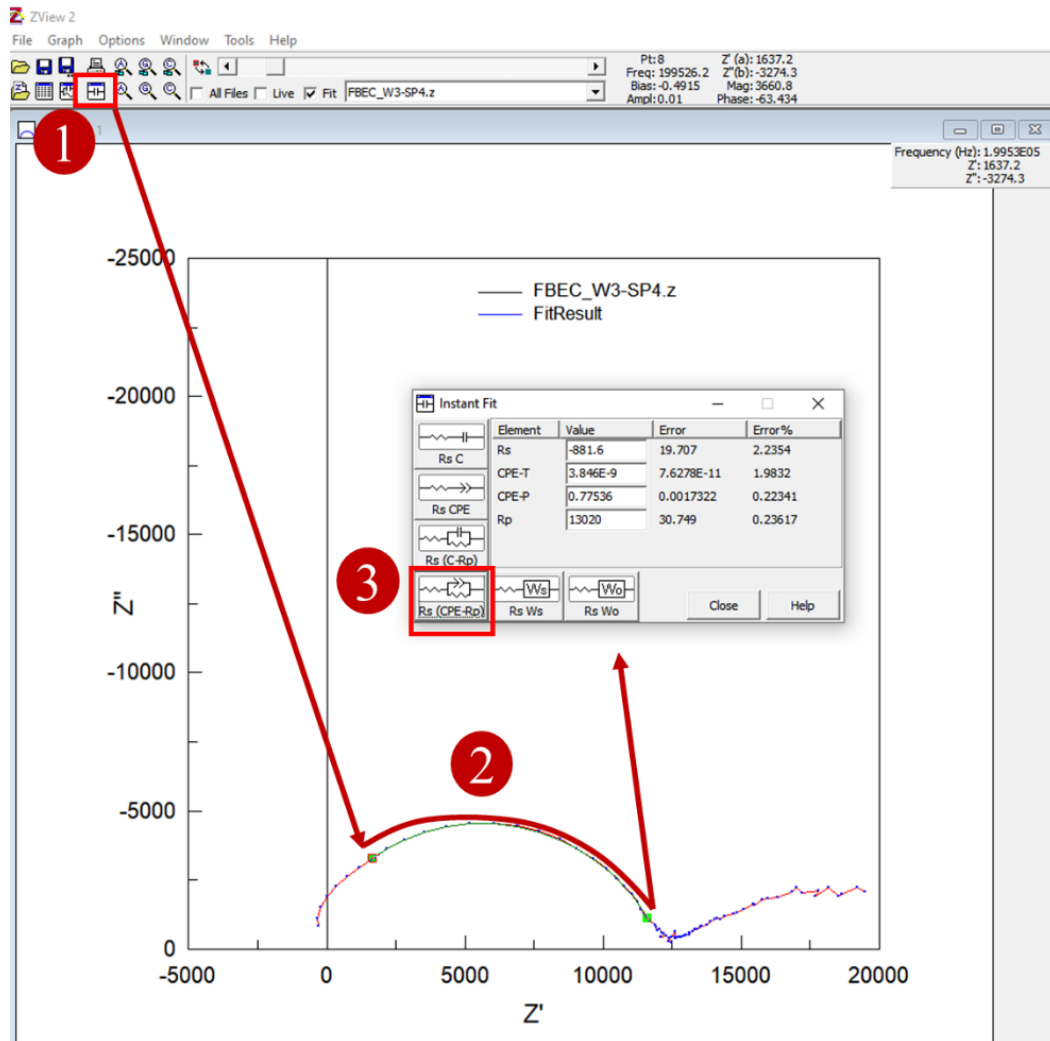ose each semicircle and fit it with R-CPE element shown in the image below. Then drag the values for each element to the main simulation dialogue box. Repeat this step for all the semicircles.

vii)   Then, run the simulation multiple times to achieve the Chi-square value ≤ 0.005 and sum of squares < 1. Error percentage of individual component less than 20%, as shown below.

This page is intentionally left blank

APPENDIX B - PROCEDURES TO DETERMINE THE CHLORIDE THRESHOLD OF UNCOATED AND COATED STEEL IN CEMENTITIOUS SYSTEMS

This method is available in SHRP 330 (Appendix F). The same procedure was adopted for determining all the chloride concentrations in this study. The procedure in detail can be found in SHRP-S/FR-92-110, Condition Evaluation of Concrete Bridges Relative to Reinforcement Corrosion, Volume 8: Procedure Manual, 1992. Below is the test method in brief.

STEPS TO DETERMINE CHLORIDE THRESHOLD OF UNCOATED STEEL REBARS

Figure 8.1 shows the steps to determine the chloride threshold of the steel-mortar interface. Note that the same process can be used for determining the chloride threshold of the steel-concrete interface. A 1.5 gm ground powdered sample is collected from mortar/concrete less than 0.5 mm depth from the steel-mortar interface. This powder was mixed with 10 ml digestion solution in an airtight container of about 125 ml capacity. Then, the container was shaken for about 30 Seconds. Then, the cap of the container was opened to release the gases formed. Then again, the container was stirred for about two minutes. Thereafter, the stabilization solution was added to this mix. Later, chloride concentration was measured using the chloride ion-specific electrode.

Impression of rebar in mortar
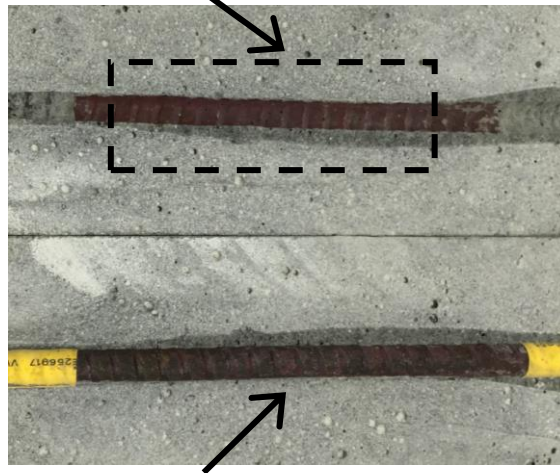
Corroded coated steel rebar

(a) Autopsied macrocell specimen

10 ml digestion solution

+

40 ml stabilization solution

(b) Powdered sample from the interface and mixing with reagents

(c)Measurement of chloride concentration

Figure 8.1 Steps for determining chloride threshold of steel-mortar interface

Apparatus

1. Grinder/filer:

➢ A needle grinder or filer is used for obtaining the powdered mortar/concrete from the mortar surface adjacent to the steel rebars.

2. Plastic bags

➢ The powdered mortar should be sealed in plastic bags with the arrangement to make it airtight to avoid contamination from dust, moisture, etc.

3. Weighing papers

➢ Clean, glossy, nonsticky papers with a size of about 50×50 mm should be used to weigh the powdered mortar samples.

4. Marking pen

➢ Permanent marking pen to label the sample number and date of testing on the plastic bags.

5. Balances

➢ Weighing balance sensitive to 0.1 gm to weigh the mortar powder, distilled water, acetic acid, and isopropanol alcohol, for preparing digestion solution; and 0.0001 gm to weigh the sodium chloride for preparing the stabilizing solution

6. Chloride ion-specific electrode

Reagents

1. Digestion solution: The digestion solution is produced by combining acetic acid, isopropyl alcohol, and distilled water. Measure 940 gm of distilled water in l-liter container. Add 60 g of glacial acetic acid and 50 gm of isopropyl alcohol to the distilled water. Thoroughly stir the solution. Dispense the solution into the 125-ml Nalgene® bottles in 20-ml volumes.

2. Stabilization solution: The stabilizing solution is a dilution, standard chloride solution. It is prepared as follows: Place 0.1545 g of sodium chloride into 1 liter of distilled water. Add 40 ml of this solution to 960 ml of distilled water. Tiffs produce a 3.75 ppm chloride solution.

3. Calibration solution: The calibration solutions are made by dissolving sodium chloride in distilled water. The concentration levels are 1.25, 0.6, 0.3, 0.03, and 0.01% by weight CI- based on a 3.0-g concrete sample. To achieve the respective concentration levels, mix the following quantities of sodium chloride with 1 liter of distilled water: 0.6169 g, 0.2961 g, 0.1481 g, 0.0148 g, and 0.0049 g. (This will result in solutions having chloride concentrations of 374, 180, 90, 9, and 3 ppm, respectively, which in turn correspond to the previously listed percentages by weight of concrete.) Dispense 20 ml into the 40-ml Nalgene®bottles and label each appropriately.

Sample preparation

➢ Obtain a powdered mortar sample. Collect at least 1.5 gm of powdered mortar. Place the collected powder in a glass container with an arrangement of the airtight cap.

➢ The degree of fit of measurements of the calibration solutions determines the suitability of the specific ion electrode in combination with the machine used. The mV response corresponding to a minimum of five calibration solution concentrations (say, 50, 100, 250, 500, 1000 ppm) measured to adequately calibrate the equipment combination. Any alterations to the combinations shall require the formulation of a new calibration equation.

➢ Calculate the log10 of the chloride concentrations (ppm) of the calibration solutions, e.g.,$- \log_{10} (374 \text{ ppm Cl}^-) = 2.573$. Perform a linear regression of the

millivolt readings (abscissa) versus the $\log_{10}$ of the chloride concentrations (ordinate) of the respective calibration solutions, producing an equation in the following format

$\text{Log}_{10}(\text{ppm Cl}) = (\text{slope} \times \text{M}) + \text{intercept}$

A sample fit of calibration of known concentration of chloride (in ppm) and potential (mV) is shown below. Once reliable R^2 values (>0.95) are obtained, the combination of multimeter and chloride ion-specific electrode is ready to use for testing,
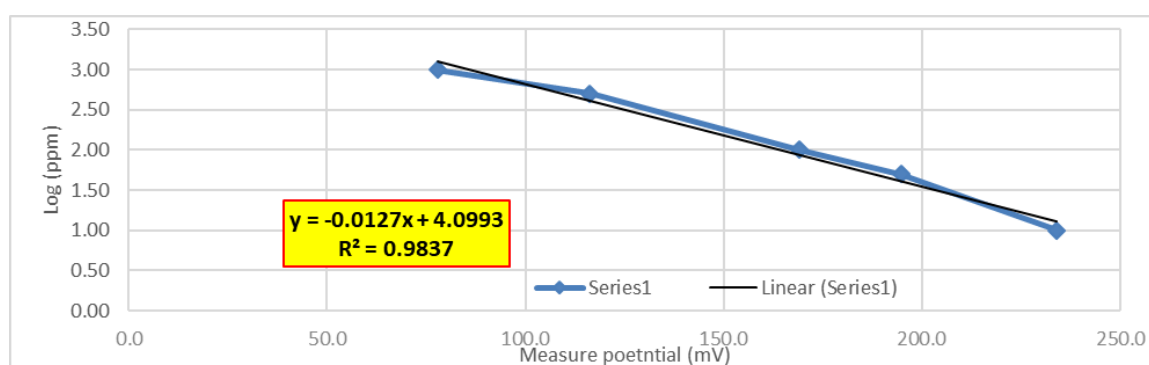

Figure 8.2 Calibration of multimeter and chloride ion-specific electrode combination

Procedure to determine the chloride concentration

- Place 10 ml of the digestion solution in a clean, dry 125 ml glass bottle. And close it to avoid losing concentration.

- Remove the powdered mortar sample from the plastic bag and weigh 1.5 ± 0.1 grams of mortar/concrete sample on a weighing paper.

- Place the concrete sample in the bottle containing the 10 ml digestion solution, place the cap on the bottle, and shake vigorously to suspend the powder in the solution. Let

the powder digest for 3 minutes. The bottle may be opened after shaking to relieve pressure from effervescence due to the reaction, and then closed immediately.

- Carefully remove the bottle cap and add 40 ml of the stabilizing solution (a 3.75 ppm chloride solution). Replace the cap and shake vigorously for 1 minute.

- Remove the bottle cap and place the electrode in the solution such that the tip of the electrode is about 10 mm below the surface of the solution.

- Wait for 3 or more minutes and record the stable millivolt reading. Millivolt reading is defined to be stable when it oscillates by less than $\pm$ 0.5 millivolts.

- After each millivolt measurement, the electrode shall be rinsed clean with distilled water.

- For calculation of %bwoc, follow the steps
    - Calculate Log Cl using the equation
    - $\text{Log}(Y) = mX + C$
    - The % of chlorides are determined by
    - $\%\,Cl^- = (10^{\,mX+C} - 3.75) \times 0.00333$
    - $Cl^- \,(lb/yd^3) = 39.15 \times Cl^- \,(\%)$
    - $Cl^- \,(kg/m^3) = 1.69 \times Cl^- \,(lb/yd^3)$
    - $Cl^- \,(\%bwoc) = Cl^- \,(kg/m^3) \times 100/$ weight of cement/binder in the concrete mix

APPENDIX C - MODIFIED SL-CHLOR PROGRAM – AN 'IN-HOUSE DEVELOPED MATLAB PROGRAM FOR ESTIMATION OF SERVICE LIFE OF RC STRUCTURES WITH COATED STEEL REBARS'

This Appendix presents the modifications made in the MATLAB® program (named as "SL-Chlor") (Rengaraju 2019) for accomodating the diffusion of chloride through FBE coating. Figure 8.3 shows the flowchart of MATLAB® program used for the estimation of service lives of RC systems with FBE/CPC coated steel rebars. In the program reported by Rengaraju (2019) an additional Function D for chloride diffusion through coating was introduced, and the same is presented in Figure 8.4.
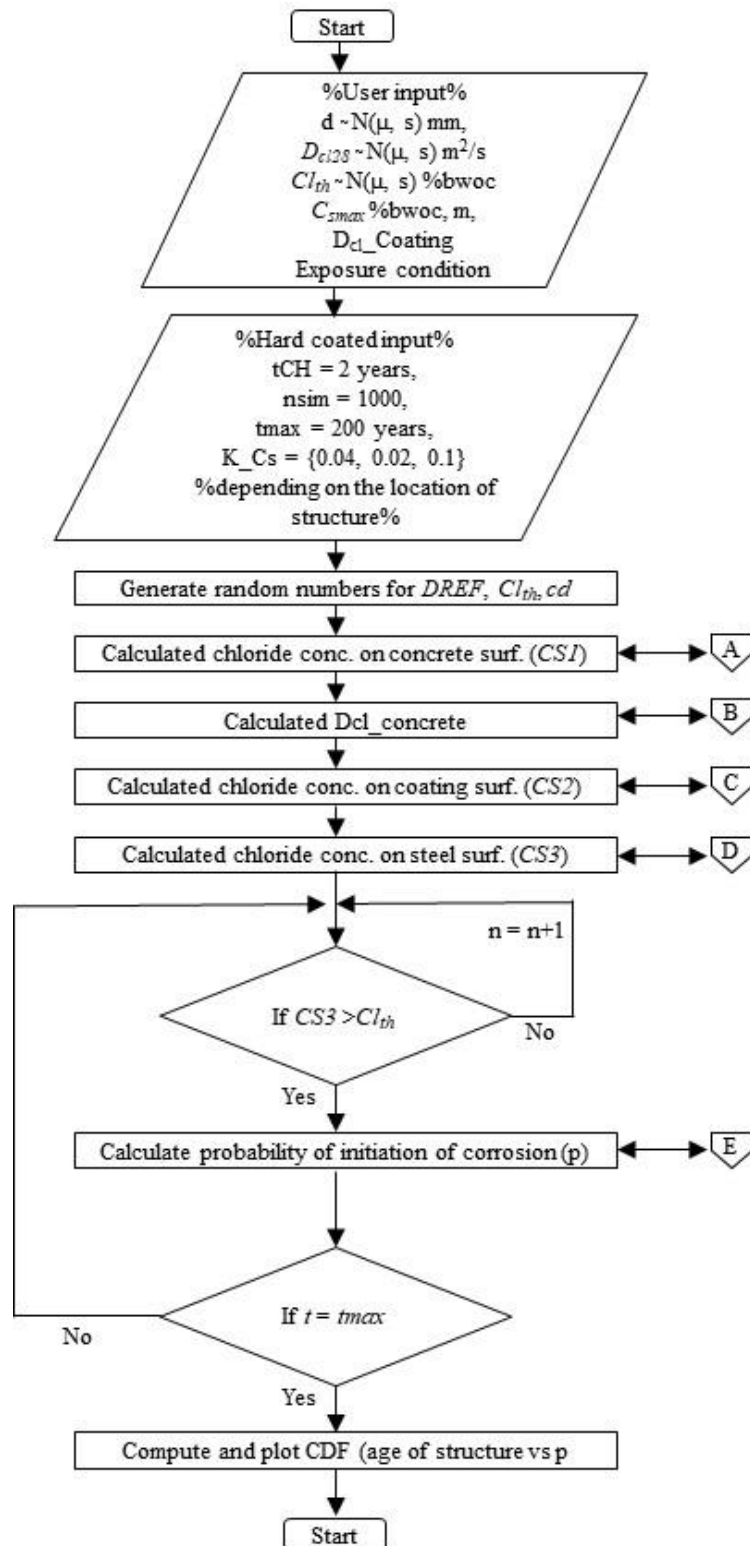
Figure 8.3 Flowchart showing the procedure to determine the service lives of RC systems with FBE coated steel rebars

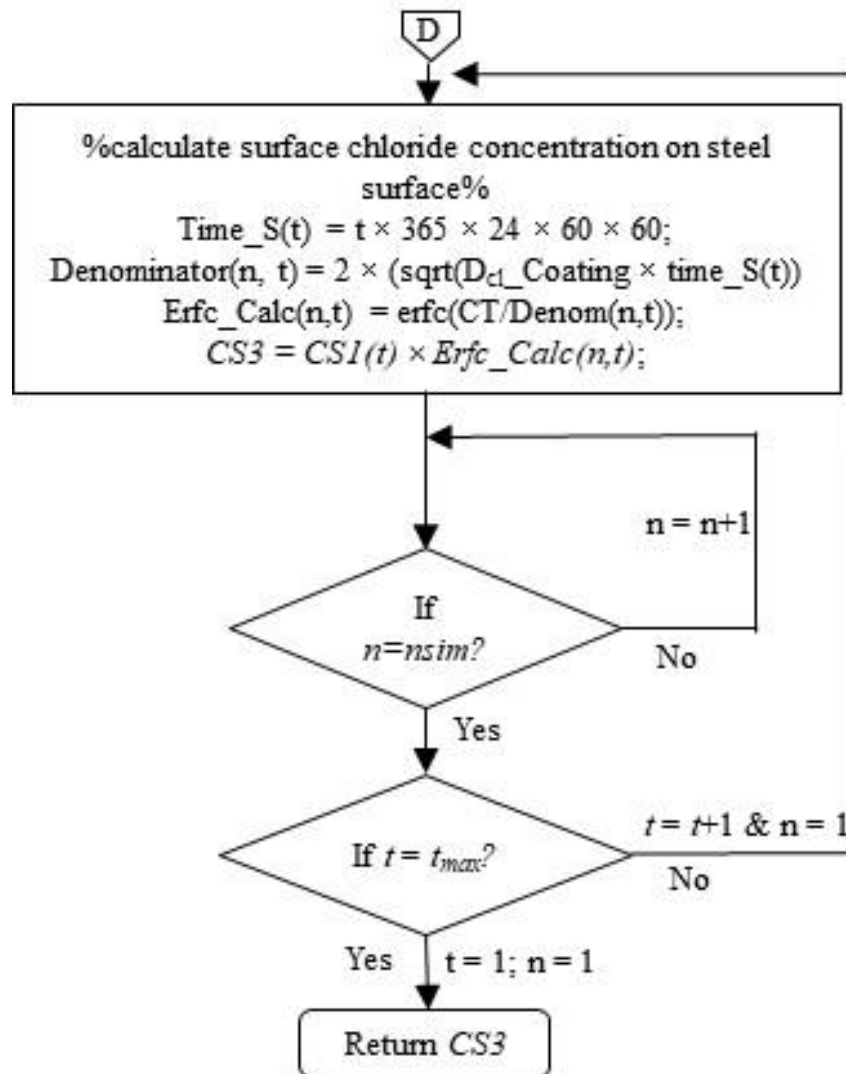**[modified SL-CHLOR reported by Rengaraju 2019]**

Figure 8.4 Function introduced for the diffusion of chloride through the coating

This page is intentionally left blank

LIST OF PUBLICATIONS BASED ON THIS THESIS

REFEREED JOURNALS

Published

[1].   **Deepak K. Kamde** and Radhakrishna G. Pillai (2020) "Effect of ultraviolet exposure on corrosion performance and service life of Fusion-Bonded-Epoxy (FBE) coated steel rebars.", *Corrosion*, NACE, https://doi.org/10.5006/3588

[2].   **Deepak K. Kamde** and Radhakrishna G. Pillai (2020) "Effect of surface preparation on corrosion of steel rebars coated with cement-polymer-composites (CPC) and embedded in concrete.", *Construction and Building Materials*, Elsevier, 237, pp 1-11, https://doi.org/10.1016/j.conbuildmat.2019.117616

In review

[3].   **Deepak K. Kamde**, Sylvia Kessler, Radhakrishna G. Pillai, and Marc Zintel "Coated Reinforcement in Cementitious Systems: Needed Modifications to Existing Service-life Models", *Journal on Sustainable and Resilient Infrastructure*

[4].   Arya E. Kandiyil, Varghese A. Ittyyeipe, **Deepak K. Kamde**, Dhanya Vinod "Service life of RC systems with cement polymer composite coated steel reinforcement.", *Indian Concrete Journal*

Draft ready

[5].   **Deepak K. Kamde** and Radhakrishna G. Pillai "A test method for electrochemical assessment of steel with non-metallic coating and embedded in cementitious systems", To be submitted to *Materials and Corrosion*, Wiley Publications

[6].   **Deepak K. Kamde** and Radhakrishna G. Pillai "Significant bond loss due to negligible corrosion of Cement-Polymer-Composite (CPC) coated steel rebars embedded in concrete", To be submitted to *Materials and Structures*, Springer

[7].   **Deepak K. Kamde**, Sylvia Kessler, and Radhakrishna G. Pillai "Condition assessment methods of fusion-bonded-epoxy (FBE) coated steel rebars in concrete – Laboratory versus field experiences.", to be submitted to *Corrosion*, NACE

CONFERENCE PUBLICATIONS

[1].   **Deepak K. Kamde**, and Radhakrishna G. Pillai "Effect of exposure to UV on the performance of fusion-bonded-epoxy (FBE) coated steel rebars", *Proceedings of the CORCON 2019*, NACE, Mumbai, Sept 23 – Sept 26, 2019 (**Best Paper Award**)

[2].   **Deepak K. Kamde**, and Radhakrishna G. Pillai "Effect of Corrosion Level on Bond

Performance of Cement-polymer-composite (CPC) Coated Rebar", *Proceedings of the* ICCRRR (International Conference on Concrete Repair, Rehabilitation, and Retrofitting), Cape Town, S outh Africa, November 2018

[3].   **Deepak K. Kamde**, and Radhakrishna G. Pillai "Electrochemical response and service life estimation of Reinforced Concrete Structures with FBEC rebars.", *Proceedings of the CORSYM 2018*, IIT Madras, NACE, Chennai, March 2018. (**Best Presentation Award**)

[4].   **Deepak K. Kamde**, and Radhakrishna G. Pillai "Short-term test methods to evaluated chloride threshold of CPC coated rebars.", *Proceedings of the CORCON 2017*, NACE, Mumbai, Sept 2017

[5].   **Deepak K. Kamde**, and Radhakrishna G. Pillai "Corrosion performance of Fusion Bonded Epoxy Coated steel rebars.", *Proceedings of the ICACMS 2017*, RILEM, Chennai, Sept 2017

[6].   **Deepak K. Kamde**, and Radhakrishna G. Pillai "Effect of surface preparation on the performance of Cement-polymer-composite (CPC) coatings for steel in concrete structures.", *Proceedings of the CORROSION 2017*, NACE, New Orleans, USA, March 2017.

[7].   **Deepak K. Kamde**, and Radhakrishna G. Pillai "Effect of surface treatment on the performance of Cement-polymer-composite (CPC) coatings for steel in concrete structures.", *Proceedings of the CORCON 2016*, NACE, Delhi, Sept 2016

RECOMMENDATION FOR MODIFICATIONS OF STANDARDS

- Indian Standard for Fusion bonded epoxy coated reinforcing bars- specification (IS 13620); *Recommendations submitted*

- Standard Specification for Epoxy-Coated Steel Reinforcing Bars (ASTM A775); *In preparation*

DOCTORAL COMMITTEE

CHAIRPERSON Dr. Manu Santhanam

Professor and Head

Department of Civil Engineering

GUIDE Dr. Radhakrishna G. Pillai

Associate Professor

Department of Civil Engineering

MEMBERS Dr. Lakshman Neelakantan

Associate Professor

Department of Metallurgical and Materials Engineering

Dr. Amlan K. Sengupta

Professor

Department of Civil Engineering

Dr. K. Ramamurthy

Professor

Department of Civil Engineering

This page is intentionally left blank

VITA

Deepak Kumar Kamde was born in Seoni, Madhya Pradesh (MP), India and was brought up in Chhindwara, MP. In May 2012, he received his Bachelor of Engineering degree in Civil Engineering from Ramdeobaba Kamla Nehru Engineering College (now, Ramdeobaba College of Engineering and Management), Nagpur, Maharashtra. In August 2014, he received his Master of Technology (M. Tech.) in Structural Engineering from Sardar Vallabbhai National Institute of Technology Surat, Gujarat. Then, he worked as an Assistant Professor at R. K. University, Rajkot, Gujarat. Later, he started his doctoral studies in Civil Engineering (with specialization in structural and material performance) in the Department of Civil Engineering, Indian Institute of Technology Madras, Chennai, Tamil Nadu. During his doctoral studies, he worked as a half-time research/teaching assistant in the Department of Civil Engineering, IIT Madras.

Deepak Kamde can be contacted at

c/o Shri. Rameshwar Kamde
28/35, Behind Pooja Lodge,
Gulabra Chhindwara
Madhya Pradesh 480 001
India
Ph. +91 94442 17698
Email: deepak.kamde89@gmail.com

This page is intentionally left blank